Identification of novel protein regulators of the HIF signaling pathway by genome-wide screening

Inaugural Dissertation
submitted to the Faculty of Medicine
in partial fulfillment of the requirements
for the PhD-Degree
of the Faculties of Veterinary Medicine and Medicine
of the Justus Liebig University Giessen

JUSTUS-LIEBIG-
UNIVERSITÄT
GIESSEN

by Ritschel, Nadja, née Utz
of Giessen, Hesse, Germany

Giessen 2023

From the Institute of Neuropathology
Director: Prof. Dr. med. Till Acker
of the Faculty of Medicine of the Justus Liebig University Giessen

Supervisor and First Reviewer:
Prof. Dr. Till Acker, Institute of Neuropathology
(Faculty of Medicine of the JLU Giessen)

Second Reviewer:
Prof. Dr. Christoph Rummel, Institute of Veterinary Physiology and Biochemistry
(Faculty of Veterinary Medicine of the JLU Giessen)

Committee Vice-Chair and Co-Supervisor:
Prof. Dr. Reinhard Dammann, Institute of Genetics
(Faculty of Biology of the JLU Giessen)

Committee Chair:
Prof. Dr. Klaus-Dieter Schlüter, Institute of Physiology
(Faculty of Medicine of the JLU Giessen)

Date of Doctoral Defense: 21st December 2023

For Kai

Table of contents

1. Introduction

1.1 Cellular oxygen-sensing via the HIF signaling pathway

In the 18th century, Carl Scheele discovered a central component of air that enabled substances to burn. This substance was first purified by Joseph Priestly and later termed "oxygen" by Antoine Lavosier [83]. In the following centuries, the essential role of oxygen for life became increasingly evident. More recently, the effects of low oxygen tension (hypoxia) have sparked interest, as this phenomenon arises in many physiological as well as pathological settings, e. g. during embryonic development or adaption to a local hypoxic microenvironment in tumor tissues. However, how cells sense oxygen levels at the molecular level was not clear until the discoveries of Semenza, Ratcliffe, Kaelin and their co-workers at the end of the 20th century. They uncovered the central, evolutionary well-conserved pathway for oxygen-sensing: The hypoxia inducible factor (HIF) signaling pathway [175, 201, 129, 73, 75]. As a scientific recognition of the importance of this work, the 2016 Albert Lasker Basic Medical Research Award, and in 2019, the Nobel Prize in Physiology or Medicine was jointly awarded to William G. Kaelin Jr., Sir Peter J. Ratcliffe and Gregg L. Semenza "for their discoveries of how cells sense and adapt to oxygen availability" [86, 152].

1.1.1 The HIF signaling pathway and its regulation

Since the studies of Kaelin, Ratcliffe and Semenza in the early 90s, the molecular network around HIFs is being extensively investigated. The key elements of the HIF signaling pathway are shown in Figure 1.1 and summarized below [173, 85]. At a physiological oxygen level (normoxia, approximately 21 % O_2; Fig. 1.1, red background), HIF1α, HIF2α (also called endothelial PAS domain-containing protein 1 (EPAS1)) and HIF3α (collectively referred to as HIFα) are hydroxylated on proline residues (HIF1α and HIF2α on two, HIF3α on one residue) by prolyl hydroxylase domain (PHD) enzymes (PHD1, -2 and -3). Among the PHD proteins, PHD2 (gene name *EGL nine homolog (EGLN)1*) was reported to be the main HIFα hydroxylase, as it has the lowest O_2 affinity among the PHDs [12]. However, PHD1 and especially PHD3 (gene name *EGLN2* and *EGLN3*, respectively) are associated with important HIF-regulatory functions as well, suggesting

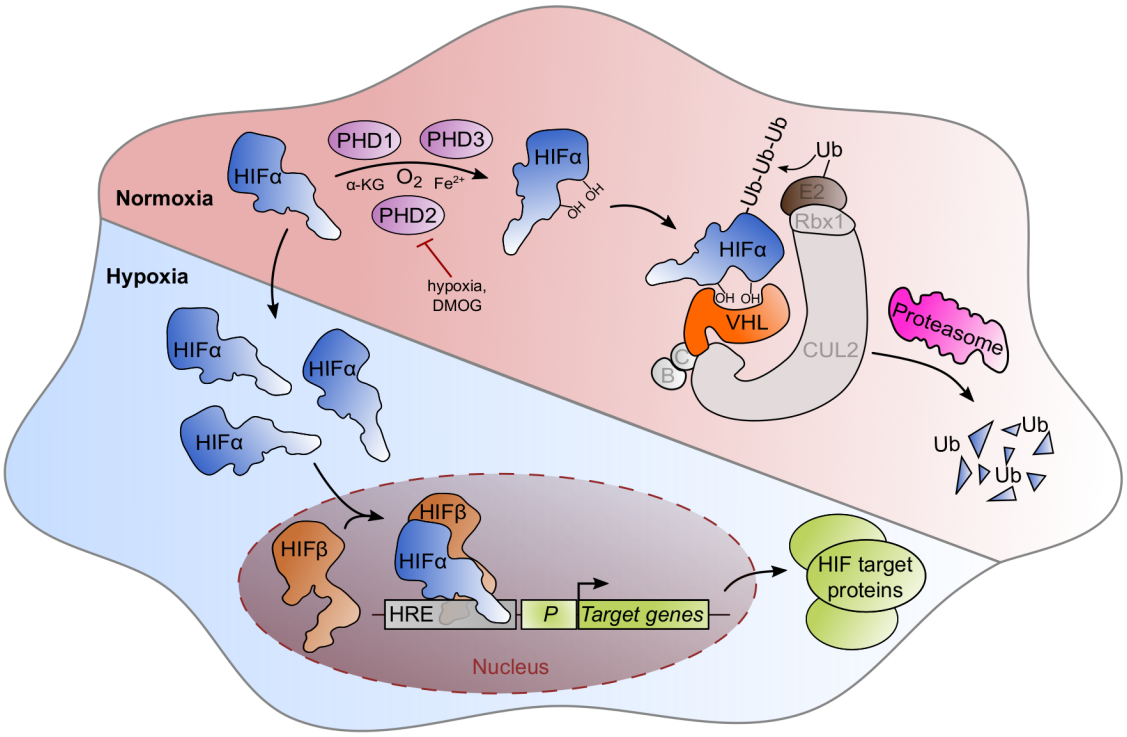

Figure 1.1: Overview of the HIF signaling pathway in human cells.
In normoxia (red background), HIFα subunits are hydroxylated (-OH) by PHD proteins (PHD1 -3) on two proline residues. PHD proteins are only active, if the co-factors/-substrates α-ketoglutarate (α-KG), oxygen (O_2) and ferrous iron (Fe^{2+}) are present. The α-KG antagonist dimethyloxaloylglycine (DMOG) inhibits PHDs. Once hydroxylated, the von-Hippel-Lindau (VHL) E3 ubiquitin ligase complex (orange and light grey) binds HIFα. Then, it interacts with the E2 ubiquitin-conjugating enzyme (dark brown) that ubiquitinates (-Ub) HIFα, thus, marking it for proteasomal degradation.
In hypoxia (blue background), due to insufficient levels of O_2, PHD proteins are inhibited. This leads to the accumulation of HIFα subunits, their translocation to the nucleus and heterodimerization with HIFβ subunits. The dimers bind to hypoxia responsive elements (HREs) at gene regulatory regions, e. g. promoters (P), and induce the transcription of HIF target genes.
Individual elements are not drawn to scale. Shape of HIFα, HIFβ and VHL are based on AlphaFold structure predictions, calculated from experimental structures summarized in UniProt entries Q99814 (HIF2α/EPAS1), P27540 (HIFβ/ARNT), P40337 (VHL). Their interactions are illustrated according to the Protein Data Bank (PDB) entries 6BVB (VHL, HIF2α, Elongin B and C, *Homo sapiens*) and 4ZPH (HIF2α and HIFβ, *Mus musculus*).

complementary roles of PHDs in HIF signaling under different cellular conditions [89, 38]. The hydroxylation activity of PHD enzymes depends on co-substrates and co-factors, namely α-ketoglutarate (α-KG) (also called 2-oxoglutarate (2-OG)), ferrous iron (Fe^{2+}), connected to this ascorbate [94], and oxygen (O_2) [167].

PHD proteins show different preferences for the major HIFα isoforms. While PHD2 prefers HIF1α (hydroxylation of P402/P564), PHD1 and PHD3 mainly hydroxylate HIF2α. There, PHD1 hydroxylates both proline substrate residues (P405/P531), whereas PHD3 hydroxylates almost exclusively one (P531) [72]. These preferences can be altered by mutations, as is the case with breast cancer-associated PHD2 R396T mutation, which

abolishes PHD2's hydroxylation activity towards the C-terminal ODD (CODD) [20].

After hydroxylation, HIFα is bound by the von-Hippel-Lindau (VHL) E3 ubiquitin ligase complex, consisting of the main subunits VHL, Elongin B and C (alternative gene names *transcription elongation factor B polypeptide (TCEB) 2* and *1*, respectively), as well as Cullin-2 (CUL2) and ring-box 1 (RBX1). The E3 ubiquitin ligase complex recruits an E2 ubiquitin-conjugating enzyme and catalyzes the poly-ubiquitination of HIFα. Subsequently, the ubiquitination is recognized by the proteasome, leading to the rapid degradation of HIFα. Therefore, HIFα protein levels are very low in normoxic cells despite constitutive basal expression of mRNA from the HIFα genes.
As pointed out by Bishop and Ratcliffe, "hypoxia" refers to levels of oxygen that are "low or sub-optimal in respect of cellular functions". Importantly, there is no defined correlation between the term "hypoxia" and the partial pressure of oxygen (pO_2) or O_2 concentration [13]. Consequently, any decrease in oxygen level that results in increased stability of HIFα protein can be called hypoxia [204]. In this study, the term hypoxia refers to 1 % (7.6 mmHg) environmental O_2 level, unless otherwise stated.

If the oxygen level decreases (hypoxia; Fig. 1.1, blue background) or PHD proteins are inhibited by other means (e. g. by iron chelation, reactive oxygen species (ROS) or dimethyloxaloylglycine (DMOG), resulting in so-called pseudohypoxia [139]), HIFα will not be hydroxylated or degraded. Therefore, HIFα proteins accumulate in the cell, translocate to the nucleus and bind to the ubiquitously-expressed HIFβ (HIF1β or aryl hydrocarbon receptor nuclear translocator (ARNT)) subunit. Together, as HIF dimers, they exert their transcription factor function. They induce the transcription of HIF target genes by binding to hypoxia responsive elements (HREs) in regulatory regions, such as enhancers or promoters, of the respective genes. As a result, HIF target proteins are expressed and act to re-establish O_2 homeostasis. This is achieved, for example, by the expression of erythropoietin (EPO) [189], which is essential for the production of erythrocytes and hence oxygen transport, or by inducing angiogenesis through expression of the vascular endothelial growth factor (VEGF) [117].

In addition, HIFα proteins exert also metabolic regulatory functions. For example, glycolytic enzymes were identified to be HIF target genes as early as the beginning of the 90s [48, 176] and the regulatory function of HIF dimers has continued to expand since then. The discoveries were fueled by technological advances, such as the application of chromatin immune precipitation sequencing (ChIP-seq) analysis, and led to the identification of hundreds of direct HIF target genes [166]. HIF has now been found to be involved in nearly all biological processes, both in areas of physiological hypoxia, e. g. embryonic development and organogenesis, and in pathological scenarios like cancer [153].

HIFα: Isoforms and protein domains

HIF activity primarily depends on the stability of the HIFα subunit, as HIFβ is ubiquitously expressed in the cells. In humans, three oxygen-dependent HIFα isoforms are known: HIF1α, HIF2α and HIF3α. Among them, HIF1α and HIF2α are the best-characterized ones. Stabilization of these isoforms results in expression of HIF target genes. In contrast, HIF3α was shown to negatively regulate the expression of HIF target genes, for example in kidney and vascular cells [5, 59]. In addition, several splice variants of HIF3α exist, which makes the analysis of this HIF isoform technically demanding [130].
The three HIFα proteins share a similar domain structure (Fig. 1.2). While the basic helix-loop-helix domain (bHLH) facilitates binding of HIFα to deoxyribonucleic acid (DNA), the two Per-ARNT-Sim (PAS) domains (PAS-1 and -2, often referred to as PAS-A and -B [161, 207]) and most likely also the PAS-associated C-terminal (PAC) domain are responsible for heterodimerization with HIFβ. The transcription regulation activity of HIFα is controlled by one (HIF3α) or two transactivation domains (HIF1α and HIF2α; N- and C-terminal). Within the C-terminal transactivation domain (CTAD), that is only present in HIF1α and HIF2α, specific asparagine residues (N804 and N847, respectively; see also Fig. 1.2) are responsible for enabling the interaction with the transcriptional coactivators CREB binding protein (CBP) and p300 [101]. Hydroxylation of this residue by factor inhibiting HIF (FIH) blocks the transcriptional activation without affecting HIFα stability and DNA binding.
Surrounding the N-terminal transactivation domain (NTAD), the oxygen-dependent degradation domain (ODD) is accountable for the stability of the protein. Within the ODD, the hydroxylation of specific proline residues (P402 and P564 in HIF1α, P405 and P531 in HIF2α, P492 in HIF3α; see also Fig. 1.2) is required for the binding to VHL. Hence, oxygen-dependent hydroxylation of those prolines leads to degradation of the HIFα isoforms.

1.1.2 Further regulatory mechanisms of HIF signaling

Besides PHD- and FIH-dependent hydroxylation-mediated regulation, HIF signaling can be regulated by other mechanisms as well. Some of them might lead to pseudohypoxia (HIF pathway activation under normoxia) or pseudonormoxia (HIF inactivation under hypoxic conditions) [71].

Transcriptional and translational regulation of HIF

HIF can be regulated by the expression levels of its subunits and through translational control. Again, the primary targets of such regulatory mechanisms are the HIFα subunits, whereas cellular HIF1β levels appear to be relatively invariant.
HIFα is regulated in response to different stimuli, for example nutrient availability, stim-

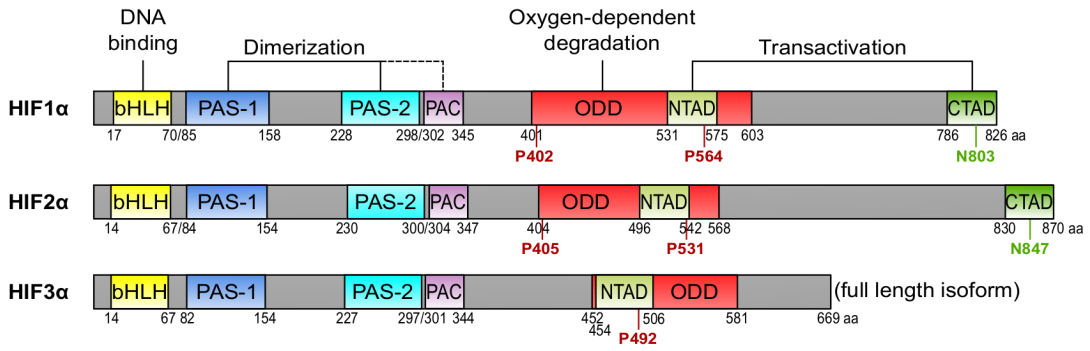

Figure 1.2: Protein domains of HIFα isoforms.
The three HIFα isoforms share most of their domains. The basic helix-loop-helix domain (bHLH) is responsible for DNA binding, Per-ARNT-Sim domains (PAS-1 and -2) and most likely also the PAS-associated C-terminal domain (PAC) are needed for heterodimerization with HIFβ. Two transactivation domains (N- and C-terminal, NTAD and CTAD) control transcription regulatory function. CTADs contain a specific asparagine residue (green) whose hydroxylation blocks transcriptional activation. The oxygen-dependent degradation domain (ODD) around the NTAD accounts for stability of the protein through hydroxylation of specific proline residues (dark red). Of the multiple isoforms of HIF3α only the full length isoform is shown here. Amino acid numbers are retrieved from UniProt entries Q16665, Q99814, Q9Y2N7.

ulation by growth factors, hormones or cytokines [71]. So far, four main pathways have been found to increase HIFα expression, which are also connected by crosstalk. Concerning the transcriptional regulation, janus kinase (JAK)/signal transducers and activators of transcription 3 (STAT3) and the nuclear factor "kappa-light-chain-enhancer" of activated B-cells (NF-κB) signaling pathways were associated with upregulated HIF1α transcription [27, 209]. Furthermore, phosphoinositide 3-kinase (PI3K)/AKT (a serine/threonine kinase) and extracellular-signal regulated kinases (ERKs) 1 and 2 pathways [92, 100], partially with involvement of reactive oxygen species (ROS), were linked to this type of regulation.
On the other hand, translational regulation was shown to be regulated by the PI3K/AKT/mammalian target of rapamycin (mTOR) pathway [104]. It is likely that other pathways are also involved in controlling transcription and translation of HIF subunits [71].

Posttranscriptional regulation of HIF levels by non-coding RNAs

As it is the case for numerous other proteins, HIFα levels can also be regulated by micro RNAs (miRNAs), e. g. miR-138 [185]. To date, more than 40 miRNAs are known to regulate HIF (HIFα and HIFβ subunits) mostly through mRNA degradation, as summarized in Serocki *et al.* [177].
In contrast to miRNAs, long non-coding RNAs (lncRNAs) can exert their regulatory functions through transcriptional interference and activation, genomic imprinting and chromatin modifications [52]. Moreover, they can function as sponges to trap miRNAs, as shown for the lncRNA homeobox transcript antisense RNA (HOTAIR) that decoys miR-

130a-3p, thereby stabilizing HIF1α messenger RNA (mRNA). To date, several lncRNAs were identified as being involved in HIF regulation [184]. However, most of them were detected in the context of cancer. The importance of this regulatory mechanism under physiological conditions is still largely unknown [177].

Posttranslational regulation of HIFα

Posttranslational regulation of HIF can occur with or without protein modifications through protein-protein interactions, that can be either oxygen-dependent or oxygen-independent, and have an activating or inactivating function. The versatility of protein interaction-mediated regulation is well illustrated in a recent report presenting a compendium of more than 100 proteins interacting with HIF1α [171]. Besides hydroxylation and subsequent ubiquitination, HIFα is regulated by several other posttranslational modifications. For instance, methylation of a lysine residue mediated by the histone-lysine N-methyltransferase SET domain containing 7 (SETD7) promotes the proteasomal degradation of HIFα [116]. Furthermore, acetylation, S-nitrosylation, phosphorylation and sumoylation of HIFα were reported as summarized in a review by Albanese *et. al* [2]. There, a special emphasis is given to phosphorylation-dependent HIFα regulation, for example through direct phosphorylation of HIF1α by protein kinase A (PKA), Polo-like kinase 3 (PLK3), glycogen synthase kinase-3β (GSK3β), ataxia telangiectasia mutated (ATM) protein, and cyclin-dependent kinases (CDKs) 1 and 5. This area is currently under extensive investigation.

Regulation of PHD proteins and other HIF signaling pathway factors

PHD proteins, key regulators of HIFα and central cellular oxygen sensors, can be regulated in various ways in addition to the aforementioned oxygen-dependent control of their enzymatic activity. First, tricarboxylic acid cycle (TCA) metabolites like succinate and fumarate can inhibit PHD proteins by competitive inhibition at the α-KG binding site [108]. Accumulation of these metabolites is often caused by defects in mitochondrial proteins acting as tumor suppressors, e. g. succinate dehydrogenase (SDH) and fumarate hydratase (FH) [170]. Second, the glycolysis product pyruvate as well as lactate were also found to inhibit PHD activity [31], although no direct effect could be observed in a cell lysate-based *in vitro* assay [146]. Third, PHD proteins, like HIFα, are targets for proteasome-mediated degradation, for example upon ubiquitination by the E3 ubiquitin ligase seven-in-absentia homolog (SIAH) [181, 141].

In addition to these regulatory mechanisms, severe damage of oxidative phosphorylation (OXPHOS) complexes might result in local accumulation of oxygen in a hypoxic environment, causing pseudonormoxia and leading to active PHD proteins and degradation of HIFα proteins [35]. In contrast, other studies show that inhibition of OXPHOS leads

to accumulation of HIFα [186], which could be explained by the tight interplay between OXPHOS and the TCA cycle. Moreover, it was suggested that increased intracellular oxygen levels would be rapidly balance with the extracellular oxygen levels, if the membrane permeability to oxygen allows. This depends on lipid metabolism, which is in turn connected to OXPHOS [71, 39]. Additionally, OXPHOS dysfunction was reported to be a source of ROS that could inhibit PHD proteins. However, the role of ROS in stabilizing HIFα is still controversial (reviewed in [139]).

As another regulatory mechanism, the transcription of PHD2 and PHD3 is upregulated during hypoxia, as their promoters contain HREs [49]. This generates a negative-feedback loop, in which increased PHD levels compensate for reduced enzymatic activity under low oxygen levels [64].

Furthermore, (epi-)genetic alterations of PHDs are able to induce pseudohypoxia. Among others, these alterations can be genetic mutations, such as point mutations, insertions, deletions or translocations, or epigenetic modifications, e. g. hypo- or hypermethylation of gene promoters [148]. For example, loss of PHD3 expression due to promoter methylation (or transforming growth factor (TGF) β exposure) can induce lung cancer metastasis by HIF-induced TGFα expression [38].

Similar to the PHD proteins, other HIF pathway components are regulated by diverse mechanisms as well. For instance, it was reported that WD repeat and SOCS box-containing protein 1 (WSB1) and mouse double minute 2 homolog (MDM2) are both negatively regulating VHL by ubiquitination and proteasomal degradation [93, 84]. Furthermore, cellular myelocytomatose oncogene (c-Myc) was found to weaken the binding between HIF1α and the VHL complex, leading to stabilization of HIF1α in normoxia and enhanced accumulation of HIF1α in hypoxia [34].
Several other proteins were also reported to either promote HIFα destruction or inhibit the necessary ubiquitination by VHL, e. g. receptor of activated protein C kinase 1 (RACK1) or heat shock protein 90 (HSP90), respectively (reviewed in [71]).

1.1.3 HIF signaling in health and disease

As outlined above, the HIF signaling pathway is regulated at many different levels, and some of the molecular regulatory mechanisms are interrelated. However, further research is needed to understand their interdependencies and context-dependent functions in various physiological and pathological settings. For instance, the HIF signaling pathway is activated during embryonic development, as embryos develop in an environment of low oxygen tension [41, 132]. Also in diseases, HIF accumulation can be protective, as exemplified by the cardio-protective function of HIF2α accumulation during reoxygenation after acute myocardial ischemia [106].

On the other hand, exploitation of the signaling pathway or mutations of its components can support or even initiate disease formation and progression [153, 173, 172]. Prominent examples for this are solid tumors, that often harbor hypoxic regions with highly activated HIF signaling [191]. Moreover, certain tumors display constitutively-active HIF signaling, like clear-cell renal carcinoma (ccRCC). In ccRCC, VHL is either mutated or silenced by promoter hypermethylation, leading to HIFα stabilization [23]. Overall, local activation of the HIF signaling pathway is a characteristic feature of most solid tumors and is associated with poor prognosis [174].

1.2 Solid tumors

As a leading cause of death worldwide, cancer was responsible for approximately ten million deaths in 2020. With more than two million estimated new cases, breast and lung cancers have the highest incidence worldwide (Fig. 1.3). Central nervous system (CNS) cancers rank 19th in terms of new cases, accounting for around 308,000 new cancer cases, but are already on rank 12th in terms of cancer deaths in 2020. The latter is led by far by lung cancer with nearly 1.8 million estimated deaths in 2020 [74].

In Germany, lung cancer accounted for 9.4 % and 13.3 % and CNS tumors for 1.3 % and 1.5 % of new cases in women and men in 2018, respectively [53]. Understanding the mechanisms of cancer development and progression as well as early detection and appropriate treatment of cancer are essential to reduce the number of cancer-related deaths.

1.2.1 Brain tumors

Among the tumors of the CNS, the group of gliomas, glioneuronal tumors and neuronal tumors compose the biggest group and can be subdivided into six different families. The family with the most common primary malignant brain tumors in adults - 75 % of them - was named “adult-type diffuse gliomas”. As the name implies, these tumors originate from glial cells (or their progenitors) in the CNS, that usually protect and support neurons in the healthy brain [47]. Thus, the family consists of tumors with an origin in astrocytes (astrocytoma; isocitrate dehydrogenase (IDH)-mutant), oligodendrocytes (oligodendroglioma; IDH-mutant and 1p/19q-co-deleted) or tumors with a not-yet clarified glial background (glioblastoma; IDH-wildtype) [118]. Glioblastoma and “astrocytoma grade 4” tumors (previously known as “glioblastoma, IDH-mutant” in the outdated WHO classification of 2016 and therefore included in all data before the new classification in 2021 as “glioblastoma”) are the most common (67.8 % and 69.3 % of the female and male patients, respectively, with malignant brain tumors in Germany, 2017 to 2018 [53]) and most aggressive adult primary brain tumors with a median age of 46.3 years at diagnosis and a median survival of only 15 months [96, 114, 144]. In Germany, the relative 5-year survival rate for patients with these tumors was only 8 % and 7 % for female and male

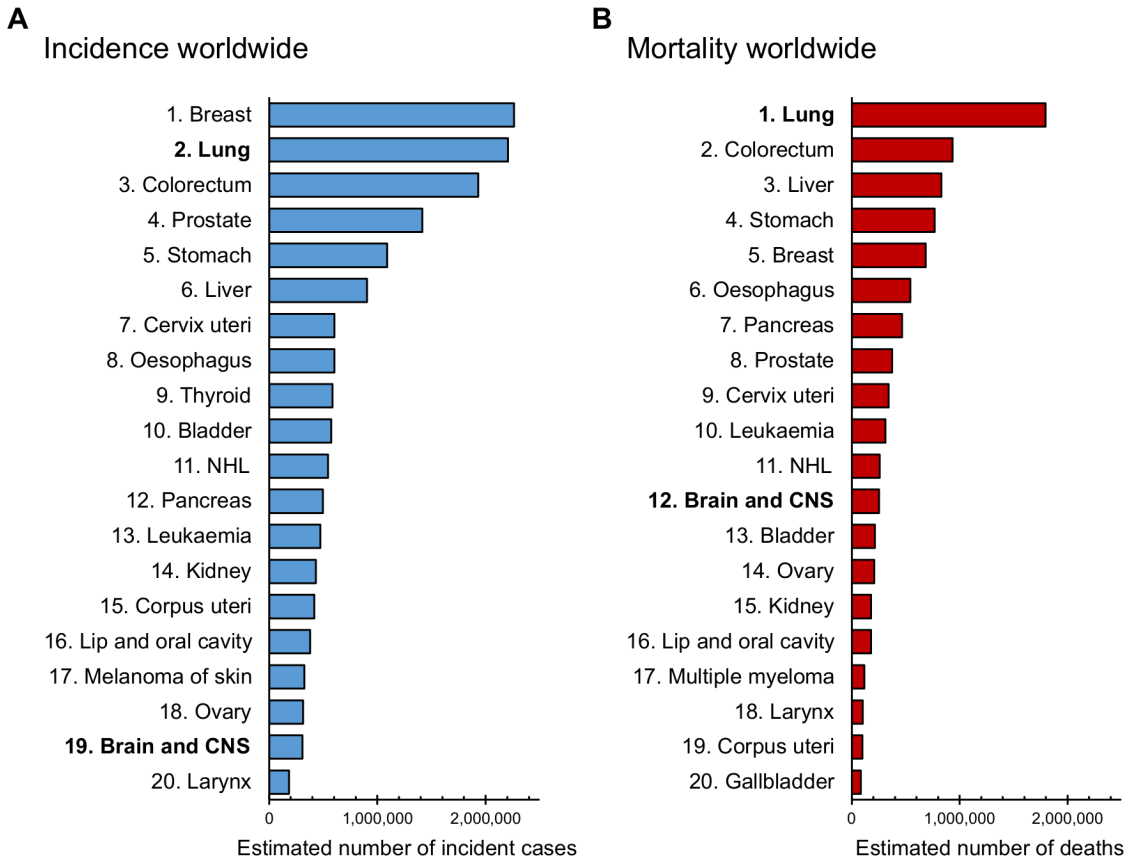

Figure 1.3: Incidence and mortality ranking of different cancers.
Estimated worldwide incidence (**A**) and mortality (**B**) of different cancer types, including all sexes and all ages in the year 2020. The 20 cancer types with the highest incidence and mortality, respectively, are shown. CNS = central nervous system; NHL = Non-Hodgkin lymphoma. Data source: GLOBOCAN 2020 [74].

patients, respectively [53]. High-grade glioma, such as glioblastoma, can either progress from a lower-grade glioma (e. g. astrocytoma) or develop rapidly *de novo*. Despite multimodal therapy options, including surgical resection, chemotherapy and radiation therapy, there is no cure for glioblastoma up to now [47].

1.2.2 Lung cancer

Lung cancer is the leading cause for cancer deaths worldwide. In Germany, lung cancer accounted for 15.8 % and 22.8 % of cancer-related deaths in women and men in 2018, respectively [53]. Lung cancer is divided into two main groups, namely non-small cell lung cancer (NSCLC) and small cell lung cancer (SCLC). With 85 % of total diagnoses, NSCLC is the largest group and within this group, adenocarcinomas are the most common subtype [190]. Although treatment and diagnosis of lung cancer were improved significantly in the past 20 years - at least in high-income countries - lung cancer remains one of the biggest health challenges worldwide. Especially challenging is the often late prognosis of lung cancer at already advanced stages [190]. By then, many patients (57 %) developed

metastases, making the therapy more complicated and the prognosis worse. The vast majority of lung cancer metastases are brain metastases and it is anticipated that 25 to 50 % of lung cancer patients will develop brain metastasis in the course of their disease [43].

1.2.3 The hypoxic tumor microenvironment

Cancer cells interact with their surrounding area, for example through direct cell-cell contacts with other tumor and non-tumor cells, like immune cells (e. g. neutrophiles or tumor-associated macrophages), tissue-specific cells (e. g. neurons and astrocytes in the brain) or endothelial cells. Apart from direct cell-cell interactions, cells communicate by exchanging chemo- and cytokines as well as extracellular vesicles and interact with the surrounding extracellular matrix (ECM) [10, 148]. This complex area within and surrounding tumors, which is characterized by a pronounced crosstalk between cancer and non-cancer cells, is referred to as the tumor microenvironment (TME) (Fig. 1.4).

Perivascular, invasive and hypoxic TME niches are tumor regions marked by specific features and cell compositions. While the invasive niche describes the areas of the tumor that are invading into the surrounding healthy tissue (Fig. 1.4, right), the perivascular niche is found in close proximity to the aberrant tumor vasculature (Fig. 1.4, left/bottom). Mostly present in the tumor core, hypoxic niches develop as rapidly growing solid tumors, e. g. glioblastoma, outgrow their blood supply, leaving the tumor cells with a deprivation of oxygen and nutrients (Fig. 1.4, top). If the supply cannot be re-established in time, tumor cells die and necrotic areas develop in the core of hypoxic niches [169].

All niches display an accumulation of cancer stem cells (CSCs) that are de-differentiated tumor cells implicated in therapy resistance and tumor recurrence [10]. It was shown, for instance, that the hypoxic niche regulates and maintains glioblastoma stem cells through the HIF signaling pathway, in particular HIF2α [169]. Due to the restricted access to oxygen, the HIF signaling pathway is activated in tumor cells residing in the hypoxic niche. These cells switch to a glycolytic metabolism, which results in increased glucose consumption as well as lactate and hydrogen proton production. Therefore, the hypoxic niche is also characterized by a lower pH (acidosis) compared to better-oxygenated TME niches [148]. In a feed-forward mechanisms, acidosis can increase HIF function and support glioma CSC maintenance [46]. Furthermore, a hypoxic TME promotes tumor cell invasion and metastasis, important hallmarks of cancer [56, 58]. Here, HIF1α and HIF2α seem to play context-dependent roles, some of which may be complementary, overlapping or even opposing, as briefly outlined below.

Different roles of HIFα isoforms in the TME

The HIF transcription program depends on cell type and shows tissue-specific features. Additionally, the different HIFα isoforms seem to exert different functions and control dif-

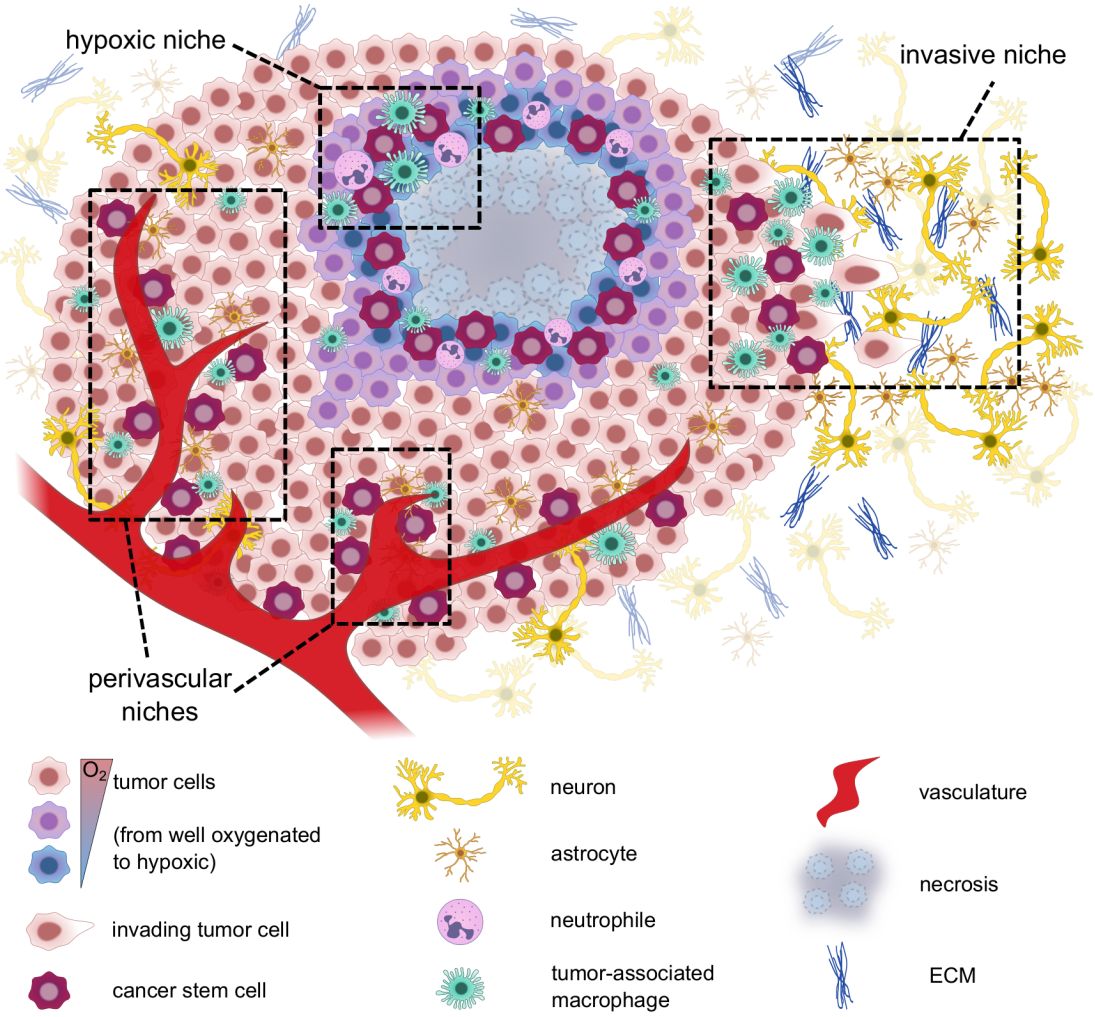

Figure 1.4: Overview of tumor microenvironment (TME) niches in glioblastoma.
The TME of glioblastoma and many other solid tumors shows three main niches (hypoxic, perivascular and invasive). All display accumulation of cancer stem cells (CSC) and immune cells (e. g. tumor-associated macrophages and neutrophiles). As tumor cells communicate with surrounding cancer and non-cancer cells (e. g. endothelial cells of the vasculature), the TME also is comprised of tissue-specific cells (e. g. neurons and astrocytes in the brain). In the invasive niche, cells invade into healthy, extracellular matrix (ECM)-rich tissue (elongated cells). The hypoxic niche is characterized by reduced oxygen levels (O_2; shown by color changes of the tumor cells with reduced O_2 levels) and resulting necrotic areas (grey with light-blue-labeled disintegrated cells).

ferent transcriptional programs and related cellular processes. Interestingly, the consensus sequence for the HRE, the DNA binding site of HIF, is the same for both isoforms (5'-RCGTG-3' with R = A or G). HIF1α was described to be the driver of metabolic response to hypoxic stimuli with suppression of mitochondrial respiration and also responsible for maintenance of intracellular pH. However, HIF2α seems to be more implicated in hypoxic induction of growth, regulation of the cell cycle and invasion processes [72]. Likewise, the induction of protein accumulation differs between HIF1α and HIF2α. While HIF1α accumulates rapidly (in the first 6 to 12 hours of hypoxic exposure) and decreases again soon after, HIF2α accumulates later and stays present longer during prolonged hypoxic

incubation [64]. These findings suggest that HIF1α plays a role in coordinating the acute response, while HIF2α tends to regulate the late response to prolonged hypoxia [72].
Recent work implies that the binding partners of HIFα subunits could determine the different functions of the isoforms. For example, HIF1α accumulation was reported to prevent c-Myc (also called MYC) from binding to its partner myc-associated factor X (MAX), leading to suppressed c-Myc-induced transcription. On the other hand, HIF2α promoted c-Myc-MAX binding, leading to increased transcriptional activity of c-Myc and promotion of tumor growth [30].

In the context of cancer, while HIF2α was found to rather have a tumor suppressor function in some gliomas [1], pro- or anti-tumorigenic activity cannot be clearly associated with the individual HIFα isoforms. Different results were reported for the two scenarios, again indicating the importance of the cellular context of HIF activity. However, a common finding is that in many tumors, including gliomas, breast cancer, and NSCLC, poor prognosis is associated with high expression of at least one of the HIF isoforms (summarized in [88]).

1.2.4 Diverse roles of PHD proteins in cancer

HIFαs are not the only target proteins of PHD-mediated regulation. Among the PHDs, PHD3 shows the widest range of non-HIF targets, implicating it in even more pathways than those that are already involved in the extended HIF signaling network. For example, PHD3 regulates epidermal growth factor receptor (EGFR) signaling in glioma by facilitating EGFR internalization, acting as a scaffolding protein for which its hydroxylase activity is not required [51]. Consequently, loss of PHD3 results in sustained EGFR activation and uncontrolled tumor growth [63].

Recent reports showed hydroxylation-mediated regulation of non-HIF targets by PHD3. PHD3 was reported to hydroxylate the beta-2 adrenergic receptor (ADRB2), the erythropoietin receptor (EPOR), the activating transcription factor 4 (ATF4) and the BH3-only protein BIM-EL, thereby promoting the degradation of those proteins by ubiquitination and proteasomal degradation [208, 62, 95, 110].
Moreover, it was shown that PHD3 hydroxylates p53 on P359, which enables interaction of p53 with the deubiquitinases USP7 and USP10, leading to p53 stabilization and apoptosis or G1 arrest induction [158]. However, the role of the enzymatic activity of PHDs in regulating non-HIF targets is controversial [24].

1.3 Genome editing with the CRISPR/Cas9 system and its application in loss-of-function studies

The Nobel Prize in Chemistry 2020 was awarded to Emmanuelle Charpentier and Jennifer A. Doudna "for the development of a method for genome editing" [151]. Although this description sounds rather simple, this development transformed the way we work today. Already in 2002, clustered regularly interspaced short palindromic repeats (CRISPR), 21 to 37 base pair (bp) short repetitive DNA sequences found in prokaryotes, and CRISPR-associated protein (Cas) genes were discovered [78]. Four years later and based on functional analyses, it was proposed that CRISPR and Cas are a part of the prokaryotic immune system and play an essential role in defending the genome against phages and plasmids [123]. This was confirmed by a study in 2007, which proved that CRISPR conveys acquired resistance of prokaryotes against viruses [9]. Soon after, Charpentier and Doudna proposed to exploit CRISPR and Cas for persistent RNA-mediated genome editing in human cells [81, 21]. Since then, different Cas proteins of different species have been identified and many applications of the CRISPR/Cas system were developed. Thus, we have an extremely versatile toolbox for molecular biology studies today.

1.3.1 Functionality and diverse applications of CRISPR/Cas9

The most widely-used and best-characterized Cas protein is Cas9 from *Streptococcus pyogenes*, also referred to as SpCas9. In order to make use of the CRISPR/Cas9 system in human cells and facilitate expression, SpCas9 was codon-optimized [178]. In this study, Cas9 always refers to the codon-optimized recombinant SpCas9 as published by Sanjana *et al.* [162].

Figure 1.5 shows the principle of CRISPR/Cas9 application in genome editing. In contrast to the original system, the RNA component was simplified by combining several RNAs into one single-guide RNA (sgRNA) consisting of a 20 to 21 bp guide sequence and a 76 bp guide RNA (gRNA) scaffold [178] (Fig. 1.5A, red). The guide sequence determines the binding specificity to the genomic DNA (gDNA) by complementarity. If the guide sequence-identical sequence on the non-binding gDNA strand is followed by a protospacer adjacent motif (PAM), which is "NGG" in the case of Cas9, Cas9 (Fig. 1.5A, yellow) will introduce a double strand break (DSB) into the gDNA (Fig. 1.5B). This means, every 20 bp sequence followed by the PAM can be targeted by Cas9 in principle. In the human genome, approximately 161 million PAM sites are present, which enables CRISPR/Cas9 targeting of nearly all genes described so far. To further expand the editable genome space, efforts are currently underway to develop a PAM-independent CRISPR/Cas system [25]. During genome editing, DSBs are introduced by enzymatic active Cas9, which activate cellular DNA repair mechanisms. These mechanisms are

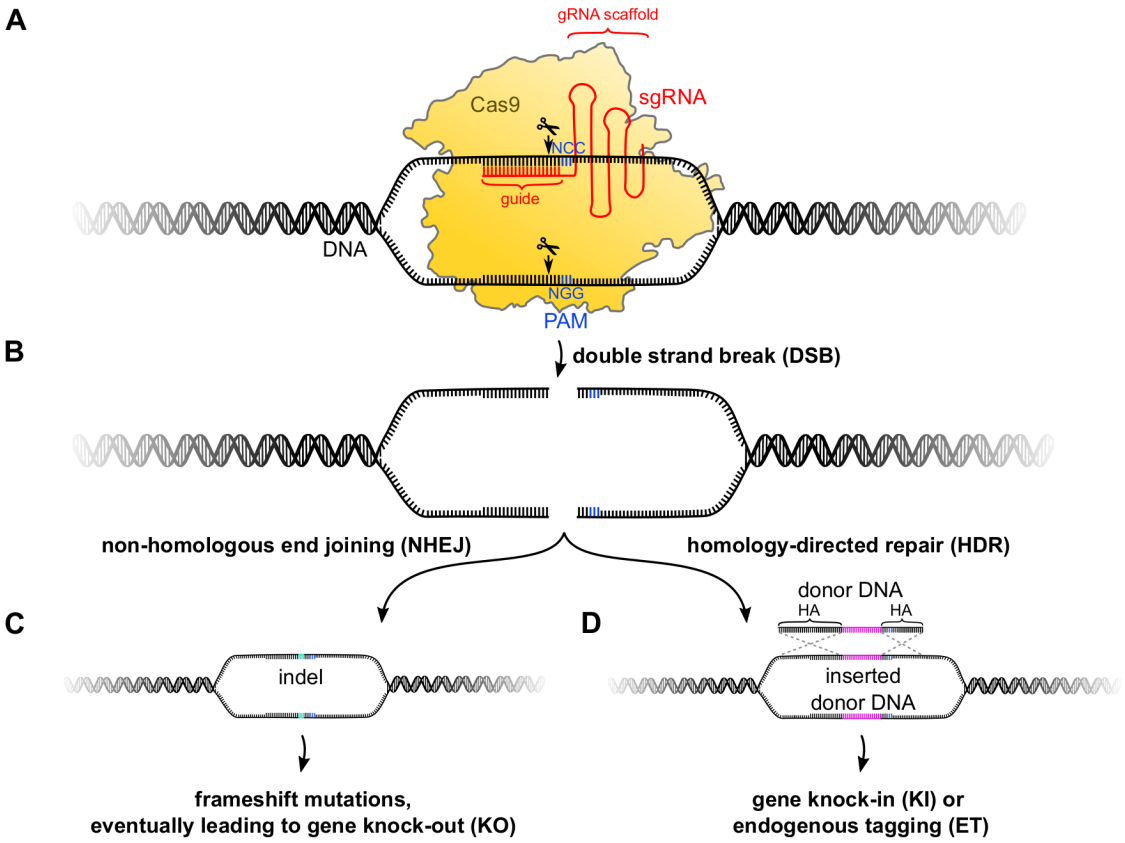

Figure 1.5: CRISPR/Cas9 system for human genome editing.
(**A**) Cas9 assembles with sgRNA (consisting of guide and gRNA scaffold) and facilitates binding of the guide to complementary DNA sequences. (**B**) If the guide is followed by a protospacer adjacent motif (PAM; in SpCas9 the bases "NGG"), Cas9 introduces a double strand break (DSB) into the DNA. This DSB will be repaired by cell-inherent repair mechanisms. (**C**) Non-homologous end joining (NHEJ) is the default but error-prone repair mechanism of the cell. Here, the DSB is repaired by introducing or deleting base pairs, leading to insertions or deletions (indels) of different sizes. (**D**) Homology-directed repair (HDR) is less common. In the example depicted here, the cell uses an exogenous template (consisting of homology arms [HA] right and left of the DNA to be introduced) to repair the DSB employing homologous recombination (HR). In non-altered cells, this template can be an intact allele. Individual elements are not drawn to scale. The shape of Cas9 is based on the Protein Data Bank (PDB) entry 5Y36.

either template-dependent or independent. Predominantly, DSBs are repaired by non-homologous end joining (NHEJ), a template-independent but highly error-prone DNA repair mechanism [210] (Fig. 1.5C). During NHEJ, the DNA ends get directly ligated. This repair process is inaccurate at nucleotide resolution and often leads to mutations like insertions or deletions (in short: indels), eventually resulting in frame shifts and the appearance of premature stop codons [210]. Therefore, if a permanent silencing of a gene (knock-out (KO)) is the aim of genome manipulation, no template is provided (Fig. 1.5C).

DSBs can also be repaired by template-dependent mechanisms, for instance by homology-directed repair (HDR) (Fig. 1.5D). HDR can be used to repair DSBs involving the use of different DNA templates. In non-modified cells, the intact, undamaged gene allele

can serve as a template. In CRISPR/Cas9 genome editing, an artificial DNA template is often introduced together with Cas9 and the sgRNA. Such templates typically contain protein-coding DNA sequences to be integrated (e. g. a fluorescent protein tag), flanked by homology arms (HAs), which are DNA sequences homologous to the DNA sequence flanking the DSB site [210]. This integration is generally called knock-in (KI). A special form of KI is endogenous tagging (ET), where a tag is introduced (e. g. a short peptide tag or a bigger protein tag).

Of note, the CRISPR/Cas9 system can be adapted to be useable in different other ways. For instance, modified Cas proteins, deficient in their nuclease function (dCas), are fused to different proteins or functional protein domains. Together with specific sgRNAs as targeting modules, they induce various site-directed modifications of DNA or chromatin. For example, DNA methyltransferase 3A (DNMT3A) and DNA methyltransferase 3 like (DNMT3L) are used to induce DNA methylation [187], while ten-eleven translocation (TET) methylcytosine dioxygenases are used for DNA demethylation as fusion partners of catalytically inactive dCas [138]. Additionally, fusions with VP64 (meaning 4 tandem copies of the Herpes Simplex Viral Protein 16) or other activating domains achieve transcriptional activation of the targeted genes (CRISPRa) [55]. In contrast, fusions with e. g. krüppel associated box (KRAB) zinc finger domains are used for transcriptional repression of genes (CRISPRi) [55]. Furthermore, induction of histone modifications are possible by fusing dCas to p300 or other histone modifiers [66].
Besides facilitating targeted, locus-specific epigenetic modifications, other uses of this multifaceted molecular toolbox were also developed, such as precise single DNA base editing by using dCas-apolipoprotein B mRNA editing enzyme catalytic polypeptide 3 (APOBEC3) fusions [65], or live-cell imaging of distinct genomic loci [18].

1.3.2 CRISPR/Cas9 screenings

The potential to target virtually all known genes in the genome by multiple sgRNAs enables the functional investigation of the effects caused by their perturbation in a large cell population simultaneously. In this cell population, each individual cell is usually targeted by a single (typically lentiviral) vector, which carries one specific sgRNA to target only one specific gene per cell. Several inherent properties of the CRISPR/Cas9 system make it a particularly powerful tool for large-scale, even genome-wide screenings: First, the system is easy to use and to adapt. Guide sequences can be readily synthesized and cloned into the appropriate vector containing the gRNA scaffold and the Cas9 protein. Second, the vectors are of lentiviral origin and the resulting virus particles allow highly-efficient infections of cells, including non-dividing cells. Third, as a result of infection, the donor DNA is integrated into the genome, enabling tracing of the integrated sgRNA. Fourth, virtually all genes can be targeted by specific gRNAs. And fifth, the diverse applications

and modifications of Cas9 developed so far (KO, KI, CRISPRa, CRISPRi, to name just a few) offer numerous possibilities and allow answering of various scientific questions.

Genetic screens using CRISPR/Cas9 depend on three main components, namely a perturbation, a model system and an assay [36].

Model systems

To address a biological question, the right choice of a model system is essential. In the context of CRISPR/Cas9 screenings, those model systems can be target cells in their natural tissue environment in animals (*in vivo*), organoids, primary cells or established cell lines (*in vitro*). Importantly, the chosen model system has to be compatible with the intended CRISPR/Cas9 screening perturbation. For instance, screenings using a genome-wide KO library require several million cells. Hence, using organoids might not be feasible to perform a genome-wide screening [36]. Therefore, initial large-scale studies are often performed in more rudimentary physiological model systems, such as established cell lines. In the present work, well-characterized glioma and lung adenocarcinoma cell lines, which are relatively easy to propagate and manipulate, were used to study the effect of genetic perturbations on the HIF signaling pathway.

Readout assays

Readout assays are designed according to the specific scientific question. A common feature of the various readout approaches is the physical separation of cell populations based on a specific phenotype [36]. After separation, sgRNAs associated with a particular phenotypic trait can be determined by targeted high-throughput sequencing of gDNA isolated from defined cell populations.

The simplest and most common applied screening assays are viability screens. Often, these are drop-out or negative selection screens, in which the KO of certain fitness genes leads to depletion of the corresponding sgRNAs from the cell pool with increasing time of cultivation [36]. Viability-based negative selection is often naturally included in other screens, as cells are cultured for extended periods of time after the perturbation.

Furthermore, positive selection can also be used in viability screens when comparing different treatment conditions (e. g. inhibitors or culture conditions). Here, the cells of interest are enriched rather than depleted over time. Both screen types, negative and positive viability screens, can also be combined in one single screen [36].

The most widely used technique for the physical separation of cell populations with a specific phenotype is flow cytometry (FC), more specifically fluorescence activated cell sorting (FACS). The careful optimization of FACS-based assays is of uttermost importance to obtain reliable and meaningful results [36]. Phenotypic traits can either be cell-intrinsic features, like increased expression of certain cell surface markers that can be marked with

fluorescently-labeled antibodies to facilitate FACS, or artificial ones. The artificial features are typically modular fluorescent reporters (FRs) introduced into the target cells via genetic engineering. A minimal FR usually consists of three modules: First, the protein of interest (POI), whose level is associated with the phenotype of interest, e. g. the stability/expression of a certain protein/gene. Second, a (typically fluorescent) reporter gene fused to the POI. Third, core gene regulatory sequences linked to the phenotypic trait of interest and controlling the expression of the fluorescent-tagged POI.
Other optional components may include, on the one hand, peptide tags for easier detection in western blot analyses, pulldown assays or as an alternative for FACS. On the other hand, extended or multimerized gene regulatory sequences can be included to enhance the signal intensity by increasing expression of the FR. However, very different compositions of FRs are possible. A widely known FR - although not useable for FACS - is the basic dual luciferase reporter (DLR) assay to study promoter activities [179].
Of note, FRs can be completely exogenous, e. g. by transferring the fluorescent POI-coding DNA by lentiviral transduction to ectopic sites where they are to be stably expressed. Alternatively, they can be generated by tagging the gene of interest with a reporter gene using ET.
Other assays - not discussed in detail here - include *in vivo* screens, usually performed in mice, as well as chromatin accessibility and gene expression screens [159]. Gene expression screens, for example, may take advantage of the feasibility of combining the CRISPR/Cas9 system with single-cell RNA sequencing. In this way, the impact of gene perturbations on the resulting phenotype can be analyzed in much greater detail by examining the transcriptome of the cells. However, these screens have their limitations, such as limited cell numbers or sequencing depth (summarized in [36]).

Genetic perturbations

Genetic perturbations using the CRISPR/Cas system can be hightly versatile as described above (KO, CRISPRa, CRISPRi, ...) and virtually all options can also be considered for screening purposes. The most commonly used perturbations in screens are KOs, mostly achieved using pooled lentiviral CRISPR knockout libraries. They are well defined, highly optimized and frequently used [36]. Table 1.1 shows the three most widely used genome-wide CRISPR KO libraries to date as available from the nonprofit plasmid repository Addgene. They all employ the same lentiviral vector, lentiCRISPRv2 [162]. However, smaller libraries that target only a specific group of genes involved in a particular metabolic, signaling or regulatory pathway already exist or can be generated [124, 203].

Of note, these often-used libraries have different compositions, e. g. the individual sgRNAs are not evenly distributed in the sgRNA pool due to the applied cloning strategies. To

Name	Number of target genes	Number of sgRNAs	sgRNAs per gene	Controls	Ref
Human sgRNA library Brunello in lentiCRISPRv2	19,114	76,441	up to 4	1,000 Non-targeting controls	[37]
Human GeCKO v2	19,050	123,411- (includes also miRNAs)	up to 6	2,000 Non-targeting controls	[178]
Toronto KnockOut version 3 library	18,053	70,948	up to 4	142 guides targeting LacZ, EGFP, luciferase	[60, 122]

Table 1.1: Human genome-wide SpCas9-based CRISPR KO libraries.
The most often used KO libraries available from Addgene with number of targeted genes, number of sgRNAs (in total and per gene), number and type of controls as well as references to the original publications.

overcome this problem, a new gRNA synthesis approach was developed recently [203]. Being aware of the limitations and pitfalls of the available libraries and their different strengths and weaknesses, they are nevertheless invaluable tools to conduct genome-wide CRISPR KO screens.

1.4 Motivation and aims

Brain and lung cancer pose a major health problem worldwide with increasing significance, e. g. due to increased life-span. Among the brain tumors, glioblastoma is the most aggressive but also the most common malignant primary brain tumor in adults. Patients diagnosed with glioblastoma have a median survival of only 15 months and the tumor is not curable with the current standard of care so far. Major contributors to the poor prognosis include a high degree of intratumoral cellular heterogeneity and plasticity, acquired infiltrative and migratory traits and the development of therapy resistance. Similarly, lung cancer is also characterized by rapid establishment of resistance against standard as well as newly developed medication. Additionally, lung cancers are prone to metastasize, frequently to the brain, contributing to the fact that it is the leading cause of cancer-related death worldwide.

Brain and lung tumor progression and dissemination largely depend on the capacity of cancer cells to adapt to microenvironmental changes, such as tumor hypoxia. In fact, several hallmarks of cancer are driven by a hypoxic TME, which can be found in virtually all solid tumors. To name the most important ones, deregulation of the cellular metabolism, the induction of vascularization, the activation of tumor invasion (especially in glioma) and metastasis, sustaining proliferative signaling and epigenetic reprogramming are con-

tributing to progression and malignancy of tumors [58]. The main signaling pathway implicated in hypoxia is the HIF signaling pathway. Here, deregulation by the hypoxic TME or mutations of pathway-related enzymes, such as VHL or PHD3, can lead to pseudohypoxia or pseudonormoxia. Thus, controlling the HIF pathway by pharmacological interventions might provide a promising option in combined treatments of cancer. However, the regulation of the HIF pathway is highly complex as well as disease- and context-dependent. As an additional layer of complexity, PHD3 is - HIF pathway-dependent as well as -independent - an important regulator of the hallmarks of cancer, e. g. by controlling EGFR internalization to overcome hypoxic growth inhibition in glioma or regulating lung cancer metastasis and drug resistance [51, 63, 38]. Thus, a better understanding of the underlying molecular mechanisms of HIF pathway regulation in general and regulation of PHD3 specifically is important to improve anti-cancer strategies and support precision medicine.

With this in mind, the aim of this work was to improve our understanding of the regulation of PHD3 and the HIF signaling pathway in glioblastoma and lung adenocarcinoma and to identify novel protein regulators of them.
To achieve this goal, *in vitro* FRs were developed, tested and transduced into glioblastoma and lung adenocarcinoma cell lines. Subsequently, the experimental conditions for a genome-wide CRISPR KO screening using the FR cell lines were optimized. After this, a screening was performed in glioblastoma cells and after extensive analysis and interpretation of the results, several known and yet unknown regulators of the HIF signaling pathway were identified. Selected candidate top regulators were comprehensively evaluated and validated in independent experiments in both glioblastoma and lung adenocarcinoma cells. Finally, initial functional analyses of a top hit, suppressor of cytokine signaling 3 (SOCS3), were performed.

2. Results

2.1 Development of an *in vitro* fluorescent reporter system for identifying HIF pathway regulator proteins

Fluorescent reporter systems (FRSs) were developed to identify novel protein regulators of the HIF signaling pathway in glioblastoma and other, potentially metastatic, cancers like lung adenocarcinomas. These FRSs are selected human cell lines expressing a FR whose fluorescence signal intensity depends on the activity of the HIF signaling pathway.

2.1.1 Selection of cell lines with a high dynamic range of HIF pathway response

To select a suitable model system, levels of key HIF signaling proteins were examined by western blot analysis in different cell lines.

2.1.1.1 Alterations in HIF pathway protein levels in glioblastoma cell lines upon hypoxia treatment

Hypoxia-induced changes in HIF pathway protein levels were compared in G55(TL), U87-MG, HGBM and G141 human glioblastoma cell lines by western blot analysis. Cells were cultured in a cell culture incubator under normoxic (approx. 21 % O_2) or in a hypoxia chamber under hypoxic conditions (1 % O_2 for 24 or 96 hours). Whole cell protein lysates were prepared and subjected to western blot analysis using antibodies against the HIF pathway proteins HIF2α, HIF1α, PHD 1-3 and Tubulin as loading control. All cell lines showed accumulation of HIF2α and HIF1α after 24 and 96 hours of hypoxia exposure (Fig. 2.1A).

Specifically, G141 and HGBM cell lines displayed high HIF2α levels after hypoxia treatment, while G55(TL) and HGBM showed predominantly high HIF1α protein amounts after hypoxia exposure. Furthermore, hypoxia-induced increase in PHD2 protein was evident in G55(TL), U87-MG and HGBM cells. In contrast, PHD3 levels were detectable only in G141 and HGBM cells. As regulation of HIF2α and HIF1α is mainly connected to PHD3 and PHD2, respectively, G141 and G55(TL) cell lines were selected to generate reporter cell lines. Both cell lines have a high dynamic range of hypoxia response in terms

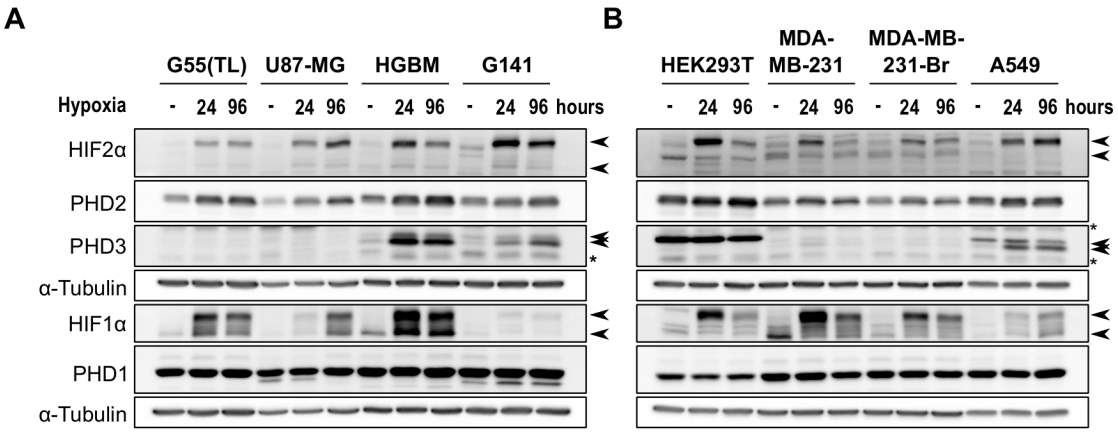

Figure 2.1: Levels of HIF signaling pathway proteins in various cell lines under normoxic and hypoxic conditions.
(**A**) Western blot analysis of the key HIFα proteins and regulatory PHD proteins in a panel of established glioma cell lines. Cells were incubated under normoxic (ambient O_2) or in hypoxic conditions (1% O_2) for 24 or 96 hours. HIF2α, PHD2 and PHD3 were detected from one gel, HIF1α and PHD1 from another gel. Tubulin served as control to monitor differences in protein loading and transfer. Arrows indicate specific protein bands where several bands are visible; asterisks indicate unspecific bands. (**B**) Western blot analyses as in (A) in epithelial cancer cell lines and immortalized human embryonic kidney cells.

of HIF2α and HIF1α protein levels. These changes correlated well with the respective PHD levels under the selected experimental conditions.

2.1.1.2 Alterations in HIF pathway protein levels in other cell lines upon hypoxia treatment

Additionally, lung (A549) and breast carcinoma cell lines (MDA-MB-231 and MDA-MB-231-Br (for "**Br**ainseeker")), which are cell culture models of cancers prone to metastasize to the brain (in particular the MDA-MB-231-Br derivative), and immortalized human embryonic kidney cells (HEK293T) were analyzed using the same experimental setup. The results revealed that all tested cell lines reacted with accumulation of HIF1α, HIF2α and PHD2 to hypoxia exposure with different amounts of accumulation after different exposure times. However, clearly increased levels of PHD3 protein after hypoxia treatment were only evident in A549 cells. Thus, and to further expand our studies, A549 cells were selected as a model system for cancers prone to metastasize to the brain.

2.1.1.3 Glioblastoma-related point mutations

To determine typical genetic markers of glioblastoma, PCR amplification of *IDH1* and *IDH2* as well as the commonly mutated *TERT* promoter loci were performed, followed by Sanger sequencing [165]. In all glioma cell lines tested, the *TERT* promoter was mutated in one of the characteristic hotspots. In detail, G55(TL) exhibited C250T mutations in

the *TERT* promoter, while G141, HGBM and U87-MG cell lines harbored C228T point mutations. Moreover, all four cell lines displayed wildtype *IDH1* and *IDH2* genes. This suggests that the cell lines present a glioblastoma-specific genetic background at these marker loci (data shown in Schmid *et al.* [165]).

2.1.2 Construction and assessment of fluorescent reporters

After selecting the cell lines, different compositions of FRs were designed and tested for applicability in high-throughput CRISPR/Cas9 KO screening for regulators of the HIF signaling pathway. These included coding sequences of core HIF pathway proteins as POIs, a reporter gene, gene regulatory elements, peptide tag-encoding sequences and antibiotic resistance genes (see also chapter 1.3.2, page 15). The viral cytomegalovirus (CMV) gene promoter, which is active in all selected cell lines, was used in all constructs where exogenous promoters were needed.

2.1.2.1 Selection of a suitable protein of interest (POI)

To engineer a FRS for identification of HIF pathway regulator proteins, PHD3- and HIFα-encoding sequences were selected as POIs based on the observed hypoxia-induced changes (Fig. 2.1).
The reporter constructs described below were cloned, and tested in G55(TL) and/or A549 and/or G141 cells.

PHD3 protein as POI

To monitor changes in PHD3 protein levels by microscopy and flow cytometry, fluorescent protein-encoding sequences were fused to the endogenous *EGLN3* gene locus in G55(TL), G141 and A549 cells. To achieve this so-called endogenous tagging (ET) of the PHD3 protein, cells were transiently transfected with two plasmids. The first one encodes the Cas9 protein and an sgRNA targeting the C-terminal region of *EGLN3* before the stop codon. The second one, the donor plasmid, contained the sequences to be fused to the *EGLN3* locus by exploiting HDR repair mechanisms of the cells following Cas9-induced DSB. Additionally, this plasmid contained each around 800 base pairs of homologous sequences left and right of the insertion site ("homology arms") of *EGLN3* to enable homologous recombination (HR) (Fig. 2.2A). Hence, transcription from a successfully endogenously-tagged *EGLN3* locus is expected to result in expression of a PHD3/fluorescent protein-fusion.

In order to obtain detectable levels of an endogenously tagged PHD3-fluorescent protein fusion, several combinations (fluorescent proteins, linker and tags) were experimentally evaluated as summarized in Table 2.1. First, mCherry was inserted right before the stop codon of *EGLN3* into the genome of G55(TL) cells (Tab. 2.1, #1). Although successful

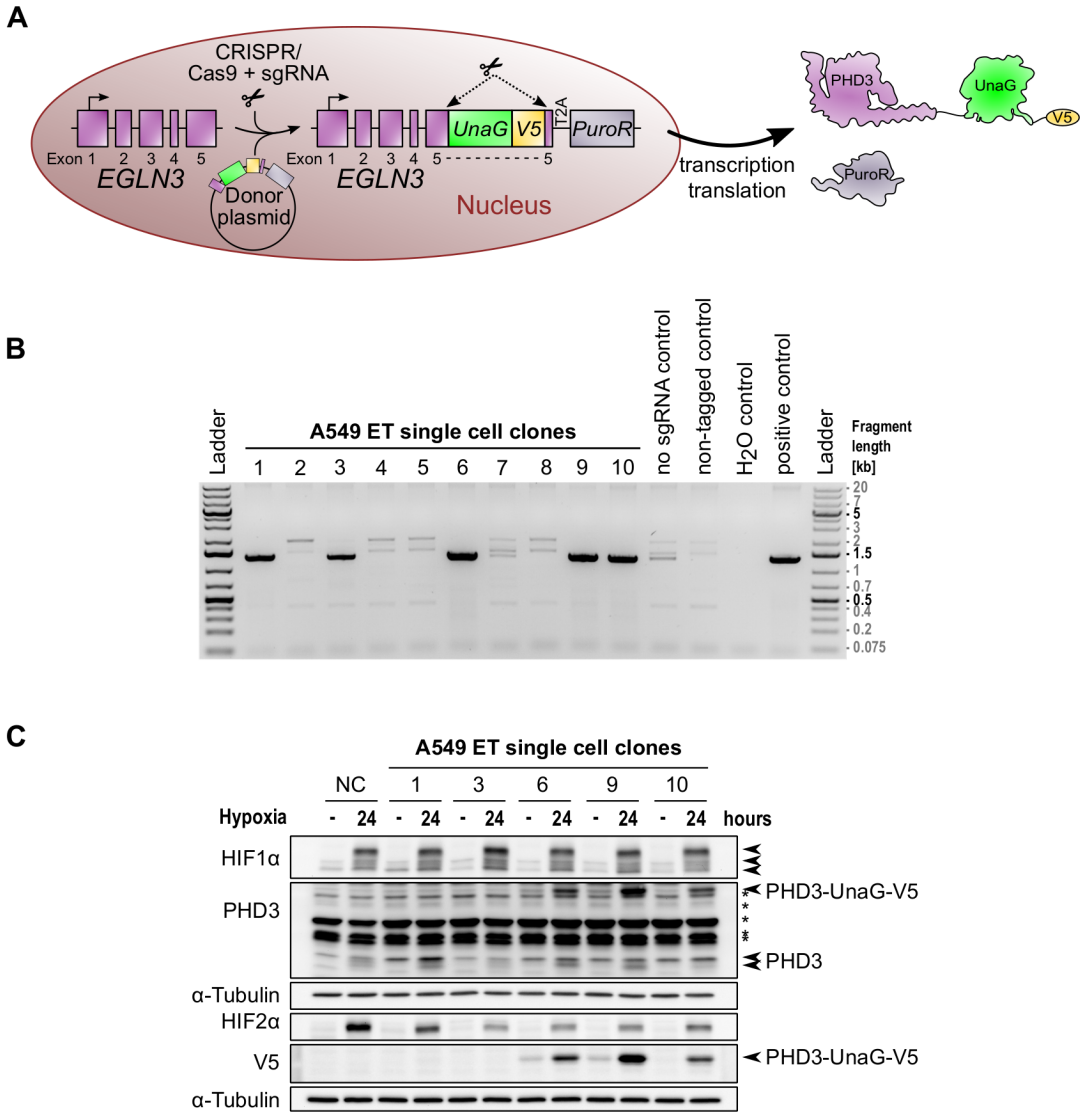

Figure 2.2: Endogenous tagging of the PHD3 gene *EGLN3*.
(**A**) Outline of the endogenous tagging (ET) approach. Cells were co-transfected with two plasmids: The first one expressing Cas9 and an sgRNA targeting the C-terminus of *EGLN3* (CRISPR/Cas9 + sgRNA), the second one harboring the donor sequence for being used for homology-directed repair (HDR) after the Cas9-induced DNA double strand break (Donor plasmid). After the insertion, PHD3 proteins are expressed containing the fluorescent protein UnaG and a V5 peptide tag as well as a puromycin N-acetyltransferase (PuroR). T2A = self-cleaving peptide from the Thosea asigna virus 2A. (**B**) Agarose gel after endpoint PCR, showing amplified products of a genomic region only present in successfully endogenously tagged cells (A549 single cell clones No. 1, 3, 6, 9 and 10) as evident by the expected size of the amplicon of around 1,350 base pairs. kb = kilo base pairs. (**C**) Western blot analysis of HIF1α, HIF2α, V5 and PHD3 in the single cell clones identified in (B). Cells were either incubated at ambient oxygen levels or exposed to 24 hours hypoxia (1 % O_2). Arrows show specific bands, asterisks show unspecific bands; NC = negative control (A549 cells transfected with empty donor plasmid).

integration of mCherry into the genome was confirmed by endpoint PCR (not shown), this approach did not result in microscopically detectable fluorescent cells. It was hypothesized that mCherry, being a red fluorecent protein, might be less well visible than a

#	Target cells	ET type	Fluorescent protein	Linker(s)	Peptide tags	Selection marker
1	G55	C-term.	mCherry	none	none	no
2	G55	C-term.	TurboGFP	GSAGSAAGSGEF [198]	V5	no
3	G55	N-term.	UnaG	GSAGSAAGSGEF [198]	Flag	no
4	A549	C-term.	UnaG	GSAGSAAGSGEF [198] (between UnaG and PHD3); GSG (between furin cleavage site and T2A)	Flag (PuroR), V5 (PHD3-UnaG)	PuroR

Table 2.1: Donor plasmids used for endogenous tagging of the PHD3 gene locus *EGLN3*. Main characteristics of the Donor plasmids used in combination with sgRNA/Cas9-expressing plasmids to facilitate endogenous tagging of the *EGLN3* locus in the shown cell lines.

green fluorescent protein and that the direct fusion without any linker sequence between PHD3 and the fluorescent protein might cause a steric hindrance. Therefore, the fluorescent protein was exchanged for TurboGFP and a GSAGSAAGSGEF linker peptide [198] was introduced between the fluorescent protein and PHD3. Furthermore, a V5 peptide tag was included on the C-terminus of TurboGFP to enable specific detection of the fusion protein by western blot analysis (Tab. 2.1, #2). G55(TL) cells were co-transfected with the donor plasmid and the sgRNA/Cas9 plasmid, gDNA und RNA were isolated and genomic insertion as well as transcription of the TurboGFP-encoding sequence was confirmed (not shown). However, the fusion protein could not be detected by western blot analysis, nor did the cells show visible green fluorescence despite DMOG treatment, which increases endogenous PHD3 levels (not shown). This indicates that the fusion protein might be too low expressed to be detected or it was expressed by a small subpopulation of cells only. To investigate whether the C-terminal fusion might have caused problems, *EGLN3* was N-terminally tagged by the green fluorescent protein UnaG, using the GSAGSAAGSGEF-linker sequence (Tab. 2.1, #3). Unfortunately, G55(TL) cells were again not showing any green fluorescence, neither with nor without induction of PHD3 protein levels by DMOG (not shown).

We wondered whether the low efficiency of the HDR mechanism, compared with the NHEJ mechanism, or competitive disadvantage of expressing the fusion protein might have led to a limited, undetectable amount of successfully tagged cells. To select for successfully tagged cells, a puromycin N-acetyltransferase (PuroR) gene was included into the donor plasmid, separated from the fusion protein by a furin cleavage site, a GSG-linker sequence as well as a Thosea asigna virus 2A (T2A) site that ensures proteolytic splitting of the translated proteins (Fig. 2.2A). Co-transfection of the new donor plasmid with the sgRNA/Cas9 plasmids in A549 (and G141 cells, not shown) was followed by 10 days of puromycin selection. Puromycin selection resulted in only a few, well dispersed single cell clones (SCCs), that were expanded individually. Then, an endpoint PCR was per-

formed to verify the integration of the tag into the genome of the A549 SCCs (Fig. 2.2B). Out of ten SCCs, five showed the successful integration of the tag. When using those SCCs (No. 1, 3, 6, 9 and 10) for western blot analysis after preparing whole-cell lysates, three of them showed expression of the tagged PHD3 protein, as shown by the V5 and the PHD3 immunoblots (Fig. 2.2C). Of note, untagged PHD3 seems to be present in the SCCs as well, shown by its induction upon 24 hours hypoxia treatment, which indicates tagging of only one allele in the single cell clones No. 6 and 9.
However, when subjecting these ET cells to microscopy or flow cytometry analyses, no increase in fluorescence signal could be detected (data not shown), even if PHD3 levels were clearly increased by hypoxia treatment (Fig. 2.2C). To verify that the PHD3-UnaG-V5 fusion protein (Tab. 2.1, #4) will fold into a fluorescent protein, an overexpression construct was cloned and transiently transfected into A549 and G141 cells. Fluorescence microscopy revealed brightly green cells (not shown), indicating successful folding of the fusion protein.

Overall, the results presented here suggest that the levels of endogenously tagged PHD3 fusion proteins are not sufficient to be detected by standard fluorescence microscopy or flow cytometry analyses. Hence, they are not usable as FRs for screening purposes.

PHD3-regulated non-HIF proteins as POIs

PHD3 was described to hydroxylate proteins besides HIFα, which could have direct or indirect effects on the HIF-PHD-signaling axis. To elucidate if PHD3-modified domains of different proteins can be used as POIs for the luminescent/fluorescent reporter system, the PHD3-regulated POI domain was fused to a *Firefly* luciferase 2 (Luc2)/tdTomato fusion protein, which should be proteasomally degraded when PHD3 is active (Fig. 2.3A).
In order to assess the usability of these reporters, the cytosolic domains of two different PHD3-regulated POIs were cloned into the Luc2/tdTomato expression plasmid, namely EPOR (amino acid (aa) 291-508) or ADRB2 (aa 330-413). G55(TL) cells - either wildtype (wt), PHD3-KO or stable PHD3-overexpression (OE) cells - were co-transfected with the respective Luc2/tdTomato fusion plasmid and a *Renilla* luciferase-expressing plasmid. In addition, DMOG was added to a subset of PHD3-OE cells. After harvesting and freezing the cell lysates, DLR assay was performed (Fig. 2.3B).
As expected, G55(TL) cells harboring a PHD3-KO showed increased relative luciferase signal in comparison to wt cells, while G55(TL) cells overexpressing PHD3 exhibited reduced reporter levels with both reporter systems in both experiments (Fig. 2.3B, left and middle panel). Surprisingly, DMOG treatment led to a reduction of the luciferase reporter. Proper function of DMOG and the transfection process itself was confirmed by using a 9xHRE FLuc reporter as positive control, which shows high accumulation of the reporter upon DMOG treatment (Fig. 2.3B, right panel).

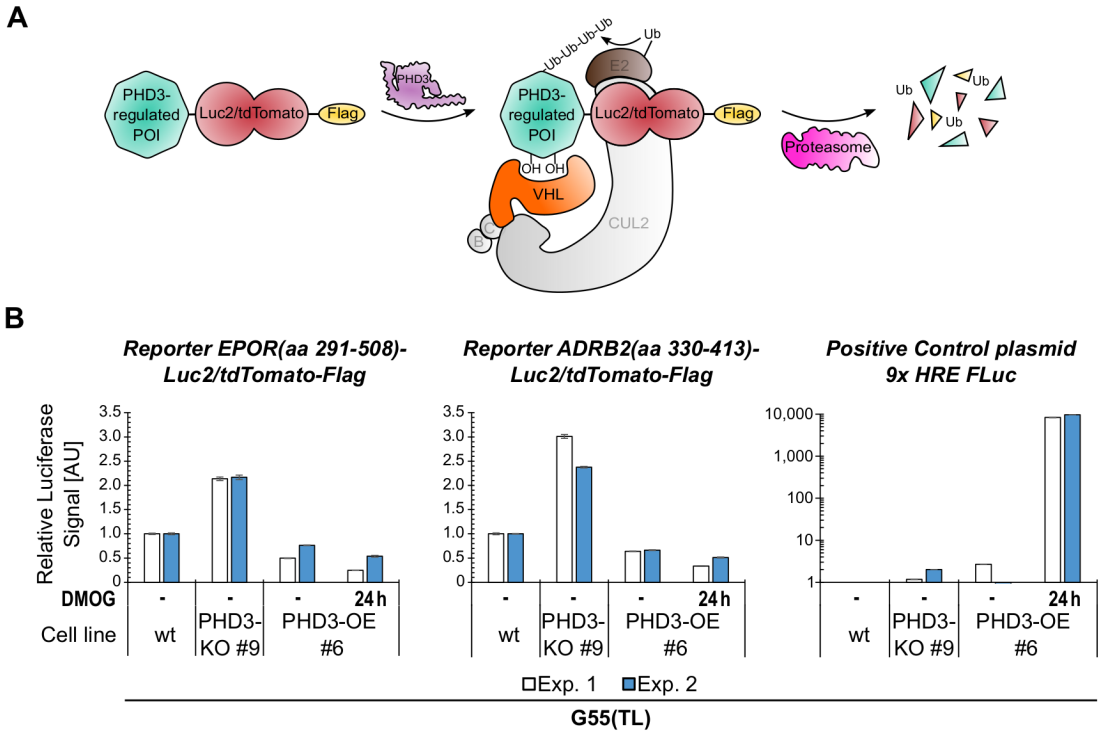

Figure 2.3: PHD3-regulated proteins are no suitable proteins of interest.
(**A**) Outline of the luminescent/fluorescent reporter system using PHD3-regulated protein targets as POIs. POIs are coupled to Luciferase2/tdTomato and a Flag tag. In theory, the reporter system will be hydroxylated by PHD3, leading to ubiquitination by the VHL E3 ubiquitin ligase complex and degradation by the proteasome. (**B**) Dual luciferase reporter (DLR) assay after transient co-transfection of the reporters or a control reporter (9xHRE FLuc) with a *Renilla* luciferase plasmid, into G55(TL) wildtype (wt), PHD3-knockout (PHD3-KO #9) or PHD3-overexpressing (PHD3-OE #6) cells. Cells were partially treated with 1 mM DMOG for 24 hours. *Firefly* luciferase reads were divided by *Renilla* luciferase reads for normalization; for comparison, untreated wt cells were set to 1. Error bars show the standard deviation of technical replicates. Results of two independent experiments are shown with white and blue columns; n_{TR} (number of technical replicates) = 3; AU = arbitrary units.

In summary, the results using ADRB2 and EPOR as POIs were not conclusive, suggesting that these domains are not usable as POIs for the FRs.

Hypoxia inducible factors (HIFs) as POIs

Next, we decided to focus on HIFα as main PHD3 target and to directly monitor HIFα stabilization. Therefore, the ODD of HIFα was employed as a POI. To prove the general usability of this approach, the ODD of HIF1α (aa 530-652) was coupled to a Luc2/tdTomato fusion protein (Fig. 2.4A). Subsequently, the plasmid was co-transfected with a *Renilla* luciferase-coding plasmid into G55(TL) cells, incubated under normoxic conditions (with or without DMOG treatment) or hypoxic conditions for 24 hours. Then, DLR assay was performed (Fig. 2.4B). Transfection with the pLenti6-ODD-Fluc-Rluc (POR) reporter plasmid served as a positive control, as this plasmid was extensively used before in our

laboratory and the expressed fusion protein was found to be only slightly stabilized by hypoxia in previous transient transfections. As shown in Figure 2.4B, both reporters were only weakly stabilized by hypoxia treatment. In contrast, DMOG treatment did not lead to increased relative luciferase signal. Importantly, DMOG strongly induced the control reporter plasmid 9xHRE FLuc, proofing the functionality of the inhibitor. Remarkably, fluorescence microscopy observations revealed that the cells transfected with the Luc2/tdTomato-HIF1α-ODD plasmid showed less fluorescent cells in the hypoxic population compared to the normoxic cells. Most of the fluorescent cells displayed only fluorescent dots around the nucleus under hypoxia and no homogenous staining of the cytoplasm was detected as observed in the cells in normoxia (not shown). This observation was also evident when fusing HIFα-ODDs to other fluorescent proteins, namely TurboGFP and mCherry. Interestingly, in some cases, stabilization of the reporters could be detected after DMOG treatment, but not with hypoxia treatment (data not shown), indicating that decreased fluorescence signal intensity is related to low oxygen tension.

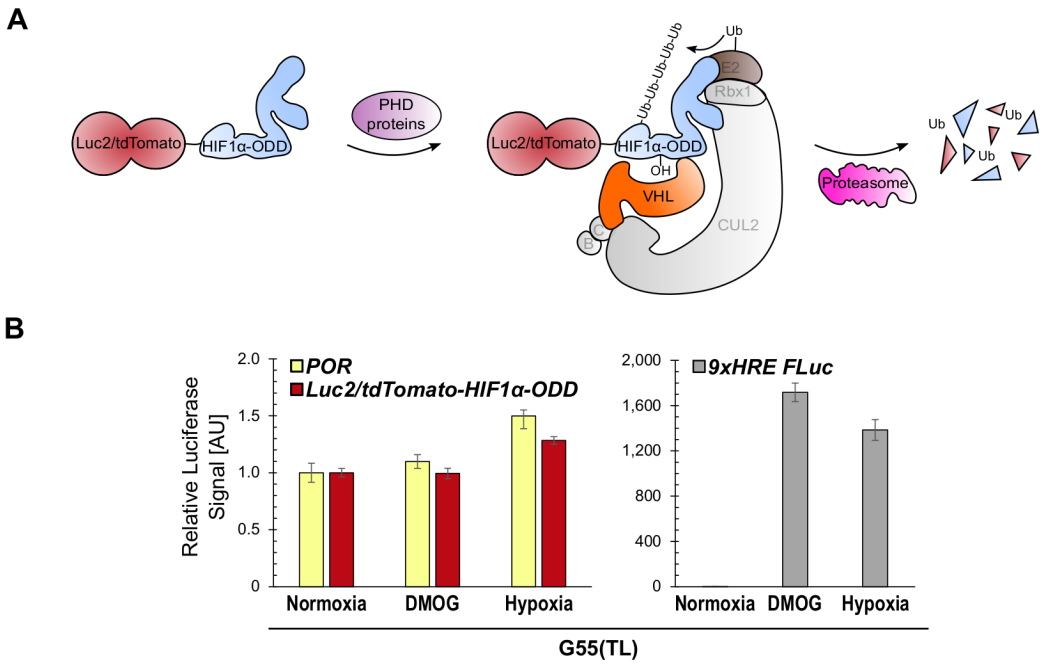

Figure 2.4: HIFα oxygen-dependent degradation domain (ODD) as POI.
(**A**) Outline of the fluorescent reporter system using HIF1α-ODD as POI. The POI is fused to Luciferase2/tdTomato. Generally, PHD protein-mediated hydroxylation of the HIF1α-ODD should result in ubiquitination of the ODD by the VHL E3 ubiquitin ligase complex and degradation by the proteasome. (**B**) DLR assay after transient co-transfection of a Luc2/tdTomato-HIF1α(aa 530-652)-ODD reporter plasmid or the 9xHRE FLuc reporter, and a *Renilla* luciferase plasmid, or the POR plasmid (containing both luciferases), into G55(TL) cells. Cells were either treated with DMOG (1 mM, 24 hours), incubated in the hypoxia chamber (1% O_2, 24 hours) or incubated under normoxic conditions; $n_{TR} = 3$; error bars show the standard deviation of technical replicates.

2.1.2.2 Selection of the oxygen-independent fluorescent reporter protein UnaG

As further evidenced by data from the literature, "standard" fluorescent proteins (e. g. GFP, mCherry, TurboGFP) require oxygen for their fluorophore maturation process [61]. Hence, these fluorescent proteins are not usable for constructing a FR that is supposed to be applicable also under hypoxic experimental conditions (1 % O_2).

In contrast, UnaG, a green fluorescent protein from the japanese eel *Anguilla japonica*, was shown to develop fluorescence completely independent of oxygen availability [98]. Importantly, UnaG requires bilirubin as a co-factor, which would be available in sufficient amounts in our experimental systems due to the use of fetal bovine serum (FBS) in our cell culture medium [42].
To construct a FR that can be used even in anoxia (absence of oxygen), UnaG was fused to the HIF2α-ODD, since HIF2α is primarily regulated by PHD3. Furthermore, a V5 tag was incorporated for easier detection by western blot analysis (Fig. 2.5A).
To test the FR, G141 cells - showing a prominent HIF2α stabilization in response to hypoxia (Fig. 2.1A) - were transduced with lentiviral particles containing the HIF2α-ODD(aa 354-581)=UnaG-V5 reporter with different multiplicities of infection (MOI) (1, 2 and 5). After selection of successfully-transduced cells, the stable cell lines were subjected to FC analysis, either after 18 hours of DMOG or hypoxia treatment (Fig. 2.5B). The resulting dot plots show a substantial portion of UnaG-positive cells in normoxia when using the lowest MOI of 1 (13.8 %). This was increased to 62.2 % and 55.2 % with 18 hours of DMOG or hypoxia treatment, respectively. With higher MOI, the percentage of UnaG-positive cells increased under all conditions, including normoxia.

To decrease the amount of UnaG-positive cells in normoxia and obtain a highly hypoxia-responsive FRS, SCCs were established. For this, reporter cells cultured under normoxic conditions were sorted for UnaG-negativity by FACS. Inducibility of the SCCs was then confirmed by 18 hours of hypoxia or DMOG treatment, followed by FC (data not shown).

Overall, a HIF2α-ODD-based reporter was found to be responsive to hypoxia and DMOG treatment and could be used for a FACS-based screening. However, the relatively high percentage of UnaG-positive cells under the normoxic control condition could lead to an unwanted high false-positive rate and limit the dynamic range of the UnaG signal changes.

2.1.2.3 Hypoxia responsive elements (HREs) increase the effective dynamic range of the fluorescent reporter

In an attempt to increase the effective dynamic range of the HIF2α-ODD(aa 354-581)=UnaG-V5 reporter, a 5xHRE enhancer, consisting of five repeats of the HRE found in the *VEGFA* promoter, was included upstream of the CMV promoter of the reporter

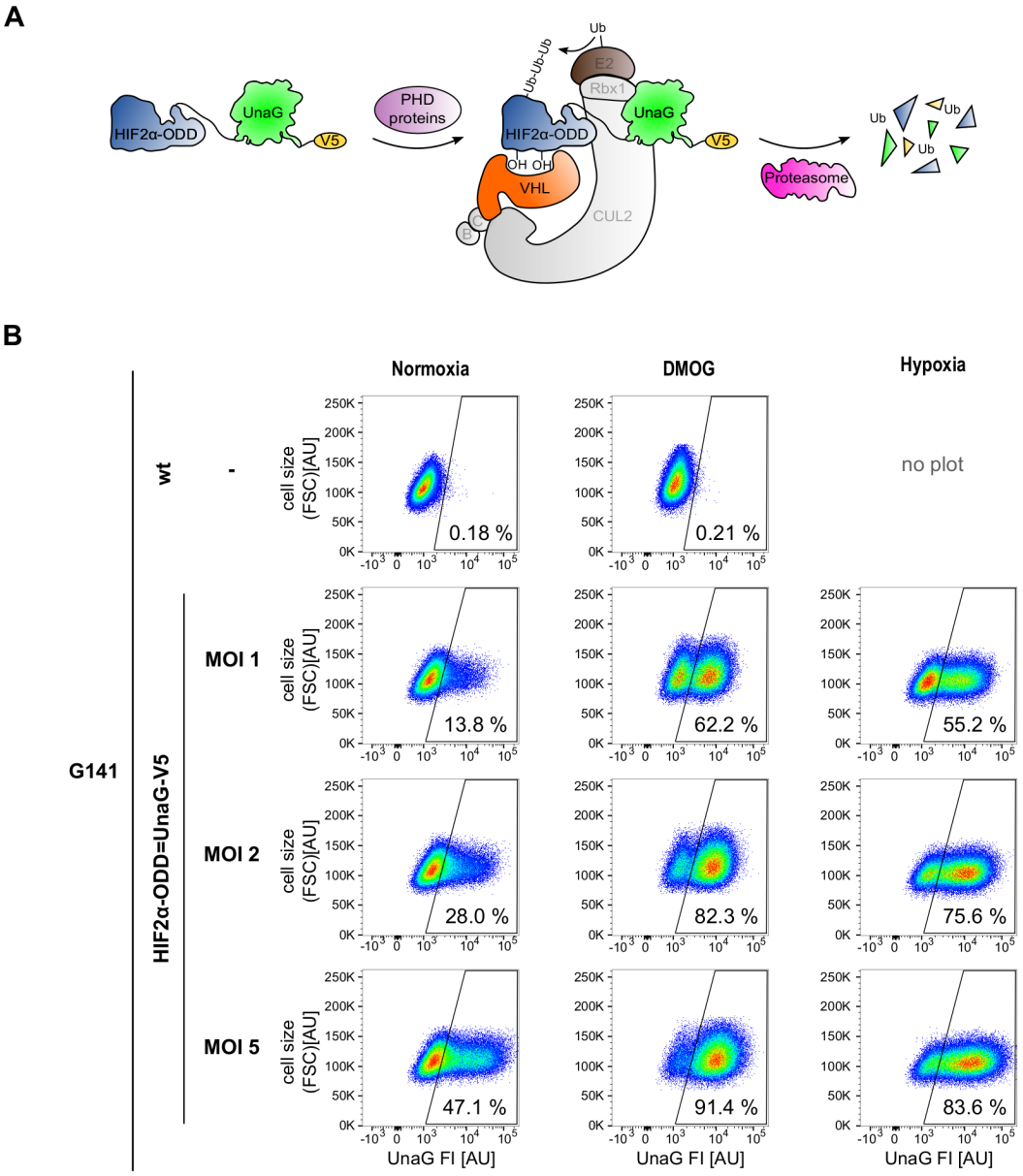

Figure 2.5: UnaG is a suitable fluorescent reporter gene for the FRS.
(**A**) Outline of the fluorescent reporter using HIF2α-ODD(aa 354-581) fused to UnaG and a V5 peptide tag. The reporter is supposed to be hydroxylated by PHD proteins, ubiquitinated by the VHL E3 ubiquitin ligase complex and degraded by the proteasome. If PHD proteins are not active, the reporter will be stabilized. (**B**) Flow cytometry analysis of G141 cells stably expressing the HIF2α-ODD(aa 354-581)=UnaG-V5 reporter (transduced with different multiplicities of infection (MOI), treated with 18 hours of hypoxia (1% O_2) or 18 hours of 1 mM DMOG; AU = arbitrary units; FSC = forward scatter; wt = wildtype; FI = fluorescence intensity.

plasmid DNA. This should increase the expression of the reporter when HIFα proteins are stabilized and bind after dimerization with HIFβ and nuclear translocation to the HREs (Fig. 2.6A).

To test this, G141 and A549 cells were transduced with lentiviral reporters with and without the 5xHRE enhancer and stable cell pools (MOI 10) were established and compared

using FC after 24 hours of normoxic or hypoxic incubation (Fig. 2.6B, left and right panel, respectively). When analyzing the G141 +/- 5xHRE reporter cell pools, the one containing the 5xHRE showed only 3.36 % of UnaG-positive cells in normoxia. In contrast, the reporter cells without the 5xHRE showed already 80.8 % of UnaG-positive cells under the same conditions. This increased to 56.7 % or 93.8 % after 24 hours of hypoxia treatment, respectively.
In A549 cells, the amount of UnaG-positive cells was with both reporters below 1 %. However, the amount of UnaG-positive cells after hypoxia treatment was significantly higher in the 5xHRE-containing FRS compared to the one without the enhancer (49.7 % vs. 3.16 %).

In summary, the low percentage of UnaG-positive cells in normoxia as well as the shift of around 50 % of cells towards UnaG-positivity after 24 hours hypoxia exposure suggested to continue the development of the FRS with the 5xHRE-containing reporter. This was further supported by live-cell microscopy data, showing the rapid accumulation of the FR with DMOG treatment over 24 hours in A549 cell pools (Fig. 2.7).

2.1.3 Selection of G141 and A549 5xHRE HIF2α-ODD(aa 354-581)=UnaG-V5 single cell clones for screening

To further reduce the percentage of UnaG-positive cells in non-treated cell populations and gain well distinguishable populations after the treatments in FC analysis, SCCs were established from the already established cell pools. To select SCCs with a high dynamic range, the 5xHRE HIF2α-ODD(aa 354-581)=UnaG-V5 cell pools (G141 and A549) were sorted by FACS in a two-step procedure (Fig. 2.8A). First, polyclonal G141 or A549 5xHRE HIF2α-ODD(aa 354-581)=UnaG-V5 cell pools were seeded, harvested and selected by FACS for low UnaG signal. “Low levels” refer to UnaG signals that are slightly higher than the signal of wildtype cells without any reporter expression. Those UnaG-low cells were further cultured as polyclonal pools. When confluent, the cells were seeded and treated with 1 mM DMOG for 18 hours to trigger the accumulation of the reporter. Subsequently, cells were sorted by FACS for UnaG positivity into only one cell per well of a 96-well plate.

To choose suitable SCCs, SCCs were seeded and incubated in normoxia, with or without DMOG treatment (1 mM, 18 hours), or in hypoxia (18 hours). After harvesting, SCCs were analyzed by FC. Data were processed using FlowJo and R and displayed as violin plots with included boxplots (Fig. 2.8B for G141 and Fig. 2.9 for A549 SCCs; descriptive statistic measures: Suppl. Tab. 4.4 and 4.5). SCCs with the best signal separation (the lowest overlap between the distributions of the normoxic versus the hypoxic or DMOG-treated cell populations) were selected, namely G141 SCCs #A1 and #B11 and A549 SCC#P3A5.

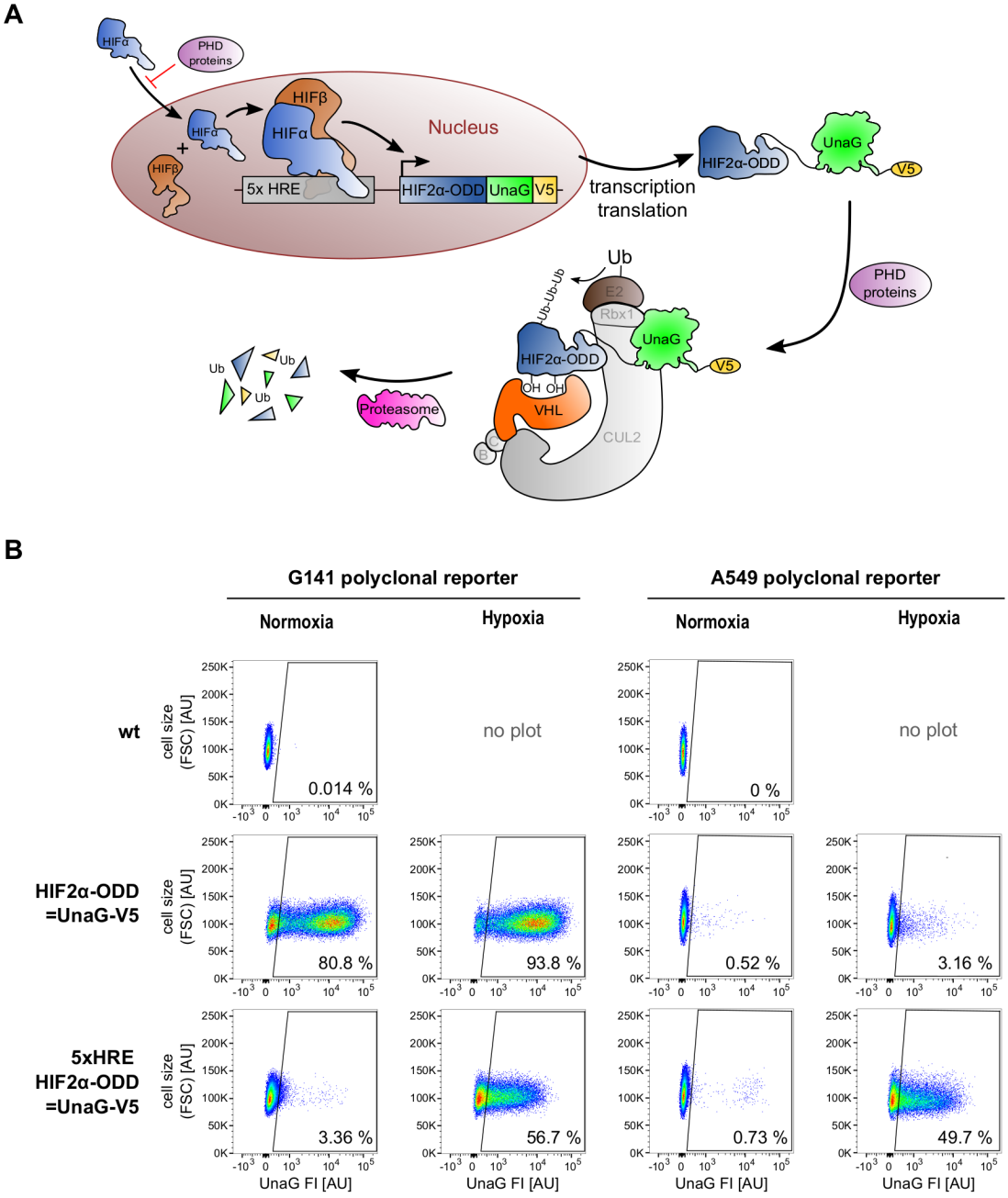

Figure 2.6: Addition of a 5xHRE enhancer increases the effective dynamic range of the reporter.

(**A**) Schematic representation of the fluorescent reporter combining 5xHREs and HIF2α-ODD(aa 354-581)=UnaG-V5. Upon activity of PHD proteins, the reporter is supposed to be hydroxylated by PHD proteins, ubiquitinated by the VHL E3 ubiquitin ligase complex and degraded by the proteasome (lower part). In contrast, when PHD protein activity is diminished, endogenous HIFα proteins (as well as the reporter proteins) are stabilized, can translocate to the nucleus, dimerize with HIFβ and bind to the 5xHREs, increasing the expression of the fluorescent reporter (upper part left). (**B**) Flow cytometry (FC) analysis of G141 (left) and A549 (right) cells transduced with the HIF2α-ODD(aa 354-581)=UnaG-V5 reporter with or without inclusion of the 5xHRE enhancer and treatment with 24 hours of hypoxia (1% O_2). FSC = forward scatter; FI = fluorescence intensity; AU = arbitrary units; wt = wildtype.

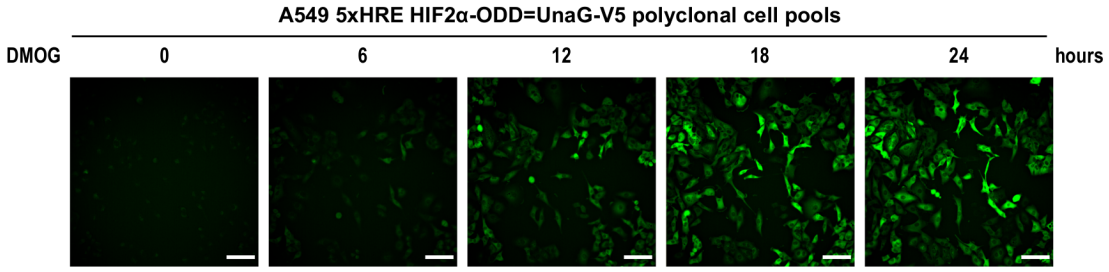

Figure 2.7: Reporter cells rapidly accumulate the fluorescent reporter (FR) upon PHD inhibition by DMOG.
Widefield live-cell microscopy pictures (Leica THUNDER Imager, Instant Computational Clearing applied with Feature Scale = 15,000 nm and Strength = 75 %) of A549 5xHRE HIF2α-ODD=UnaG-V5 reporter cell pools (MOI 10) treated with 1 mM DMOG for the indicated time. Scale bar = 100 µm.

2.1.4 Comparison of the single cell clones to their parental cell lines

In order to ensure that the selected SCCs display critical features comparable to their parental cell lines, protein levels of the key HIF pathway proteins as well as markers for epithelial-to-mesenchymal transition (EMT) were evaluated by western blot analysis in the different cell lines. For this, cells were either treated with 18 hours of hypoxia or DMOG or incubated at normoxia (Fig. 2.10A).

In summary, G141 wt and SCC#A1 showed comparable levels of HIFα proteins as well as PHD2 and N-Cadherin (Fig. 2.10A, first six lanes). Only PHD3 levels differed between the polyclonal pool and the single cell clone, as SCC#A1 cells showed higher levels of PHD3 in normoxia, hypoxia and with DMOG treatment.
In contrast, A549 wt cells remarkably differed from the SCC#P3A5 (Fig. 2.10A, lanes seven to twelve). Except for PHD2, all other protein levels were altered in this FRS in comparison to its parental cell line. Most notably, E-Cadherin levels were reduced while N-Cadherin levels were increased in SCC#P3A5, suggesting that the single cell clone had a more mesenchymal phenotype than the wildtype.

When comparing the morphology of the cells by widefield microscopy, no differences were observed between the G141 wt and the SCC#A1 cell lines (Fig. 2.10B). In general, the cell populations were morphologically homogeneous in both cases.
Conversely, the A549 wt cell population already showed morphological differences between the individual cells (Fig. 2.10C, left). Areas with densely packed, more epithelial-like cells were as well present as areas with more elongated, mesenchymal-like cells. When comparing the SCC#P3A5 to the wt cells (Fig. 2.10C), the packed, epithelial-like cells disappeared completely in the SCC, in good agreement with the different expression

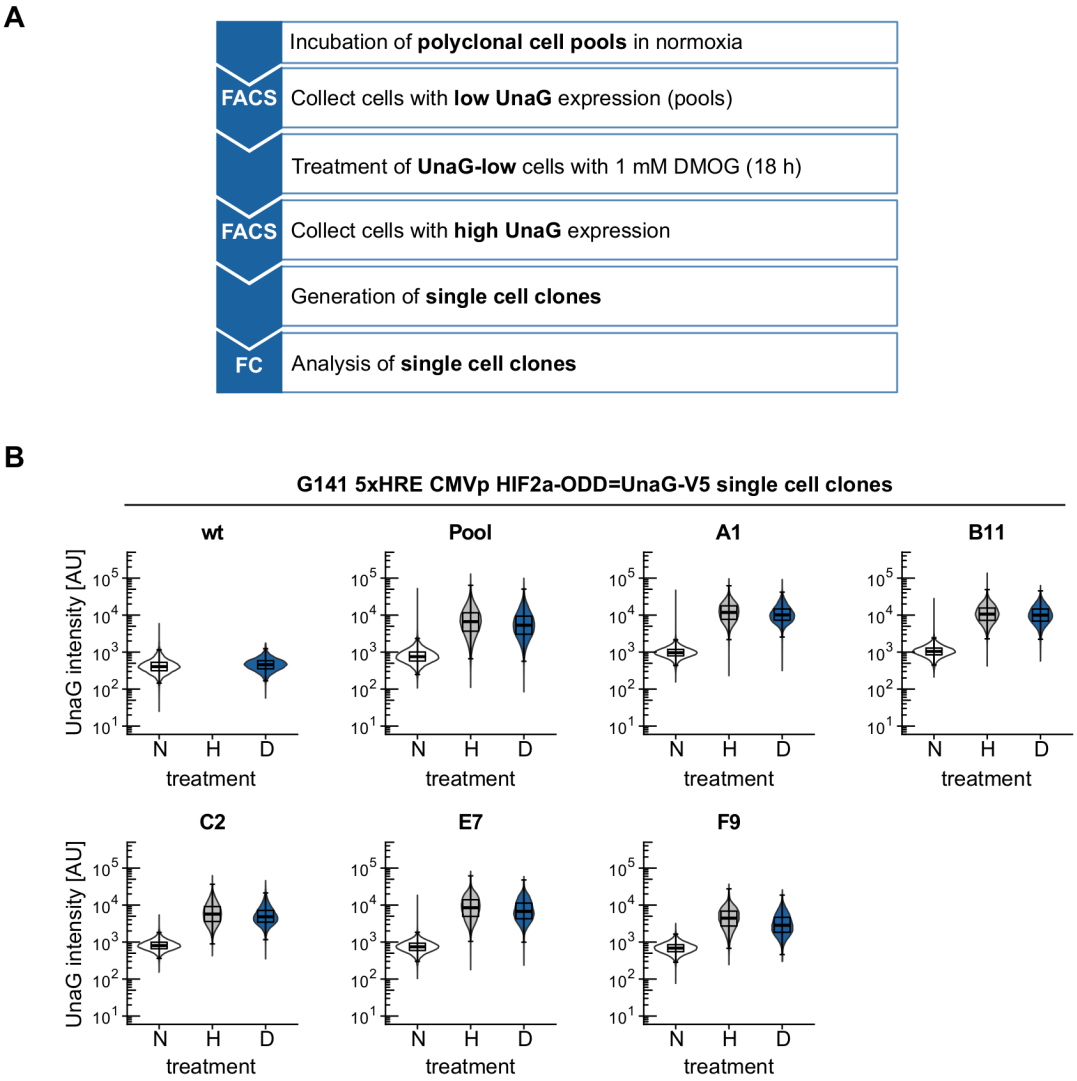

Figure 2.8: Selection procedure and inducibility profiles of G141 5xHRE HIF2α-ODD(aa 354-581)=UnaG-V5 single cell clones.
(**A**) Outline of the two-step fluorescence activated cell sorting (FACS)-based selection procedure to obtain single cell clones (SCCs) for screening purposes. (**B**) Subset of candidate G141 5xHRE HIF2α-ODD(aa 354-581)=UnaG-V5 SCCs in comparison to the wt G141 cells and the cell pool prior sorting. Cells were analyzed by FC, data were processed by FlowJo and distributions of the UnaG fluorescence intensity in arbitrary units (AU) are displayed as violin plots. Descriptive statistics are shown as box plots within the violin plots (data points outside the whiskers [1.5x interquartile range (IQR)] are considered outliers by R). Normoxic (N) cells are compared to cells incubated in hypoxia for 18 hours (H) or cells treated with DMOG for 18 hours (1 mM; D). SSCs were derived from a single 96-well plate. Descriptive statistic measures are listed in Suppl. Tab. 4.4 in the appendix (page 160).

of N- and E-Cadherin seen in the western blot analysis (Fig. 2.10A).
In line with the literature [69], the A549 wt cell line showed a spectrum of epithelial and mesenchymal-like cells. Thus, western blot analysis of these cells showed the average protein expression of the different cell states. Hence, the expression pattern differences between the heterogeneous wt and the mesenchymal-like SCC#P3A5 were to be expected.

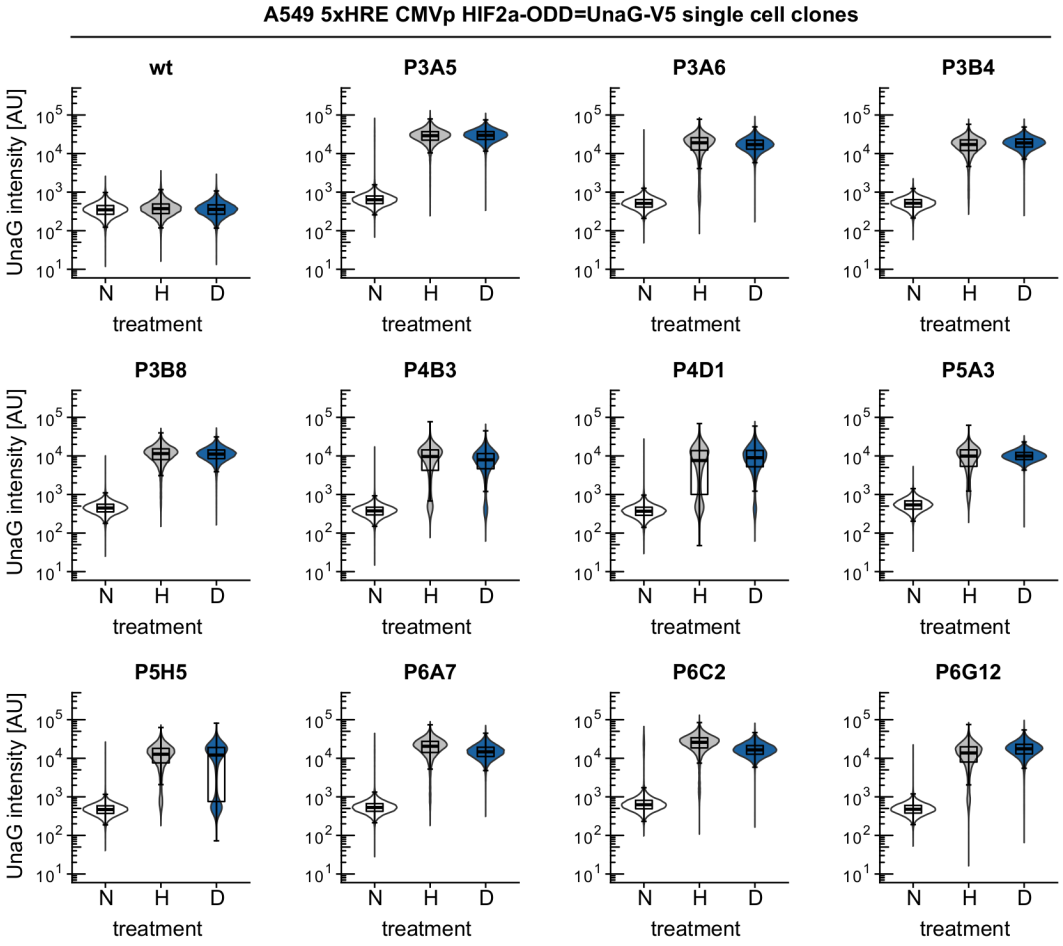

Figure 2.9: Selection procedure and inducibility profiles of A549 5xHRE HIF2α-ODD(aa 354-581)=UnaG-V5 single cell clones.
Subset of candidate A549 5xHRE HIF2α-ODD(aa 354-581)=UnaG-V5 SCCs in comparison to the wt A549 cells. Cells were analyzed by FC, data were processed by FlowJo and distributions of the UnaG fluorescence intensity in arbitrary units (AU) are displayed as violin plots. Descriptive statistics are shown as box plots within the violin plots (data points outside the whiskers [1.5x IQR] are considered outliers by R). Normoxic (N) cells are compared to cells incubated in hypoxia for 18 hours (H) or cells treated with DMOG for 18 hours (1 mM; D). SSCs were derived from different 96-well plates. Descriptive statistic measures are listed in Suppl. Tab. 4.5 in appendix (page 161).

Consequently, both SCCs sufficiently resembled (at least parts of) their parental cell lines and could be used for FACS-based screening.

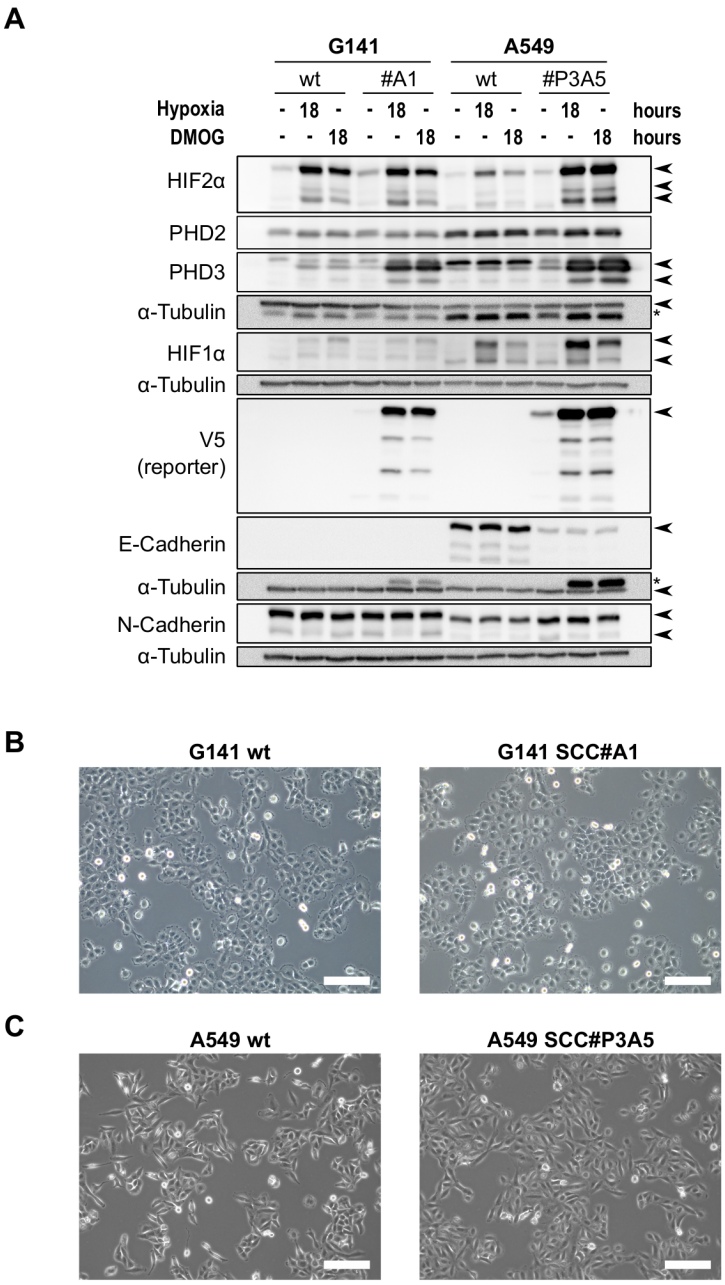

Figure 2.10: Protein and cell morphology-based comparison of the FR SCCs with their parental cell lines.
(**A**) Western blot analysis showing the protein levels of wt cell lines G141 and A549 in comparison to 5xHRE CMVp HIF2α-ODD=UnaG-V5 single cell clones (SCCs) G141 #A1 and A549 #P3A5. Arrows show specific protein bands; asterisks indicate unspecific bands (in Tubulin blots: Residual signal from PHD2 and V5 blots). Cells were treated with DMOG (1 mM) or incubated in the hypoxia chamber for each 18 hours. (**B**) Widefield brightfield microscopy images showing the morphology of G141 wt vs. SCC#A1. Scale bar = 200 μm. (**C**) Widefield brightfield microscopy images showing the morphology of A549 wt vs. SCC#P3A5. Scale bar = 200 μm.

2.2 Optimization of the experimental parameters for CRISPR-screening

To determine the optimal conditions for the FACS-based CRISPR/Cas9-mediated genome-wide screening experiment, the following parameters were experimentally evaluated.

2.2.1 Definition of the optimal cell confluency for FC data collection

In preliminary experiments, the SCCs exhibited varying amounts of UnaG-positive cells at different degrees of cell culture confluency at the time of harvesting for FC analysis. This was particularly evident in the G141 SCC#A1 FRS and especially at very low or very high levels of confluency.

To systematically assess the dependency of the UnaG signal in the FC experiments on the cell confluency of the population, different amounts of G141 SCC#A1 and A549 SCC#P3A5 cells were seeded, grown under normoxia, with or without DMOG treatment (18 hours, 1 mM), or hypoxia, and subsequently harvested (Fig. 2.11). FC analysis revealed a shift of the UnaG signal towards higher positivity with increasing cell amount in G141 SCC#A1 cells in normoxia and after DMOG treatment (Fig. 2.11A). This shift was even larger after hypoxic exposure. Here, not only a shift but also a broadening of the distribution of the UnaG fluorescence intensity was present with low seeding density compared to higher cell numbers. As a result, the distributions of normoxia and hypoxia samples did overlap, making it impossible to reliably distinguish populations and set sorting gates for FACS.
In contrast, A549 SCC#P3A5 cells showed only little variation in their fluorescence intensities at the same densities (Fig. 2.11B).

Based on these measurements and to avoid pseudohypoxic phenotypes induced by high cell confluency, a seeding amount of 150,000 cells per well of a standard 6-well plate (scaled accordingly if different cell culture plastic was used) was chosen for further FC analyses and FACS.

2.2.2 The harvesting procedure influences UnaG fluorescence intensity

Conducting a screen using a genome-wide CRISPR/Cas9 library requires culturing of ten to several hundred million cells. When performing a screen under hypoxic conditions, harvesting the cells in normoxia would simplify the handling. To clarify whether harvesting of hypoxia-treated cells in normoxia impacts UnaG signal intensity, G141 SCC#A1 and A549 SCC#P3A5 cells were seeded, treated with 18 hours hypoxia (or 1 mM DMOG

as a control) and harvested either inside or outside of the hypoxia chamber (Fig. 2.12). Cells were then analyzed by FC.

FC analysis revealed a clear difference in UnaG fluorescence intensity (FI) between

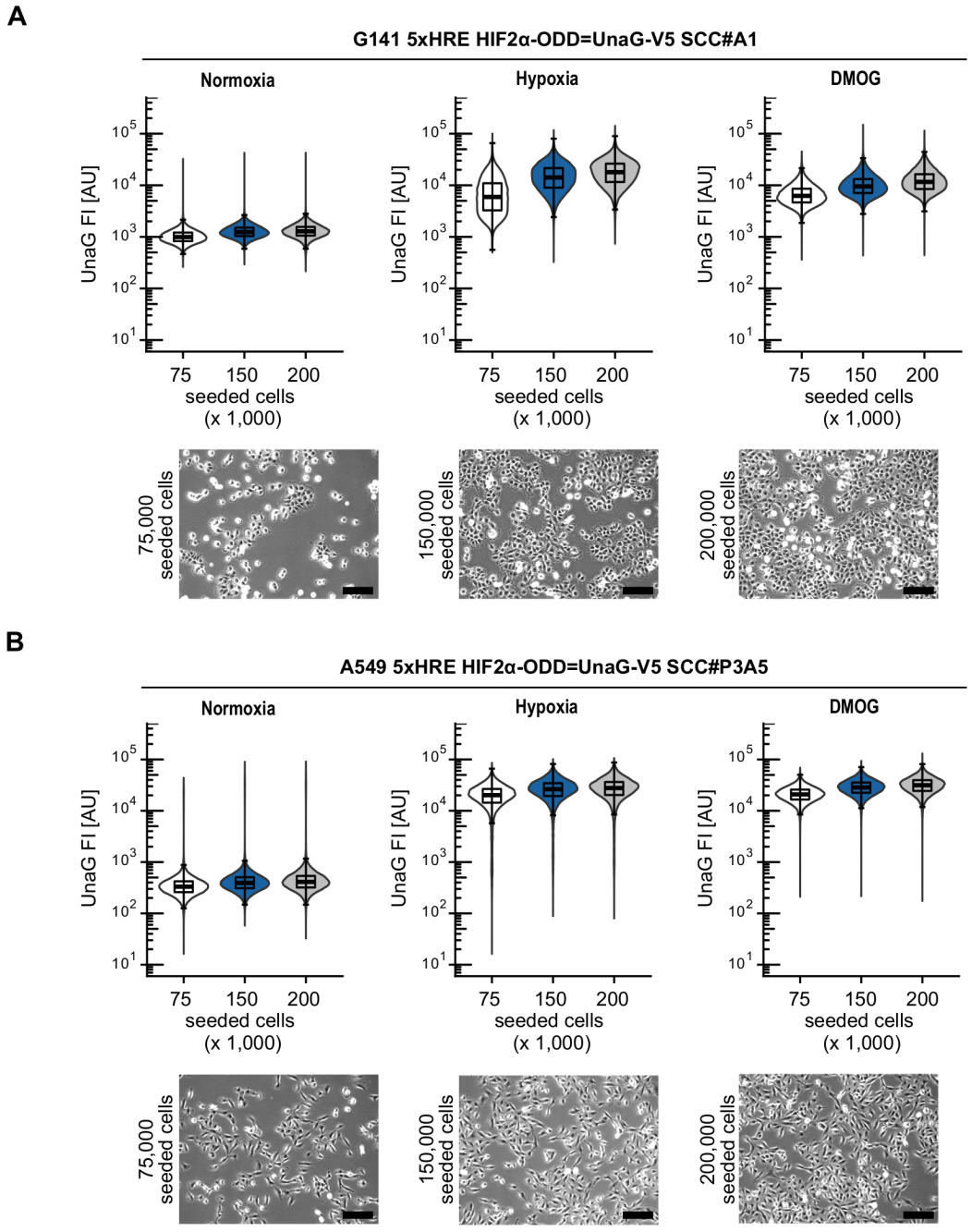

Figure 2.11: UnaG signal dependency on cell confluency.
Flow cytometry analysis (top) and brightfield microscopy images (bottom) of G141 SCC#A1 (**A**) and A549 SCC#P3A5 (**(B)**) cells seeded with different cell amounts and treated with 18 hours of hypoxia or DMOG (1 mM) or untreated (normoxia).
Descriptive statistics are shown as box plots within the violin plots (whiskers show 1.5x IQR). Descriptive statistic measures are listed in Suppl. Tab. 4.6 in appendix (page 162). Scale bar: 200 µm. n = 2; one representative experiment is shown. AU = arbitrary units.

hypoxia-treated G141 SCC#A1 cell populations harvested inside versus outside of the hypoxia chamber (Fig. 2.12A). Not only the overall median of the UnaG fluorescence intensity was reduced in cells harvested outside of the hypoxia chamber (e. g. a UnaG fluorescence intensity median of 17,227.2 AU in G141 SCC#A1 harvested inside versus median of 12,676.2 AU in the cells harvested outside the hypoxia chamber; Suppl. Tab. 4.7), but also its distribution broadened under this condition.
Interestingly, the same experiment in A549 SCC#P3A5 did not result in remarkable UnaG FI changes between the populations harvested inside or outside the hypoxia chamber (Fig. 2.12B).
These results imply that both reporter systems are differently sensitive to changes in oxygen levels shortly before harvesting and at least the FRS G141 SCC#A1 should be harvested under hypoxic conditions when conducting a hypoxia screening.

Additionally, harvesting of high cell amounts needs considerable amounts of FACS buffer, which requires the addition of FBS as the donor for bilirubin (co-factor of UnaG) and to maintain cell viability. To evaluate how much FBS should be added to the FACS buffer in order to obtain reliable results, different concentrations of fetal bovine serum (FBS) (10 %, 5 % or 1 % FBS) were added to the FACS buffer used in the already described experiment (Fig. 2.12).
Only a slight increase in UnaG FI was detectable when comparing cells kept in FACS buffer containing 1 % versus 5 or 10 % FBS in both SCCs. Furthermore, the relative amount of living cells slightly dropped gradually with decreased FBS concentration, but most strikingly between the 1 % and the 5 % FBS buffer (data not shown). Therefore, further experiments were conducted with either 5 % or 10 % FBS in FACS buffer.

2.2.3 Prolonged incubation before FC/FACS influences UnaG signal intensity only slightly

Sorting several million cells at the FACS machine takes several hours. To monitor UnaG signal stability when cells are kept for a prolonged time on ice prior to FC or FACS, G141 SCC#A1 and A549 SCC#P3A5 cells were seeded, subjected to 18 hours of hypoxia and harvested at different time points in 10 % FBS FACS buffer. Then, the cells were incubated on ice, covered with aluminum foil to restrict light exposure, for the indicated amount of time before FC measurement (Fig. 2.13).
In both reporter cell lines, prolonged incubation time on ice prior to FC analysis led to a shift towards a reduced median UnaG FI (see also Suppl. Tab. 4.8). Again, the G141 reporter SCC#A1 was more sensitive, as evident from the stronger reduction of median UnaG FI with increasing incubation time (Fig. 2.13A).
In contrast, changes in the A549 SCC#P3A5 were barely visible (Fig. 2.13B).
However, UnaG-negative cells could be still well separated from UnaG-positive cells even

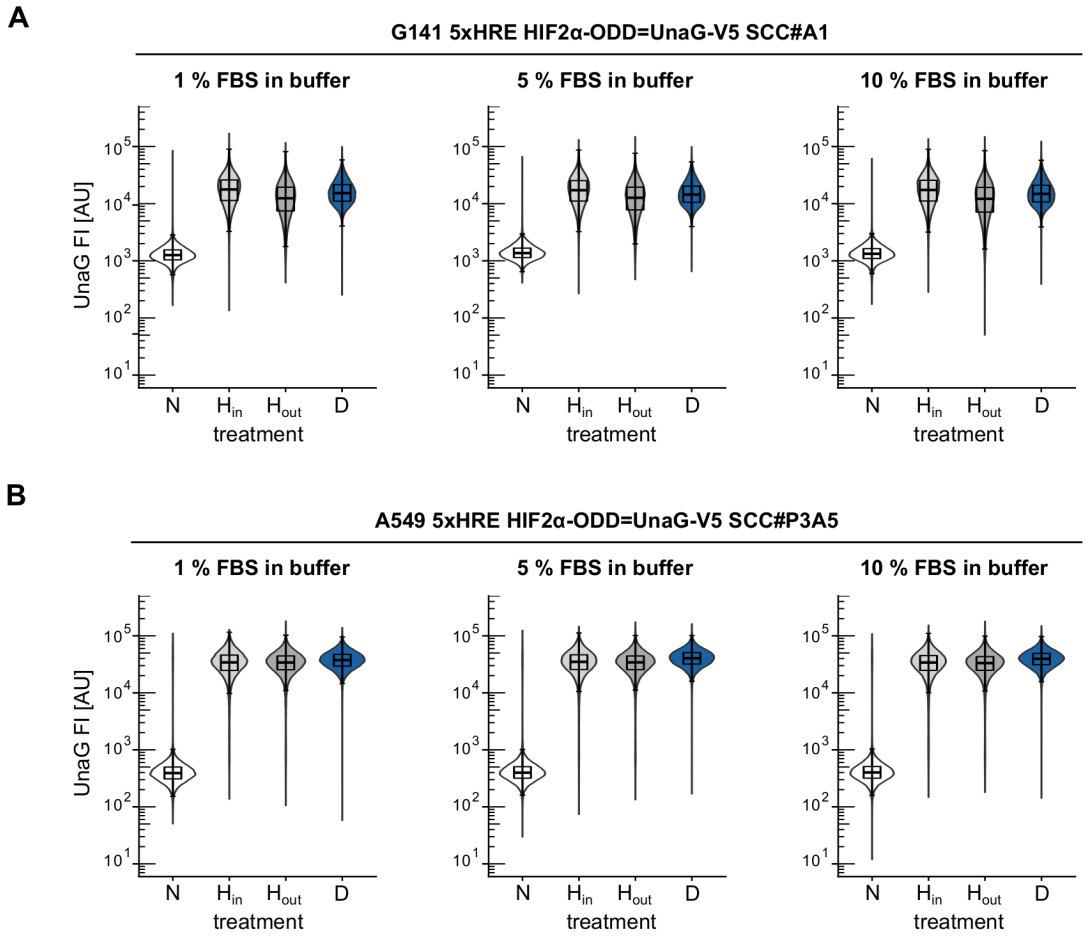

Figure 2.12: Differences in UnaG fluorescence intensities according to the harvesting procedure.
Flow cytometry analyses of G141 SCC#A1 (**A**) or A549 SCC#P3A5 (**B**) FRS cells, treated with hypoxia (H_{out} and H_{in}; 18 h), DMOG (D; 1 mM, 18 h) or not treated (N). Hypoxic cells were harvested either inside (H_{in}) or outside of the hypoxia chamber (H_{out}). All cells were kept in FACS buffer containing the indicated percentage of fetal bovine serum (FBS). n = 2; one representative experiment is shown. FI = fluorescence intensity. Descriptive statistics are shown as box plots within the violin plots (whiskers show 1.5x IQR). Descriptive statistic measures are listed in Suppl. Tab. 4.7 in appendix (page 163).

in G141 SCC#A1 cells after 3 hours of incubation.

Overall, cells, especially G141 SCC#A1, should be kept on ice as short as possible even if prolonged incubation times do not strongly alter the UnaG FI of the main population. For CRISPR-screening, in order to keep the UnaG signal stable and the cell viability high, cells should be harvested in a way that they do not remain longer than two to three hours on ice before they are sorted by FACS.

2.2.4 Selection of control sgRNA constructs

In order to set the gates for the FACS sorting of the screening experiment, several positive and negative sgRNA controls were evaluated.

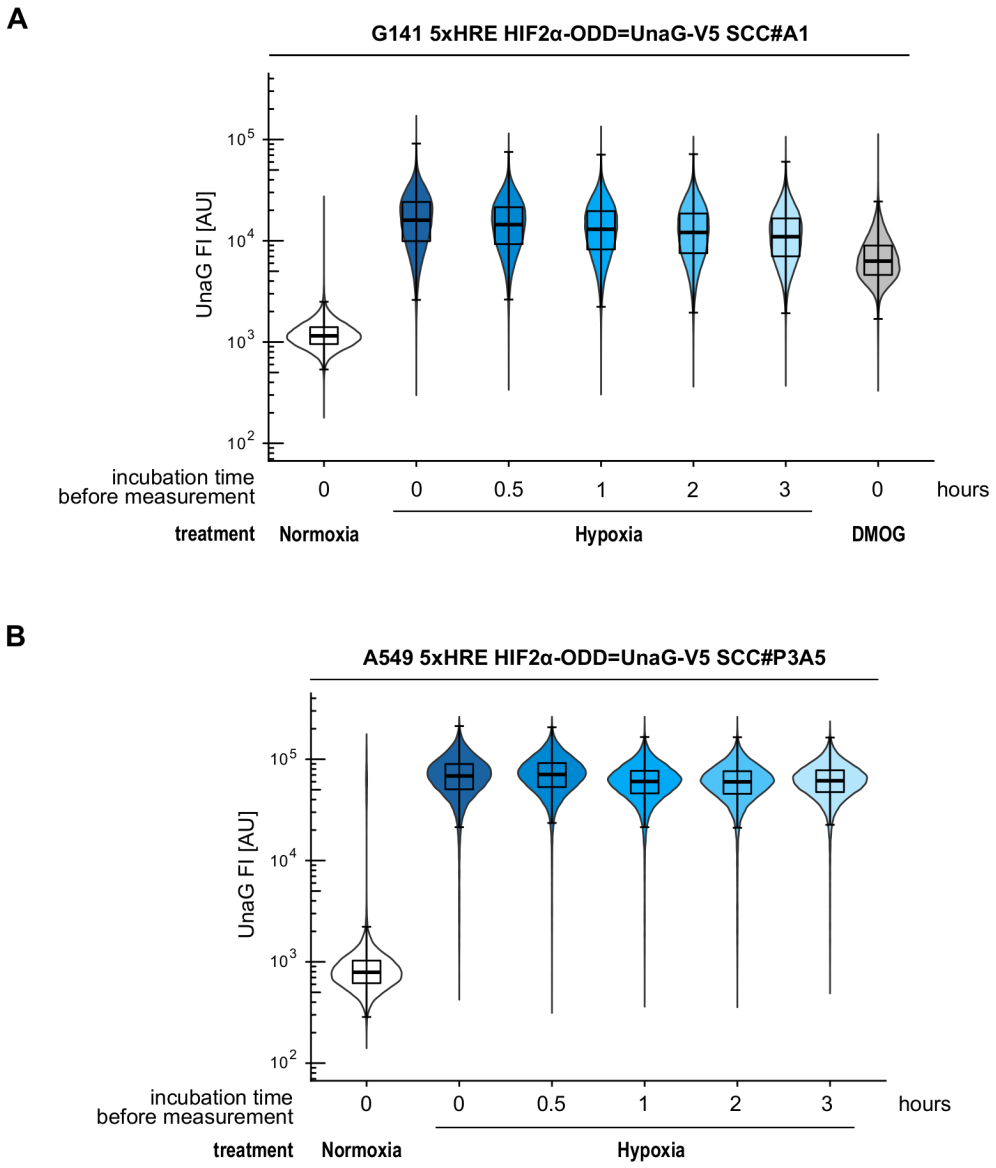

Figure 2.13: Prolonged incubation prior measurement influences UnaG signal intensity.
Flow cytometry analyses of G141 SCC#A1 (**A**) or A549 SCC#P3A5 (**B**) cells, treated for 18 hours with hypoxia, DMOG (1 mM) or not treated (Normoxia). Cells were harvested and, protected from light, incubated on ice for the indicated amount of time before measurement.
Descriptive statistics are shown as box plots within the violin plots (whiskers show 1.5x IQR). Descriptive statistic measures are listed in Suppl. Tab. 4.8 in appendix (page 164). n = 1; FI = fluorescence intensity; AU = arbitrary units.

First, three sgRNAs of the 1,000 non-targeting controls (NTCs) of the Brunello library, namely #524, #681 and #776, termed now NC#1, NC#2 and NC#3, respectively, were randomly selected as negative controls (NCs). Those sgRNAs do not bind in the human genome and therefore do not induce DNA DSBs.
Second, sgRNAs targeting PHD2, PHD3 and VHL (two different sgRNAs) were chosen as candidates for positive controls (PCs), as a KO of those genes is expected to lead to accumulation of the FR.

To test the selected NCs and PCs, the sgRNAs were cloned into the (p)LentiCRISPR v2 (Puro) vector, lentiviruses were produced, titered and transduced into the SCCs (MOI 0.5). After ten days of puromycin selection, cells were seeded, incubated in normoxia or hypoxia for 18 hours, harvested and analyzed by FC and western blot analysis (Fig. 2.14 and Fig. 2.15).
FC analysis revealed that NC#1 was the sgRNA leading to the smallest increase of median UnaG FI in G141 SCC#A1 cells in normoxia compared to non-transduced SCCs (Fig. 2.14A). From the PCs, the sgRNA targeting PHD3 did not result in a significant shift of fluorescence signal towards a higher UnaG FI, while the sgRNA targeting PHD2 resulted in a well-detectable broadening of the UnaG FI distribution towards a higher UnaG FI. This shift was even more evident with the sgRNAs targeting VHL, with VHL-sgRNA#2 showing a nearly complete shift of the UnaG-negative population towards UnaG FI values as seen in hypoxia-treated samples.
Subsequently, to assess the impact of the different sgRNAs on key HIF pathway proteins and the FR, western blot analysis was performed (Fig. 2.14B). As expected, the expression levels of HIF2α, HIF1α, PHD3, PHD2 and the FR (shown by V5 immunoblot) in cells expressing the NC#1 sgRNA were equal to cells without any sgRNA. Furthermore, PHD3- and PHD2-KOs led to a visible reduction of PHD3 and PHD2 protein levels in the respective KO cells. In good agreement with the FR changes detected by FC analysis, the largest alteration on the steady-state levels of key HIF pathway enzymes was observed with the sgRNA #2 targeting VHL. There, HIF2α, HIF1α, PHD3, PHD2 and the FR were highly induced already in normoxia.

Similar experiments were conducted in A549 SCC#P3A5 cells as well (Fig. 2.15). Here, the FC analysis showed no differences in the mean UnaG FI values between the three NCs (Fig. 2.15A). Additionally, PHD2-KO had only a minor effect on the FR, while PHD3-KO had no detectable impact.
Furthermore, the western blot analyses of the steady-state levels of key HIF pathway enzymes showed a comparable pattern to G141 SCC#A1 for the tested sgRNAs (Fig. 2.15B).

Taken together, NC#1 was identified as a suitable NC/non-targeting control (NTC) and VHL-sgRNA#2 as a good PC in these experiments. Accordingly, these sgRNAs were used in the screening experiment as controls.
Moreover, these data revealed that the FRS is responsive to genetic perturbations mediated by CRISPR/Cas9-induced DSBs, leading to knockout of genes and consequently depletion of proteins that regulate the HIF signaling pathway.

Altogether, the FRS, the experimental conditions and in particular the cell lines G141 SCC#A1 and A549 SCC#P3A5 were comprehensively validated. They were found to be suitable for screenings with the aim to identify regulators of the HIF signaling pathway.

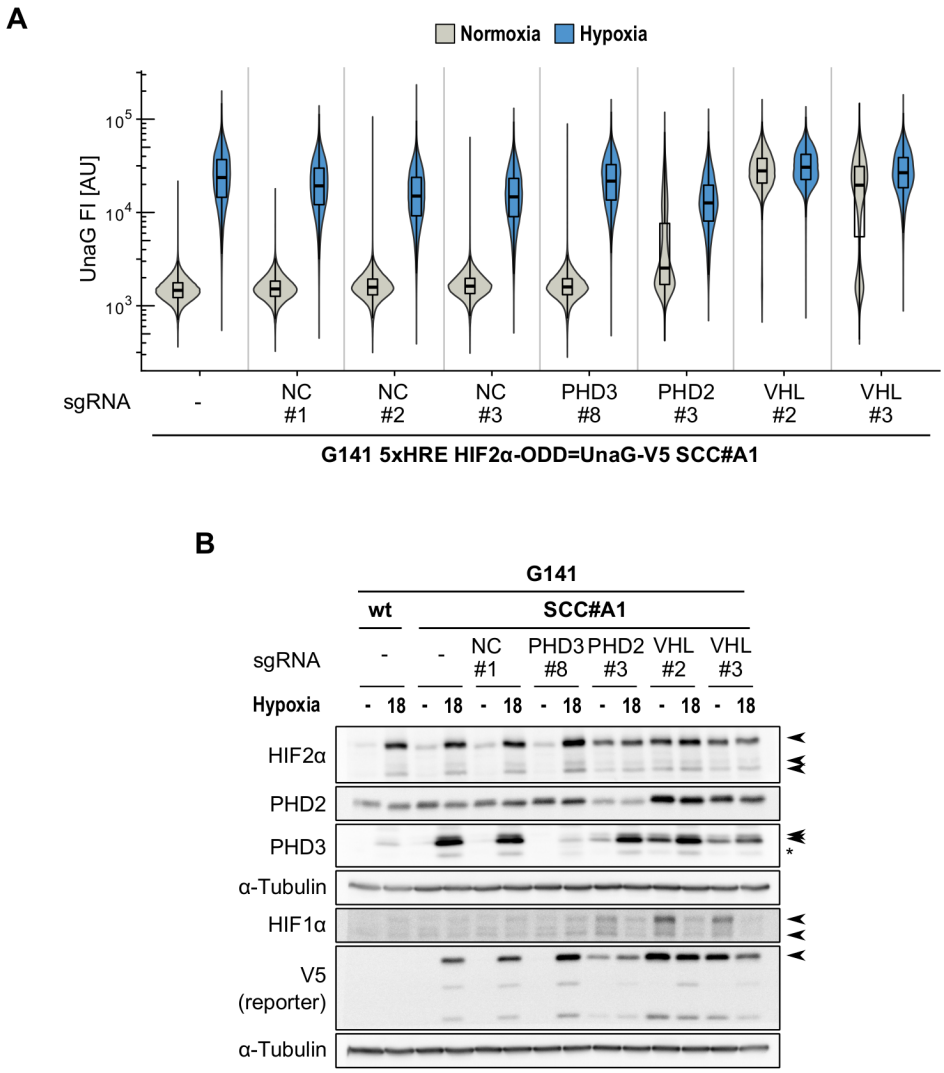

Figure 2.14: Selection of control sgRNAs for the screening experiment.
(**A**) Flow cytometry analyses of G141 SCC#A1 cells transduced with virus particles harboring the coding sequence for the Cas9 protein as well as the indicated sgRNA (x-axis), treated with hypoxia or not treated (normoxia). Descriptive statistics are shown as box plots within the violin plots (whiskers show 1.5x IQR). Descriptive statistic measures are listed in Suppl. Tab. 4.9 in appendix (page 165). AU = arbitrary units; FI = fluorescence intensity. (**B**) Western blot analysis corresponding to the FC data shown in (A). Arrows show specific protein bands; asterisks indicate unspecific bands. wt = wildtype.

2.3 Screening for regulators of the HIF pathway and validation of hits

After development and characterization of the FRSs as well as optimization of the experimental parameters, the CRISPR/Cas9-mediated genome-wide KO screening and validation experiments were conducted.

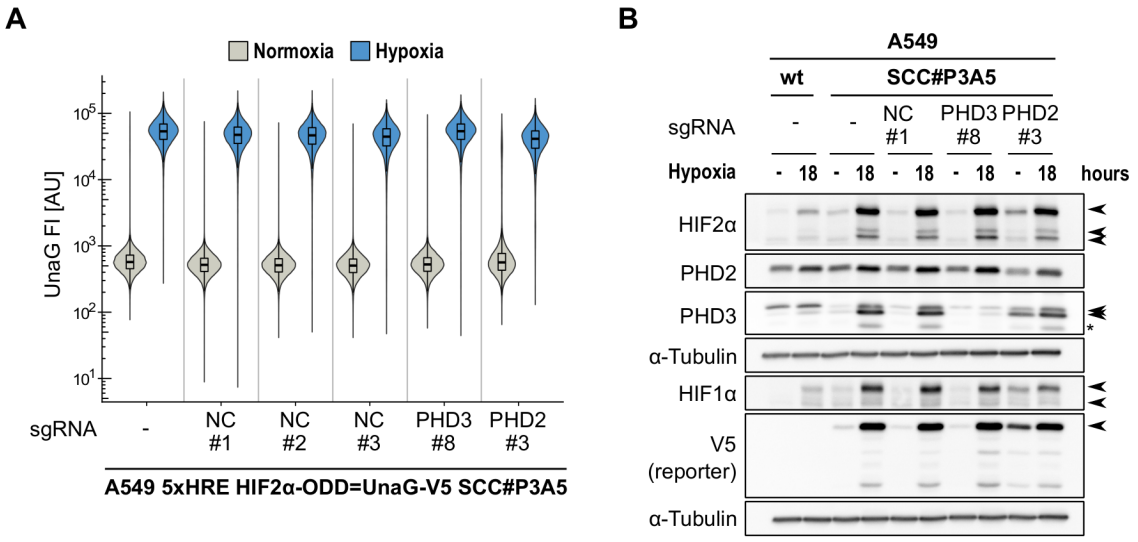

Figure 2.15: Validations of control sgRNAs for the screening experiment in A549 SCC. (**A**) Flow cytometry analyses of A549 SCC#P3A5 **(A)** cells transduced with virus particles harboring the coding sequence for the Cas9 protein as well as the indicated sgRNA (x-axis), treated with hypoxia or not treated (normoxia). Descriptive statistics are shown as box plots within the violin plots (whiskers show 1.5x IQR). Descriptive statistic measures are listed in Suppl. Tab. 4.9 in appendix (page 165). AU = arbitrary units; FI = fluorescence intensity. (**B**) Western blot analysis corresponding to the FC data shown in (A). Arrows show specific protein bands; asterisks indicate unspecific bands. wt = wildtype.

2.3.1 Genome-wide knockout screen proposes several HIF regulatory proteins

To identify novel negative HIF pathway regulator proteins - proteins that downregulate HIF signaling under normoxia as e. g. PHD proteins - genome-wide CRISPR/Cas9-based KO screen experiments were performed in two biological replicates under normoxic conditions using the G141 5xHRE HIF2α-ODD=UnaG-V5 SCC#A1 FRS.

An outline of the screening procedure until the day of harvesting is shown in Figure 2.16. In brief, ten million G141 SCC#A1 cells were seeded and transduced with viral particles containing the human genome-wide CRISPR Brunello knockout pooled library [37]. To increase the probability that each cell takes up only one lentivirus, transduction was performed with MOI 0.4. To ensure that every sgRNA is represented in the cells, a coverage of 50x was used (76,441 sgRNAs x 50 : 0.4 MOI = approx. 10,000,000 cells). Cells were selected using puromycin for in total ten days. On day five and eight, cells were passaged while keeping the theoretical 50x coverage. On day eleven, cells were seeded for FACS in the density determined before (chapter 2.2.1) and again with keeping the 50x coverage. On the following day, medium was changed and FACS was performed on day 13 with the assistance of Monika Heiner and Stefanie Jarmer (Department of Medicine V, Internal Medicine, Infectious Diseases and Infection Control, Justus Liebig University Giessen).

In total, approximately 30 million cells were sorted in each of both screens. During harvesting, a proportion of cells was kept as an unsorted control sample (unsorted control; approx. 9.5 % of all cells in the screen). All sorted UnaG-positive cells and a subset of sorted UnaG-negative cells were separately seeded and kept in culture for additional seven days, as the amount of UnaG-positive cells was insufficient for direct gDNA isolation. This was due to a low percentage of UnaG-positive cells (mean percentage of 0.504 % UnaG-positive cells), which was only slightly above the background as determined by the percentage of UnaG-positive cells in NC#1-transduced cells (Fig. 2.17). Cells were harvested on day 20, gDNA was extracted, diluted and sent for further analysis to the Gene Editing Group, Institute of Biochemistry II, Goethe University Frankfurt. There, the sequencing library was prepared (by Alkmini Kalousi) and submitted to next generation sequencing (NGS) (by Yves Matthess). Subsequently, the sequencing data were assessed concerning their quality and the results were analyzed using a bioinformatic pipeline based on the MAGeCK algorithm (by Martin Wegner) [111].

2.3.1.1 NGS quality controls

In order to determine if the NGS data were appropriate for bioinformatic analysis, the sequencing depth was examined first. NGS resulted in slightly higher than theoretically expected read counts (e. g. UnaG-positive cells of screen 1: 2,097,301 reads). The expected read counts were approximately 1.7 million reads for samples collected on day 20 and 48.6 million reads for samples collected on day 13 as well as the Brunello library used for virus production. These numbers were calculated according to the theoretical amount of cells in the sample, which was determined by FACS for the day 13 samples and estimated for the day 20 samples according to the doubling time of G141 cells (20 hours, not

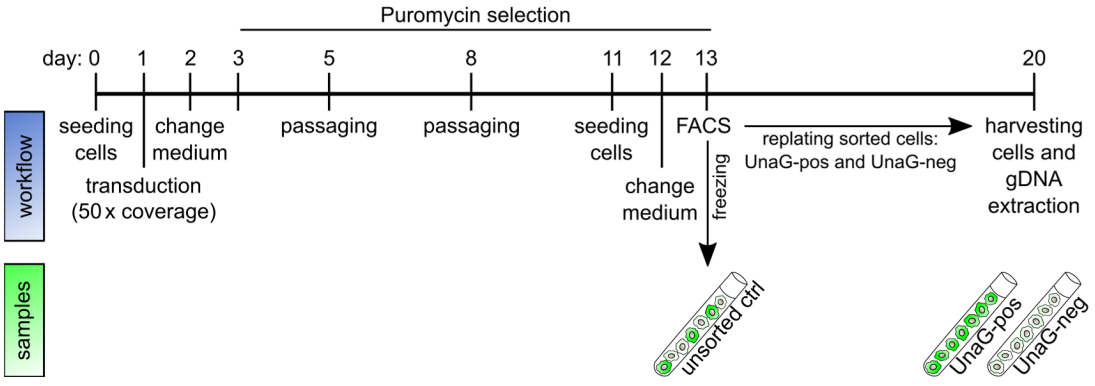

Figure 2.16: Outline of the cell culture part of the screening experiment.
Schematic representation of the workflow (blue) and the most important sample collection steps (green). The indicated samples were subjected to sequencing and further bioinformatical analysis in order to identify regulators of the HIF signaling pathway.

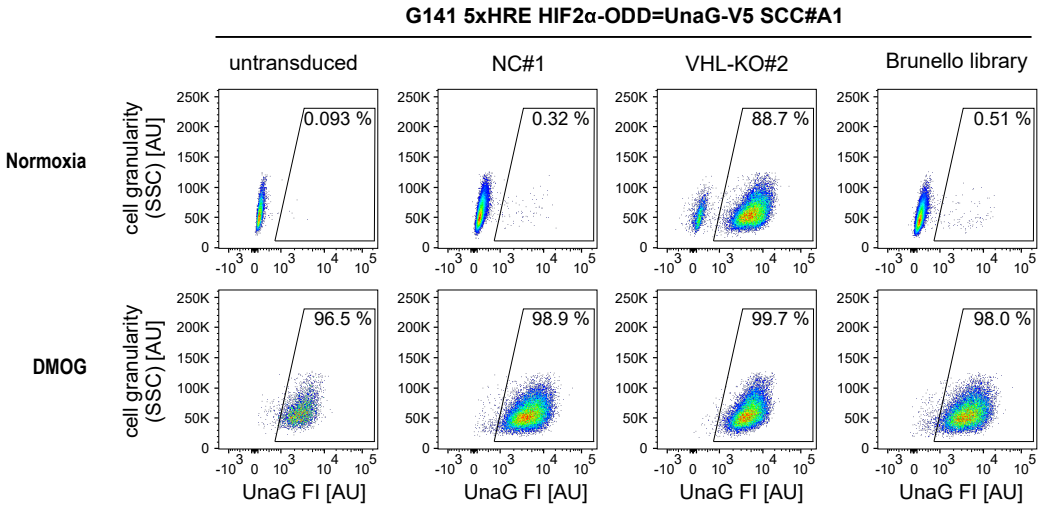

Figure 2.17: FACS analyses of the genome-wide CRISPR-KO screen and control experiments.
Dot plots obtained by FACS of screening replicate No. 1 (out of 2). Controls (first three columns) and samples (right column) are shown in the upper row. The bottom row shows additional matched controls with 18 hours of DMOG treatment. Normoxic, untreated Brunello library-transduced cells were harvested in two batches of each eight FACS tubes. Dot plot of tube #10 is shown, as its UnaG-positive cell percentage is close to the mean of all 16 tubes ($\bar{x}$ = 0.504 %). SSC = side scatter; AU = arbitrary units; FI = fluorescence intensity.

shown).

To further assess the quality of the sequencing data, raw read counts were normalized to counts per million (cpm) (see Methods section). Furthermore, the sgRNA read counts were aggregated on gene level by using the median count of the four sgRNAs per gene. Additionally, log-fold changes (LFCs) were individually calculated as the log2 fold change of the cpm-normalized sgRNA and gene read counts.
Pairwise sample correlation on cpm-normalized read counts per gene revealed that the UnaG-positive samples of screening replicate 1 and 2 correlated well (Pearson's correlation coefficient [ρ] = 0.8) (Fig. 2.18A). The same was true for the unsorted control samples (Pearson's ρ = 0.85). In contrast, the UnaG-negative samples of screening 1 and 2 did not correlate well (Pearson's ρ = 0.54). Instead, the UnaG-negative sample of screen 2 correlated surprisingly well with the Brunello library, even better than the unsorted control samples (Pearson's ρ = 0.94), indicating a mistake in the library preparation or a following step.

As a further quality measure, the dropout of essential genes [60] and the accumulation of NTCs in the unsorted control samples versus the Brunello library itself was assessed. Consistent in both screen replicates, the vast majority of sgRNAs corresponding to essential genes were depleted during the course of the experiment (Fig. 2.18B, red circles). On the other hand, NTC sgRNAs accumulated during the experiment due to the growth

advantage over cells with induced DSBs.

Taken together, the overall quality of the NGS data resulting from the genome-wide screening was considered sufficient for further analyses with the exception of the UnaG-negative sample of screen 2. As this observation suggested an error during library preparation, this sample was excluded from further analyses.

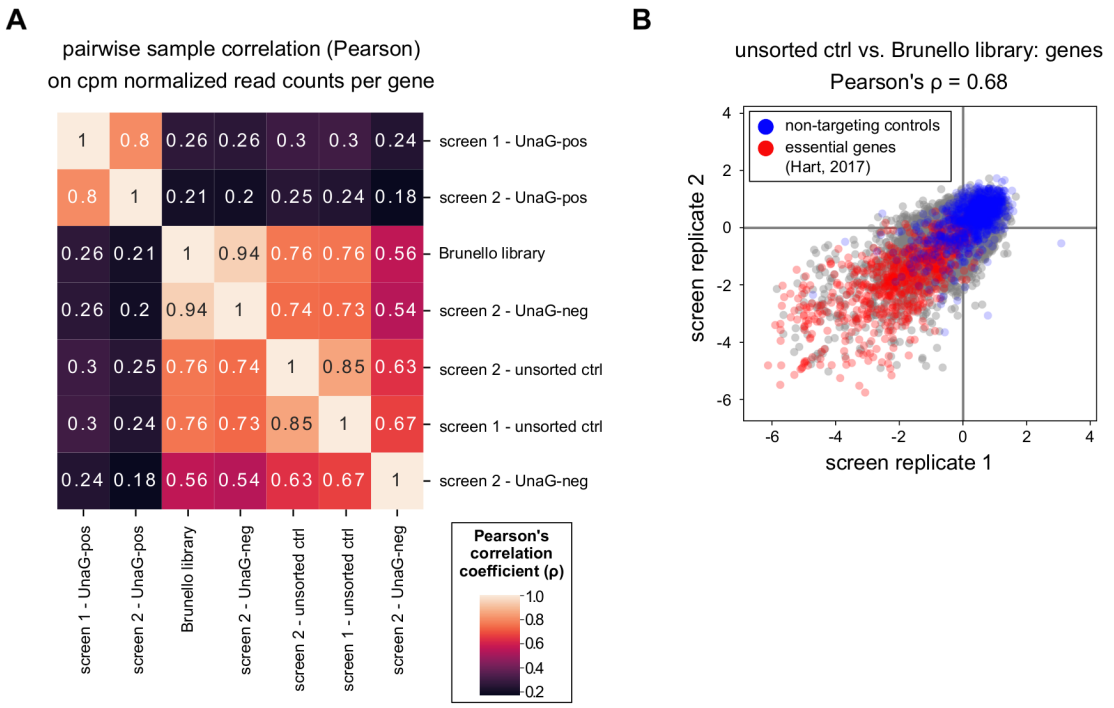

Figure 2.18: Pairwise correlation analysis of processed NGS datasets of screen replicates. (**A**) Heat map showing the pairwise sample correlation (Pearson's ρ) on counts per million (cpm)-normalized read counts per gene. (**B**) Correlation of unsorted control samples versus Brunello library of both screen replicates. SgRNAs of genes were aggregated to genes, sgRNAs of non-targeting controls were kept as sgRNAs.
Figures were computed by Martin Wegner (Gene Editing Group, Institute of Biochemistry II, Goethe University Frankfurt) and adapted by us.

2.3.1.2 Identification of novel and known regulators of the HIF signaling pathway in the screening data

To identify HIF pathway regulator proteins, sgRNA enrichment analyses using the MAGeCK algorithm was employed on raw gRNA read counts [111]. For this, the following samples were used: The UnaG-positive samples of both screens, the unsorted control samples of both screens and the UnaG-negative sample of screen 1.
In brief, to analyze the sequencing data from the screening experiments, read counts from different samples were median-normalized to counts per million (cpm). Then, sgRNA read counts were aggregated on gene level by using the median count of the four sgRNAs per gene. Subsequently, a negative binomial model was used to test if the sgRNA abun-

dance is significantly differing between the UnaG-positive samples versus the unsorted control samples and between the UnaG-negative sample and the unsorted control samples (resulting in *p*-values). Additionally, LFCs of the UnaG-positive or UnaG-negative samples in respect to the unsorted control samples were calculated.

To rank the genes, MAGeCK uses a special robust rank aggregation (RRA) algorithm. Since we excluded the UnaG-negative sample of screen 2, and, thus, lost analytical power in the LFC calculations of UnaG-negative samples, the ranking was adopted as follows: First, I decided to focus on the *p*-value of the comparison between UnaG-positive samples and unsorted control samples. Therefore, the genes were divided in six different *p*-value groups:

$p < 0.00005$
$0.00005 \leq p < 0.0005$
$0.0005 \leq p < 0.005$
$0.005 \leq p < 0.05$
$0.05 \leq p < 0.5$
$p \geq 0.5$

As a second, less stringent measure, the difference between the LFCs of the gene reads of UnaG-positive versus unsorted control and UnaG-negative versus unsorted control samples was calculated (ΔLFC). The assumption was that the higher the difference, the more likely it is that the respective gene is a true hit, as the gene is differently abundant in UnaG-positive and UnaG-negative samples (in relation to the unsorted control sample). To filter out likely false-positive hits, genes with a ΔLFC of <1 were excluded. During the final review of the top 60 genes, genes with no reads in the UnaG-negative sample were also excluded, as in this case no reliable LFC could be calculated. For this reason, one gene, ATP13A1, was excluded from the top 60 screening hits.

With the aforementioned strategy, a ranking list of top 25 screening hits was compiled (Tab. 2.2). Among the top hits were several genes whose products are known to be involved in HIF regulation, like the main HIF regulator PHD2 (rank #2). Furthermore, central components of the VHL-E3 ubiquitin ligase complex, responsible for the ubiquitination of HIFα, were scoring very high (VHL [rank #5], TCEB1 [rank #4], TCEB2 [rank #3] and CUL2 [rank #7]). These results strongly validated the screen to identify (negative) regulators of the HIF signaling pathway.

Other hits, that are less known or not known to be implicated in HIF signaling, also scored high, e. g. STK11 (rank #1), members of the SWI/SNF family (SMARCB1 [rank #6] and ARID1A [rank #15]), SOCS3 (rank #13), mitochondrial proteins (NDUFA11 [rank #8], MRPS21 [rank #10] and MRPS2 [rank #11]) and several others (Tab. 2.2, Suppl. Tab. 4.10 in appendix).

Rank	Gene-ID	Protein Name	*p*	ΔLFC
1	STK11	LKB1	0.00000233	9.68
2	EGLN1	PHD2	0.00000026	8.89
3	TCEB2	ELOB	0.00000026	8.86
4	TCEB1	ELOC	0.00000026	8.82
5	VHL	VHL	0.00000026	8.59
6	SMARCB1	BAF47	0.00000855	7.33
7	CUL2	Cullin-2	0.00000181	7.06
8	NDUFA11	NDUFA11	0.00003548	6.83
9	MANEAL	MANEAL	0.00004999	5.88
10	MRPS21	MRPS21	0.00002409	5.80
11	MRPS2	MRPS2	0.00000285	5.63
12	SOCS3	SOCS3	0.00000026	5.60
13	ORM2	ORM2	0.00003963	5.11
14	AIP	AIP	0.00000285	4.93
Excl.	ATP13A1	AT131	0.00000803	4.56
15	ARID1A	ARID1A	0.00004170	4.45
16	AHR	AHR	0.00000026	4.36
17	LIPT2	LIPT2	0.00000803	3.71
18	RPUSD3	RPUSD3	0.00000389	2.94
19	ACO1	ACO1	0.00005569	12.18
20	BOLA3	BOLA3	0.00007589	9.12
21	DNAJC19	TIM14	0.00015410	8.03
22	FASTKD2	FASTKD2	0.00026444	7.68
23	CDCA7L	CDCA7L	0.00041310	7.21
24	NDUFA8	NDUFA8	0.00046956	6.75
25	CBFB	CBFB	0.00006242	6.66

Table 2.2: Top 25 hits of the screenings ranked by *p*-value and ΔLFC.
Genes identified by the genome-wide CRISPR/Cas9-mediated knockout screening using the FRS G141 5xHRE HIF2α-ODD=UnaG-V5 SCC#A1. Hits were ranked by first *p*-value group, followed by ΔLFC.
p = *p*-value of the comparison between UnaG-positive and unsorted control cells using a negative binomial model within the MAGeCK algorithm; LFC = log fold change of a gene found in UnaG-positive or UnaG-negative cells compared to unsorted control samples; ΔLFC = difference of the LFC of UnaG-positive minus UnaG-negative cells; Excl. = Excluded gene from further analyses.

2.3.2 Validation of hits using an independent sgRNA

In order to perform the validation experiments, first, the set of control sgRNAs was expanded. As a DSB control without influence on HIF signaling, a sgRNA targeting the PPP1R12C gene was selected. Furthermore, the NTC#29 sgRNA from the Brunello library was chosen as a non-targeting control, as this NTC did not show any impact on our FRS during the screenings. These sgRNAs were cloned into the (p)LentiCRISPR v2 (Puro) plasmid, virus particles were produced and G141 SCC#A1 cells were transduced with them. After puromycin selection, cells were seeded, treated with hypoxia or DMOG or kept untreated. Whole-cell protein lysates were prepared and the impact of the cho-

sen controls on HIFα or PHD levels was monitored by western blot analysis. The results clearly showed that neither HIF2α, HIF1α nor PHD2 and PHD3 levels were significantly different between untransduced cells and the cells transduced with control sgRNAs in the three tested conditions (Fig. 2.19). Only a slight increase in the FR levels (shown by the V5 blot) was observed under hypoxia. As the experiments to validate the top ranking hits were planned in normoxia, the novel sgRNAs were considered appropriate controls.

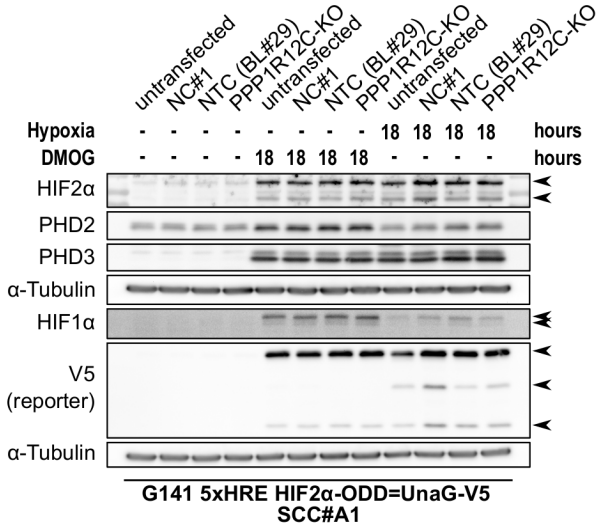

Figure 2.19: Selection of controls for screening hit validation experiments.
(**A**) Western blot analysis of the former non-template control (NTC) NC#1 as well as the newly selected controls (NTC#29 from the Brunello library and PPP1R12C-KO) without treatment or with 18 hours of hypoxia or DMOG (1 mM) treatment. Arrows show specific protein bands.

To confirm the key screening hits, sgRNAs targeting genes of the top 25 screening hits were designed using the GPP tool of the Broad Institute (https://portals.broadinstitute.org/gpp/public/). Caution was taken that the designed sgRNAs were not already part of the Brunello library and therefore independent of the screening. The hits TCEB1 and -2, VHL, CUL2 and PHD2 were excluded from the validation experiments, as they are already well-described regulators of the HIF signaling pathway.
All designed sgRNAs were cloned into the (p)LentiCRISPR v2 (Puro) plasmid, followed by virus particle production and transduction into the FRSs G141 SCC#A1, G141 SCC#B11 and A549 SCC#P3A5. The control sgRNAs verified above and VHL-sgRNA#2 as PC were transduced in the same way in parallel. Cells were further handled as in the screening experiments, performed in a smaller scale. On day 13, cells were harvested and analyzed by FC (Fig. 2.20, 2.21 and 2.22). For comparison, gates were set to define the UnaG-positive cell percentage in the measured population.
To define a threshold for successful validation of a screening hit, the mean of the UnaG-positive percentages of cells transduced with NC#1, NTC#BL29 (not shown in dotplots) and PPP1R12C-KO sgRNAs was calculated and multiplied by two, resulting in a threshold

of 0.31, 0.23 and 0.55 for G141 SCC#A1, SCC#B11 and A549 SCC#P3A, respectively. If a higher UnaG-positivity percentage was measured in the cells transduced with an sgRNA targeting a top ranking hit, the hit was considered validated. For the FRS G141 SCC#A1, 15 hits were validated, while 18 hits were validated in G141 SCC#B11 and 8 hits in A549 SCC#P3A in this manner.
The results were summarized and ranked according to the rank sum of their performances in the individual FR cell lines in Table 2.3. Finally, eight genes were chosen (Tab. 2.3, rank 1 to 7 and AIP, in bold italics) for further exploration.

To address that the eight identified gene products are true regulators of the HIF signaling pathway and not only affecting the artificial FR, cells generated during the validation FC experiments were seeded and harvested after 48 hours cell culture in normoxia. DMOG treatment of the PPP1R12C-KO cells served as a control for HIF pathway induction. Whole-cell protein lysates were prepared and levels of HIF2α, HIF1α, PHD2, PHD3 and the reporter (V5 blot) were detected by western blot analysis (Fig. 2.23). All investigated G141 SCC#A1-based KO cell lines showed accumulation of endogenous HIF2α,

	G141 SCC#A1		**G141 SCC#B11**		**A549 SCC#P3A5**		
sgRNA target gene	**UnaG-pos cells [%]**	**Rank**	**UnaG-pos cells [%]**	**Rank**	**UnaG-pos cells [%]**	**Rank**	**Total rank**
SOCS3	2.84	1	1.23	8	37.20	1	**1 / 2**
ARID1A	1.88	4	2.17	3	2.80	3	**1 / 2**
ACO1	2.40	2	1.24	6	0.89	5	**3**
MRPS2	1.89	3	3.70	1	0.42	10	**4**
SMARCB1	1.64	6	1.79	4	0.60	7	**5 / 6**
LIPT2	1.24	8	1.24	7	3.67	2	**5 / 6**
BOLA3	1.04	12	3.00	2	1.50	4	**7**
MRPS21	1.74	5	0.69	11	0.39	11	**8**
NDUFA11	1.20	9	1.11	9	0.16	17	**9**
NDUFA8	1.36	7	0.54	13	0.23	16	**10 / 11**
AIP	1.10	11	1.74	5	0.03	20	**10 / 11**
CDCA7L	0.25	18	0.60	12	0.58	8	**12**
AHR	0.75	13	0.77	10	0.16	18	**13 / 14**
CBFB	0.28	16	0.18	19	0.63	6	**13 / 14**
MANEAL	0.23	19	0.42	14	0.55	9	**15**
ORM2	0.45	15	0.40	15	0.36	13	**16**
RPUSD3	1.14	10	0.38	16	0.13	19	**17**
STK11	0.75	14	0.17	20	0.33	14	**18**
DNAJC19	0.14	20	0.35	17	0.38	12	**19**
FASTKD2	0.27	17	0.31	18	0.26	15	**20**

Table 2.3: Validation of hits: Ranking of the targeted genes by UnaG-positivity percentage. Individual and total ranks according to UnaG-positivity. Genes with shared ranks are indicated by "/" and two numbers. SgRNA target genes chosen for further analysis are depicted in bold and italics. Genes with UnaG-positive percentages in grey writing are considered "not confirmed".

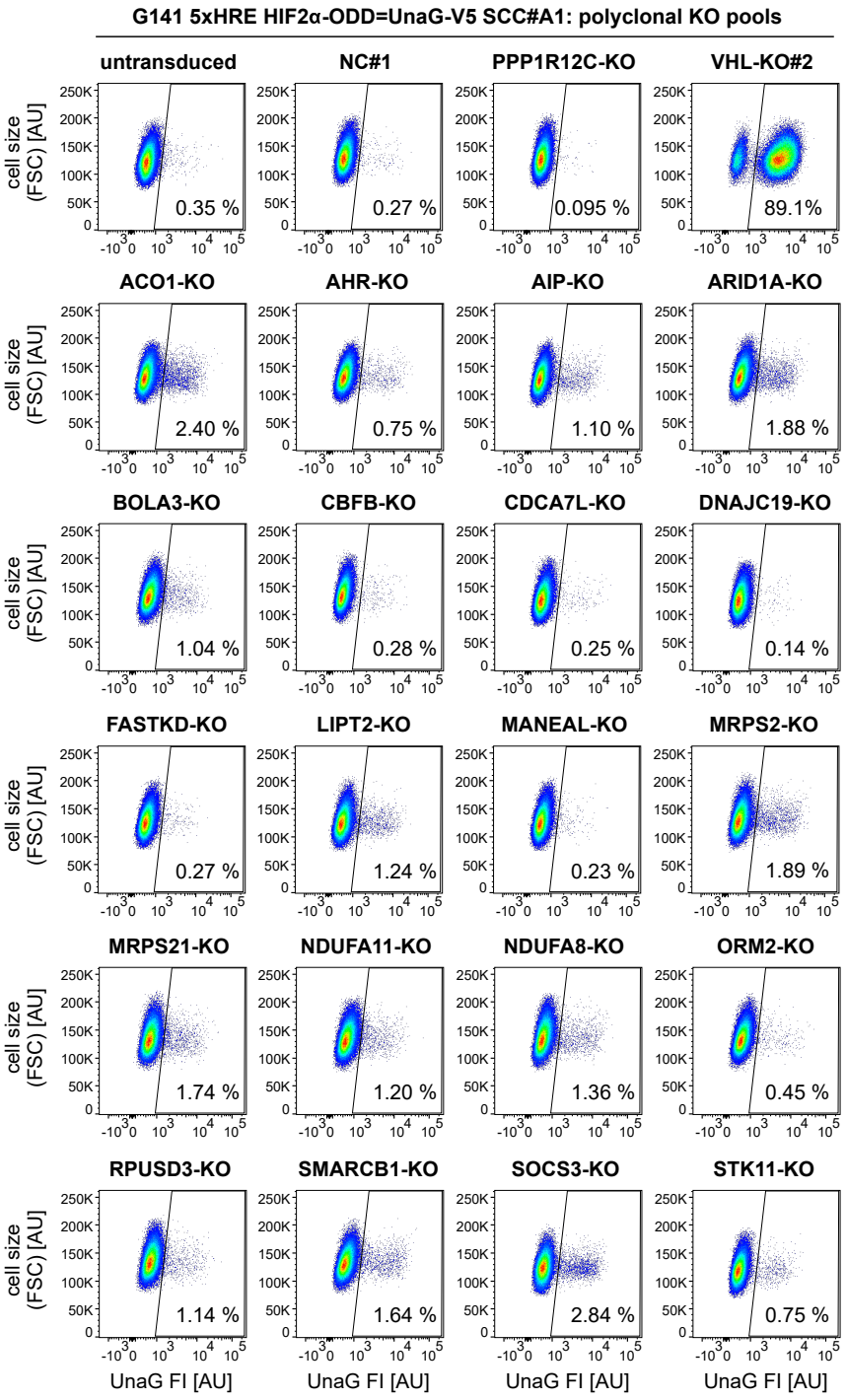

Figure 2.20: Flow cytometry-based validation of screening hits in G141 SCC#A1.
Flow cytometry analysis of the *in vitro* fluorescence reporter system G141 SCC#A1 transduced with specific sgRNAs targeting the indicated genes. The top 25 hits (excluding TCEB1, TCEB2, PHD2 and CUL2) are shown. Gates and indicated percentage refer to UnaG-positive cells. FSC = forward scatter; AU = arbitrary units; FI = fluorescence intensity.

PHD3 as well as V5-tagged FR. Changes in HIF1α levels could not be clearly observed under the same conditions. Interestingly, SOCS3-KO led to a very strong accumulation of HIF2α, PHD2, PHD3 and the V5-tagged FR. These changes in the protein levels were

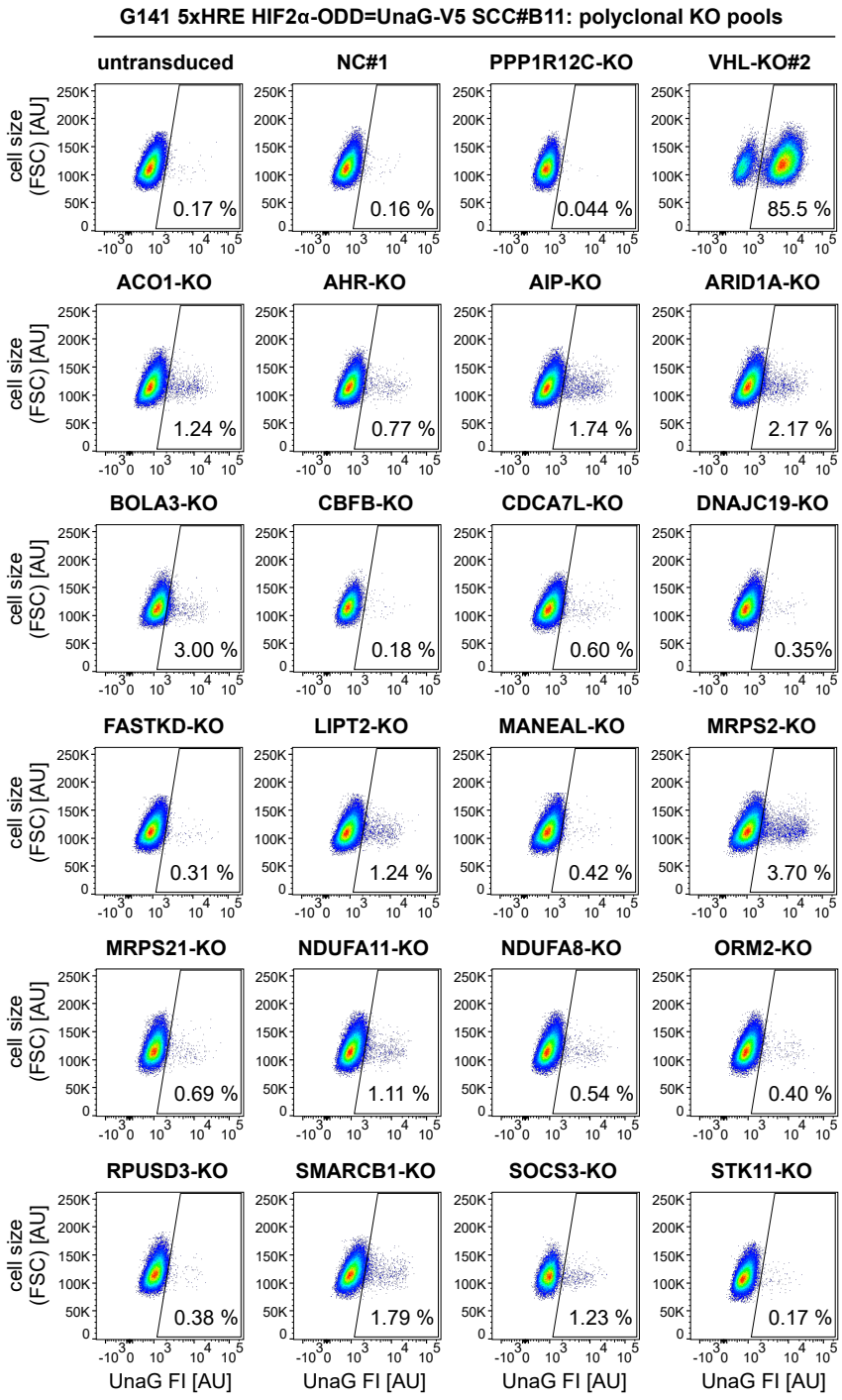

Figure 2.21: Flow cytometry-based validation of screening hits in G141 SCC#B11.
Flow cytometry analysis of the *in vitro* fluorescence reporter system G141 SCC#B11 transduced with specific sgRNAs targeting the indicated genes. The top 25 hits (excluding TCEB1, TCEB2, PHD2 and CUL2) are shown. Gates and indicated percentage refer to UnaG-positive cells. FSC = forward scatter; AU = arbitrary units; FI = fluorescence intensity.

comparable to the changes observed in the positive control VHL-KO cells.

Of note, STAT3, a binding partner of SOCS3 known to regulate the HIF signaling pathway in a SOCS3-dependent manner, was in the sixth *p*-value group ($p > 0.5$) and was also not

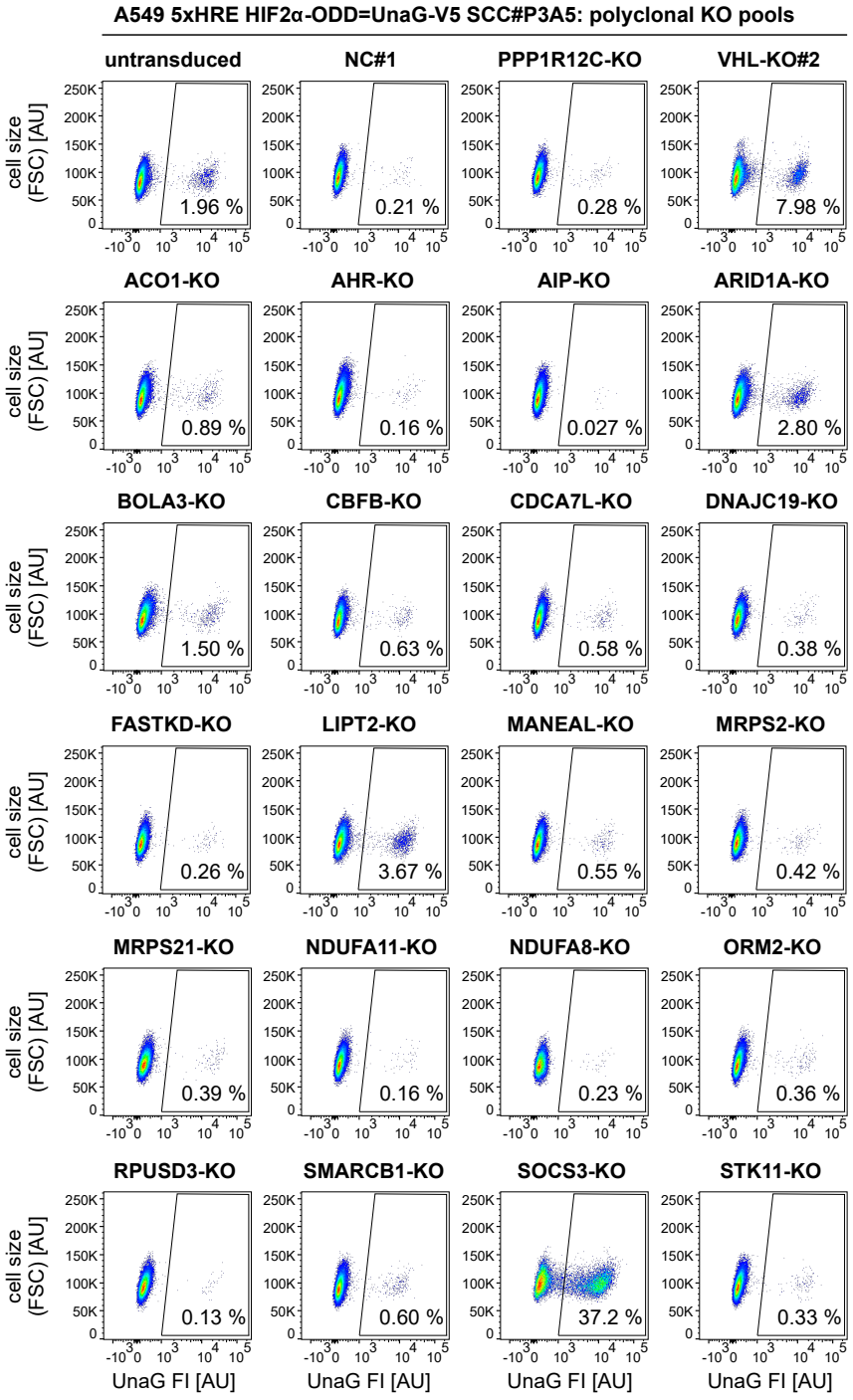

Figure 2.22: Flow cytometry-based validation of screening hits in A549 SCC#P3A5. Flow cytometry analysis of the *in vitro* fluorescence reporter system A549 SCC#P3A5 transduced with specific sgRNAs targeting the indicated genes. The top 25 hits (excluding TCEB1, TCEB2, PHD2 and CUL2) are shown. Gates and indicated percentage refer to UnaG-positive cells. FSC = forward scatter; AU = arbitrary units; FI = fluorescence intensity.

identified as an essential gene.

Taken together, these data suggest a potential novel regulatory way of the HIF signaling pathway and identify SOCS3 as a highly interesting candidate for further analyses.

In addition, the screening revealed several novel protein regulators of the HIF signaling pathway, whose functions remain to be revealed in future investigations.

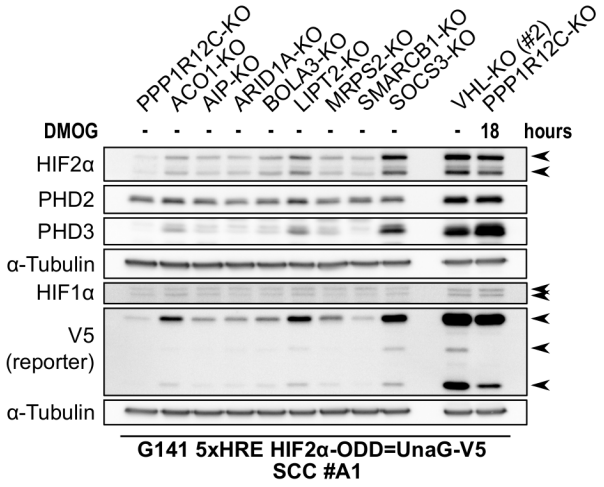

Figure 2.23: Knock-out of the selected genes increases HIF signaling pathway protein levels. Western blot analysis of *in vitro* FRS G141 SCC#A1 additionally transduced with sgRNAs targeting the indicated genes. PPP1R12C-KO cells were treated with 1 mM DMOG as an additional positive control. Arrows point to specific protein bands where multiple bands are visible.

2.4 Knockout of SOCS3 leads to stabilization of HIF in cell culture models of different tumor entities

To further confirm the effect of SOCS3-KO on the HIF signaling pathway and exclude SCC-specific effects, SOCS3 was investigated in the parental cell lines of the FR cell lines as well as in other established glioma and ccRCC cell lines.
The established glioma cell lines G141, G55(TL) and U87-MG as well as the lung adenocarcinoma cell line A549 and the VHL-deficient ccRCC cell lines RCC10 and 786-O were transduced with viral particles containing (p)LentiCRISPR v2 (Puro) plasmid harboring the SOCS3 sgRNA that worked most potently in the screening (Brunello Library SOCS3-sgRNA No. 3, in short BL#3). In parallel, control cell lines (NTC BL#29 and PPP1R12C-KO) were established as well. After 8 to 12 days of puromycin selection, cells were seeded and harvested after 48 hours, either incubated for 24 hours in hypoxia or without treatment. Subsequently, western blot analysis was performed to assess the effect of SOCS3-KO on the key HIF signaling pathway proteins HIF2α and HIF1α, PHD3 (ccRCC only) and on SOCS3 itself (Fig. 2.24).
All tested cell lines except G55(TL) displayed an at least moderate accumulation of HIF2α upon SOCS3-KO when cultured in normoxia (Fig. 2.24A-C, E). HIF1α protein amount was elevated less prominently in most cell lines. HIF1α levels were not remarkably altered in G55(TL) cells and in U87-MG cells they were even reduced.
After hypoxia treatment, accumulation of HIF2α protein was evident in G141, G55(TL), the ccRCC cell lines and partially A549, when comparing SOCS3-KO lines with NTC#29 or PPP1R12C-KO cell lines. However, in U87-MG cells, HIF2α levels were not changed. In VHL-deficient 786-O and RCC10 cells, PHD3 protein levels were examined and showed upregulation upon SOCS3-KO (Fig. 2.24E). In line with this, especially HIF2α levels were consistently increased in SOCS3-KO cells, despite the fact that HIFα levels are already elevated in those cells due to the VHL deficiency [97]. This suggests a VHL-independent regulation of the HIF signaling pathway by SOCS3.

Taken together, HIF2α accumulation upon SOCS3-KO was not only present in the FR cell lines but also in their parental cell lines as well as in other established glioma cell lines and VHL-deficient ccRCC cell lines. These results indicate a general, at least partially VHL-independent role for SOCS3 in the regulation of the HIF signaling pathway and exclude that the effect of SOCS3-KO on HIF2α protein is an artifact of the rather artificial *in vitro* FRSs.

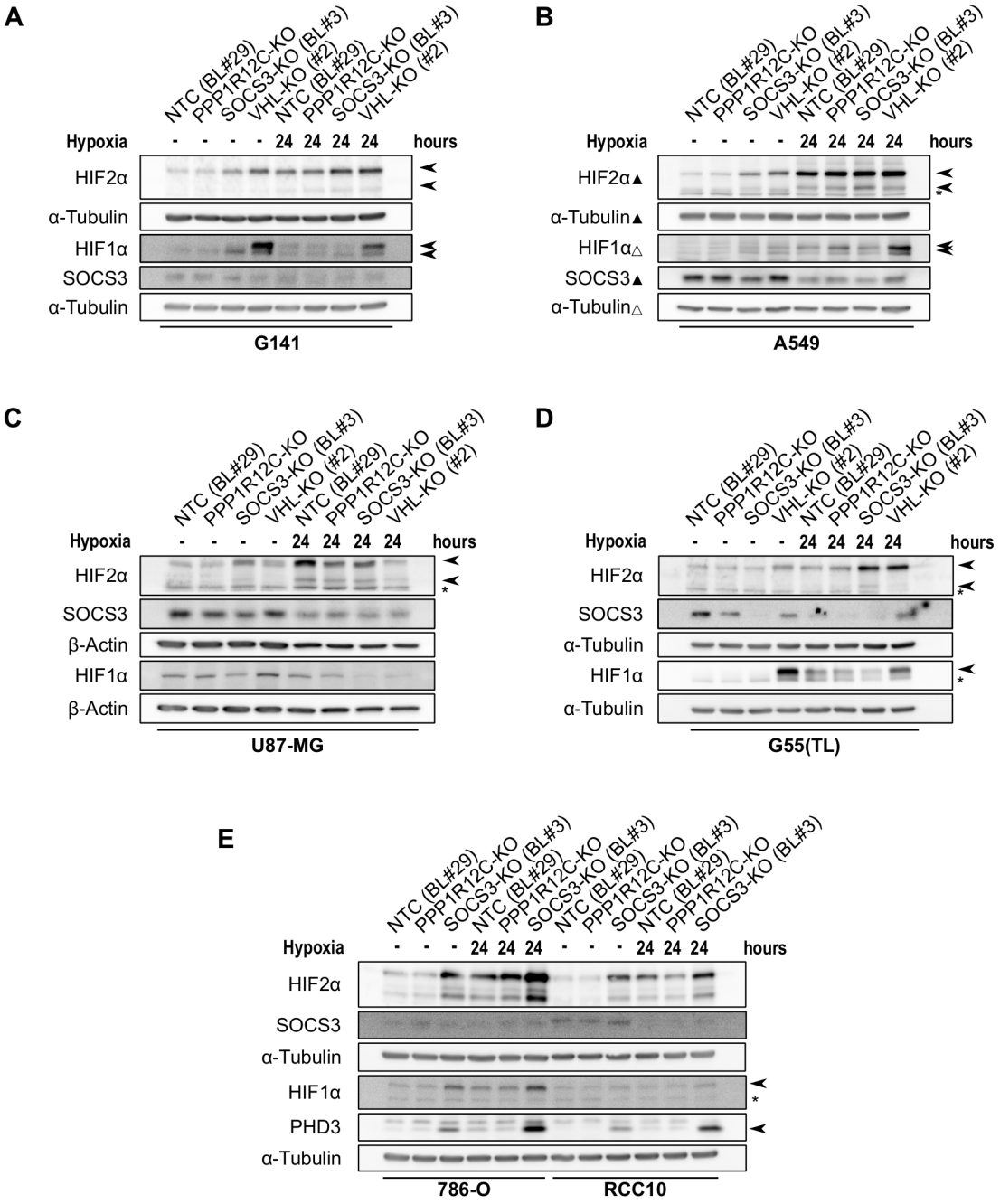

Figure 2.24: Effect of SOCS3-KO on HIF pathway protein levels in different cell lines. Western blot analyses of the parental cell lines of the *in vitro* FRSs used in this study, G141 (**A**) and A549 (**B**), as well as further glioblastoma cell lines G55(TL) (**C**) and U87-MG (**D**) and the VHL-deficient renal cell carcinoma cell lines 786-O and RCC10 (**E**). Cells were either not treated or incubated in hypoxia for 24 hours. Arrows show specific protein bands; asterisks indicate unspecific bands; triangels indicate which blots belong together (A549 cells only, due to changed order of blots). The western blot analyses shown here were in part performed with the technical assistance of Weam Maddadeh (Institute of Neuropathology, Justus Liebig University Giessen).

3. Discussion

Brain and lung cancer are major health problems worldwide. Glioblastoma, the most common malignant brain tumor in adults [47], as well as lung adenocarcinoma, the most common lung cancer subtype [190], are solid tumors with diverse TMEs. As extensively documented in the literature and discussed in numerous review articles (for recent ones see [10, 148]), hypoxic niches of the TME contribute to cancer progression by sustained activation of the HIF signaling pathway. This can be caused - additionally or alternatively to hypoxia - by genomic mutations or epigenetic regulation, for example. In any case, aberrant HIF signaling in tumors can foster invasion, metastasis, immune escape and overall tumor progression [155, 197]. However, the HIF signaling pathway and its regulation is complex and not yet fully understood. Therefore, the aim of this study was to deepen the understanding of the HIF signaling pathway regulation in glioblastoma and lung adenocarcinoma by identifying novel protein regulators.

In order to achieve this goal, *in vitro* FRs were developed to monitor the activation status of the HIF signaling pathway in cell lines. First, we focused on PHD3 and proteins specifically regulated by PHD3, as PHD3 was shown to link oxygen-sensing via the HIF signaling pathway with several hallmarks of cancer, such as EMT, invasion and metastasis [38]. Then, we moved on to use the ODD of HIF2α as POI, because HIF2α was reported to be mainly regulated by PHD3 [72]. Moreover, it seems to be the master regulator of prolonged HIF signaling activity and was also implicated in hypoxic induction of invasion processes in tumors [72].
On the basis of the HIF2α-ODD, novel FRSs were developed, genome-wide CRISPR/Cas9-mediated KO screenings were performed, HIF pathway regulators were identified and selected top hits from the screen were independently validated. A regulator with an unexpectedly strong impact on HIF signaling, SOCS3, was further investigated and subjected to broader validation.
In this chapter, the results of this study are summarized, interpreted and discussed. Moreover, limitations are highlighted and recommendations for further research are proposed.

3.1 Development of the fluorescent reporter system

3.1.1 Selection of cell lines

Given the fact that tumor cell lines display remarkable diversity in their molecular responses to reduced oxygen levels, as it was also observed in our laboratory [64], glioblastoma and lung adenocarcinoma cell lines with different HIF pathway responses were selected to construct *in vitro* HIF signaling pathway FRSs.
Comparing the different glioblastoma cell lines G55(TL), U87-MG, HGBM and G141, all cell lines reacted to hypoxia treatment by accumulation of HIF2α and HIF1α, although to different extents and with different steady-state levels of the proteins in the normoxic control cells (Fig. 2.1A). In line with previous results, G55(TL) cells showed a pronounced accumulation of HIF1α and PHD2, while G141 cells rather accumulated HIF2α and PHD3, indicating a tight connection between the different HIF and PHD isoforms in the respective cell lines [64]. To cover cell lines with a well-detectable response to hypoxia either focused on HIF1α or HIF2α, G55(TL) and G141 were selected as model systems for the FRSs.

Additionally, all tested glioma cell lines harbored *TERT* promoter point mutations and lacked *IDH1* and *IDH2* mutations, presenting the typical glioblastoma-specific genetic background and confirming their origin [165, 118].

To be able to expand the upcoming findings to a cancer entity prone to metastasize to the brain [80, 157], the breast cancer cell lines MDA-MB-231, MDA-MB-231-Br, the lung adenocarcinoma cell line A549 and immortalized human embryonic kidney cells (HEK293T) were compared regarding their HIF signaling response to hypoxia (Fig. 2.1B). As in G141, the A549 cell line accumulated predominantly and long-lasting HIF2α and PHD3 protein upon hypoxia exposure, while the other cell lines typically exhibited reduction of HIFα levels after a peak at 24 hours of hypoxia treatment and no pronounced PHD3 accumulation. As the model cell line should be useable for PHD3 ET as well, A549 cells were chosen as a model system for cancers prone to metastasize to the brain.

Admittedly, established cell lines might not represent the most adequate model for glioblastoma and lung adenocarcinoma as they are growing as monolayers and, moreover, lack the complex heterogeneous TME. For example, 3D organoids or even animals developing tumors based on certain mutations are model systems closer to the tumor patient situation. However, these model systems are less suitable for genome-wide screenings, where millions of cells have to be modified. Therefore, it was suggested to start out with a less complex model system for the screening and then carry out further studies on potential screening hits in more complex model systems closer to the clinical setting [36].
Additionally, development of the FR itself would not have been feasible in those complex

model systems. Hence, *in vitro*-cultured tumor cell lines were selected as model systems representing a trade-off between biological meaningfulness and methodical feasibility.

3.1.2 Selection of FR components

3.1.2.1 PHD3 is not a suitable POI for ET-based screening

Recently, PHD3 was shown to link oxygen-sensing via the HIF signaling pathway with EMT, metastasis and therapy resistance in lung cancer [38]. In order to investigate the regulation of PHD3 as part of the HIF signaling pathway further, the endogenous *EGLN3* gene locus of G55(TL) or A549 cell lines was tagged with different fluorescent proteins and tags (Tab. 2.1). For this, co-transfection of a sgRNA/Cas9-expressing plasmid and a donor plasmid, containing the fluorescent protein and tag, was performed (Fig. 2.2A). Several iterations of donor plasmids were tested (Tab. 2.1#1 to #4). However, no accumulation of visible fluorescence could be detected by microscopy or flow cytometry measurements under conditions leading to PHD3 accumulation. This lack of fluorescence in the tagged cells suggested that the endogenous levels of PHD3 were not sufficient to be detected with flow cytometry or standard microscopy. Hence, this reporter system was considered not usable for the intended screening procedure using FACS as the method for discrimination of the populations.

These data indicated that it would be in general difficult to use endogenous proteins as the basis for the FR. Thus, the following approaches were based on exogenous, artificial reporters for the activity status of the HIF signaling pathway. Nonetheless, the method of ET is a powerful tool that might be used to investigate the underlying mechanisms of HIF regulation of screening hits found in this study. For example, putative HIF regulatory proteins without available antibodies could be tagged and detected by western blot analysis via the introduced tag, e. g. after tag-mediated immunoprecipitation.

3.1.2.2 Reported PHD3-regulated POIs are not suitable as FRs

Several proteins were found to be directly regulated by PHD3. The stability of some of those was described to be dependent on hydroxylation, for example p53 [158], ATF4 [95], EPOR [62] and ADRB2 [208]. Others can be modulated by PHD3 by other means, e. g. EGFR where PHD3 mediates the internalization of the receptor by functioning as a scaffolding protein [63]. To elucidate the regulation of PHD3 as a main modulator of the HIF signaling pathway, reported PHD3-regulated proteins were employed as POIs for the FR.

Here, the focus was set to hydroxylation-dependent regulation of PHD-regulated POIs, as hydroxylation is the main modification regulating the HIF signaling pathway. Thus, the cytosolic domains of the reported PHD3-regulated proteins EPOR and ADRB2 were

attached to a Luc2/tdTomato-Flag fusion protein, transfected into G55(TL) cells and subjected to a DLR assay (Fig. 2.3).
As expected, transient transfection of both reporters into PHD3-KO cells led increased reporter signal intensities compared to wt cells. Additionally, overexpression of the reporters in PHD3-OE cells resulted in a reduction of the reporter levels in those cells compared to wt cells. These data strengthened the assumption that EPOR and ADRB2 are indeed PHD3-regulated proteins.
However, unexpectedly, 24 hours of PHD hydroxylase activity inhibition by DMOG did not result in increased reporter levels in PHD3-OE cells compared to non-treated cells (Fig. 2.3B). Proper functioning of the inhibitor DMOG was controlled for by transient transfection with a 9xHRE FLuc plasmid, which showed the expected accumulation of the reporter in PHD3-OE cells treated with DMOG (Fig. 2.3B, right panel).

While performing these studies, Cockman *et al.* reported the reactivity of all previously identified reported PHD-regulated proteins with recombinant PHD enzymes [24]. Interestingly, they could not detect any prolyl-hydroxylase activity on any of the reported PHD-regulated proteins, among them EPOR and ADRB2, although they were using different mass spectrometry methods, radiochemical assays and employed several controls to validate their approaches. However, they also acknowledged the possibility that they missed hydroxylation as the assays were optimized for the HIF controls. Moreover, the hydroxylation of non-HIF proteins might be more complex than hydroxylation of HIFα, e. g. requiring adapter proteins available in cells but not in their hydroxylation assays.
Of note, the study by Cockman *et al.* questions only the hydroxylation of non-HIF substrates by PHD proteins and does not comment on hydroxylation-independent functions of PHD proteins, e. g. the PHD3-mediated internalization of EGFR [63].

As the data generated in this study were repeatedly inconclusive and the study by Cockman *et al.* convincingly questioned the possible hydroxylation of non-HIF substrates by PHD proteins, the reported PHD3-regulated proteins were excluded as possible POIs for the construction of the FR.

3.1.2.3 ODDs of HIFs are suitable POIs

Stabilization and therefore accumulation of HIFα shows an activated HIF signaling pathway in the cells (Fig. 1.1). Thus, one of the most direct approaches to follow the activation status of the HIF signaling pathway is to visualize HIFα levels. As the stability of HIFα is dependent on hydroxylation of proline residues in the ODD [161, 207] and in order to create a minimal FR, only the ODDs of HIF1α and HIF2α were examined as POIs. For HIF1α, the amino acids 530 - 652 (as described in Safran *et al.* [160]) were used. During these studies, work by others was published, showing that HIF1α fragments from aa 338 to 608 [42] and from aa 530 to 603 [143, 15] can be successfully used as POIs to monitor

accumulation of HIF1α in the cells, too.
For HIF2α, the protein fragment from aa 354 to 581 was used, as it was successfully employed in previous work in our laboratory (pLenti6-ODD-Fluc-Rluc(POR) plasmid by Omelyan Trompak).

The first tested HIFα-based FR was based on the ODD of HIF1α fused to Luc2/-tdTomato. Due to the inclusion of Luc2, DLR assays were conducted to assess the reporter performance. Indeed, the DLR assay showed a slight stabilization of the reporter after hypoxia treatment compared to normoxic G55(TL) cells (Fig. 2.4B). However, accumulation of fluorescence could not be detected via fluorescence microscopy. The formation of fluorescent dots around the nucleus rather than homogenous accumulation of fluorescence in hypoxia-treated cells indicated an issue with the fluorescent protein tdTomato. Therefore, the Luc2/tdTomato fusion was exchanged with TurboGFP or mCherry and the transient transfection experiments were repeated. Essentially, the same fluorescent signal patterns were detected in these experiments. In some cases, stabilization of the reporter could be achieved after DMOG treatment, but never with hypoxia. As the same pattern was observed with different fluorescent proteins and accumulation was visible with DMOG but not hypoxia, it was hypothesized that the lack of signal accumulation might be related to the low oxygen levels in the hypoxia chamber. Since the reporter was working in the DLR assays, the putative problematic component of the FR was pinpointed to the fluorescent protein. Thus, a connection between hypoxia and malfunction of fluorescent proteins was explored. Indeed, chromophore formation of fluorescent proteins, such as green fluorescent protein (GFP), requires molecular oxygen, which can quickly become a limiting factor in hypoxia. Before the final oxidation step, the protein does not acquire visible absorbance and hence no fluorescence is emitted [61, 156, 194]. This is equally true for GFP-, DsRed- (as tdTomato and mCherry) and TurboGFP-based fluorescent proteins [57, 44]. As a result, those fluorescent proteins were considered not useful for a FR that should be usable also under hypoxic conditions.

3.1.2.4 UnaG as fluorescent reporter gene in the FRS

To date, only few fluorescent proteins were described that do not rely on oxygen for fluorophore formation. On the one hand, developed in 2007, flavin mononucleotide (FMN)–based fluorescent proteins (FbFP) are proteins that are fluorogenic in aerobic and anaerobic biological systems [40]. Furthermore, they were shown to be functional in mammalian cells as well [199].
On the other hand, a green fluorescent protein from the japanese freshwater eel Unagi (*Anguilla japonica*) was discovered recently. Similar to the fish's name, this fluorescent protein was termed UnaG [98].

As one of the aims of this study was to construct a FRS usable in different environmental

conditions, including hypoxia and anoxia, an oxygen-independent fluorescent protein was required. To find an optimal solution, four criteria had to be fulfilled:

1. The fluorescent protein has to be fluorogenic under different environmental conditions, including hypoxia and anoxia.
2. To avoid steric hindrance and dimerization or aggregation, the size of the fluorescent protein should be equal to or smaller than the POI and it must be monomeric.
3. The emission of fluorescence after excitation must be well detectable (brightness) with standard FACS systems (excitation/emission spectra).
4. The fluorescent protein must not require media supplements that might impact the HIF signaling pathway.

Fulfilling the first two requirements, FbFPs are fluorogenic even at anaerobic conditions [199] and the protein is around 260 aa (referring to "evoglow-Bs1"-FbFP), that is only slightly bigger than the POI (HIF2α-ODD around 228 aa). However, possibly violating the third demand, FbFPs display a much weaker total quantum yield than most GFP derivatives [145]. Moreover, a yet unsolved question addresses the point, whether or not expression of FbFPs could lead to an exhaustion of free flavin in the cells, leading to increased flavin biosynthesis [145]. How this would impact HIF signaling is unknown. With this in mind, FbFPs were excluded as possible fluorescent proteins for the FR.

UnaG on the other hand, in accordance with our first demand, shows fluorescence independent of the oxygen levels, as shown by experiments applying 0.1 % O_2 [98]. Furthermore, the protein consists of 139 aa and thus is smaller than the HIF2α-ODD. Additionally, UnaG is a monomeric fluorescent protein [98], in contrast to e. g. tdTomato. Fulfilling the third requirement, the brightness of UnaG is comparable to eGFP and mCherry [98]. Additionally, its emission and excitation spectra are similar to those of fluorescein isothiocyanate (FITC) and GFP, making it easily detectable with commercial FACS machines and microscopes. The final requirement for the fluorescent protein was also fulfilled by UnaG, as it binds non-covalently to unconjugated bilirubin, a heme metabolite present in the human body in all cells (albeit with varying concentrations [188]) and, importantly, in the FBS added to the cell culture medium (7-10 pmol/mL [188]).

As UnaG fulfilled all criteria for a suitable fluorescent protein for constructing the FR, it was fused to the HIF2α-ODD and transduced into G141 cells (Fig. 2.5A). As expected, FC analysis demonstrated that the HIF2α(aa 354-581)=UnaG-V5 reporter accumulated with DMOG or hypoxia treatment. However, the percentage of UnaG-positive cells without any treatment was too high for screening purposes (Fig. 2.5B) and the generation of SCCs could not solve this issue. Thus, it was hypothesized that the dynamic range between the FI of UnaG-positive and UnaG-negative cells was too low.

3.1.2.5 Inclusion of a 5xHRE motif increases the dynamic range of the FRS

HREs (consensus sequence: 5'-RCGTG-3' with R = A or G) are found in regulatory regions of certain genes, such as enhancers or promoters. Once bound by HIF dimers and their complex partners, transcription from the target genes is initiated [206, 166].

To increase the dynamic range of the reporter constructed here, a 5xHRE motif - based on the HRE found in the *VEGFA* gene promoter [42, 180] - was added upstream of the CMV promoter driving the expression of the FR (Fig. 2.6A).
Direct comparison of stably-transduced cell lines (G141 and A549) with and without the 5xHRE revealed a larger difference in fluorescence intensities between normoxic cells and cells incubated in the hypoxia chamber for 24 hours when the 5xHRE was present (Fig. 2.6B). These results clearly demonstrated that the inclusion of the 5xHRE improves the dynamic range. Also, visible accumulation of the reporter during PHD hydroxylase activity inhibition by DMOG could be shown by live-cell fluorescence microscopy (Fig. 2.7).

As inclusion of the 5xHRE increased the dynamic range but did not eliminate completely the UnaG signal in non-treated cells, SCC were generated and selected based on their signal separation. As a result, the SCCs G141 #A1 and #B11 as well as A549 #P3A5 showed the smallest overlap between the fluorescence intensity distributions of the normoxic versus the hypoxic or DMOG-treated cell populations and were chosen for further studies.

While inclusion of the 5xHRE supported the construction of a highly-responsive FRSs, it also added another layer of complexity to the reporter. Without HREs, the reporter signal intensity was only dependent on the stability conveyed by the HIF2α-ODD fragment. With adding the 5xHRE, changes in endogenous HIFα levels can also influence the signal intensity, as binding of endogenous HIF dimers to 5xHRE increases FR transcription. This has to be considered when interpreting the results of the genome-wide CRISPR screening.

3.1.2.6 Single cell clones still represent the parental cell lines

Established cell lines might contain a variety of different cell states, such as it is the case for the A549 cell populations that contain both, epithelial- as well as mesenchymal-like cells [69]. Furthermore, lentiviral transduction of the FR could impact individual cells differently. These inherent variations might have contributed to the emergence of cell populations that responded non-uniformly to hypoxia or DMOG treatment. To reduce these inconsistencies and obtain reproducible and clear responses of the FR, SCCs were generated.

However, the generation of SCCs should not result in a loss of cell line-typical features, such as protein expression levels. This would be problematic, as the selected cell lines

would no longer represent their parental tumor types. Importantly, western blot analyses revealed similar protein levels of HIF1α, HIF2α, PHD2 and the mesenchymal marker N-Cadherin in G141 SCC#A1 and G141 wt cells. Only PHD3 levels were increased in the G141 SCC#A1 compared to the parental cell line (Fig. 2.10A), which might reflect the response of the cell line to the continuously expressed but readily degraded FR.

In A549 cells, the differences were more pronounced, as both the response to hypoxia and DMOG treatment were increased in the reporter SCC (HIF1α, HIF2α and PHD3) (Fig. 2.10A). Furthermore, SCC #P3A5 cells displayed lower E-Cadherin levels (epithelial marker) and higher N-Cadherin levels (mesenchymal marker). This difference is well explainable considering that A549 parental cells contain both, epithelial- as well as mesenchymal-like cells [69], displaying an EMT spectrum. Thus, the proper comparison of the SCC to its parental line would require at least the division of the cell line into epithelial- and mesenchymal-like cell populations.
As A549 SCC#P3A5 showed a rather mesenchymal-like cell state also when observed by transmitted light microscopy (Fig. 2.10C), it can be speculated that this SCC might be more aggressive than the parental cells, as Huang *et al.* could show this for more mesenchymal-like cells [69]. In any case, this difference between wt and SCC has to be taken into account when interpreting the screening results.

3.2 Optimization of experimental conditions for screening

Once the single cell clones were selected, the experimental conditions for the FACS-based CRISPR/Cas9-based knockout screen had to be determined. Thus, several critical parameters were optimized for reproducible flow cytometry results and hence for a robust screening experiment.

3.2.1 Confluency influences readout

Cell-cell contacts and density are well-known factors having considerable impact on the cell's physiological state. For instance, density-dependent regulation of VHL protein stability and subcellular localization have been demonstrated (stability in [6, 135], nucleocytoplasmic shuttling in [109]), affecting HIF-signaling. Thus, the effect of different cell population densities on the UnaG FI was investigated.
G141 SCC#A1 cells were found to be more sensitive to varying cell confluencies than A549 SCC#P3A5 cells (Fig. 2.11). In G141 SCC#A1 cells, the mean UnaG FI dropped with lower confluency and the distribution broadened, which was most evident after hypoxia treatment. Since the oxygen concentration in the cell culture medium in the hypoxia chamber drops dependently on how many cells consume oxygen [204], the medium of the

subconfluent cells (seeding amount 75,000 cells per well of a 6-well plate) might still contain a higher oxygen concentration than the one with more cells initially seeded and therefore a higher confluency. Hence, the HIF pathway is not yet as triggered in the subconfluent cells as in the more confluent ones. In line with that, there is also an increase in the mean UnaG FI between the cells seeded with 150,000 and 200,000 cells per well, albeit not as evident as between the 75,000 and the 150,000 seeded cells per well sample. In support of the oxygen-availability hypothesis, the broadening of the distribution is not seen in the DMOG-treated cells in which the HIF signaling pathway is activated by inhibition of the PHD proteins independently of oxygen availability. However, an increase in mean UnaG FI with increased confluency is also detectable here, as well as in the normoxia untreated controls. This supports the notion that O_2 in resting, meaning not-stirred, cultures is reaching the bottom of the dish only by diffusion, which is limited to approximately 100 to 200 µm, while the medium height in a cell culture dish usually exceeds 1 to 2 mm [204]. Thus, normoxic cells consume oxygen, thereby reducing the oxygen concentration in their surrounding medium. This would result in a lack of oxygen that could trigger the HIF signaling pathway despite being in a normoxic environment (pseudohypoxia).

Of course, other factors might contribute to a pseudohypoxic phenotype in denser cultures, such as accumulation of metabolic waste products, e. g. TCA cycle intermediates inhibiting PHD proteins. This could induce stress in the cells with accumulation of stress-induced ROS that might activate HIF transcription by the PI3K/Akt/mTOR pathway axis [139]. However, the role of ROS in HIF regulation is still under debate [139] and was not investigated here.

In order to clarify whether the slightly increased UnaG FI signal with increasing cell confluency, being a mirror of HIF signaling activity, is due to the aforementioned phenomena, different experiments could be performed. For example, HIF levels in cells whose medium was agitated during culture could be compared with cells that were not agitated at all. Furthermore, oxygen concentration could be measured with sensors in the close proximity of the cells [204]. With the aim to limit lack of oxygen in normoxic cultures, cell culture plates using a gas-permeable foil bottom instead of thick plastic as usual could also be used.

Taken together, the confluency of cell cultures prior harvesting is critical for experiments using the FRSs, as well as other tools when investigating HIF signaling. Therefore, the optimal confluency has to be experimentally determined and kept constant between experiments.

3.2.2 Harvesting and preparation of cells for FC/FACS

Reported findings and own experiments robustly demonstrate that reoxygenation after hypoxia exposure rapidly activates the PHD proteins, thereby inducing the process of HIFα protein degradation [26, 42].

As the aim of this study was to develop FRs for the identification of HIF signaling pathway regulators that can be used under various environmental conditions, such as normoxia and hypoxia, the impact of the different conditions had to be monitored after harvesting of the cells. Harvesting large amounts of cells in a hypoxia chamber is cumbersome and might not be absolutely necessary. To test this, it was analyzed whether harvesting of hypoxia-treated cells in normoxia alters the UnaG FI in comparison to harvesting in the hypoxia chamber .
The cell confluency experiments already suggested that G141 SCC#A1 cells are more sensitive to parameter changes than A549 SCC#P3A5 (Fig. 2.12), which could be observed also here. While G141 SCC#A1 cells showed a lower median UnaG FI and a slightly broader distribution when harvested in normoxia vs. hypoxia, A549 SCC#P3A5 cells did not show any differences between these two settings. This suggests that, in a hypoxic screening experiment with the FRS G141 SCC#A1, cells should be harvested under hypoxic conditions. On the other hand, this does not seem to be necessary when using the FRS A549 SCC#P3A5. However, the reason for this discrepancy is unknown and thus these findings might not apply to other G141 or A549 SCCs.

During the same experiments, the impact of using different FBS concentrations in the FACS buffer was investigated. Usually, this buffer contains around 0.5 % bovine serum albumin (BSA) (and no FBS) to avoid apoptosis, sticking of the cells to the FACS tubes and non-specific staining when staining with antibodies is necessary [46]. As UnaG requires the addition of bilirubin as cofactor for fluorophore maturation [98], BSA was replaced by FBS. Since high concentrations of FBS can cause autofluorescence and foster clumping of the cells, it was experimentally determined how much FBS is required to obtain reliable FC results. When comparing the UnaG FI of cells kept in FACS buffer containing 1 % versus 5 or 10 % FBS, only small changes were detectable but the amount of living cell dropped with decreasing FBS concentrations. Thus, 5 or 10 % FBS were used as concentrations for the FACS buffer in further experiments.

3.2.3 Effect of time between cell harvesting and FI measurement

CRISPR/Cas9-mediated genome-wide screening requires the sorting of several million cells by FACS [36], which in total takes several hours of non-stop sorting. During this time, cells are stored in ice-cold FACS buffer under normoxic conditions with limited light exposure, possibly influencing the FR signal intensity over time. Thus, it was evalu-

ated, if the cells can be harvested at once and then measured one after the other or if several batches should be prepared as a loss of UnaG FI is visible when cells are kept for a prolonged time on ice prior FACS. For this, hypoxic G141 SCC#A1 and A549 SCC#P3A5 cells were harvested and incubated on ice without light exposure for up to three hours before measurement.
Both FRSs displayed gradually decreasing median UnaG FI with increased incubation time before measurement (Fig. 2.13). However, this tends to be only a problem in the G141 FRS, as the FIs of the UnaG-negative and UnaG-positive populations are in a closer proximity and start to overlap from one hour of incubation before measurement on (compare whiskers of the box plots in Fig. 2.13A). In contrast to the G141 FRSs, the A549 SCC#P3A5 cell line does not show an overlap of the whiskers at any time point. Thus, as seen before in the other optimization experiments, this FRS is less sensitive to varying conditions.

In summary, the G141 FRS SCC#A1 is prone to loose UnaG FI signal if the cells are incubated for a prolonged time before the measurement. Moreover, this loss of UnaG FI can interfere with proper separation of the UnaG-positive and -negative populations, as their FIs are quite close to each other. Hence, one has to consider the slight loss of fluorescence after the relative short time period of only one hour when setting the gates for the sorting process. Therefore, those cells need to be harvested in batches to limit the incubation period before FACS.
Due to the fact that the UnaG-positive and -negative populations are well separated in A549 SCC#P3A5 cells, the slight loss of UnaG FI over time can be considered negligible in these cells. However, cell viability decreased with increased time on ice. Thus, even the A549 FRS should be used in a way that incubation time on ice prior measurement or sorting takes less than three hours.

3.2.4 Selection of sgRNA quality controls to monitor FRS performance

The sorting process using FACS requires reliable controls to set meaningful gates [36]. With incubation of a subset of cells in hypoxia or administration of DMOG, the UnaG-positive gates can be roughly set by using external factors. However, transduction of the FR cells with viruses containing, among other elements, Cas9 protein and a sgRNA, might induce unpredictable changes. Moreover, the effect of impacting the HIF pathway on a knockout level might result in a different extent of FR accumulation than hypoxia or PHD hydroxylase activity inhibition.
Therefore, different possible sgRNA controls were compared by FC and western blot analysis (Fig. 2.14 and 2.15). All of them were based on the (p)LentiCRISPR v2 (Puro) plasmid used also in the genome-wide Brunello library for screening. Finally, one positive

and one negative control was selected. As NC#1 (corresponding to the non-targeting control #524 in the Brunello library) was displaying the lowest impact on UnaG FI and on the key HIF pathway proteins HIF2α, HIF1α, PHD3 and PHD2, this sgRNA was used as a negative control or non-targeting control that does not induce double strand breaks. As a positive control, a sgRNA targeting VHL was chosen, as the HIF pathway was robustly activated as demonstrated by the FC and western blot results in both FRSs.
Of note, the VHL-targeting sgRNA might not only lead to accumulation of HIFα, but also to accumulation of other VHL targets, such as EGFR, Sprouty2, or ADRB2 [213].

Surprisingly, the PHD3-knockout sgRNA was not successful in inducing accumulation of the HIF2α-ODD-based FR, even if there was a clear reduction of the protein, which is only detectable after hypoxia treatment, in both FRSs (Fig. 2.14B and 2.15B). This was not expected, as HIF2α is reported to be mainly hydroxylated by PHD3 [3], while HIF1α is mainly regulated by PHD2 [12]. It should also be noted that PHD3 is reported to have no hydroxylation activity towards the N-terminal ODD (NODD) [3, 67, 196], but the FR contains both, the NODD and CODD. Hydroxylation of one proline residue should be sufficient for proteasomal degradation [67], suggesting that PHD3 should be able to mediate FR degradation. Thus, the reason for the missing effect of PHD3-KO on the FR is elusive.

In contrast to PHD3-KO, PHD2-KO led to a detectable but non-complete shift of UnaG FI signal in at least G141 SCC#A1 cells, indicating that PHD2 plays a critical role in the regulation of the FR. This is supported by the finding that PHD2 protein levels are upregulated in PHD3-KO cells in these cells, possibly compensating for the loss of PHD3. Vice versa, knockout of PHD2 increases PHD3 protein levels in both FRSs cell lines. This indicates a compensatory role of PHD3 in PHD2-KO cells on HIFα and reporter protein regulation. Interestingly, accumulation of the FR upon PHD2-KO in the A549 FRS was detected by western blot analysis, however, it did not translate into a substantial increase in UnaG-positive cell populations as shown by FC (Fig. 2.15).

Admittedly, the FR presented here is not only regulated by the stability of the introduced HIF2α-ODD but also partly by the introduced 5xHRE motif. This motif is responsible for the increased expression of the FR upon HIF pathway activation. Of note, both heterodimers HIF1α/HIFβ and HIF2α/HIFβ should be able to bind the *VEGF*-based HREs, although HIF2α seems to be more potent in facilitating the transactivation of a *VEGF* promoter Luciferase reporter construct [206]. However, a direct comparison is not possible as the 5xHRE motif used herein (5 repetitions of a 35 bp fragment -1483 to -1448 relative to the transcription start site) is way shorter and less complex than the *VEGF* promoter fragment used in the cited study (1,786 bp; -1288 to +480 relative to the transcription start site). Thus, the long *VEGF* promoter fragment contains further HREs and other transcription factor binding sites contributing to the shown transactivation activity difference.

To conclude, a PC and NC were successfully selected and verified in both FRSs. A sgRNA controlling for the generation of DSBs in a gene independent of HIF signaling pathway, and thus induction of the DSB repair pathway, had also to be included to complete the sgRNA control panel, but not for setting gates for the cell sorting in screening experiments. As detailed below, a PPP1R12C-KO sgRNA has been selected for this purpose. These three carefully selected and validated sgRNA controls can and were already used also in other projects in the laboratory (unpublished).

3.3 Screening for regulators of the HIF pathway and validation of screening hits

3.3.1 The 5xHRE HIF2α-ODD-based FRS identifies regulators of the HIF signaling pathway

In normoxia, HIFα protein levels are kept low, mainly by PHD-induced hydroxylation, followed by VHL-mediated ubiquitination and proteasomal degradation [173, 85]. However, other HIFα-regulatory mechanisms might contribute to this as well. Thus, in order to identify (negative) protein regulators of the HIF signaling pathway under normoxic oxygen levels, a CRISPR/Cas9-mediated genome-wide screening, using the FRS G141 SCC#A1 and the Brunello library as perturbation, was performed in biological duplicate experiments (Fig. 2.16 and Fig. 2.17). Quality control of the NGS data revealed contamination in one control sample (UnaG-negative sample of screen 2, Fig. 2.18A). Therefore, the MAGeCK analysis pipeline was adapted to calculate a meaningful ranking despite the missing sample (see Material and Methods section).

The ranking identified several known proteins that regulate HIF signaling, which collectively confirmed the usefulness of the experimental setting of our screening approach, the robust functionality of the 5xHRE HIF2α-ODD-based FRS and the analysis pipeline. For example, the main HIFα regulator PHD2 was ranked on #2, while several central components of the VHL E3 ubiquitin ligase complex, namely VHL itself, TCEB2, TCEB1 and CUL2, were positioned on rank #5, 3, 4 and 7, respectively. This clearly shows that the G141 5xHRE HIF2α-ODD=UnaG-V5 FRS is suitable to identify regulators of the HIF signaling pathway in a screening setting as presented here. However, a direct or indirect interaction of the putative HIF regulatory proteins with HIFα cannot be determined with our FRS only, as the HIF pathway can be disturbed by the gene knockout on several positions. These are, for example, the proline hydroxylation by PHD proteins or the asparagine hydroxylation by FIH, the ubiquitination by the VHL E3 ubiquitin ligase complex or the proteasomal degradation process.

In summary, the results clearly show that the 5xHRE HIF2α-ODD-based FRS is useful

to identify regulators of the HIF signaling pathway. Thus, this system is a novel and unique tool to investigate the HIF signaling pathway, which is only dependent on the availability of the ubiquitous bilirubin as co-factor and can be used under normoxic and hypoxic conditions. Moreover, the FR can be inserted in virtually all model systems, such as other cell lines or primary cells, *ex vivo* cultures, e. g. organoids, or *in vivo* tumor models.

3.3.1.1 Comparison to similar studies

Over the course of these studies, another research group (laboratory of James A. Nathan, University of Cambridge, UK) developed and published similar reporter systems. Burr *et al.* presented a 3xHRE SV40 HIF1α-ODD(aa530-603)-GFP FR that was introduced into the near-haploid chronic myelogenous leukemia line KBM7 [15]. Using a forward genetic screen employing gene-trap retroviruses and validation in reporter HeLa cells, they were able to validate PHD2 and VHL and identify lipoic acid synthetase (LIAS) and oxoglutarate dehydrogenase (OGDH) as regulators of HIF1α stability. Similarly to the screen presented here, the Burr screen was performed under normoxic conditions, cells were sorted for high fluorescence and insertions were identified by NGS.
In comparison to their FR, the 5xHRE HIF2α-ODD=UnaG-V5 FR developed herein possesses several additional features. First, using UnaG instead of GFP increases the application possibilities, as screenings under conditions with limited oxygen availability are possible, such as in hypoxia or in hypoxic areas of organoids or animals, e. g. hypoxic niches in a tumor. Second, the use of HIF2α instead of HIF1α might result in different screening hits, although PHD2 and VHL were identified as relevant hits in both screens. Third, including five HREs instead of only three HREs - as the used *iNOS* HRE minimal promotor region contains three HREs [107, 131] - might increase the dynamic range of the reporter system, as binding of several HIF heterodimers could increase transcription of the reporter gene. However, this should be experimentally tested. Additionally, the HREs used in the Burr *et al.* study are based on *iNOS*, while the ones used here are based on *VEGF-A* gene regulatory regions.
Another difference to the screening shown here is the use of a near-haploid cell line. This should allow for stronger phenotypes of gene knockouts, as only one copy of most genes is available in these cells (only chromosome 8 and a 30 megabase fragment on chromosome 15 are diploid [14]). Thus, loss of one gene copy cannot be compensated by the other gene copy. Often, in CRISPR/Cas9 knockout experiments, only one allele is fully knocked out while the other allele is intact or altered in a way that compensates a knockout effect. Consequently, single cell clones are isolated to gain a cell line with a full knockout background in many studies using gene knockouts by CRISPR/Cas9. As this is not possible during a screening experiment, it was also considered to use a haploid cell line, eHAP, for this screen as well in order to increase the amount of cells with a full knockout

after the perturbation was applied. In fact, this idea was discarded as such a cell line does not reflect the glioma and lung cancer background. However, despite the usage of the near-haploid cell line KDM7, only few putative HIF regulatory proteins were identified in the Burr screen [15].

Shortly later, the same group exchanged the GFP for mCherry [133], which was then used to conduct a CRISPR/Cas9-mediated screening [143]. Again, several differences in comparison to the screen presented here can be pointed out. First, their aim was to identify genes necessary for activation of the HIF pathway response under hypoxia. Therefore, they subjected the cells to hypoxia and sorted twice for the cells that remain with a low mCherry FI despite hypoxia treatment. This kind of screen can easily be conducted with the FRSs shown here as well, as all necessary controls and experimental conditions were already established during this study. Second, instead of the Brunello library, the Toronto human knockout library (TKO, see Tab. 1.1 for comparison) was used. This time, the authors used HeLa cells for screening, switching from the near-haploid cell line to a cell line with a hypotriploid karyotype [102]. HeLa cells were used in their previous study only for validation experiments.
These reports already illustrate how valuable a versatile screening system for the analysis of the HIF signaling pathway can be. Although the FR presented here is similar to the ones developed by the Nathan group, the aforementioned differences of the FRSs led to overlapping, but different results. This notion is supported by a comparison of the identified regulatory protein hits later in this chapter.

An interesting CRISPR-based knockout screen performed by Jain *et al.* identified gene knockouts that confer fitness defects in high or low oxygen tensions by systematically comparing knockout cells cultured at 21 %, 5 % and 1 % oxygen [76]. As a result, they found that low oxygen levels buffer the negative cell fitness effects caused by loss of mitochondrial and iron-sulfur biosynthetic pathways in normoxia. On the other hand, the effects of lipid metabolism or peroxisome gene knockouts were exacerbated by low oxygen tension [76].
In line with the screen presented here, Jain *et al.* used the Brunello library as well. Apart from this similarity, the screens have little in common, as the research questions are very different. For example, the screen by Jain *et al.* was performed using the chronic myelogenous leukemia cell line K562, which is cultured in sphere culture. Additionally, no reporter constructs were used as the screen aimed to compare fitness genes under different oxygen levels and not the regulation of the HIF signaling pathway specifically.

Another CRISPR/Cas9 screening combined several techniques shown here. Zaini *et al.* modified the endogenous *EPAS1* (HIF2α gene) locus to co-express mCherry when HIF2α is expressed [212]. Both genes are separated with a T2A self-cleaving peptide motif to enable ribosome skipping [212, 33]. With this approach, only the transcription of HIF2α can

be monitored, but not the regulation of its protein stability. However, using endogenous proteins instead of artificially overexpressed FRs has certainly also advantages. Although no direct chromatin regulator was identified in this focused CRISPR/Cas9-based screening approach, the usability of the reporter system was shown. It was demonstrated that an endogenous tagging approach of HIF2α could be promising, because the simultaneous expression of mCherry resulted in a visible shift in FI when different single cell clones were compared to the parental untagged control cell line UOK101, a VHL-mutant ccRCC cell line with accumulation of HIF2α [212].

Before the CRISPR/Cas9 KO system emerged, screenings in the field of HIF signaling were mainly performed by RNA interference using small interfering RNA (siRNA) [168, 87, 68, 19, 113, 32]. In some studies, this approach was combined with the use of small molecule libraries [68, 113].

Importantly, loss-of-function effects achieved by RNA interference or small molecule inhibitors and KOs achieved by CRISPR/Cas9 do not always lead to the same phenotypic outcome. The reasons for this may include different levels of loss-of-function, off-target effects or compensatory mechanisms [147]. In contrast to the screen performed herein and other genome-wide CRISPR/Cas9 screens, siRNA screens typically involve much less targets. Thus, these studies often concentrated on a specific enzyme family, such as kinases [168, 19] or phosphatases [87].

Although these siRNA-based screens were very similar in the method of perturbation, the readout assays were quite variable. While Hsu *et al.* used an endogenous HIF1α-NanoLuc reporter, where a luciferase gene is introduced into one allele of exon 15 of HIF1α [68], others used cell lines stably [113] or transiently [87, 19] expressing an HRE-luciferase reporter. Additionally, Schoolmeesters *et al.* used a cell imaging-based approach where HIF1α-EGFP is stably expressed [168].

The results of these studies can only partially be compared to the results of the genome-wide screen performed here. First, in contrast to our work, some of the studies were performed under hypoxia [19, 87, 113, 32]. There, SMG1 nonsense mediated mRNA decay associated PI3K related kinase (SMG1) [19] and protein phosphatase 3 catalytic subunit alpha (PPP3CA) [87] were identified as negative regulators of HIF activity in hypoxia. Perturbation of these genes did not lead to activation of the HIF pathway in our normoxia screening, and only the results of an additional screening under hypoxic conditions could be meaningfully compared to these studies.

Second, some studies focused on transcriptional activity of HIF - by using HRE-Luciferase constructs - without taking the stability of the HIF protein into consideration [87, 19, 113, 32]. As our FRSs combine monitoring of transcriptional activity and protein stability, the HIF pathway regulators identified in these studies should also be detectable with our screening but only under similar conditions, e. g. using the same cell line.

Third, one study by Dekanty *et al.* was performed in *Drosophila melanogaster* S2 cells.

Although the mechanisms mediating adaption to hypoxia are very similar in diverse animal species [32], differences in the complexity of the systems between animals are evident. However, for example, components of the SWI/SNF complex were also identified as regulators of HIF signaling in the Dekanty study [32].
Interestingly, the study by Lin *et al.* identified several compounds of different molecule classes that inhibit hypoxia-induced HIF reporter activity through targeting mitochondria and blocking mitochondrial ROS production. This suggests an essential role of mitochondria in HIF pathway regulation [113]. In line with that, the screen described here also identified several mitochondrial proteins as potential regulators of the HIF signaling pathway that were also validated (Tab. 2.3). However, as the screening by Lin *et al.* was performed under hypoxia, the effects of mitochondrial perturbations on the HIF pathway cannot be directly compared to our study. Moreover, cancer type- or cell line-specific settings may also play a role, as most mitochondrial hits could not be validated in the A549 FRS.

Taken together, although several approaches have been developed to unravel the regulatory network around the HIF signaling pathway, the FRSs described in this study outperform them in the glioma and lung cancer field of research not only by using UnaG instead of oxygen-dependent fluorescent proteins (such as GFP or mCherry) but also by using cell lines matching our research area of interest and by applying a genome-wide screening approach.

3.3.2 Validation experiments support involvement of the top screening hits in HIF pathway regulation

In general, validation experiments after screenings can be performed either using different methods or with the same method in other model systems [36]. For example, the first validation approach was used by Burr *et al.* to verify the hits from their gene trap screening using CRISPR/Cas9-mediated knockout [15]. However, often, broad and deep validations of screenings are not shown in publications, as a focus is set on one specific protein (or a specific group of proteins) that is further investigated. These selected hits are then validated in depth using several methods.

Here, in order to validate the putative HIF-regulatory proteins, a sgRNA not included in the Brunello library was used to perform a screening-independent validation. Additionally, this sgRNA was not only used in the FRS G141 SCC#A1 used for screening, but also in the FRS G141 SCC#B11 and the FRS A549 SCC#P3A5 to provide additional cell line- and clone-independent proofs. Furthermore, a PPP1R12C-KO sgRNA was included as a DSB/DSB-repair control, as this sgRNA was not enriched in UnaG-positive samples. Besides this, the NTC#29 from the Brunello library was chosen, as it was not enriched in

the UnaG-positive samples and, thus, had no influence on HIF signaling (Fig. 2.19).

In the validation experiments employing the three different FRSs, FC was used to assess the percentage of UnaG-positive cells in cell populations transduced with the respective sgRNAs not included in the Brunello library (Fig. 2.20, Fig. 2.21 and Fig. 2.22). According to the ranks in the individual cell lines, a total rank was calculated (Tab. 2.3). Using this approach, all hits were validated in one or more of the tested cell lines, although not all of them could be validated in the original screening FRS G141 SCC#A1, namely CDCA7L, CBFB, MANEAL, DNAJC19 and FASTKD2. Strikingly, several hits that were validated in the G141 FRSs could not be confirmed in the A549 FRS, such as MRPS2, MRPS21, NDUFA1, NDUFA8, AIP, AHR, ORM2, and RPUSD3. This indicates that the HIF regulatory mechanism displays cell line- or cancer type-specific characteristics.
Moreover, the top hit in the initial screening experiment, STK11 (also known as LKB1), could only be validated in the screening FRS G141 SCC#A1. This could pinpoint to the possibility that the chosen fifth sgRNA might not be as potent as the four (or a subset of the four) used in the Brunello library. Indeed, accumulation of HIF2α was detected by western blot analysis when knocking out STK11 in G141 wildtype cells with any of the two STK11-sgRNAs from the Brunello library that showed accumulation in the UnaG-positive population in both screen replicas (data not shown). Thus, it should be considered that the incomplete validation of hits might be a result of low efficacy of the chosen sgRNA rather than a false-positive screening hit.

To further validate a subset of hits and their impact on HIF2α protein levels, western blot analysis was performed in G141 SCC#A1 cells. All cell lines showed accumulation of HIF2α, supporting the involvement of the hits in HIF pathway regulation further (Fig. 2.23). Most prominently, the KO of SOCS3 increased HIF2α levels to a point that was comparable with HIF2α accumulation after PHD protein inhibition by DMOG, indicating a strong negative regulatory function of SOCS3 towards the HIF signaling pathway in normoxic conditions.

3.3.3 Top 25 hits partially overlap with known HIF pathway regulators

As all top 25 screening hits were verified at least in one FRS, they were further considered putative regulators of HIF signaling. Importantly, the identified proteins can be functionally grouped by either their association in specific protein complexes or by subcellular localization.

3.3.3.1 Mitochondrial dysfunction activates HIF signaling

While the connection between mitochondrial dysfunction and HIF signaling is becoming increasingly clear, the understanding of the underlying mechanisms is far from being complete [71, 15, 183, 77]. Here, at least nine of the top 25 hits identified in the screens, whose loss might activate HIF signaling, are directly linked to mitochondria: the mitochondrial ribosomal protein (MRP)S2 and S21 as well as RNA pseudouridine synthase D3 (RPUSD3) are involved in mitochondrial protein biosynthesis. Loss of RPUSD3 leads to defects in oxidative phosphorylation (OXPHOS), as identified in a genome-wide CRISPR/Cas9 death screen [4].
Furthermore, NADH dehydrogenase ubiquinone 1 alpha subcomplex subunit (NDUFA) 8 and 11 are subunits of the NADH dehydrogenase (ubiquinone) complex in the mitochondrial inner membrane. Loss of one of both NDUFA subunits leads to mitochondrial complex 1 deficiency, the most common respiratory chain defect [11, 193].
Additionally, the gene *DnaJ heat shock protein family (Hsp40) member C19 (DNAJC19)* is coding for mitochondrial import inner membrane translocase 14 (TIM14), a part of the TIM23 complex and thus important for the import of nuclear-encoded proteins into the mitochondria [137].
FAST kinase domains 2 (FASTKD2) is largely localized in the mitochondrial inner compartment and was linked to cytochrome C oxidase deficiency [54]. In addition, members of the FASTK family were shown to be altered in several cancers [121].
Apart from this, lipoyl(octanoyl) transferase 2 (LIPT2), as well as BolA family member 3 (BOLA3) are involved in the mitochondrial lipoylation pathway [105]. There, LIPT2 catalyzes the transfer of octanoic acid to lipoate-dependent enzymes and BOLA3 produces iron-sulfur clusters to support the maturation of lipoate-containing proteins and the assembly of the respiratory chain complexes.

Not obviously linked to mitochondria, aconitase 1 (ACO1) is a mostly cytoplasmic enzyme and regulates the levels of iron inside the cells. As shown before, loss of ACO1 leads to mitochondrial DNA instability, at least in yeast [45]. Of note, ACO2, the aconitase that is an essential protein of the mitochondrial TCA cycle [22], was not identified in the screening, nor other TCA cycle proteins (first three *p*-value groups), such as IDH1 and 2. However, not much is reported about ACO1 and even its localization is not fully clarified in the literature. Thus, ACO1 might be involved in maintaining functional mitochondria.

The connection between mitochondrial dysfunction and HIF signaling is still controversial [71]. Some experimental evidence suggests that OXPHOS damage may not change HIF regulation [35]. Other data implies that a defect in OXPHOS blocks HIF1α stabilization due to a relative increase in oxygen tension following decreased oxygen consumption due to disrupted OXPHOS [150]. Again, others indicate that HIFα accumulates when OXPHOS is impaired due to elevated ROS levels [17, 8].

As shown in the screening by Burr *et al.*, defects in the lipoylation pathway, there in LIAS and OGDH, resulted in accumulation of HIFα due to accumulation of L-2-HG and thus inhibition of PHD proteins. Interestingly, OGDH did not appear as a significant hit in the screen shown here. However, LIPT2 and BOLA3 rank very high and are implicated in the same pathway. Moreover, LIAS ranks #120, implicating that significant non-top hits even from the *p*-value group 4 could be considered as potential HIF regulatory proteins. This is supported by the finding that also the HIF-regulatory PHD3 gene *EGLN3* ranks in the same group (rank #110).

Altogether, the frequent appearance of mitochondrial proteins in the top 25 hits in this screen clearly indicates a pivotal role of mitochondrial (dys)function in the regulation of the HIF signaling pathway. Furthermore, this seems to be cancer type- or at least cell line-specific, as most mitochondrial genes, with the exception of LIPT2 and BOLA3, could not be validated in the FRS A549 SCC#P3A5. However, our results underscore the importance of mitochondrial dysfunction in HIF pathway regulation in glioblastoma and support further investigations into this direction.

3.3.3.2 SWI/SNF complex and HIF signaling

SWItch/sucrose non-fermentable (SWI/SNF) complexes are chromatin remodeling complexes containing eight to twelve subunits including an ATPase [90, 128]. Several of this subunits are shared between different SWI/SNF complexes, including one of the genes identified as HIF regulatory gene here, namely SWI/SNF related, matrix associated, actin dependent regulator of chromatin, subfamily B, member 1 (SMARCB1) (also known as BAF47, INI1, SNF5) [136]. A further screen hit and part of the SWI/SNF complex is ARID1A (also known as BAF250A, SMARCF1). In 2009, Kenneth *et al.* showed that HIF1α is a SWI/SNF target, where overexpression of SWI/SNF components resulted in increased transcription [90]. There, siRNA-mediated downregulation of different SWI/SNF complex subunits resulted in reduced transcription from an HRE reporter gene and no changes in HIF1α levels in normoxia but reduced accumulation in hypoxia. These findings are in contrast to the results shown here, as loss of two specific SWI/SNF complex components resulted in accumulation of the FR in this study. However, the SWI/SNF complex subunits identified here were not specifically investigated in the Kenneth *et al.* study [90]. Thus, their findings might not apply to all SWI/SNF subunits.

Interestingly, approximately 25 % of all cancers harbor mutations in subunits of the SWI/SNF complex, mostly in the BAF subunits [134, 163]. For example, SMARCB1 mutations are found in nearly all cases of rhabdoid tumors. Furthermore, ARID1A mutations are prevalent in several cancers with a prevalence of up to 50 %, such as different ovarian cancer types and gastric adenocarcinoma. This makes ARID1A the most common SWI/SNF subunit being mutated across cancer types [134].

As SMARCB1 is a shared subunit of several SWI/SNF complexes, it is interesting to notice that ARID1A was so far only described as part of the canonical BAF SWI/SNF complex subfamily [134]. However, apart from those two subunits, none of the subunits - neither shared ones nor subfamily-dependent ones - were significantly enriched in the screening presented here. This could indicate a SWI/SNF complex-independent role of SMARCB1 and ARID1A in the regulation of HIF in G141 glioblastoma cells. Interestingly, SMARCB1 has been shown to act as an E3 ubiquitin ligase in complex with CUL2, elongin (ELO)B and ELOC [112], thus sharing structural similarities with VHL-containing and other ubiquitin ligase complexes [16].
Another possibility is that these two subunits are essential in G141 cells, while the loss of the other subunits can be compensated for to exert the HIF restrictive role in normoxia.

Remarkably, both hits of the SWI/SNF complex could be validated in G141 and A549 FRSs, indicating that the mechanism of action is not specific to a certain cancer type. However, no information is available on whether knockout of other subunits of the SWI/SNF complex induces HIFα accumulation in A549 cells, as the screen was only performed in the FRS G141 SCC#A1.

Taken together, little is known about the interplay between the SWI/SNF complex and the HIF signaling pathway so far and conflicting results to our screening have been reported at least concerning HIF1α. Therefore, further investigation into unraveling this connection is needed.

3.3.3.3 Role of aryl hydrocarbon receptor complex in HIF signaling

Another two screening hits identified here are the aryl hydrocarbon receptor (AHR) and the aryl hydrocarbon receptor-interacting protein (AIP) (also known as XAP-2). AHR is a ligand-activated transcription factor that is - as well as HIFα proteins - involved in metabolic reprogramming towards higher (aerobic) glycolysis rates [50]. In glioblastoma, AHR was found to be regulated by tumor environmental tryptophane derivatives. In immune cells, AHR cooperates with HIF1α to control immune cells [127].
Since it is known that glioblastoma show aberrant tryptophan catabolism and glioma cells produce the tryptophan-based AHR ligand kynurenine, it was suggested that the kynurenine-AHR pathway contributes to glioblastoma tumor progression [142].

AHR and AIP are part of the AHR/HSP90/cellular sarcoma (c-SRC) complex. This complex is triggered by ligand binding, followed by conformational changes leading to exposure of the protein kinase C target site. Phosphorylation of this site leads to dissociation of the complex and translocation of AHR to the nucleus, where it binds to HIF1β (also known as ARNT) and initiates target gene transcription [50]. With that, AHR and HIFα share at least two interactions partners, namely HSP90 and HIF1β.
Moreover, AHR and HIF1α seem to regulate metabolic remodeling in a staggered manner

in lymphocytes, where HIF1α facilitates the early reprogramming, followed by AHR on a later time point. Then, AHR is suspected to induce the degradation of HIF1α by increased PHD protein expression [127]. In line with the fact that loss of either AHR or AIP results in accumulation of the FR described here, Mascafroni *et al.* also reported increased HIF1α expression in Ahr^{mut} T cells as well as increased AHR binding to PHD protein genes [127].

These findings again support the functionality of our FRSs and the screening performed with them. However, it remains elusive, how the crosstalk between HIFα and the AHR-based complex in glioblastoma exactly works. In fact, the screening hits AHR and AIP could not be validated in A549 cells, suggesting cancer type-specific signaling. Therefore, in order to unravel the mechanisms, further experiments need to be conducted.

3.3.3.4 Other hits

Six other screening top hits could not be assigned to specific protein groups or complexes. As shown above, two of them were validated in one or both G141 FRSs and additionally in the A549 FRS, namely SOCS3 and cell division cycle associated 7 like (CDCA7L). Other hits could only be verified in one FRS, namely core-binding factor subunit beta (CBFB), serine/threonine kinase 11 (STK11) (also known as LKB1) and mannosidase endo-alpha like (MANEAL). Among those, CBFB and MANEAL were not confirmed as hits in the FRS G141 SCC#A1 used for the screening, suggesting that the sgRNA had a low on-target activity. Thus, these hits should be further validated and potentially investigated.

Furthermore, orosomucoid 2 (ORM2) could be verified in both G141 FRSs but not A549, indicating a cancer type-specific regulatory function as already seen with other hits.

For several of these top 25 screening hits, such as the widely unstudied proteins MANEAL, ORM2, CDCA7L and CBFB, no connections to the HIF signaling pathway could be identified in the scientific literature. However, CDCA7L was shown to be a C-MYC target gene and a protein promoting glioma proliferation [79], suggesting a link to HIF signaling via MYC.

On the other hand, two of the top 25 screening hits, STK11 and SOCS3, were already associated with HIF signaling.
STK11 is a tumor suppressor that is most often mutated in kirsten rat sarcoma virus (KRAS)-mutant lung adenocarcinoma (31 to 34 %) [182]. Of note, KRAS and STK11 are both mutated in A549 cells, therefore no HIF activation would be expected upon STK11-targeted sgRNA expression in these cells. However, appearance of STK11 as a screening hit suggests that G141 cells do not harbor a STK11 loss-of-function mutation, which should be experimentally verified.
STK11 is responsible for phosphorylation of 5’ AMP-activated protein kinase (AMPK),

which in turn inactivates other proteins by phosphorylation to restrain energy metabolism when ATP levels are low. One of the targets is mTOR complex 1 (mTORC1) [99]. As previously shown, HIFα levels depend on mTORC1 function [192]. Thus, loss of STK11/AMPK signaling might lead to upregulated HIFα levels via mTORC1 accumulation. This hypothesis could be tested and followed up in further studies.

In additions, SOCS3 was also linked to the HIF signaling pathway, which will be discussed in the following chapter in detail.

3.4 SOCS3 as a potential regulator of HIF signaling in different cancer types

So far, only a few publications indicate a link between SOCS3 and the HIF signaling pathway (65 PubMed-indexed publications with the search terms “SOCS3 AND hypoxia” and 22 with “SOCS3 AND HIF”, as of 2022-09-16) and just some of them show mechanistic findings, e. g. references [211, 200]. Yet, SOCS3 was identified as HIF regulatory gene on rank #12 in the genome-wide screening using the FRS G141 SCC#A1, indicating a strong connection between SOCS3 function and HIF signaling in these cells. Remarkably, the *p*-value, calculated by the comparison of UnaG-positive and unsorted control samples, was together with PHD2 (EGLN1), VHL, TCEB1 and 2 and AHR the lowest in the whole screen, indicating a true positive hit (see Tab. 2.2). Importantly, validation of SOCS3 as a HIF regulatory protein was successful in all three tested FRSs. Moreover, UnaG-positivity in the A549 SCC#P3A5 FRS exceeded by far all other tested screening hits, even the positive control VHL-KO (Tab. 2.3). Thus, SOCS3 ranked in the validation results on shared rank #1/2.
In western blot analysis of the screening FRS, we showed that SOCS3-KO results in an accumulation of HIF2α that is comparable with DMOG-treated PPP1R12C-KO DSB control cells (Fig. 2.23).

In order to exclude FRS-specific effects, SOCS3 was further investigated in other glioma cell lines as well as in ccRCC cell lines with VHL deficiency. These cells were transduced with the controls and SOCS3-KO lentiviral particles and examined for expression of HIFα proteins, SOCS3 and in some cases PHD3. Accumulation of HIF2α upon SOCS3-KO was robust in nearly all tested cell lines in normoxia (except in G55(TL) cells) and partially also after 24 hours of hypoxia treatment (except in U87-MG cells). These findings indicate a key regulatory role of SOCS3 in HIF pathway regulation.
Interestingly, only a modest reduction in SOCS3 levels was detected in SOCS3-KO cells (Fig. 2.24), suggesting that either a complete knockout is lethal for the cells or the sgRNA used here was not very efficient. Since essential genes did drop out in the screening experiment, the first scenario is unlikely. Thus, the incomplete knockout might be rather

explained by a low sgRNA KO efficiency.

3.4.1 Different functions of SOCS3 in cytokine-induced signaling

SOCS3 is an "essential physiological inhibitor of signaling by interleukin-6 and G-CSF family cytokines" [205] with different domains (Fig. 3.1). In short, cytokines (such as interleukins (ILs), growth factors or interferons (IFs)) bind to their receptors, thereby inducing homo- or heterodimerization and phopshorylation of receptor-associated JAK proteins [205, 82] (Fig. 3.2A). In turn, JAKs phosphorylate the receptors, which leads to the recruitment of signal transducers and activators of transcriptions (STATs) that are phosphorylated by JAKs that are now in close contact. Phosphorylation of STATs enables translocation to the nucleus, protein dimerization and hence regulation of target genes by binding to gamma activated sites (GASs) in the DNA. One of these target genes is SOCS3. SOCS3 binds to JAK1, JAK2 and tyrosine kinase 2 (TYK2) with its kinase inhibitory region (KIR) domain and inhibits further STAT activation in a negative regulatory feedback loop, especially the one of STAT3. Furthermore, SOCS3 interacts with its Src-homology 2 (SH2) domain with phosphotyrosines on JAK2 and several cytokine receptors, such as the co-receptor gp130 that is shared by IL-6, IL-11, leukemia inhibitory factor (LIF), oncostatin M (OSM) and ciliary neurotrophic factor (CNTF) - partially at the same time [91]. Additional cytokine receptors bound by the SH2 domain of SOCS3 include granulocyte colony stimulating factor receptor (G-CSFR), leptin receptor (LEP-R), EPOR, IL-12 receptor β2 (IL-12Rβ2), growth hormone receptor (GHR) and insulin receptor (IR) (summarized in [205]).

Apart from this function, SOCS family proteins contain a SOCS box domain, that is responsible for binding ELOB and ELOC, as well as Cullin-5 (Fig. 3.2B). This complex further binds to RING box protein 2 (RBX2), forming an E3 ubiquitin ligase complex, similar to the VHL complex but with another central Cullin subunit. Thus, substrates bound via the SH2 domain by SOCS3 are ubiquitinated and, thus, marked for proteasomal degradation with the help of an E1 ubiquitin-activating enzyme and an E2 ubiquitin-conjugating enzyme. Reported targets of SOCS3 specifically are insulin receptor substrate (IRS)1/2,

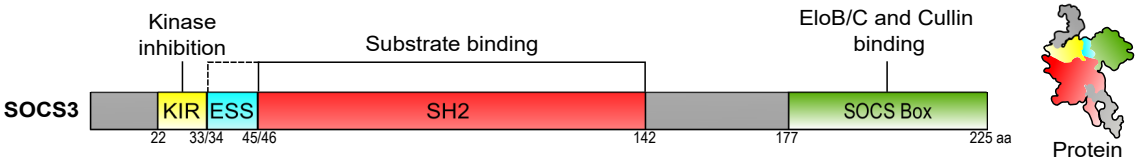

Figure 3.1: Protein domains of SOCS3.
SOCS3 consists of an N-terminal domain (grey), a Kinase inhibitory region (KIR, yellow) , an extended Src-homology 2 (SH2) subdomain (ESS, cyan), a SH2 domain (containing a PEST sequence, not indicated; red) and a SOCS Box (green). A scheme of the folded protein is depicted on the right, indicating the positions of the different domains in the protein. Protein structure is based on AlphaFold structure prediction v4, Uniprot number O14543.

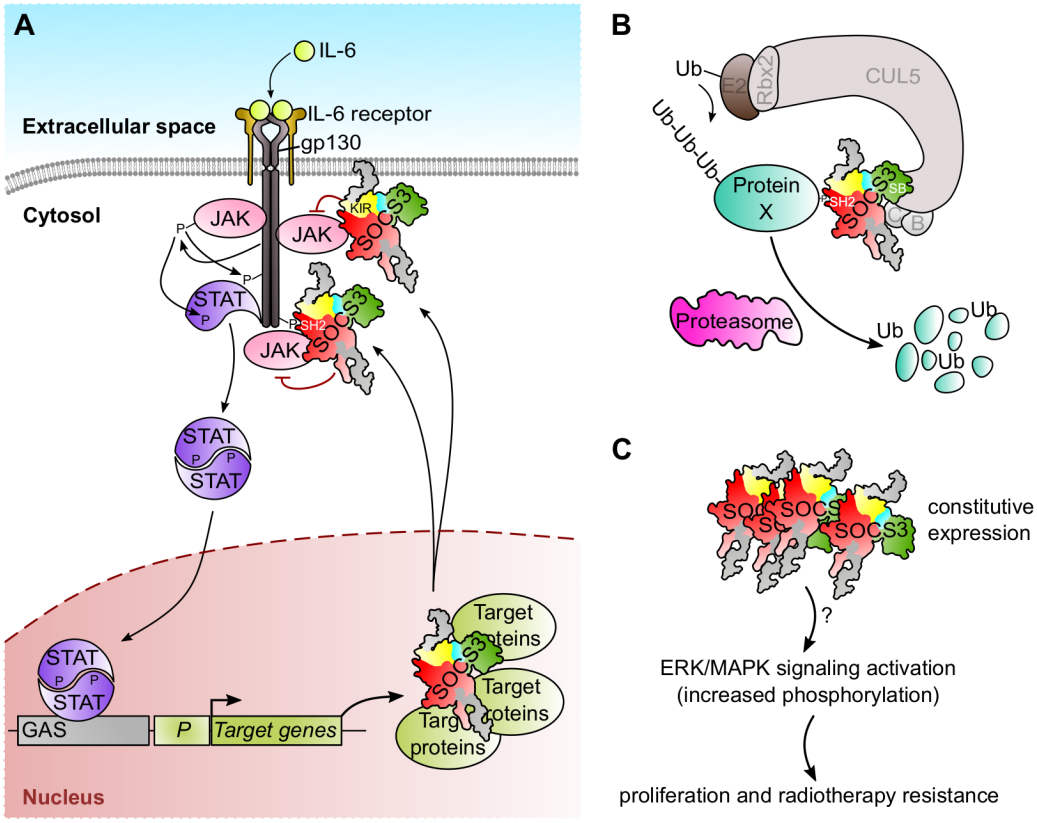

Figure 3.2: Functions of SOCS3 in cytokine-induced signaling and cancer.
(**A**) Canonical function of SOCS3 using the example of interleukin 6 (IL-6) signaling. IL-6 binds to its receptor, thereby inducing heterodimerization with gp130 and phosphorylation (P) of Janus kinases (JAKs) which in turn trigger the phosphorylation of signal transducer and activators of transcription (STATs). Activation of STATs by tyrosine phosphorylation leads to their dimerization and translocation to the nucleus, where they bind to gamma activated sites (GAS) upstream of promoters (*P*, green) to regulate transcription of target genes, among them SOCS3. SOCS3 in turn can bind to JAK via its SH2 domain (red) and inhibit JAK via its kinase inhibitory region (KIR, yellow). (**B**) Binding of SOCS3 to substrate proteins (Protein X, turquoise) via SOCS3's SH2 domain (red) triggers the assembly of the E3 ubiquitin ligase complex, where SOCS3 binds via its SOCS Box (SB, green) to Elongin B and C (B, C, both grey) and Cullin-5 (CUL5, grey). As a result, the substrate is ubiquitinated and degraded via the proteasome (pink). (**C**) SOCS3 is involved in the regulation of several other pathways, e. g. the extracellular-signal regulated kinases (ERK)/mitogen-activated protein kinase (MAPK) pathway (Zhou *et al.*, 2007). ? = mechanism unclear.

sialic acid binding Ig-like lectin (Siglec)7 and 3 (also known as CD33), indolamin-2,3-dioxygenase (IDO), focal adhesion kinase 1 (FAK1) (also known as PTK2) and G-CSFR [205].

3.4.2 SOCS3 and cancer

Since SOCS3 inhibits cytokine-induced JAK/STAT3 signaling, which drives cell growth and proliferation, SOCS3 was suspected to be a tumor suppressor gene [115]. Indeed, an

increasing amount of data suggests a role of SOCS3 in carcinogenesis [28].
In glioma, SOCS3 promoter hypermethylation, leading to decreased protein levels, was reported to be associated with a poor prognosis in a small patient cohort [126]. In line with that, loss of SOCS3 increased the invasive capacity of glioma cells [115]. Interestingly, SOCS3 promoter hypermethylation is mostly absent in glioblastoma with EGFR amplification and/or overexpression [115]. However, recent analyses using large TCGA data sets rather found that upregulation of SOCS3 is associated with poor overall survival in glioblastoma, low-grade glioma and other cancers [29]. Furthermore, SOCS3 was found to be necessary for glioma stem cell growth, and its loss in glioma stem cells led to downregulation of several stem cell fitness genes and to the upregulation of neuronal progenitor-associated genes, indicating differentiation [120].
Thus, the role of SOCS3 in glioblastoma might be context-dependent and requires further research.

SOCS3 seems to be implicated in the regulation of several other pathways besides the JAK/STAT pathway, such as ERK/MAPK signaling (Fig. 3.2C). There, in glioblastoma cells, SOCS3 is constitutively expressed and induces the activation of ERK/MAPK pathway, as shown by increased phosphorylation of ERK. A therapeutically potentially relevant finding is that blocking SOCS3 in this scenario sensitizes the cells to radiation-induced cell death [214].

3.4.3 SOCS3 and HIF signaling

According to Yokogami *et al.*, in glioblastoma, SOCS3 levels are decreased in hypoxia, enabling STAT3 accumulation and increased *VEGF* expression by binding to a sis-inducible element (SIE)-like (SIEL) element proximal of the HRE in the VEGF promoter [211] (Fig. 3.3A). In line with this, SOCS3 levels were indeed decreased in all cell lines tested after 24 hours of hypoxia treatment (Fig. 2.24). However, STAT3 or VEGF protein and expression levels were not analyzed here. Highly interesting, Yokogami *et al.* speculated about a molecular interaction of STAT3 with HIFα via common activators, such as CBP/p300, as a similar bridging mechanism involving STAT3 and Smad1 was described in the fetal brain before [140, 211]. Admittedly very speculative, those findings suggest connections between SOCS3 and HIF signaling.

Further evidence towards a link between SOCS3 and HIF pathway regulation was provided by Wan *et al.* in SCLC [200]. The authors showed that HIF1α is downregulated upon SOCS3 overexpression. Furthermore, VEGF-A and cell proliferation are also inhibited in that experimental system. These finding would be in agreement with the data presented here, showing SOCS3 downregulation-mediated accumulation of HIF2α and partially HIF1α. Mechanistically, Wan *et al.* argue that HIF1α expression is inhibited by SOCS3 via inhibition of the Akt pathway and not the STAT3 pathway (Fig. 3.3B). How-

ever, a direct inhibitory mechanism, potentially acting via the ubiquitin ligase function of SOCS3, was not proposed.

With the screening performed here, the mechanism behind the regulation of HIF signaling via SOCS3 in normoxia cannot be unraveled, as loss of HIF pathway activators, such as Akt or STAT3 pathway members, would result in a down- and not in an upregulation of the FR levels. In line with that, neither PI3K genes (such as *PIK3CA*, *PIK3R1*, *PIK3C2A* or *PIK3C3*), pyruvate dehydrogenase kinase 1 (PDK1) nor Akt (genes *AKT1*, *2* and *3*) itself appeared as screening hits ($p > 0.05$). To clarify if and to which extent Akt and STAT3 signaling are involved in the HIF-regulatory function of SOCS3, further experiments have to be conducted.

Remembering that SOCS3 can function in an E3 ubiquitin ligase complex very similar to VHL and VHL is the main regulator of HIFα proteins [129], one could speculate about HIFα ubiquitination by SOCS3 (Fig. 3.3C). This mechanism could explain why knocking out SOCS3 leads to accumulated HIF2α and HIF1α protein levels in VHL-deficient ccRCC cell lines 786-O and RCC10, as shown in Fig. 2.24E. However, until now, no data hint directly into this direction. Furthermore, SOCS3 was only shown to build complexes with Cullin-5 [7], which was also no hit in the screening presented in this study.

Another possibility to be explored is whether SOCS3 could modulate the HIF-regulatory function of VHL, e. g. by binding or modifying HIFs, ELOB/ELOC or VHL itself (Fig. 3.3D). Other indirect regulatory mechanisms involving PHDs (Fig. 3.3E) or other HIF regulators identified in the screening are also conceivable and could be considered for further investigation.

Taken together, knockout of SOCS3 results in accumulation of HIF2α in several glioblastoma cell lines, one lung adenocarcinoma cell line (A549) and two VHL-deficient ccRCC cell lines. The mechanisms behind this regulation are yet to be investigated. In the cellular model systems presented, it also remains to be clarified whether SOCS3 negatively regulates HIF2α - as has been shown for HIF1α [200] - since only the loss of SOCS3 but not its overexpression was investigated here so far.

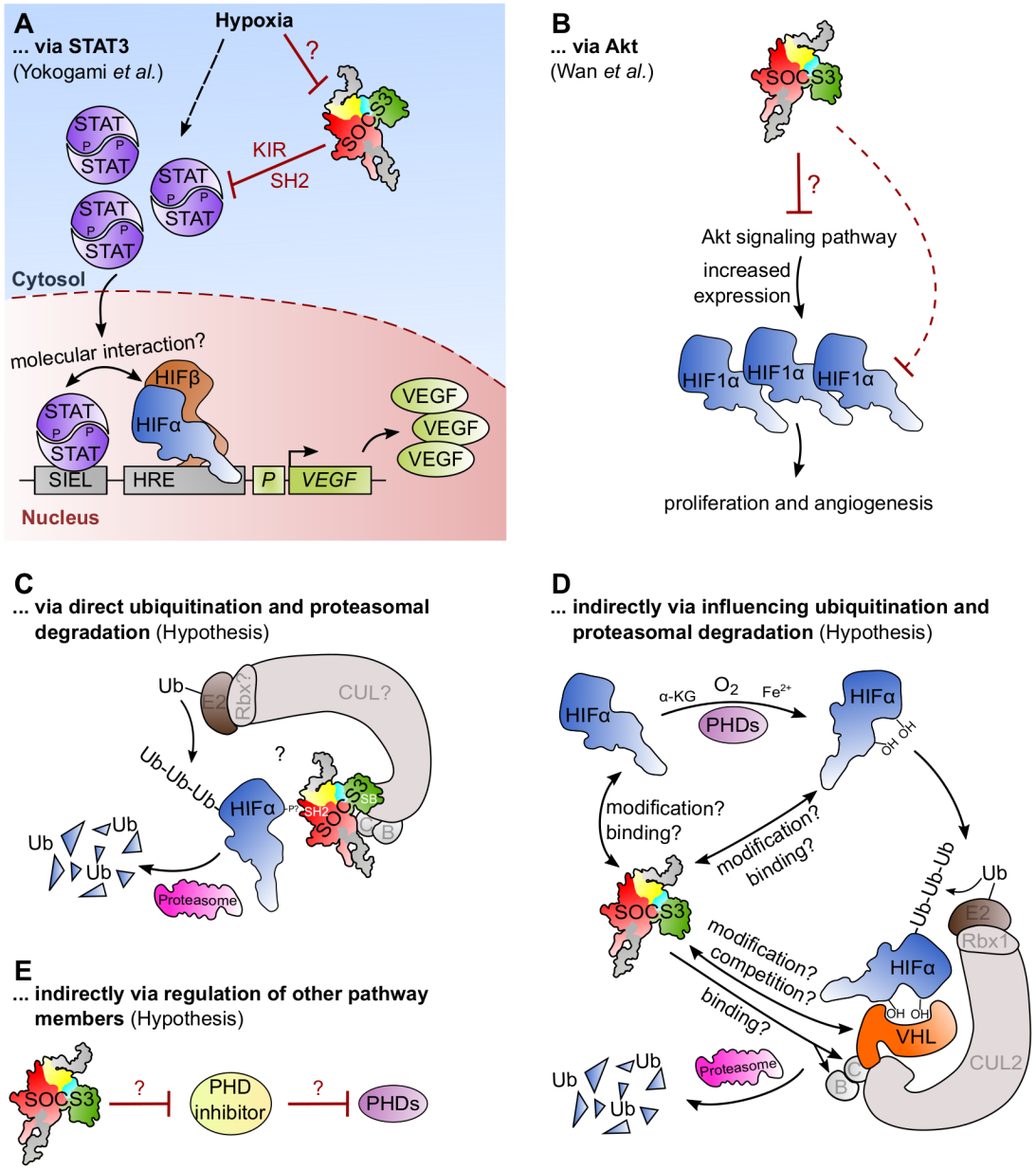

Figure 3.3: Reported and hypothetical roles of SOCS3 in HIF pathway regulation.
(**A**) Regulation of HIF signaling pathway by SOCS3 according to Yokogami *et al.*: Hypoxia results in decreased SOCS3 levels and hence accumulation of STAT3. Dimerized STAT3 binds to sis-inducible element (SIE)-like (SIEL) elements proximal to hypoxia responsive elements (HREs), enhancing transcription of the HIF target gene *vascular endothelial growth factor (VEGF)*. (**B**) Regulation of HIF signaling pathway by SOCS3 as proposed by Wan *et al.*: HIFα is inhibited by SOCS3 via inhibition of the Akt signaling pathway and not the STAT(3) pathway. (**C**) Own hypothesis: SOCS3 might regulate HIFα by its E3 ubiquitin ligase function in complex with Elongin B and C and a yet to be defined Cullin (CUL) and Rbx isoform, leading to HIFα reduction via ubiquitination and proteasomal degradation. (**D**) Own hypothesis: SOCS3 might regulate the HIF signaling pathway by not directly targeting HIFα as proposed in (C) but in an indirect way, e. g. by modifying or binding to HIFα and thus influencing binding to VHL or competing with VHL for binding to Elongin B and C. (**E**) Own hypothesis: SOCS3 might regulate regulators of HIF pathway proteins, e. g. inhibitors of the prolyl hydroxylase domain (PHD) proteins. ? = mechanisms unclear; OH = hyroxylation; -P = phosphorylation; Ub = ubiquitin; E2 = ubiquitin-conjugating enzyme; KIR = kinase inhibitory region; SH2 = Src-homology 2 domain; SB = SOCS Box.

3.5 Concluding summary and perspectives

Cancer is still a widely unmet medical challenge. Brain and CNS cancers as well as lung cancers provide a global health problem with high incidences and nearly as high mortality rates. The TME plays a pivotal role in the development and progression of tumors. Especially the hypoxic niche drives metastasis and invasion of tumors by prolonged activation of the HIF signaling pathway. Additionally, many cancers display pseudohypoxia or -normoxia, i. e. HIF pathway activation despite high oxygen tension or no HIF signaling response to low oxygen levels. Thus, in order to identify possible therapy targets, the aim of this study was to identify novel HIF signaling pathway regulatory proteins (Fig. 3.4A).

To achieve this, FRSs were developed that mirror the activation status of the HIF signaling pathway in real time (Fig. 3.4B). First, the host cell lines were selected, then different FRs were engineered and tested. Finally, a 5xHRE HIF2α-ODD=UnaG-V5 FR was introduced into the host cell lines G141 (glioblastoma) and A549 (lung adenocarcinoma) and single cell clones were selected.

Next, the experimental conditions were carefully optimized in order to obtain meaningful and reproducible results (Fig. 3.4C). This included the determination of the culture confluency at timepoint of harvesting, the harvesting procedure (hypoxia vs. normoxia), the optimal concentration of FBS in the FACS buffer and the effect of prolonged incubation time on ice prior to measurement. This was completed by the selection of suitable controls to define the appropriate gating parameters for the sorting process.

As a proof of principle, a CRISPR/Cas9-mediated genome-wide KO screen was carried out in the FRS G141 SCC#A1 under normoxic conditions (summarized in Fig. 3.4D). Here, negative regulators of the HIF signaling pathway that restrict HIF signaling under normoxic conditions were identified (Fig. 3.4E). Appearance of key HIF regulatory proteins, such as the PHD2 gene *EGLN2* and E3 ubiquitin ligase complex subunits VHL, TCEB1, TCEB2 and CUL2, in the top ranks confirmed the usability of the FRS and the screening approach to identify HIF pathway regulators. Apart from those mentioned, several other proteins were identified and validated as putative negative HIF regulators, with proteins being involved in mitochondrial (dys)function, the SWI/SNF complex or the AHR signaling. Some of these screening hits could be linked to HIF signaling by findings already reported in the literature. Other screening hits, such as MANEAL, ORM2, CDCA7L and CBFB, are not yet known to be associated with HIF signaling.
The most prominent screening hit of the validation process, SOCS3, was further investigated by examining the effect of SOCS3-KO on HIFα in several glioblastoma, one adenocarcinoma as well as two VHL-deficient renal cell carcinoma cell lines. However, further research is needed to unravel whether SOCS3 and several other screening hits negatively regulate HIF(2)α and by which mechanisms.

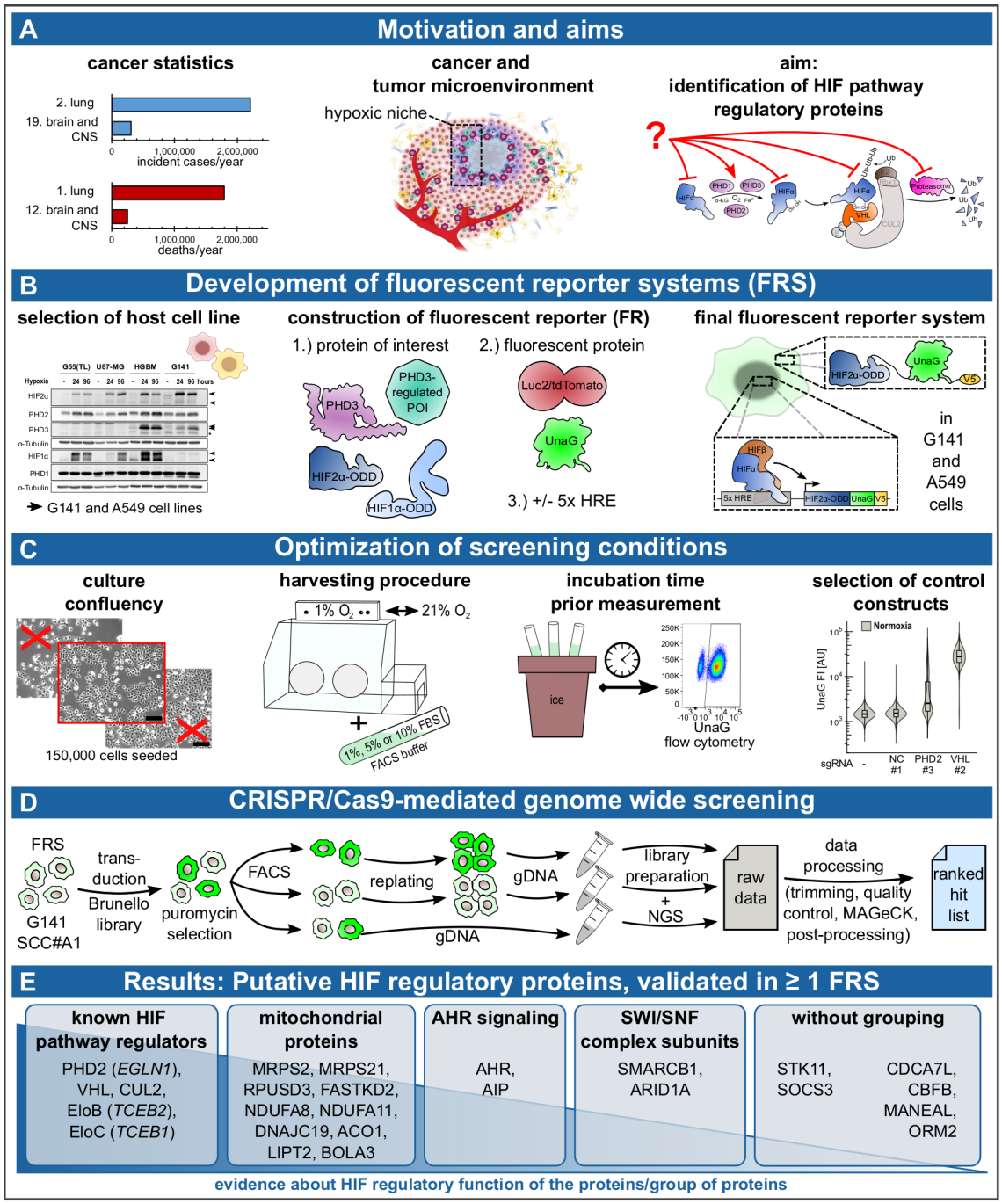

Figure 3.4: Graphical abstract of this study.
Outline of this study shown from the initial "motivation and aims" to the final screening results in the FRS G141 SCC#A1, identifying (putative) HIF regulatory proteins.

Furthermore, only the top 25 screening hits were validated here. The appearance of HIF regulatory proteins beyond rank 100 (e. g. the PHD3 gene *EGLN3* on rank #110) suggests that this screening has uncovered many more putative novel proteins regulating the HIF pathway that could be further investigated. Besides the identification of new regulators of the HIF signaling pathway, the FRSs developed here can be applied under different environmental conditions. Thus, screenings under hypoxia can easily be conducted to e. g. look for activators or enhancers of hypoxia/HIF signaling during hypoxia, thanks

to the application of the oxygen-independent green fluorescent UnaG protein. Moreover, the FRs engineered here have the potential to be used in other model systems as well, for example in primary cell cultures, organoid cultures or even animals. Hence, this study lays the foundation of virtually innumerable studies on HIF regulation in different model systems and under different environmental cues, such as hypoxia or anoxia.

Understanding the HIF signaling pathway is key to understand the mechanisms how brain and lung tumors develop, adapt to low or fluctuating oxygen tensions and use the HIF signaling pathway for their own purposes, e. g. to induce invasion and metastasis. Moreover, this understanding might enable pharmacological interventions with the aim to target only tumor tissue and to prevent invasion and metastasis, a deadly hallmark of advanced cancers. With the development and application of the tools engineered in this study, a step towards understanding the HIF signaling pathway in different cancers was taken, which can now be followed up in the future to achieve the overall goal of better therapy options for cancer patients.

4. Materials and methods

4.1 Materials

Most materials were purchased from Sigma-Aldrich (München, Germany), Merck KGaA (Darmstadt, Germany), Thermo Fisher Scientific (Waltham, USA), Promega Corporation (Mannheim, Germany), Carl Roth GmbH +Co. KG (Karlsruhe, Germany), InvivoGen (San Diego, USA), Becton Dickinson and Company (BD) (Franklin Lakes, USA), GE Healthcare (Little Chalfont, UK), AppliChem GmbH (Darmstadt, Germany), New England Biolabs (NEB) (Ipswich, USA) and Qiagen (Hilden, Germany) in pro analysis quality.

Plastic ware, such as petri dishes, multiwell plates or serological pipettes, was purchased from Greiner Bio-One GmbH (Frickenhausen, Germany) and SARSTEDT AG & Co. KG (Nürnbrecht, Germany).

4.1.1 Standard chemicals

Standard laboratory chemicals were mostly purchased from Carl Roth, Merck and Sigma-Aldrich.

4.1.2 Transfection and transduction reagents

The substances listed below were used for transfection or transduction of cell lines:

Reagent	**Order number**	**Producer**	**DNA:reagent ratio [µg/µL]**
FuGene HD Transfection Reagent	#E2312	Promega	1:3
Lipofectamine 2000	#11668027	Thermo Fisher Scientific	1:3
PEI 25K (Polyethylenimine)	# 23966-1	Polysciences (Warrington, USA)	1:3
Polybrene (Hexadimethrine bromide)	#H9268-5G	Sigma-Aldrich	final conc.: 8 µg/mL

4.1.3 Antibiotics

Antibiotics were dissolved in distilled water and sterile filtered before use (0.22 µm, #83.1826.001, SARSTEDT) or purchased as a commercial stock solution.

Antibiotics for bacterial selection

Antibiotics	Order number	Producer	Stock solution	Final concentration
Ampicillin sodium salt	#A9518-25MG	Sigma-Aldrich	100 mg/mL	100 µg/mL
Kanamycin sulfate	#T832.1	Carl Roth	50 mg/mL	50 µg/mL
Chloramphenicol	#C0378	Sigma-Aldrich	25 mg/mL	25 µg/mL

Mammalian cell culture antibiotics

Antibiotics	Order number	Producer	Stock solution	Final concentration
Blasticidin S HCL	#R210-01	Invitrogen	6 mg/mL	varying*
Puromycin	#ant-pr	InvivoGen	10 mg/mL	varying**
Amphotericin B	#A2942-100ML	Sigma-Aldrich	250 µg/mL	2.5 µg/mL
Gentamicin	#15750-045	Thermo Fisher Scientific	50 mg/mL	50 µg/mL
Plasmocin	#ant-mpt-1	InvivoGen	25 mg/mL	25 µg/mL
Plasmocure	#ant-pc	InvivoGen	100 mg/mL	50 µg/mL

* = 4 µg/mL (G141, A549, MDA-MB231), 6 µg/mL (G55(TL), RCC10, 786-O)

** = 1 µg/mL (G141, A549, MDA-MB231), 2 µg/mL (G55(TL), RCC10, 786-O)

4.1.4 Antibodies

Antibodies used in this study are listed below, divided in primary and secondary antibodies.

4.1.4.1 Primary antibodies

Primary antibodies were purchased from Dianova (Hamburg, Germany), Sigma-Aldrich, Cayman Chemical (Ann Arbor, Michigan, USA), BD, Novus Biologicals (NB) (Centennial, Colorado, USA), Cell Signaling Technology (CST) (Danvers, Massachusetts, USA) and Thermo Fisher Scientific:

Antigen	Species	Order number	Producer	Dilution
α-Tubulin	mouse	#DLN09992	Dianova	1 : 8,000
β-Actin	mouse	#A5316	Sigma-Aldrich	1 : 10,000
HIF1α	rabbit	#10006421	Cayman Chemical	1 : 5,000
HIF2α	rabbit	#NB100-122	NB	1 : 500
E-Cadherin	mouse	#610181/2	BD	1 : 1,000
N-Cadherin	mouse	#610920	BD	1 : 1,000
PHD1	rabbit	#NB-100-31	NB	1 : 1,000
PHD2	rabbit	#NB100-137	NB	1 : 2,000
PHD3	rabbit	#NB100-303	NB	1 : 1,000
SOCS3 (D6E1T)	rabbit	#52113	CST	1 : 1,000
V5	mouse	#R960-25	Thermo Fisher Scientific	1 : 500

4.1.4.2 Secondary antibodies

All secondary antibodies were purchased from Jackson ImmunoResearch (Ely, UK). They were used in a 1:5,000 dilution except for combination with SOCS3 primary antibody. For SOCS3 detection, the secondary antibody was diluted 1:50,000:

Antibody	Order number	Dilution
goat-anti mouse-HRP	#115-035-146	1 : 5,000
goat-anti-rabbit-HRP	#111-035-144	1 : 5,000

4.1.5 Inhibitors

Inhibitors were used according to the following table:

Inhibitor	Order number	Producer	Stock solution	Final concentration
DMOG	#400091-50MG	Merck Millipore	1 M	1 mM
MG-132	#474790-10MG	Merck Millipore	10 mM	10 µM
Chloroquine	#C6628-25G	Sigma-Aldrich	10 mM	10 µM

4.1.6 Solutions, buffers and media

4.1.6.1 SDS PAGE and western blot

The following buffers were used for SDS PAGE and western blot experiments:

Buffer/solution	Recipe
SDS PAGE running buffer	25 mM TRIS, 190 mM Glycine, 0.1 %SDS, pH 8.3
Upper buffer (for stacking gel)	0.5 M TRIS, 0.4 % SDS, pH 6.8
Lower buffer (for separating gel)	1.5 M TRIS, 0.4 % SDS, pH 8.8
Ammonium persulfate solution	10 % (w/v) Ammonium persulfate (#A1142, AppliChem)
Laemmli lysis buffer	10 mM TRIS-HCL (pH 7.5), 2 % SDS, 2 mM EGTA, 20 mM NaF
Stripping buffer	200 mM Glycine, 0.05 % Tween-20, pH 2.5
Sample buffer (4x)	40 mL 10 % SDS solution, 16 mL 1 M TRIS (pH 6.8), 20 mL 100 % glycerol, 19 mL water. Per 800 µL of this buffer, 200 µL 1 % bromphenolblue solution and 50 µL β-mercaptoethanol is added.
Washing buffer (PBS-T)	0.1 % Tween-20 (#A4974,0100, AppliChem) in 1x PBS
Wet transfer buffer	20 mM TRIS, 150 mM Glycine, 20 % methanol
8 % separating gel	Per single-percentage gel: 4.65 mL water, 2.6 mL lower buffer, 2.7 mL 30 % acrylamide, 100 µL 10 % APS, 5 µL TEMED
10 % separating gel	Per single-percentage gel: 3.95 mL water, 2.6 mL lower buffer, 3.35 mL 30 % acrylamide, 100 µL 10 % APS, 5 µL TEMED
12 % separating gel	Per single-percentage gel: 3.5 mL water, 2.6 mL lower buffer, 4.0 mL 30 % acrylamide, 100 µL 10 % APS, 5 µL TEMED
4 % stacking gel	Per two gels: 3.05 mL water, 1.3 mL upper buffer, 0.65 mL 30 % acrylamide, 50 µL 10 % APS, 5 µL TEMED
5 % milk blocking buffer	1x PBS, 0.1 % Tween-20, 5 % milk powder

Furthermore, the following commercially available solutions were used:

Solution	Order number	Producer
DC Protein Assay Reagents Package	#500-0116	BIO-RAD
Pierce ECL Western Blotting Substrate	#32106	Thermo Fisher Scientific
Western Lightning Plus ECL	#0RT2655	Perkin Elmer
SuperSignal West Pico PLUS Chemiluminescent Substrate	#34577	Thermo Fisher Scientific
Super Signal West Femto Maximum Sensitiviy Substrate	#34095	Thermo Fisher Scientific
PageRuler protein ladder (10 -180 kDa)	#26617	Thermo Scientific
Spectra High Range protein ladder (40 -300 kDa)	#26625	Thermo Scientific

4.1.6.2 Agarose gel electrophoresis

The following buffers were used for agarose gel electrophoresis:

Buffer/solution	Recipe
TAE buffer (1x)	40 mM TRIS, 20 mM glacial acetic acid, 1 mM EDTA
Agarose gel	0.5 to 2 % (w/v) Agarose NEEO ultra quality (#2267.4, Carl Roth)

Furthermore, the following commercially available solutions were used:

Solution	Order number	Producer
Gel Loading Dye, Orange (6x)	#B7022S	NEB
Gel Loading Dye, Purple (6x)	#B7024S	NEB
GeneRuler 1 kb Plus DNA Ladder	#SM1333	Thermo Scientific
SYBR Safe DNA gel stain	#S33102	Thermo Fisher Scientific

4.1.6.3 Dual-Luciferase Reporter assay

The solutions required for performing the DLR assay were prepared as follows:

Solution	Recipe
Reagent A	25 mM Glycyl-glycin ($C_4H_8N_2O_3$), 15 mM Kaliumdihydrogenphosphat (KH_2PO_4), 4 mM EGTA ($C_{14}H_{24}N_2O_{10}$), 2 mM ATP ($C_{10}H_{14}N_5Na_2O_{13}P_3$), 1 mM Dithiothreitol ($C_4H_{10}O_2S_2$), 15 mM Magnesiumsulfat ($MgSO_4 \cdot 7H_2O$), 0,1 mM Coenzyme A ($C_{21}H_{33}Li_3N_7O_{16}P_3S \cdot 2H_2O$), 75 µM Beetle Luziferin ($C_{11}H_7N_2O_3S_2 \cdot K$)
Reagent B	1.1 M NaCl, 2.2 mM Na_2-EDTA ($C_{10}H_{14}N_2Na_2O_8 \cdot 2H_2O$), 0.22 M KH_2PO_4, 0.44 mg/mL BSA, 1.3 mM NaN_3
Reagent C	1.43 µM Coelenterazine ($C_{26}H_{21}N_3O_3$)
1x Passive Lysis Buffer	5x Passive Lysis Buffer (Promega) was dilutet to 1x with distilled water

Reagent C has to be mixed with Reagent B (1:50) freshly before use.

4.1.6.4 gDNA isolation for NGS

TEX buffer was prepared for gDNA isolation as follows:

Solution	Recipe
TEX buffer	10 mM Tris-HCl (pH 7.5), 1 mM EDTA (pH 7.9), 0.5 % SDS; sterile filtered

4.1.6.5 Buffers and media for cell culture

The following buffers were prepared for cell culture maintenance and FACS/FC experiments:

Solution	Recipe
Basic culture medium	1x Dulbecco's Modified Eagle Medium (DMEM) high glucose, pyruvate +10 % FBS
Freezing medium	90 % [DMEM +10 % FBS] +10 % DMSO
FACS buffer	1x PBS buffer, 2 mM EDTA, FBS (1 to 10 %, variable)
Capture buffer	1x PBS buffer, 2 mM EDTA, 20 % FBS
Post-sorting medium	1x DMEM, 10 to 20 % FBS, 2.5 µg/mL Amphotericin B, 50 µg/mL Gentamicin
Crystal violet staining solution	0.5 % Crystal violet in 20 % Methanol
Live-cell microscopy medium	FluoroBrite DMEM +4 mM L-Glutamin +10 % FBS

The following buffers and media were purchased ready-to-use:

Solution	Order number	Producer
1x Dulbecco's Modified Eagle Medium (DMEM) high glucose, pyruvate	#41966029	Thermo Fisher Scientific
Fetal Bovine Serum (FBS)	#F7524	Sigma-Aldrich/Merck
1x PBS (pH 7.4)	#10010023	Thermo Fisher Scientific
0.05 % Trypsin-EDTA	#25300-054	Thermo Fisher Scientific
CASY ton solution	#5651808	OMNI Life Sciences, Bremen, Germany
FluoroBrite DMEM	#A1896701	Thermo Fisher Scientific
Opti-MEM Reduced Serum Medium	#11058021	Thermo Fisher Scientific
DMSO	#A994.1	Carl Roth
Crystal violet	#61135	Fluka/Honeywell, Charlotte, North Carolina, USA
200 mM L-Glutamin	#25030.024	Thermo Fisher Scientific

4.1.6.6 Buffers and media for bacterial culture

The buffers for bacterial culture were ready-to-use or prepared as indicated by the manufacturer:

Solution	Order number	Producer
LB medium (Lennox)	#X964.1	Carl Roth
LB agar (Lennox)	#X965.2	Carl Roth
S.O.C. medium	#15544-034	Thermo Fisher Scientific
0.9 % NaCl solution	#9511121	Braun, Melsungen, Germany

LB medium and LB agar were autoclaved after preparation and stored at 4 °C.

Preparation of competent *E. coli.*

Competent *E. coli.* bacteria were prepared using the following buffers:

Buffer	Recipe
TfBI buffer	100 mM RbCl, 50 mM MnCltextsubscript2•2H_2O, 30 mM KAc, 10 mM $CaCl_2$•2H2O, 15 % Glycerin (v/v)
TfBII buffer	10 mM MOPS, 10 mM RbCl, 75 mM $CaCl_2$, 15 % Glycerin (v/v)

4.1.6.7 Other solutions

Other solutions were purchased as follows:

Solution	Order number	Producer
Sytox blue	#S11348	Thermo Fisher Scientific

4.1.7 Enzymes

4.1.7.1 Restriction endonucleases

The following enzymes were used for cloning purposes:

Enzyme	Order number	Producer
Eco32I (EcoRV) (10 U/µL)	#ER0301	Thermo Fisher Scientific
BpiI FastDigest	#FD1014	Thermo Fisher Scientific
Esp3I FastDigest (BsmBI)	#FD0454	Thermo Fisher Scientific
DpnI (10 U/µL)	#ER1701	Thermo Fisher Scientific
SmaI (10 U/µL)	#ER0662	Thermo Fisher Scientific
NheI (10 U/µL)	#ER0971	Thermo Fisher Scientific
BamHI (10 U/µL)	#ER0051	Thermo Fisher Scientific
XhoI (10 U/µL)	#ER0692	Thermo Fisher Scientific
MluI (10 U/µL)	#ER0561	Thermo Fisher Scientific
BcuI (SpeI) (10 U/µL)	#ER1251	Thermo Fisher Scientific
Bsu15I (ClaI) (10 U/µL)	#ER0141	Thermo Fisher Scientific

4.1.7.2 Polymerases

The following polymerases were used for PCRs in this thesis:

Enzyme	Order number	Producer
Q5 Hot Start High-Fidelity DNA Polymerase	#M0493S	NEB
Phusion Hot Start II DNA-Polymerase	#F549S	Thermo Fisher Scientific
OneTaq DNA Polymerase	#M0509L	NEB
HotStarTaq DNA Polymerase	#203203	Qiagen

4.1.7.3 Other enzymes

Other enzymes used in this work are listed below:

Enzyme	Order number	Producer
Proteinase K	#3719.1	Carl Roth
RNAse A (10 mg/mL)	#7156.1	Carl Roth
NEBuilder HiFi DNA Assembly Master Mix	#E2621S	NEB
FastAP (1 U/µL)	#EF0654	Thermo Fisher Scientific
T4 PNK	#M0201S	NEB
T4 DNA Ligase (5 U/µL)	#EL0014	Thermo Fisher Scientific

4.1.8 Bacterial strains

Bacterial strains used in this study are listed below:

Strain	Order number	Producer
One Shot Stbl3 Chemically Competent *E. coli*	#C737303	Thermo Fisher Scientific
E. coli DH5α Competent Cells for Sublconing	#EC0111	Thermo Fisher Scientific
E. coli K12 ER2925 (Dam-Dcm-) bacteria	#E4109	NEB

4.1.9 Mammalian cell lines

4.1.9.1 Glioblastoma cell lines

The following glioblastoma cell lines were used in this study:

Cell line	Source
G141	Manfred Westphal (Hamburg, Germany)
G55(TL)	Manfred Westphal (Hamburg, Germany)
G55(TL) PHD3-OE#6 tet-off	Anne-Theres Henze (Giessen, Germany)
HGBM	Herbert A. Weich (Braunschweig, Germany)
U87-MG	ATCC (#HTB-14)

4.1.9.2 Other cell lines

The following non-glioblastoma cell lines were used in this study:

Cell line	Information	Source
A549	Human lung adenocarcinoma cells	ATCC (#CCL-185)
MDA-MB-231	Human breast carcinoma cells	Massimiliano Mazzone (Leuven, Belgium)
MDA-MB-231-Br	Human breast carcinoma cells selected for increased brain metastasis capacity	Joan Massagué (New York, USA)
HEK293T	Human embryonic kidney cells, for virus production	Invitrogen/Thermo Fisher Scientific

4.1.9.3 Cell lines produced in this study

Stable cell lines generated by lentiviral transduction and selection

The following FRS cell lines were generated during this study using lentiviral transduction and selection:

Cell line	Reporter construct	MOI	Single cell clones
G141	pLenti6 CMVp HIF2α-ODD(aa354-581)=UnaG-V5	1 or 2 or 5	yes, several
G141	pLenti6 5xHRE CMVp HIF2α-ODD(aa354-581)=UnaG-V5	10	yes, several; mainly used here: #A1 and #B11
A549	pLenti6 5xHRE CMVp HIF2α-ODD(aa354-581)=UnaG-V5	10	yes, several; mainly used here: #P3A5

Furthermore, the stable FRSs G141 5xHRE CMVp HIF2α-ODD(aa354-581)=UnaG-V5 SCC#A1 and #B11 as well as A549 5xHRE CMVp HIF2α-ODD(aa354-581)=UnaG-V5 SCC#P3A5 were transduced with (p)LentiCRISPR v2 (Puro) plasmids No. 14 to 42 (see chapter 4.1.11.2 starting on page 108) to induce gene knockouts. For this, a MOI of 2 was used in all cell lines.

Additionally, the (parental) cell lines G141, A549 , U87-MG and G55(TL) were transduced with the (p)LentiCRISPR v2 (Puro) plasmids No. 19 (VHL-KO) and 41 to 43 (PPP1R12C-KO, NTC#29 and SOCS3-KO#BL3) (see chapter 4.1.11.2 starting on page 108). Also, 786-O and RCC10 cells were transduced with the (p)LentiCRISPR v2 (Puro) plasmids 41 to 43 (PPP1R12C-KO, NTC#29 and SOCS3-KO#BL3) (see chapter 4.1.11.2 starting on page 108). For this, a MOI of 2 was used in all cell lines.

Stable cell lines generated by transient transfection and selection (endogenous tagging or gene knockout using transient transfection)

The following cell lines were generated during this study:

Parental cell line	Reporter construct/plasmid	Single cell clones
G55(TL)	pUC57 PHD3-ET C-term mCherry	-
G55(TL)	pUC57 PHD3-ET C-term GSAGSAAGSGEF-Linker TurboGFP-V5	-
G55(TL)	pUC57 PHD3-ET N-term GSAGSAAGSGEF-Linker UnaG-Flag	-
G141	pUC57 PHD3-ET C-term GSAGSAAGSGEF-Linker UnaG-Flag GSG-Linker Furin/T2A PuroR	-
A549	pUC57 PHD3-ET C-term GSAGSAAGSGEF-Linker UnaG-Flag GSG-Linker Furin/T2A PuroR	#1 to #10
G55(TL)	pSpCas9(BB)-2A-Puro (PX459) V2.0 PHD3-KO	several; used here: #9

4.1.10 Oligonucleotides

4.1.10.1 PCR amplification

The following primers were used for PCR reactions with the purpose of cloning plasmids (see chapter 4.2.3.11, page 128):

No.	Final plasmid	Sequence (5'-3')
1	pUC57 PHD3-ET C-term mCherry and pUC57 PHD3-ET C-term GSAGSAAGSGEF-Linker TurboGFP-V5	GAGCTCGGTACCTCGCGAATGCATCTAGATTATATTTTTC-CTTTCATTTAAATTTAAATTCCATTC
2	pUC57 PHD3-ET C-term mCherry	GAGCTGTACAAGTGATGACCGTGCTCTGAAATCTG
3	pUC57 PHD3-ET C-term mCherry	CTCGCCCTTGCTCACGTCTTCAGTGAGGGCAGATTC
4	pUC57 PHD3-ET C-term mCherry and pUC57 PHD3-ET C-term GSAGSAAGSGEF-Linker TurboGFP-V5	CCTCTGCAGTCGACGGGCCCGGGATCCGATGTTAACCAGT-CAAATGTAACATTAAATTTTG
5	pUC57 PHD3-ET C-term mCherry	TTCAGAGCACGGTCATCACTTGTACAGCTCGTCCATGC
6	pUC57 PHD3-ET C-term mCherry	GCCCTCACTGAAGACGTGAGCAAGGGCGAGGAGGA
7	pUC57 PHD3-ET C-term GSAGSAAGSGEF-Linker TurboGFP-V5	GGTCTCGATTCTACGTAATGACCGTGCTCTGAAATC
8	pUC57 PHD3-ET C-term GSAGSAAGSGEF-Linker TurboGFP-V5	GCTCTCGTCGCTCTCGAATTCGCCAGAACCAGCAGCG-GAGCCAGCGGATCCGTCTTCAGTGAGGGCAGATTC
9	pUC57 PHD3-ET C-term GSAGSAAGSGEF-Linker TurboGFP-V5	TTCAGAGCACGGTCATTACGTAGAATCGAGACCGAGGA-GAGGGTTAGGGATAGGCTTACCTTCTTCACCGGCATCTGCATC
10	pUC57 PHD3-ET C-term GSAGSAAGSGEF-Linker TurboGFP-V5	CTGGTTCTGGCGAATTCGAGAGCGACGAGAGCGGC
11	pUC57 PHD3-ET N-term GSAGSAAGSGEF-Linker UnaG-Flag	CGGTACCTCGCGAATGCATCTAGATAGTGCTTTTGTA-GAAATCTCTTCTGAC
12	pUC57 PHD3-ET N-term GSAGSAAGSGEF-Linker UnaG-Flag	CTGGTTCTGGCGAATTCCCCCTGGGACACATCATGAG
13	pUC57 PHD3-ET N-term GSAGSAAGSGEF-Linker UnaG-Flag	CAAATTTCTCGACACTAGTTTTATCATCATCATCTTTATAATC-CATCTCGCCCGCAGAATCGA
14	pUC57 PHD3-ET N-term GSAGSAAGSGEF-Linker UnaG-Flag	GCAGTCGACGGGCCCGGGATCCGATTACCTCC-TAATCTCTCAGTGGC

No.	Final plasmid	Sequence (5'-3')
15	pUC57 PHD3-ET N-term GSAGSAAGSGEF-Linker UnaG-Flag	TGTGTCCCAGGGGGAATTCGCCAGAACCAGCAGCG-GAGCCAGCGGATCCACTAGTTTCCGTCGCCCTCCGGTAGC
16	pUC57 PHD3-ET N-term GSAGSAAGSGEF-Linker UnaG-Flag	ATGATGATGATAAAACTAGTGTCGAGAAATTTGTTGGCAC-CTGGAAG
17	pUC57 PHD3-ET C-term GSAGSAAGSGEF-Linker UnaG-Flag GSG-Linker Furin/T2A PuroR	ATTTCTCGACGAATTCGCCAGAACCAGCAG
18	pUC57 PHD3-ET C-term GSAGSAAGSGEF-Linker UnaG-Flag GSG-Linker Furin/T2A PuroR	ACAAAGACGATGACGACAAGTGACCGTGCTCTGAAATCTG
19	pUC57 PHD3-ET C-term GSAGSAAGSGEF-Linker UnaG-Flag GSG-Linker Furin/T2A PuroR	CTTGTCGTCATCGTCTTTGTAGTCGGCAC-CGGGCTTGCGGGTCA
20	pUC57 PHD3-ET C-term GSAGSAAGSGEF-Linker UnaG-Flag GSG-Linker Furin/T2A PuroR	CTCCTCGGTCTCGATTCTACGCGTCGAAAGCGAGGAAGCG-GAGAGGGCAGAGGAAGTCTGCTAACATGCG
21	pUC57 PHD3-ET C-term GSAGSAAGSGEF-Linker UnaG-Flag GSG-Linker Furin/T2A PuroR	CGTAGAATCGAGACCGAGGAGAGGGTTAGGGATAGGCTTAC-CTTCCGTCGCCCTCCGGTAGC
22	pUC57 PHD3-ET C-term GSAGSAAGSGEF-Linker UnaG-Flag GSG-Linker Furin/T2A PuroR	TGGCGAATTCGTCGAGAAATTTGTTGGCACCTGGAAG
23	pLenti6/V5-DEST CMVp ADRB2-Luc2/tdTomato-Flag	TCCAGTGTGGTGGAATTCTGCAGATGCCACCATGCC-CGGGCCAGATTTCAGGATTGCCTTC
24	pLenti6/V5-DEST CMVp ADRB2-Luc2/tdTomato-Flag	TCCTCCACCGCTAGCCAGCAGTGAGTCATTTGTAC
25	pLenti6/V5-DEST CMVp ADRB2-Luc2/tdTomato-Flag	TGACTCACTGCTGGCTAGCGGTGGAGGAGGTAGCGGAGGTG-GAGGTAGCATGGAAGATGCCAAAAACATTAAG

No.	Final plasmid	Sequence (5'-3')
26	pLenti6/V5-DEST CMVp ADRB2-Luc2/tdTomato-Flag	TCGAGCGGCCGCCACTGTGCTGGATTTACTTGTCGT-CATCGTCTTTGTAGTCCTTGTACAGCTCGTCCATGC
27	pLenti6/V5-DEST CMVp EPOR-Luc2/tdTomato-Flag	GTCATGCCCGGGTCGAGCGAGTTTGAAGGCCTCT
28	pLenti6/V5-DEST CMVp EPOR-Luc2/tdTomato-Flag	GTCATGGCTAGCAGAGCAAGCCACATAGCTGG
29	pLenti6/V5-DEST CMVp Luc2/tdTomato-HIF1α-ODD(aa530-652)	GGGAGCATCGCCACCGAATTCAAGTTGGAATTGGTA-GAAAAACTTTTTGC
30	pLenti6/V5-DEST CMVp Luc2/tdTomato-HIF1α-ODD(aa530-652)	TTAAGTAGTTTCTTTATGTATGTGGGTAGGAGATGGAGATG-CAATC
31	pLenti6 CMVp HIF2α-ODD(aa354-581)=UnaG-V5 reporter plasmid	CTCCTTGGATCCTTCGCCACCATGGAATTCAAGTTGGAATTG-GTAGAAA
32	pLenti6 CMVp HIF2α-ODD(aa354-581)=UnaG-V5 reporter plasmid	GTATGCCTCGAGAGTAGTTTCTTTATGTATGTGGGTAGGA
33	pLenti6 CMVp HIF2α-ODD(aa354-581)=UnaG-V5 reporter plasmid	TGACTGCTCGAGGAGAGCGACGAGAGCGG
34	pLenti6 CMVp HIF2α-ODD(aa354-581)=UnaG-V5 reporter plasmid	GTATGCACGCGTCGGCCGCTACTTGTACATTATTCTTCA
35	pLenti6 CMVp HIF2α-ODD(aa354-581)=UnaG-V5 reporter plasmid	GTCATGACTAGTATGGTCGAGAAATTTGTTGGCACCT
36	pLenti6 CMVp HIF2α-ODD(aa354-581)=UnaG-V5 reporter plasmid	GTCATGACTAGTTTCCGTCGCCCTCCGGTAG
37	pLenti6 CMVp HIF2α-ODD(aa354-581)=UnaG-V5 reporter plasmid	GTCATGCTCGAGTTCTCCATGGACCAGACTGAA
38	pLenti6 CMVp HIF2α-ODD(aa354-581)=UnaG-V5 reporter plasmid	GTCATGCTCGAGACTGTGCGGGGCTACAGG
39	pLenti6 5xHRE CMVp HIF2α-ODD(aa354-581)=UnaG-V5 reporter plasmid	GTCATGATCGATAAAAGTGCCACCTGACGTCA
40	pLenti6 5xHRE CMVp HIF2α-ODD(aa354-581)=UnaG-V5 reporter plasmid	GTCATGATCGATTTTACCAACAGTACCGGAATGC

4.1.10.2 Cloning sgRNAs into knockout vectors

The following oligonucleotides were used to insert specific target sequences (sgRNAs) into the pSpCas9(BB)-2A-Puro V2.0 (PX459 V2.0) or (p)LentiCRISPR v2 (Puro) (in short: LentiCRISPR v2) vector backbones in order to use them for endogenous tagging (ET) - either C-terminally (C-term.) or N-terminally (N-term.) - or gene knockout (KO) (see chapter 4.2.3.11, page 128):

No.	Vector backbone	Purpose	Target gene	Sequence (5'-3')
41	PX459 V2.0	ET	PHD3 C-term. #A	CACCGAGCACG-GTCAGTCTTCAGTG
42	PX459 V2.0	ET	PHD3 C-term. #A	AAACCACTGAAGACTGACCGT-GCTC
43	PX459 V2.0	ET	PHD3 C-term. #B	CACCGCACGGTCAGTCTTCAGTGA
44	PX459 V2.0	ET	PHD3 C-term. #B	AAACTCACTGAAGACTGACCGTGC
45	PX459 V2.0	ET	PHD3 N-term. #A	CACCGAGCCTCATGATGTGTCCCAG
46	PX459 V2.0	ET	PHD3 N-term. #A	AAACCTGGGACACATCATGAG-GCTC
47	PX459 V2.0	ET	PHD3 N-term. #B	CACCGTCTGCGGGCGAGATGCC-CCT
48	PX459 V2.0	ET	PHD3 N-term. #B	AAACAGGGGCATCTCGCCCGCA-GAC
49	PX459 V2.0, LentiCRISPR v2	KO	PHD3	CACCGTGGACAACCCCAACGGTGA
50	PX459 V2.0, LentiCRISPR v2	KO	PHD3	AAACTCACCGTTGGGGTTGTCCAC
51	LentiCRISPR v2	KO	NC#1	CACCGAAATGCTATGCTTCGGTTC
52	LentiCRISPR v2	KO	NC#1	AAACGAACCGAAGCATAGCATTTC
53	LentiCRISPR v2	KO	NC#2	CACCGGCTTACGTGGGGGGCAAAA
54	LentiCRISPR v2	KO	NC#2	AAACTTTTGCCCCCCACGTAAGCC
55	LentiCRISPR v2	KO	NC#3	CACCGTTGGCATATTGGCCCAGAC
56	LentiCRISPR v2	KO	NC#3	AAACGTCTGGGCCAATATGCCAAC
57	LentiCRISPR v2	KO	PHD2#3	CACCGTGCAGCAGTAGAAG-GAGCTG

No.	Vector backbone	Purpose	Target gene	Sequence (5'-3')
58	LentiCRISPR v2	KO	PHD2#3	AAACCAGCTCCTTCTACTGCTGCAC
59	LentiCRISPR v2	KO	VHL#2	CACCGCGATTGCAGAAGATGACCT
60	LentiCRISPR v2	KO	VHL#2	AAACAGGTCATCTTCTGCAATCGC
61	LentiCRISPR v2	KO	VHL#3	CACCGAGTTCACCGAGCGCAGCAC
62	LentiCRISPR v2	KO	VHL#3	AAACGTGCTGCGCTCGGTGAACTC
63	LentiCRISPR v2	KO	NTC#29	CACCGAAGAAGAATTGGGGATGATG
64	LentiCRISPR v2	KO	NTC#29	AAACCATCATCCCCAATTCTTCTTC
65	LentiCRISPR v2	KO	PPP1R12C	CACCGCTGGACTCCACCAACGCCGA
66	LentiCRISPR v2	KO	PPP1R12C	AAACTCGGCGTTGGTGGAGTCCAGC
67	LentiCRISPR v2	KO	STK11	CACCGTGATGGAGTACTGCGTGTG
68	LentiCRISPR v2	KO	STK11	AAACCACACGCAGTACTCCATCAC
69	LentiCRISPR v2	KO	SMARCB1	CACCGTGGCACGGCATCTAAGTGGT
70	LentiCRISPR v2	KO	SMARCB1	AAACACCACTTAGATGCCGTGCCAC
71	LentiCRISPR v2	KO	NDUFA11	CACCGCAGTACTGGGATATCCCCGA
72	LentiCRISPR v2	KO	NDUFA11	AAACTCGGGGATATCCCAGTACTGC
73	LentiCRISPR v2	KO	MANEAL	CACCGGCGTGTTGCGGATCGAATG
74	LentiCRISPR v2	KO	MANEAL	AAACCATTCGATCCGCAACACGCC
75	LentiCRISPR v2	KO	MRPS21	CACCGATTATGAGAAGCCATGCTGC
76	LentiCRISPR v2	KO	MRPS21	AAACGCAGCATGGCTTCTCATAATC
77	LentiCRISPR v2	KO	MRPS2	CACCGGCCCTTATGATCCGCGAGT
78	LentiCRISPR v2	KO	MRPS2	AAACACTCGCGGATCATAAGGGCC
79	LentiCRISPR v2	KO	SOCS3	CACCGTACTGGAGCGCAGTGACCGG
80	LentiCRISPR v2	KO	SOCS3	AAACCCGGTCACTGCGCTCCAGTAC
81	LentiCRISPR v2	KO	ORM2	CACCGTTCTCAGAGAGTACCAGACC
82	LentiCRISPR v2	KO	ORM2	AAACGGTCTGGTACTCTCTGAGAAC
83	LentiCRISPR v2	KO	AIP	CACCGCAACCGGTTGTACCGCGAG
84	LentiCRISPR v2	KO	AIP	AAACCTCGCGGTACAACCGGTTGC
85	LentiCRISPR v2	KO	ARID1A	CACCGCAATAGATGACCTCCCCATG
86	LentiCRISPR v2	KO	ARID1A	AAACCATGGGGAGGTCATCTATTGC

No.	Vector backbone	Purpose	Target gene	Sequence (5'-3')
87	LentiCRISPR v2	KO	AHR	CACCGAGACTCATCTTGTTGCATCA
88	LentiCRISPR v2	KO	AHR	AAACTGATGCAACAAGATGAGTCTC
89	LentiCRISPR v2	KO	LIPT2	CACCGTGACGCCCGAGGAAACTGCG
90	LentiCRISPR v2	KO	LIPT2	AAACCGCAGTTTCCTCGGGCGTCAC
91	LentiCRISPR v2	KO	RPUSD3	CACCGAGAAGTACTTCACCCATGCA
92	LentiCRISPR v2	KO	RPUSD3	AAACTGCATGGGTGAAGTACTTCTC
93	LentiCRISPR v2	KO	ACO1	CACCGATGCTGTGAAAAAGTTAGG
94	LentiCRISPR v2	KO	ACO1	AAACCCTAACTTTTTCACAGCATC
95	LentiCRISPR v2	KO	BOLA3	CACCGCCCTGCCCACGCTCACCCCG
96	LentiCRISPR v2	KO	BOLA3	AAACCGGGGTGAGCGTGGGCAGGGC
97	LentiCRISPR v2	KO	DNAJC19	CACCGTTTGCAAGCCATGAAGCATA
98	LentiCRISPR v2	KO	DNAJC19	AAACTATGCTTCATGGCTTGCAAAC
99	LentiCRISPR v2	KO	FASTKD2	CACCGCTTCACGCCATAGTGAAGCT
100	LentiCRISPR v2	KO	FASTKD2	AAACAGCTTCACTATGGCGTGAAGC
101	LentiCRISPR v2	KO	CDCA7L	CACCGTCTGACGAGAGGGTTTCCAT
102	LentiCRISPR v2	KO	CDCA7L	AAACATGGAAACCCTCTCGTCAGAC
103	LentiCRISPR v2	KO	NDUFA8	CACCGAAAGTTTGACGAGTGTGTGC
104	LentiCRISPR v2	KO	NDUFA8	AAACGCACACACTCGTCAAACTTTC
105	LentiCRISPR v2	KO	CBFB	CACCGAGAAGCAAGTTCGAGAACG
106	LentiCRISPR v2	KO	CBFB	AAACCGTTCTCGAACTTGCTTCTC
107	LentiCRISPR v2	KO	SOCS3 BL#3	CACCGTCAGCGTCAAGACCCAGTCT
108	LentiCRISPR v2	KO	SOCS3 BL#3	AAACAGACTGGGTCTTGACGCTGAC

4.1.11 Plasmids

4.1.11.1 Plasmids used in this study

The following plasmids were used for cloning, virus production or directly in experiments as they are:

Plasmid	Producer or cloned by
(p)LentiCRISPR v2 (Puro)	Addgene #52961; gift from Feng Zhang
(p)LentiCRISPR v2 Brunello library	Addgene #73179; gift from David Root and John Doench
9x HRE Fluc	Gift from Massimiliano Mazzone
pcDNA3 HIF2a-ODD-Luciferase-Flag	Gift from Richard Bruick
pcDNA3.1(+)/Luc2=tdT	Addgene #32904; gift from Christopher Contag
pCI-VSVG	Addgene #1733; gift from Garry Nolan
pEF/myc/cyto 5xHRE CMVp dUnaG	Gift from Friedemann Kiefer
pGIPZ nsc (A0055)	Horizon Discovery Ltd., Cambridge, UK
pLenti6/V5-DEST CMVp Luc2/tdTomato	Cloned by Omelyan Trompak; based on pLenti6/V5-DEST and pcDNA3 Luc2/tdTomato
pLenti6/V5-DEST CMVp SmaI-dead	Thermo Fisher Scientific; modified by Omelyan Trompak
pLenti6-ODDFluc-Rluc(POR)	Cloned by Omelyan Trompak; based on pLenti6/V5-DEST CMVp SmaI-dead
pLenti6-V5/DEST CMVp SmaI-dead, EcoRV digested and religated	Cloned by Omelyan Trompak; based on pLenti6/V5-DEST CMVp SmaI-dead
pmCherry-C1	Clontech Laboratories, Inc., Mountain View, USA
pRL SV40 (Renilla Plasmid)	Promega
psPAX2	Addgene #12260; gift from Didier Trono
pSpCas9(BB)-2A-Puro (PX459) V2.0	Addgene #62988; gift from Feng Zhang
pUC57	Thermo Fisher Scientific
PX459 V2.0 PHD3-KO #8	Cloned by Alina Filatova

4.1.11.2 Plasmids created for the thesis project

The following plasmids were cloned in the course of this study with the purpose to perform endogenous tagging (ET), establish fluorescent reporters (FR) or induce CRISPR/Cas9-mediated gene knockouts (KO):

No.	Plasmid	Relevant main components	Purpose
1	pUC57 PHD3-ET C-term mCherry	PHD3 homology arms, C-terminal mCherry tag	ET
2	pUC57 PHD3-ET C-term GSAGSAAGSGEF-Linker TurboGFP-V5	PHD3 homology arms, GSAGSAAGSGEF-Linker, C-terminal TurboGFP-V5 tag	ET
3	pUC57 PHD3-ET N-term GSAGSAAGSGEF-Linker UnaG-Flag	PHD3 homology arms, GSAGSAAGSGEF-Linker, N-terminal UnaG-Flag tag	ET
4	pUC57 PHD3-ET C-term GSAGSAAGSGEF-Linker UnaG-Flag GSG-Linker Furin/T2A PuroR	PHD3 homology arms, GSAGSAAGSGEF-Linker, C-terminal UnaG-Flag tag, GSG-Linker, Furin cleavage site and T2A, Puromycin resistance gene	ET
5	PX459 V2.0 EGLN3 C-term. #A	Cas9 and sgRNA against C-terminus of EGLN3 (sgRNA: AGCACGGTCAGTCTTCAGTG)	ET
6	PX459 V2.0 EGLN3 C-term. #B	Cas9 and sgRNA against C-terminus of EGLN3 (sgRNA: GCACGGTCAGTCTTCAGTGA)	ET
7	PX459 V2.0 EGLN3 N-term. #A	Cas9 and sgRNA against N-terminus of EGLN3 (sgRNA: AGCCTCATGATGTGTCCCAG)	ET
8	PX459 V2.0EGLN3 N-term. #B	Cas9 and sgRNA against N-terminus of EGLN3 (sgRNA: TCTGCGGGCGAGATGCCCCT)	ET
9	pLenti6/V5-DEST CMVp SmaI-dead [EcoRV] ADRB2(aa330-413)=Luc2=tdTomato-Flag-tag	Cytosolic domain of ADRB2(aa330-413), GGGGSGGGS-Linker, Luciferase 2, GGGGSGGGS-Linker, tdTomato-Flag tag	FR
10	pLenti6/V5-DEST CMVp SmaI-dead [EcoRV] EPOR(aa291-508)=Luc2=tdTomato-Flag-tag	Cytosolic domain of EPOR(aa291-508), GGGGSGGGS-Linker, Luciferase 2, GGGGSGGGS-Linker, tdTomato-Flag tag	FR

No.	Plasmid	Relevant main components	Purpose
11	pLenti6 CMVp Luc2/tdTomato-HIF1α-ODD(aa530-652)	Luciferase2, GGGGSGGGS-Linker, tdTomato, HIF1α-ODD aa530-652	FR
12	pLenti6 CMVp HIF2α-ODD(aa354-581)=UnaG-V5	HIF2α-ODD aa354-581, UnaG-V5 tag	FR
13	pLenti6 5xHRE CMVp HIF2α-ODD(aa354-581)=UnaG-V5	5xHRE, HIF2α-ODD aa354-581, UnaG-V5-tag	FR
14	LentiCRISPR v2 (Puro)NC#1	Cas9 and sgRNA targeting nothing in the human genome (sgRNA: GAAATGCTATGCTTCGGTTC)	KO
15	LentiCRISPR v2 (Puro)NC#2	Cas9 and sgRNA targeting nothing in the human genome (sgRNA: GGCTTACGTGGGGGGCAAAA)	KO
16	LentiCRISPR v2 (Puro)NC#3	Cas9 and sgRNA targeting nothing in the human genome (sgRNA: GTTGGCATATTGGCCCAGAC)	KO
17	LentiCRISPR v2 (Puro)PHD3-KO#8	Cas9 and sgRNA targeting EGLN3 (sgRNA: GTGGACAACCCCAACGGTGA)	KO
18	LentiCRISPR v2 (Puro)PHD2-KO#3	Cas9 and sgRNA targeting EGLN1 (sgRNA: TGCAGCAGTAGAAGGAGCTG)	KO
19	LentiCRISPR v2 (Puro)VHL-KO#2	Cas9 and sgRNA targeting VHL (sgRNA: GCGATTGCAGAAGATGACCT)	KO
20	LentiCRISPR v2 (Puro)VHL-KO#3	Cas9 and sgRNA targeting VHL (sgRNA: GAGTTCACCGAGCGCAGCAC)	KO
21	LentiCRISPR v2 (Puro) ACO1-KO	Cas9 and sgRNA targeting ACO1 (sgRNA: GATGCTGTGAAAAAGTTAGG)	KO
22	LentiCRISPR v2 (Puro) AHR-KO	Cas9 and sgRNA targeting AHR (sgRNA: AGACTCATCTTGTTGCATCA)	KO
23	LentiCRISPR v2 (Puro) AIP-KO	Cas9 and sgRNA targeting AIP (sgRNA: GCAACCGGTTGTACCGCGAG)	KO
24	LentiCRISPR v2 (Puro) ARID1A-KO	Cas9 and sgRNA targeting ARID1A (sgRNA: CAATAGATGACCTCCCCATG)	KO
25	LentiCRISPR v2 (Puro) BOLA3-KO	Cas9 and sgRNA targeting BOLA3 (sgRNA: CCCTGCCCACGCTCACCCCG)	KO

No.	Plasmid	Relevant main components	Purpose
26	LentiCRISPR v2 (Puro) CBFB-KO	Cas9 and sgRNA targeting CBFB (sgRNA: GAGAAGCAAGTTCGAGAACG)	KO
27	LentiCRISPR v2 (Puro) CDCA7L-KO	Cas9 and sgRNA targeting CDCA7L (sgRNA: TCTGACGAGAGGGTTTCCAT)	KO
28	LentiCRISPR v2 (Puro) DNAJC19-KO	Cas9 and sgRNA targeting DNAJC19 (sgRNA: TTTGCAAGCCATGAAGCATA)	KO
29	LentiCRISPR v2 (Puro) FASTKD2-KO	Cas9 and sgRNA targeting FASTKD2 (sgRNA: CTTCACGCCATAGTGAAGCT)	KO
30	LentiCRISPR v2 (Puro) LIPT2-KO	Cas9 and sgRNA targeting LIPT2 (sgRNA: TGACGCCCGAGGAAACTGCG)	KO
31	LentiCRISPR v2 (Puro) MANEAL-KO	Cas9 and sgRNA targeting MANEAL (sgRNA: GGCGTGTTGCGGATCGAATG)	KO
32	LentiCRISPR v2 (Puro) MRPS2-KO	Cas9 and sgRNA targeting MRPS2 (sgRNA: GGCCCTTATGATCCGCGAGT)	KO
33	LentiCRISPR v2 (Puro) MRPS21-KO	Cas9 and sgRNA targeting MRPS21 (sgRNA: ATTATGAGAAGCCATGCTGC)	KO
34	LentiCRISPR v2 (Puro) NDUFA11-KO	Cas9 and sgRNA targeting NDUFA11 (sgRNA: CAGTACTGGGATATCCCCGA)	KO
35	LentiCRISPR v2 (Puro) NDUFA8-KO	Cas9 and sgRNA targeting NDUFA8 (sgRNA: AAAGTTTGACGAGTGTGTGC)	KO
36	LentiCRISPR v2 (Puro) ORM2-KO	Cas9 and sgRNA targeting ORM2 (sgRNA: TTCTCAGAGAGTACCAGACC)	KO
37	LentiCRISPR v2 (Puro) RPUSD3-KO	Cas9 and sgRNA targeting RPUSD3 (sgRNA: AGAAGTACTTCACCCATGCA)	KO
38	LentiCRISPR v2 (Puro) SMARCB1-KO	Cas9 and sgRNA targeting SMARCB1 (sgRNA: TGGCACGGCATCTAAGTGGT)	KO
39	LentiCRISPR v2 (Puro) SOCS3-KO	Cas9 and sgRNA targeting SOCS3 (sgRNA: TACTGGAGCGCAGTGACCGG)	KO
40	LentiCRISPR v2 (Puro) STK11 -KO	Cas9 and sgRNA targeting STK11 (sgRNA: GTGATGGAGTACTGCGTGTG)	KO
41	LentiCRISPR v2 (Puro) PPP1R12C-KO	Cas9 and sgRNA targeting PPP1R12C (sgRNA: CTGGACTCCACCAACGCCGA)	KO
42	LentiCRISPR v2 (Puro) NTC#29	Cas9 and sgRNA targeting nothing in the human genome (sgRNA: AAGAAGAATTGGGGATGATG)	KO
43	LentiCRISPR v2 (Puro)SOCS3-KO (BL#3)	Cas9 and sgRNA targeting SOCS3 (sgRNA: TCAGCGTCAAGACCCAGTCT)	KO

4.1.12 Software

The following software was used in this study:

Software	Version	Producer	Purpose
Geneious Prime	2019.2.3	Biomatters Ltd.	*In silico* cloning, plasmid map creation
BD FACSDiva	varying	BD	Flow cytometry measurement
ChemoStarTS	0.5.54.0	Intas Science Imaging Instruments GmbH, Göttingen, Germany	Western blot imager software
FlowJo	10.8.1	FlowJo, LLC; part of BD	Analysis and gating of FC data
MikroWin 2010	5.24	Labsis Laborsysteme GmbH, Neunkirchen-Seelscheid, Germany	Plater reader software for protein measurements and DLR assay
R Studio	1.2.1335	RStudio, Inc	Analysis, descriptive statistics and display og FC data
Excel	2016	Microsoft Corporation	Analysis DLR assay, ranking after MAGeCK analysis
Inkscape	1.0.1	Inkscape development team	All figures of this study
ImageJ	1.52p	Wayne Rasband, National Institutes of Health, USA	Western blot analysis, combined with Inkscape
TeXnicCenter	2.02	The TeXnicCenter Team	Thesis typesetting
LAS X	3.7.4.23463	Leica Microsystems	Live-cell imaging

4.2 Methods

4.2.1 Working with bacteria

4.2.1.1 Preparation of chemically competent bacteria

Chemically competent *Stbl3*, *DH5α* and *K12 ER2925* bacteria were prepared as follows: 50 µL of bacteria solution was added to 15 mL LB medium and incubated over night at 37 °C and 225 rpm (pre-culture). On the next day, 400 mL LB medium was inoculated with the whole pre-culture and incubated at 37 °C and 225 rpm until the optical density measured at 550 nm reached 0.4 to 0.5. Then, bacteria were incubated on ice for 10 minutes and centrifuged in a pre-cooled 4 °C centrifuge for 15 min at 4,700 rpm. LB medium was removed and pellet was resuspended in 120 mL pre-cooled TfBI buffer. After 45 minutes, bacteria were centrifuged in a pre-cooled 4 °C centrifuge for 15 min at 4,700 rpm. TfBI buffer was removed and the pellet resuspended in 16 mL pre-cooled TfBII buffer. Bacteria were then aliquoted, snap-frozen in liquid nitrogen and stored at -80 °C.

4.2.1.2 Preparation of LB medium and agar plates

LB medium powder and LB agar powder were prepared using distilled water as recommended by the manufacturer. The mixtures were sterilized by autoclaving. After cooling down to approximately 50 °C, either ampicillin was added to a final concentration of 100 µg/mL or kanamycin was added to a final concentration of 50 µg/mL. LB agar was poured into 10 cm Petri dishes under the sterile hood, let dry and stored at 4 °C. LB medium was also stored at 4 °C.

4.2.1.3 Bacterial transformations

Aliquots of *Stbl3*, *DH5α* or *K12 ER2925* competent *E. coli* were thawn on ice. Per sample, 50 µL of bacteria were transferred to ice-cold reaction tubes and the ligation or HiFi DNA assembly reaction (up to 5 µL) was added. The tubes were flicked several times and incubated for 30 minutes on ice. Heat shock (42 °C) was applied to the bacteria for 45 seconds. Subsequently, bacteria were incubated on ice for two minutes. 150 µL S.O.C. medium was added to the cell suspension. Cells were incubated in a 37 °C heat block at 800 rpm continuous shaking for up to one hour. Different volumes of the bacteria suspension (20 and 180 µL) were streaked onto LB agar plates containing the appropriate antibiotics and incubated at 37 °C overnight. As a positive control, bacteria were transformed with the parental vector.

4.2.1.4 Inoculation of liquid cultures

After overnight incubation, single bacterial colonies on the LB agar plates were picked and transferred to LB medium containing the appropriate antibiotic. These liquid cultures were incubated at 37 °C at 225 rpm overnight in a Multitron Incubator Shaker (Infors AG, Bottmingen, Switzerland). They were subsequently used for small-scale plasmid purification, the inoculation of medium- or large-scale cultures or preparation of glycerol stocks.

4.2.1.5 Preparation of glycerol stocks

For long-term storage of the plasmid-containing bacteria, glycerol stocks of bacteria suspension were prepared by mixing 500 µL 60 % Glycerol (in LB medium, autoclaved) and 500 µL of the liquid cultures. The stocks were stored at -80 °C.

4.2.1.6 Plasmid isolation

To isolate plasmids out of bacteria, different kits were used according to the manufacturer's protocols.
For small-scale plasmid purification, the DNA-spin Plasmid DNA Purification Kit (#17098, iNtRON Biotechnology, South Korea) was used.
For medium-scale plasmid purification and large-scale plasmid purification, the PureLink HiPure Plasmid Midiprep Kit and PureLink HiPure Plasmid Maxiprep Kit (#K210004 and #K210007; both Thermo Fisher Scientific) were used.

4.2.2 Working with cell lines

4.2.2.1 Culture of mammalian cell lines

All human cell lines were cultured in 1x DMEM supplemented with 10 % FBS on tissue culture plastic ware (SARSTEDT and Greiner Bio-One). Cells were split when the cultures reached 60 to 80 % confluency. For this, cells were washed with 1x PBS. Then, 0.05 % Trypsin-EDTA was added to detach the cells and incubated for up to four minutes at 37 °C. Cells were then transferred to fresh 1x DMEM + 10 % FBS and centrifuged for three minutes at 1,000 rpm in a tabletop centrifuge (Rotina 420(R), Andreas Hettich GmbH and Co. KG, Tüttlingen, Deutschland). Medium was removed and the cell pellet was resuspended in fresh 1x DMEM + 10 % FBS. A part of this cell suspension was plated on new plastic ware for further culture.

The cultures were incubated in a CO_2 copper incubator (Thermo Scientific Heracell) with 5 % CO_2 and 95 % humidity.

4.2.2.2 Treatments

Hypoxia

Hypoxia treatment was carried out in a hypoxic glove box (either Coy Laboratory Products Inc., Grass Lake, Michigan, USA; or Toepffer Lab Systems, Göppingen, Deutschland) with 5 % CO_2 and 1 % O_2. Cells treated with hypoxia were also harvested in the hypoxia chamber unless otherwise stated.

PHD protein inhibition

PHD protein inhibition was achieved by the addition of DMOG to the cell culture medium. At the beginning of the treatment, medium of all cultures was changed to fresh medium (1x DMEM + 10 % FBS). The medium for the cultures to be treated were supplemented with 1 mM DMOG (final concentration) for 18 or 24 hours prior harvesting.

Proteasome inhibition

Inhibition of the proteasomal degradation was performed by the addition of MG-132 to the cell culture medium. At the beginning of the treatment, medium of all cultures was changed to fresh medium (1x DMEM + 10 % FBS). The medium for the cultures to be treated was supplemented with 10 µM MG-132 (final concentration) for 6 hours prior harvesting.

4.2.2.3 Cell counting

Cells were counted using the CASY Cell Counter and Analyzer System Model TT (Roche Innovatis AG, Reutlingen, Germany). By electronic pulse area analysis, cell number, size distribution and viability of a cell suspension is measured. Counting was performed by diluting 100 µL cell suspension in 10 mL CASY ton solution and measurement according to the manufacturer's protocol with individual programs stored for every cell line used.

4.2.2.4 Cryopreservation of cells

For storage of cell lines in liquid nitrogen tanks, cells were prepared as follows: A 60 to 80 % confluent culture was washed with 1x PBS. To detach the cells, cells were incubated for up to four minutes in 0.05 % Trypsin-EDTA at 37 °C. Cells were then transferred to fresh 1x DMEM + 10 % FBS and centrifuged for three minutes at 1,000 rpm in a tabletop centrifuge (Rotina 420(R)). Medium was removed and the cell pellet was resuspended in freezing medium containing 10 % DMSO, sterile filtered beforehand. Cell solution was transferred to Cryo vials (Cryo.S.; #123277, Greiner Bio-One) and placed in a container used to ensure a slow temperature drop in the vials (by isopropyl alcohol or styrofoam). The container was placed in a -80 °C freezer for at least 24 hours. For long-term storage,

cryo vials were transferred to liquid nitrogen tanks.

4.2.2.5 Thawing of cells

To thaw cryopreserved cells, the vials were rapidly transferred to a 37 °C water bath until mostly thawn. Then, cells were transferred to a 15 mL tube containing 5 mL 1x DMEM + 10 % FBS. Cells were centrifuged for three minutes at 1,000 rpm in a tabletop centrifuge and medium was removed. Subsequently, the cell pellet was resuspended in fresh 10 mL DMEM + 10 % FBS and cell solution was transferred to 10 cm (diameter) cell culture plastic ware.

4.2.2.6 Transient transfections

Endogenous tagging

Endogenous tagging required the co-transfection of two plasmids, namely the donor template and the Cas9- and sgRNA-expressing plasmid. Cells were seeded at a density of 1.5×10^6 in 10 cm tissue culture dishes in 10 mL 1x DMEM + 10 % FBS. On the next day, transfection was performed in a molar ratio of donor plasmid vs. Cas9/sgRNA plasmid 2 to 1 in 1 mL Opti-MEM. Thus, 15 µg donor plasmid was mixed with 15 µg Cas9-/sgRNA-expressing plasmid and 90 µL FuGene HD Transfection Reagent, resulting in a DNA vs. transfection reagent ratio of 1 to 3. Mixes were incubated for 15 minutes at room temperature. In the meantime, medium of the cells was changed to 5 mL 1x DMEM + 10 % FBS. Then, the transfection mix was added dropwise under soft shaking to the cells and cells were incubated at 37 °C overnight.

On the next day, cells were split to 10 new 10 cm dishes. The following day, medium was changed to 10 mL 1x DMEM + 10 % FBS containing the cell line-specific amount of puromycin to select for cells that transiently took up the Cas9/sgRNA plasmid. If the donor plasmid encoding the endogenous tag contained a puromycin resistance gene, the selection period was extended from two to ten days to select for cells expressing the tagged *EGLN3* gene. Then, in the case of A549 cells, single cell clones were isolated and expanded for further analyses.

DLR assay

Cells were seeded with a density of 40,000 cells/well in 24-well plates in 1 mL 1x DMEM + 10 % FBS. On the next day, 2 hours before transfection, medium was changed to 0.5 mL 1x DMEM + 10 % FBS. Then, 675 ng of the test plasmid - containing ADRB2, EPOR, or HIF1α-ODD coupled to the Luc2/tdTomato fusion protein - was added to 50 µL Opti-MEM. Additionally, 25 ng of the Renilla luciferase-encoding plasmid pRL (#E2231, Promega) was added. 2.1 µL of Lipofectamine 2000 was mixed into 50 µL of Opti-MEM.

Subsequently, both mixes were combined and incubated for 5 minutes at room temperature. Then, the whole mix was added to one well of the 24-well plate and incubated for four hours in the 37 °C incubator. Then, the medium was changed to 1 mL 1x DMEM + 10 % FBS. On the next day, treatments were performed and one day later, cells were harvested for the DLR assay.

4.2.2.7 Working with lentiviruses

All steps were performed in a S2 (biosafetly level 2) laboratory with all the necessary permissions granted.

Lentivirus production

Per virus to be produced, two T75 cell culture flasks (SARSTEDT) were used. Per flask, 4.5 x 10^6 HEK293T cells were seeded in 10 mL 1x DMEM + 10 % FBS.

On the next day, two hours before transfection, medium was changed to 6 mL 1x DMEM + 10 % FBS. In a sterile 1.5 mL reaction tube, 500 µL Opti-MEM was mixed with 7.5 µg of the specific plasmid - containing the to-be-expressed DNA. Additionally, 2.63 µg of the envelope plasmid pVSVG as well as 4.88 µg of the packaging plasmid psPAX was added. PEI 25K was equilibrated to room temperature and mixed. Then, 45 µL PEI were added to the plasmid-Opti-MEM-mix under vortexing and vortexing was continued for ten seconds. The DNA/PEI mix was incubated at room temperature for 20 minutes. In the meantime, 6 µL of 10 mM chloroquine (final concentration: 10 µM) were added to the cells and mixed well.
The DNA/PEI mix was then added in a dropwise manner to the cells under soft shaking and cells were incubated for 18 to 24 hours in the 37 °C incubator.

On day 2, the medium of the transfected cells was changed to 10 mL 1x DMEM + 10 % FBS.

48 hours post-transfection, on day 3, the virus-containing supernatant was collected in 50 mL tubes and stored at 4 °C. Cells were supplemented with fresh 10 mL 1x DMEM + 10 % FBS.

Finally, on day 4, the virus-containing supernatant was collected in 50 mL tubes and centrifuged with the previously collected supernatant for five minutes at 250 x g to remove cells and debris. Subsequently, the virus supernatant was filtered through a 0.45 µm PVDF filter (#P667.1, Carl Roth).

Lentivirus concentration

To obtain high viral titers, lentivirus particles were concentrated.
First, ultracentrifugation tubes (#253060, Herolab GmbH Laborgeräte,Wiesloch, Deutsch-

land) were added to each centrifuge bucket (#52427, Thermo Fisher Scentific). To each ultracentrifugation tube, approximately 20 mL of virus supernatant was added in a way that all buckets end up with the same weight. Viruses were then spun down at 20,000 rpm (or 22,500 rpm) for four hours (or 1.5 hours) at 4 °C in an ultracentrifuge (Sorvall WX ULTRA, Thermo Fisher Scientific) using the AH-629 rotor (Thermo Fisher Scientific).

After centrifugation, supernatant was removed and the tubes were left upside-down to dry on UV-lighted tissue paper for up to ten minutes. Then, the pellet was resuspended in 70 to 100 µL 1x DMEM and the UZ tubes were incubated at 4 °C for 20 minutes. After that, viruses of the same plasmid were resuspended again and combined in a 1.5 mL reaction tube, spun down for three minutes at 13,000 rpm at 4 °C. The supernatant was then aliquoted and frozen to -80 °C for storage.

Titration of lentiviral particles using crystal violet

5×10^4 cells per well were seeded in 6-well plates, 9 wells per virus to be titered. On the next day, the virus aliquots were thawn on ice and dilutions were prepared in dilution medium (1x DMEM + 10 % FBS + 8 µg/mL Polybrene) as follows: 11 µL of the virus was dissolved in 1,089 µL of dilution medium, and resuspended well (1:100 dilution). 110 µL of this dilution were transferred to 990 µL dilution medium and resuspended well (1:1,000 dilution). Again, 110 µL of this dilution were transferred to 990 µL dilution medium and resuspended well (1:10,000 dilution). This was continued up to a 1:1,000,000,000 dilution. Then, medium was removed from the cells and the virus dilutions were added to the cells and incubated for 18 to 24 hours in the 37 °C incubator. In the last well, only dilution medium without viral particles was added as mock control.

On the next day, medium was changed to 1x DMEM + 10 % FBS. One day later, at day 3, the medium was replaced with 1x DMEM + 10 % FBS containing selective antibiotics as required by the used plasmid and in the amount tolerated by the transduced cells (cell line-specific). Selection medium was changed every 2 to 3 days until day 16 or 17. By day 7 latest, all cells in the mock control should have died.

On day 16 or 17, the colonies that have formed during the experiment were stained. For this, the cells were washed twice with 1x PBS. Then, 1 mL 1x DMEM was added to the cells together with 100 µL crystal violet staining solution. Cells were incubated for 15 minutes at room temperature. After this, the staining solution was discarded and the cells were washed two to three times with 1x PBS until the colonies were well visible. Subsequently, the plates were scanned (EPSON Perfection V700 Photo Scanner, Suwa, Nagano, Japan) and colonies were quantified using Fiji (based on ImageJ) [164]. To determine the titer in transducing units per mL (TU/mL), the amount of colonies in one well was multiplied by the dilution factor (e. g. 100,000). The titer of several wells (at least two) was calculated and the mean was calculated to obtain the titer of the virus particles.

Transduction of cell lines with lentiviral particles

To stably integrate plasmid-coded DNA into the genome of cells, viral transduction was used here. For this, 10,000 or 25,000 cells were seeded in 48-well or 24-well plates in 1x DMEM + 10 % FBS, respectively. On the next day, transduction mixes were prepared: 1x DMEM (150 or 250 µL), 8 µg/mL polybrene and concentrated virus solution according to the required MOI were combined. Medium was removed from the cells and the transduction mixes were added. Cells were then incubated for 18 to 24 hours in the 37 °C incubator.

On the next day, medium was changed to 1x DMEM + 10 % FBS. One day later, at day 3, the medium was replaced with 1x DMEM + 10 % FBS containing selective antibiotics as required by the used plasmid and in the amount tolerated by the transduced cells (cell line-specific). In the following days, selection medium was changed every 2 to 3 days and cells were expanded whenever they reached 80 % confluency.

4.2.2.8 Microscopy

Standard microscopy

Standard microscopy was performed using a standard wide field inverted microscope (DMIL, Leica Microsystems, Wetzlar, Germany).

Live-cell microscopy

For live-cell microscopy, cells were seeded in microscopy-grade 96-well CELLSTAR plates (Greiner Bio-One). Here, to reduce the autofluorescence of phenol-red present in the 1x DMEM, live-cell microscopy medium (based on FluoroBrite DMEM) was used. One day after seeding the cells, medium was changed and DMOG was added where applicable. Promptly, the plate was inserted in the pre-incubated THUNDER Imager Microscope (Leica Microsystems) equipped with a live-cell incubation chamber (WSKMX, Tokai Hit, Co, Ltd, Fujinomiya, Japan) and imaging was started for the indicated amount of time. The incubation chamber ensured supply with 5 % CO_2 (using the STXF and STXCO2O2 controllers, Tokai Hit) and a high humidity to limit evaporation.

4.2.2.9 Flow cytometry and FACS

Preparation of cells

Unless otherwise stated, 150,000 cells per well were seeded in 6-well plates in 1x DMEM + 10 % FBS. On the following day, medium of all cells was changed and treatments were started where applicable. On the next day, cells were harvested by removing the medium and washing the cells once with 1x PBS. Then, 400 µL Trypsin-EDTA was added and the

cells were incubated for up to four minutes at 37 °C. One mL 1x DMEM + 10 % FBS was added and cells were stored in an ice box until all cells were harvested. Then, cells were centrifuged in a pre-cooled 4 °C centrifuge for three minutes at 1,000 rpm. Subsequently, medium was removed and cells were washed in 3 mL FACS buffer and transferred in FACS tubes (SARSTEDT) through a cell strainer (Corning Incorporated, Corning, New York, USA). Then, cells were centrifuged in a pre-cooled 4 °C centrifuge for three minutes at 1,000 rpm and the buffer was removed by inverting the FACS tube. Cells were washed once more using 1 mL FACS buffer and vortexing, then centrifuged in a pre-cooled 4 °C centrifuge for three minutes at 1,000 rpm. Buffer was discarded by inverting the tube and sample (with approximately 100 µL buffer left) was stored on ice with aluminum foil as light protection. Five minutes before measurement, 1 µL SYTOX blue nucleic acid stain was added to every sample. To prepare a dead-cell control, wildtype cells were prepared as described and supplemented with 70 µL of 100 % ethanol.

Flow cytometry

For flow cytometry - pure measurement of the samples without sorting - a BD FACSCanto II cell analyzer (BD) and the corresponding software BD FACSDiva was used. Control samples were used to set meaningful gates. First, forward scatter (FSC) and side scatter (SSC) were used to define the main cell population(s). Then, SYTOX blue nucleic acid stain was used to determine the living cells. Finally, FITC (having very similar excitation and emission spectra as UnaG) was used to discriminate UnaG-positive and -negative cell populations. Mostly, a medium flow rate was used and the system was flushed after every sample.

FACS for single cell clone generation

Sorting for single cell clones was achieved in two steps using a BD FACSAria III cell sorter (BD) and the corresponding BD FACSDiva software. Control samples were used to set meaningful gates. First, forward scatter (FSC) and side scatter (SSC) were used to define the main cell population(s) and exclude dirt. Then, SYTOX blue nucleic acid stain (represented by 'Pacific Blue') was used to determine the living cells. Finally, FITC (having very similar excitation and emission spectra as UnaG) was used to discriminate UnaG-positive and -negative cell populations.

As a first sorting step, polyclonal G141 or A549 5xHRE HIF2α-ODD(aa 354-581)=UnaG-V5 cell pools were seeded and harvested as described above. Cells were sorted by FACS for low UnaG signal, which was slightly higher than the signal of wildtype cells without any reporter expression. Here, cells were sorted in tubes with capture buffer to keep polyclonal pools, which were then further cultured in post-sorting medium. Cells were kept in post-sorting medium to avoid fungal or bacterial contamination, as the sorting process

was not sterile.
In the second step, cells were seeded as described above and treated with 1 mM DMOG for 18 hours to trigger the accumulation of the fluorescent reporter. Subsequently, cells were sorted by FACS for UnaG positivity into only one cell per well of a 96-well plate into post-sorting medium. Cells were then grown and expanded until they could be frozen and examined.

Analysis and display of data

To analyze and display flow cytometry and FACS data, raw data were exported from BD FACSDiva as FCS3.0 files and imported into FlowJo (BD).
In FlowJo, gates were set as described above and either dot plots were created (as e. g. in Fig. 2.6) or the living cells (meaning the Pacific Blue-negative cells) were exported as csv files including FITC measurements.

Csv files were imported in R Studio using the library 'readr'. Then, experimental information was added to each sample, such as cell line, treatment or seeded cell density. Individual samples were clustered to one dataset and filtered to exclude negative values that would interfere with display of data in a logarithmic view. Then, violin plots with integrated box plots were compiled using the libraries 'ggridges', 'ggplot2', 'scales', 'ggstance', 'cowplot' and 'dplyr' (as e. g. shown in Fig. 2.8). Additionally, descriptive statistics were calculated by using the 'summary' R function to yield the mean, median, 25^{th} and 75^{th} quartiles, minimum value and maximum value of every sample (see appendix). In the graphs, whiskers show the 1.5-fold interquartile range (IQR), which can be considered the reasonable extremes of the data.

4.2.2.10 CRISPR screening

To conduct the CRISPR/Cas9-mediated KO screening, ten million G141 SCC#A1 cells were seeded in a total of 40 75 cm^2 tissue culture (TC) flasks in DMEM + 10 % FBS and 1.2 µg/mL blasticidin (day 0). On the next day, cells were transduced with viral particles containing the human genome-wide CRISPR Brunello knockout pooled library that targets 19,114 genes with each four sgRNAs per gene [37]. Transduction was performed with a MOI of 0.4 to increase the probability that each cell takes up only one lentiviral particle and with that only one sgRNA. Furthermore, a coverage of 50x was used, meaning that theoretical - assuming every sgRNA is equally abundant in the virus particle preparation - every sgRNA should be present in 50 cells after transduction (76,441 sgRNAs x 50 : 0.4 MOI = approx. 10,000,000 cells). For transduction, plain DMEM medium was used supplemented with 8 µg/mL polybrene.
On the following day (day 2), medium was changed to DMEM + 10 % FBS, omitting antibiotics for recovery. From day 3 on, cells were selected using 1 µg/mL puromycin

for in total ten days. 1.2 µg/mL blasticidin was added as well to avoid loss of the FR in the cells. On day five and eight, cells were passaged while keeping the theoretical 50x coverage. On day eleven, cells were seeded for FACS in the density determined before (chapter 2.2.1; applying to 10 cm TC plates: 1.3 million cells per plate) and again with keeping the 50x coverage. On the following day, medium was changed.

FACS was then performed on day 13. Cells were prepared as described above (chapter 4.2.2.9) with the exception that 900 µL FACS buffer was added in the end to dilute the sample, which was necessary for the sorting process. In agreement with the higher amount of cells and the bigger volume, 5 µL SYTOX blue nucleic acid stain was added per sample. Cell sorting was performed using a 100 µm nozzle in the BD Aria III sorting machine. During the sorting process, UnaG-positive and UnaG-negative cells were sorted into tubes with capture buffer. After this, the cells were transferred to post-sorting medium, centrifuged, medium was removed and new post-sorting medium was added. Cells were counted using CASY counter and seeded at a density of 10,000 cells/well in 6-well TC plates. Cells were kept in post-sorting medium to avoid fungal or bacterial contamination. Like this, all UnaG-positive cells and a number-matching subset of UnaG-negative cells were separately seeded and kept in culture for additional seven days to increase the amount of UnaG-positive cells for gDNA extraction. Those cells were harvested on day 20 by trypsination and two PBS washes before freezing the cell pellets to -20°C.

In total, approximately 30 million cells were sorted in each of both screens. During harvesting, a proportion of cells was kept as an unsorted control sample (unsorted control; approx. 9.5 % of all cells in the screen).

Genomic DNA isolation and further processing was performed as described (chapter 4.2.3.8, page 123).

4.2.3 Working with DNA

4.2.3.1 Standard gDNA isolation

To isolate gDNA from human cell cultures for all purposes except NGS after the screening, the PureLink Genomic DNA Mini Kit (#K182001, Thermo Fisher Scientific) was used according to the manufacturer's instructions.

4.2.3.2 Endpoint Polymerase Chain Reactions

Fragments for cloning purposes and Sanger sequencing

Most endpoint PCRs - e. g. for cloning purposes or Sanger sequencing - were performed using Q5 Hot Start High-Fidelity DNA Polymerase. In rare cases where am-

plification was not successful using Q5, Phusion Hot Start II DNA-Polymerase was used. Both polymerases were used according to the manufacturer's manual. For Q5, primer annealing temperatures were determined using the NEB Tm calculator tool (https://tmcalculator.neb.com). For Phusion, primer annealing temperatures were determined using the Thermo Tools Tm Calculator (https://www.thermofisher.com/).

Colony PCRs

In order to determine if bacterial colonies contained the intended plasmid, colony PCRs were performed. For this, 0.5 mL tubes were labeled and filled with 6 µL 0.9 % NaCl solution. A OneTaq DNA Polymerase PCR master mix was prepared according to the manufacturer's instructions and 19 µL were dispensed into each 0.2 mL PCR tube. A bacterial colony was picked from the LB agar plate with a 10 µL pipette tip, pipetted up and down in the 0.5 mL tube and transferred 1 µL to the PCR tube. PCR programme was set according to the manual and the primer annealing temperatures were determined using the NEB Tm calculator tool (https://tmcalculator.neb.com).

Mycoplasma PCR

Mycoplasma PCR was performed using HotStarTaq DNA Polymerase according to Pisal *et al.* [149] and using primers and internal control plasmid as specified in Uphoff and Drexler [195].

4.2.3.3 Agarose gel electrophoresis

In order to analyze the results of a PCR or a control restriction digestion, a 0.5 % to 2 % agarose gel was prepared as follows: 0.5 g to 2 g of NEEO agarose was added to each 100 mL 1x TAE buffer and boiled until it was completely dissolved (microwave). Volume was adjusted to the respective gel tray (60, 120 or 180 mL). After cooling down to approximately 50 °C, 4 µL SYBR Safe DNA gel stain (10 mg/ml) were added and the gel was poured into the gel tray. The gel was left to polymerize for at least 30 min under a digestorium.
6x gel loading dye (orange or purple) was added to the PCR or digestion samples, which were then loaded onto the gel placed in a gel chamber filled with 1x TAE buffer. DNA ladder GeneRuler 1kb Plus allowed for the assessment of the DNA fragment lengths. The electrophoresis was running for about 40 minutes at 120 V in a gel electrophoresis chamber (Model H5 Series 1087, Thermo Fisher Scientific). Afterwards, the DNA was visualized using a blue/green light-equipped gel documentation system (FastGene FAS-V Imaging System, NIPPON Genetics EUROPE GmbH, Düren, Germany). If elution of the DNA was desired, the correct DNA fragments were excised using a clean scalpel. The gel slices were transferred to a 2 mL microcentrifuge tube and stored at -20 °C until further use.

4.2.3.4 DNA isolation out of agarose gel (gel extraction)

The recovery of DNA from gel slices was performed using the QIAquick Gel Extraction Kit (Qiagen) according to the manufacturer's instructions. The DNA was eluted in 30 µL nuclease-free water instead of 50 µL, as recommended, in order to obtain a higher concentrated DNA solution. The DNA solution was then purified (see below) and used for e. g. cloning of plasmids.

4.2.3.5 PCR cleanup

To clean up PCR products (with or without previous gel extraction) for downstream applications, the E.Z.N.A. Cycle Pure Kit (Omega Bio-tek, Inc., Norcross, USA) was used according to the manufacturer's instructions. The DNA was eluted in up to 30 µL nuclease-free water.

4.2.3.6 Determination of DNA concentration and quality

DNA and RNA concentrations and quality were measured on a NanoDrop 2000 Spectrophotometer (Thermo Fisher Scientific). For determination of RNA and DNA concentration in solution, the absorbance at 260 nm was measured. To assess the purity of the RNA or DNA sample, the ratio of absorbance at 260 nm and 280 nm was calculated. A ratio of ~1.8 shows pure DNA and a ratio of~2.0 is accepted as pure RNA. Lower ratios indicate contaminations with for example proteins (absorbance at 280 nm) or phenoles (absorbance at 230 nm). As a secondary measurement of RNA and DNA purity, the ratio of absorbance at 260 nm and 230 nm was calculated. Lower ratios than 2.0 to 2.2 indicate contaminations with for example EDTA, carbohydrates or phenoles.

4.2.3.7 Sanger sequencing

In order to verify the correct sequences of PCR products or plasmids, and to determine point mutations in gDNA of cell lines, PCR fragments or plasmids were sent for sequencing to Microsynth AG (Balgach, Switzerland) according to the requirements set by the service provider.

4.2.3.8 Next Generation Sequencing

gDNA isolation for Next Generation Sequencing

gDNA isolation in the course of the CRISPR/Cas9-mediated genome-wide screening was performed as follows:
Per cell amount that equals a 10 cm TC plate, 1 mL TEX buffer together with 12.5 µL Proteinase K (final concentraion: 250 µg/mL) was added to the cell pellet and mixed by pipetting. The solution was transferred to a 2 mL reaction tube and incubated at 37 °C

with 400 rpm shaking overnight.

On the next day, 350 µL 5 M NaCl solution was added and vortexed vigorously, then incubated for 30 minutes on ice. Then, the samples were centrifuged in a table-top centrifuge at 13,000 rpm for 30 minutes at 4 °C. Supernatant was transferred to a new 2 mL reaction tube. To precipitate the DNA, 1 mL absolute ethanol was added and mixed well. Mixes were incubated for 45 minutes at -80 °C and then centrifuge at 13,000 rpm for 30 minutes at 4 °C. Supernatant was decanted and pellet was washed with 1 mL ice-cold 70 % ethanol and then centrifuge at 13,000 rpm for 30 minutes at 4 °C. Supernatant was carefully removed and the pellet dried at room temperature for approximately 15 minutes. The dry pellet was then dissolved in 150 µL nuclease-free water which was preheated at 37 °C.

Ribonuklease A treatment

To remove RNA from the sample, samples were treated with RNAse A. For this, per 100 µL gDNA, 1 µL boiled RNAse A (10 mg/mL) was added to the samples. The reaction tubes were incubated at 37 °C with 400 rpm shaking for 30 minutes. Then, 35 µL 5 M NaCl solution was added and mixed well, followed by 200 µL absolute ethanol (ice-cold). Samples were vortexed well. Mixes were incubated for 45 minutes at -80 °C and then centrifuge at 13,000 rpm for 30 minutes at 4 °C. Supernatant was decanted and pellet washed with 500 µL ice-cold 70 % ethanol and then centrifuge at 13,000 rpm for 30 minutes at 4 °C. Supernatant was carefully removed and the pellet dried at room temperature for approximately 15 minutes. The dry pellet was then dissolved in 50 µL nuclease-free water which was preheated at 37 °C.

DNA concentrations of the solutions were determined using Nanodrop. To verify the successful removal of RNA, a small sample of gDNA before and after the RNAse treatment was loaded onto a 0.8 % agarose gel. Disappearance of the two sharp bands below 3,000 bp (28S and 18S ribosomal RNA) as well as the diffuse bands at approximately 250 bp (small and/or degraded RNAs) indicated successful removal of RNA.

NGS library preparation

Genomic DNA solutions were sent to the Biochemistry II department at the Goethe-University Frankfurt (Germany) for library preparation by Alkmini Kalousi.
NGS library preparation was generated using two PCR reactions: The first one is used to amplify the sgRNA-containing part of the (p)LentiCRISPR v2 (Puro) plasmid that was inserted into the genome of the cells by lentiviral transduction. The second PCR reaction is used to add barcodes and indices to the fragments needed for the actual sequencing.

For the first PCR (PCR-1), the gDNA was divided in up to 2 µg per 50 µL PCR reaction. Per sample, 10 µg gDNA were used. PCR was performed using the NEBNext

High-Fidelity 2X PCR Master Mix (NEB) and 2.5 µL of each 10 µM PCR-1 forward and reverse primer. The reactions were incubated in a thermo cycler as follows: Initial denaturation at 98 °C for 7 min, followed by 20 cycles of 2 min denaturation at 98 °C, 55 s annealing at 60 °C and 1 min elongation at 72 °C. Then, a 10 min final elongation step at 72 °C followed before the samples were cooled down to 4 °C.

Following PCR-1, the PCR reactions of the same sample were pooled. This was then used as template for PCR-2 (12.5 µL). Additionally, 25 µL NEBNext High-Fidelity 2X PCR Master Mix (NEB), 2.5 µL PCR-2 forward and reverse primers (containing Illumina adaptors and barcodes, each 10 µM) and ddH_2O up to 50 µL reaction volume were added. The reactions were incubated in a thermo cycler as follows: Initial denaturation at 98 °C for 3 s, followed by 10 cycles of 1 min denaturation at 98 °C, 55 s annealing at 68 °C and 55 s elongation at 72 °C. Then, a 10 s final elongation step at 72 °C followed before the samples were cooled down to 4 °C.

After the PCRs, the reactions were run on a 3 % agarose gel using SYBR Safe DNA gel stain and run for 35 min at 100 V. Bands were excised and purified using Nucleospin Gel and PCR Cleanup kit (Macherey-Nagel, Düren, Germany) according to the manufacturer's instructions. All DNA suspensions of the same sample were pooled and measured using Qubit.

Sequencing

Samples were sent for NGS to GENEWIZ Germany GmbH (Leipzig, Germany) by Yves Matthess (Biochemistry II department at the Goethe-University Frankfurt). They were sent as a single pool, pooling all 13 samples. Those 13 samples were:

Brunello library (Maxipreparation used for virus generation)
UnaG-positive sample, harvested at day 20 (one per screen)*
UnaG-negative sample, harvested at day 20 (one per screen)*
unsorted control sample, harvested on day 13 (one per screen)*
UnaG-negative sample, harvested at day 13 (one per screen)
unsorted control sample, harvested on day 20 (one per screen)
cells directly harvested without preparation for FACS, harvested on day 13 (one per screen)

* = samples were used for MAGeCK analysis and subsequent ranking

Sequencing configuration was 'Illumina 2x150bp configuration' and the Single Index Illumina Index Chemistry was used, providing 6gp Indices. Sequencing and Indexing Primers were standard Illumina Primers. The samples were complemented with 5 % PhiX control library spike-in to monitor run quality measures such as cluster generation and sequencing. Samples were sequenced on a Illumina HiSeq machine. Results were provided

as FASTQ files, and a Quality Report was added as well.

Analysis of data

The resulting sequencing data were analyzed in collaboration with the Department of Biochemistry II at the Goethe University Frankfurt. Of note, Martin Wegner performed all analysis steps and calculations (incl. quality control and enrichment analyses/MAGeCK analysis), except the final ranking based on the MAGeCK calculations.
Visualizations in Fig. 2.18 were created with Python3, matplotlib 3.2.1 [70] and the seaborn 0.11.0 package [202] by Martin Wegner and adapted for better visualization of relevant data.

Quality Control: In short, data were downloaded as fastq files from GENEWIZ. Raw read counts were determined using cutadapt 2.8 [125], bowtie2 2.3.0 [103] and a custom Python3 pipeline (Wegner, M., unpublished). Raw read counts were then normalized to counts per million (cpm). Subsequently, gRNA read counts were aggregated on gene level by using the median count of the four gRNAs per gene. LFCs were individually calculated as the log2 fold change of cpm normalized gRNA and gene read counts.

Enrichment analyses: Enrichment analyses were performed using Model-based Analysis of Genome-wide CRISPR/Cas9 Knockout (MAGeCK version 0.5.9.2) [111] on raw gRNA read counts, normalization set to 'median'. Samples used for MAGeCK analysis were:

UnaG-positive samples, harvested at day 20 (both screens)
UnaG-negative sample, harvested at day 20 (only screen replicate 1)
unsorted control samples, harvested on day 13 (both screens)

In short, read counts are first median-normalized to reduce the effect of read count distribution and library sizes. Here, data from both screens are used (except for UnaG-negative sample of screen 2). Subsequently, the variance of read counts is calculated by estimation. Last but not least, a negative binomial model is used to test if sgRNA abundance differs between the sorted samples (UnaG-positive or -negative) and the unsorted control samples. The resulting *p*-values are used for the ranking later on (see next paragraph). Of note, MAGeCK usually ranks using an α robust ranking aggregation (α-RRA) algorithm. In this case, UnaG-positive and -negative samples would have been used. As we were able to incorporate only one UnaG-negative sample, the α-RRA approach was not used, as it might have been highly impacted by having only one UnaG-negative sample.

Ranking: To achieve a ranking, the *p*-values resulting from the binomial model (comparisons between UnaG-positive and unsorted control samples) were used. These *p*-values were grouped in different *p*-value groups:

$p < 0.00005$

$0.00005 \leq p < 0.0005$
$0.0005 \leq p < 0.005$
$0.005 \leq p < 0.05$
$0.05 \leq p < 0.5$
$p \geq 0.5$

To sort the genes within a *p*-value group, the difference between the LFCs of the gene reads of UnaG-positive versus unsorted control and UnaG-negative versus unsorted control samples was calculated (ΔLFC).

To filter out likely false-positive hits, genes with a ΔLFC of <1 were excluded. During the final review of the top 60 genes, genes with no reads in the UnaG-negative sample were also excluded, as in this case no reliable LFC could be computed. For this reason, only one gene, ATP13A1, was excluded from the top 60.

4.2.3.9 Traditional restriction enzyme cloning

Restriction digestion

In order to introduce an insert (PCR product or other DNA fragments) into a plasmid, the circular plasmid had to be enzymatically digested. The used restriction enzymes are listed in chapter 4.1.7.1 (page 96). The digestions were performed as recommended by the manufacturer, depending on the restriction enzyme and amount of vector fragment or PCR product used. Higher amounts of DNA required longer incubation periods for digestion. Afterwards, the enzyme was heat-inactivated at 65 °C or 80 °C, if recommended by the manufacturer.

Dephosphorylation of plasmids

To prevent religation of single-digested plasmids, the phosphate residues of used plasmids were removed by alkaline phosphatase. Therefore, the FastAP enzyme was added to the restriction digestion reactions according to the manufacturer's instructions.

Ligation

Ligation was performed using T4 DNA Ligase according to the manufacturer's manual.

4.2.3.10 HiFi DNA Assembly

Assemblies of more complex plasmids, i. e. donor plasmids for endogenous tagging, were performed by using the NEBuilder HiFi DNA Assembly Master Mix (NEB) according to the manufacturer's instructions. Primers for the assembly were designed using the NEBuilder Assembly Tool (NEB, https://nebuilder.neb.com).

4.2.3.11 Cloning of plasmids in this thesis

Here, cloning of the plasmids engineered in this study is described. All PCR amplifications were performed using Q5 Hot Start Poylmerase. Of note, plasmid sequences were always verified by Sanger sequencing and analysis was done using the software Geneious Prime. If not otherwise stated, plasmid were transformed into *Stbl3* bacteria after ligation or assembly reactions and plasmids were isolated by small-scale plasmid isolation. Primer sequences are listed in chapter 4.1.10, starting on page 100.

Donor plasmids for endogenous tagging (#1 to #4)

pUC57 PHD3-ET C-term mCherry (Tab. 2.1, #1): Left and right homology arms of *EGLN3* were PCR amplified from gDNA (anonymous) using primers No. 1 and 2, and No. 3 and 4, respectively. MCherry was PCR amplified from the *pmCherry-C1* plasmid using primers No. 5 and 6. Reactions were run on a 1.5 % agarose gel and bands were excised and extracted from the gel. *PUC57* plasmid was EcoRV digested and dephosphorylated using FastAP enzyme. Then, the reaction was run on a 0.7 % agarose gel and band was excised and gel extraction was performed. The three inserts were introduced into the *pUC57* plasmid using the NEBuilder HiFi DNA Assembly Master Mix.

pUC57 PHD3-ET C-term GSAGSAAGSGEF-Linker TurboGFP-V5 (Tab. 2.1, #2): Left and right homology arms of *EGLN3* were PCR amplified from gDNA (anonymous) using primers No. 1 and 7, and No. 8 and 4, respectively. TurboGFP was PCR amplified from the *pGIPZ nsc* plasmid using primers No. 9 and 10. Reactions were run on a 1.5 % agarose gel and bands were excised and extracted from the gel. *PUC57* plasmid was EcoRV digested and dephosphorylated using FastAP enzyme. Then, the reaction was run on a 0.7 % agarose gel and band was excised and gel extraction was performed. The three inserts were introduced into the *pUC57* plasmid using the NEBuilder HiFi DNA Assembly Master Mix.

pUC57 PHD3-ET N-term GSAGSAAGSGEF-Linker UnaG-Flag (Tab. 2.1, #3): Left and right homology arms of *EGLN3* were PCR amplified from gDNA (anonymous) using primers No. 11 and 12, and No. 13 and 14, respectively. UnaG was PCR amplified from the *pEF dUnaG* plasmid using primers No. 15 and 16. Reactions were run on a 1.5 % agarose gel and bands were excised and extracted from the gel. *PUC57* plasmid was EcoRV digested and dephosphorylated using FastAP enzyme. Then, the reaction was run on a 0.7 % agarose gel and band was excised and gel extraction was performed. The three inserts were introduced into the *pUC57* plasmid using the NEBuilder HiFi DNA Assembly Master Mix.

pUC57 PHD3-ET C-term GSAGSAAGSGEF-Linker UnaG-Flag GSG-Linker Furin/T2A PuroR (Tab. 2.1, #4): This plasmid is based on the *pUC57 PHD3-ET C-term*

GSAGSAAGSGEF-Linker TurboGFP-V5 plasmid. The plasmid backbone was amplified using primers No. 17 and 18. Afterwards, the reaction was digested with DpnI to digest template full-length backbone. The T2A-Puro-Flag cassette was PCR amplified from the *pSpCas9(BB)-2A-Puro (PX459) V2.0* plasmid with the primers No. 19 and 20. UnaG was amplified using the plasmid *pEF/myc/cyto 5xHRE CMVp dUnaG* as template and the primers No. 21 and 22. All reactions were run on a 0.7 % agarose gel and bands were excised and gel extraction was performed. Additionally, E.Z.N.A. Cycle Pure Kit was used to purify the reactions. The three fragments were then assembled using the NEBuilder HiFi DNA Assembly Master Mix.

pLenti6/V5-DEST CMVp ADRB2-Luc2/tdTomato-Flag

The *pLenti6-V5/DEST CMVp SmaI-dead* plasmid was digested using EcoRV, dephopshorylated using FastAP enzyme, run on 0.7 % agarose gel and the large fragment excised and purified. The cytosolic domain of ADRB2 was PCR amplified from gDNA (anonymous) using primers No. 23 and 24 and purified using the E.Z.N.A. Cycle Pure Kit. The Luciferase2-tdTomato fusion cDNA was PCR amplified from the *pcDNA3.1(+)/Luc2=tdT* plasmid using primers No. 25 and 26, run on 0.7 % agarose gel and the large fragment excised and purified. NEBuilder HiFi DNA Assembly Master Mix was used to assemble the two inserts into the pLenti6 backbone, using two times more insert than vector backbone.

pLenti6/V5-DEST CMVp EPOR-Luc2/tdTomato-Flag

To construct the *pLenti6/V5-DEST CMVp EPOR-Luc2/tdTomato-Flag* plasmid, the *pLenti6/V5-DEST CMVp ADRB2-Luc2/tdTomato-Flag* plasmid was modified as follows: The plasmid was digested using SmaI and NheI, run on a 0.7 % agarose gel and the larger fragment excised and gel extracted. The cytosolic domain of EPOR was PCR amplified using primers No. 27 and 28 and the anonymous gDNA. After running the reaction on a 1.5 % agarose gel, the lower band was excised and the DNA was purified by gel extraction. Fragment was digested using SmaI and NheI.
Both fragments (backbone and EPOR) were purified by E.Z.N.A. Cycle Pure Kit. Then, they were ligated using T4 DNA Ligase.

pLenti6/V5-DEST CMVp Luc2/tdTomato-HIF1α-ODD(aa530-652)

The *pLenti6/V5-DEST CMVp Luc2/tdTomato-HIF1α* plasmid was engineered as follows: *The pLenti6/V5-DEST CMVp Luc2/tdTomato* plasmid (cloned by Omelyan Trompak, Institute of Neuropathology, JLU Giessen) was digested with SmaI and dephosphorylated using FastAP enzyme according to manufacturer's instructions. Afterwards, the reaction was run on a 0.7 % agarose gel and the DNA was extracted from the gel.

The HIF1α-ODD(aa530-652) was amplified from gDNA obtained from GBM46x cells (established by Sascha Seidel, Institute of Neuropathology, JLU Giessen) with primers No. 29 and 30. PCR reaction was purified using the E.Z.N.A. cycle pure kit.
Ligation was done using T4 Ligase and appropriate buffers.

pLenti6 CMVp HIF2α-ODD(aa354-581)=UnaG-V5 reporter plasmid

The *pLenti6 CMVp HIF2α-ODD(aa354-581)=UnaG-V5* reporter plasmid was cloned in multiple steps. First, the *pLenti6-V5/DEST CMVp SmaI-dead* plasmid was digested using EcoRV and then religated. Second, the resulting plasmid was digested with BamHI and XhoI according to the manufacturer's instructions. The reaction was run on a 0.7 % agarose gel and the DNA was extracted from the gel.
HIF1α-ODD was PCR amplified from *pLenti6/V5-DEST CMVp Luc2/tdTomato-HIF1α-ODD(aa530-652)* using primer No. 31 and 32. Then, the reaction was purified using the E.Z.N.A. cycle pure kit and then digested with BamHI and XhoI. Ligation was carried out using T4 DNA Ligase and respective buffers. Plasmid was transformed into *Stbl3* bacteria and plasmid isolated by small-scale plasmid isolation.

The resulting *pLenti6 CMVp HIF1α-ODD* plasmid was digest with XhoI and MluI, run on a 0.7 % agarose gel and the respective DNA band was extracted from the gel. TurboGFP was amplified from *pGIPZ nsc* plasmid using primer No. 33 and 34, followed by PCR cleanup with E.Z.N.A. cycle pure kit and digestion with XhoI and MluI. Ligation was carried out using T4 Ligase according the manufacturer's recommendations and yielded the *pL6 CMVp HIF1α(aa530-603)-ODD=TurboGFP-V5* plasmid. Plasmid was transformed into *Stbl3* bacteria and plasmid isolated by small-scale plasmid isolation.

The *pLenti6 CMVp HIF1α(aa530-603)-ODD-TurboGFP-V5* plasmid was digested with BcuI to release the TurboGFP cassette. The backbone was excised from the agarose gel and gel extracted. UnaG was PCR amplified from the *pEF dUnaG* plasmid using primers No. 35 and 36, then digested with BcuI and purified with the E.Z.N.A. cycle pure kit. Ligation was carried out as before. Plasmid was transformed into *Stbl3* bacteria and plasmid isolated by small-scale plasmid isolation.

Subsequently, the *pLenti6 CMVp HIF1α(aa530-603)-ODD=UnaG-V5* plasmid was digested with XhoI to release HIF1α(aa530-603) and dephosphorylated using FastAP according to manufacturer's instructions. The respective DNA band was excised from the gel and purified. HIF2α was PCR amplified from the *pcDNA3 HIF2α-ODD-Luciferase-Flag* plasmid (generous gift of Richard Bruick, UT Southwestern Medical Center) using the primers No. 37 and 38. Reaction was purified using the E.Z.N.A. cycle pure kit, followed by XhoI digestion. Plasmid was transformed into *K12 ER2925* (Dam- Dcm-) bacteria and plasmid isolated by small-scale plasmid isolation.

pLenti6 5xHRE CMVp HIF2α-ODD(aa354-581)=UnaG-V5 reporter plasmid

The final *pLenti6 5xHRE CMVp HIF2α-ODD(aa354-581)=UnaG-V5* reporter plasmid is based on the *pLenti6 CMVp HIF2α-ODD(aa354-581)=UnaG-V5* plasmid. The *pLenti6 CMVp HIF2α(aa354-581)-ODD=UnaG-V5* plasmid was digested with Bsu15I to release the CMV promoter and dephosphorylated using FastAP. The 5xHRE CMVp cassette was PCR amplified from *pEF dUnaG* using primer No. 39 and 40, purified and digested with Bsu15I. Ligation was carried out as before.

sgRNA cloning into pSpCas9(BB)-2A-Puro (PX459) V2.0 plasmid

Cloning of PHD3 sgRNAs for endogenous tagging (C- and N-terminal) into the *pSpCas9 (BB)-2A-Puro (PX459) V2.0* backbone was performed as described by Ran *et al.* [154]. Briefly, target sequences were designed using the CRISPR Design Tool (Massachusetts Institute of Technology, Cambridge, USA) or later the GPP Web Portal (Broad Institute of MIT and Harvard, Cambridge, USA). Based on the selected target sequences, oligonucleotides were designed and ordered (Sigma-Aldrich; primer no. 41 to 48, chapter 4.1.10.2 on page 104) as sense and antisense oligos. Oligos were then phosphorylated and annealed, using PNK enzyme, ATP and the respective buffer. A digestion-ligation reaction using the restriction enzyme BpiI digested the *pSpCas9(BB)-2A-Puro (PX459) V2.0* backbone and included the oligo duplex with the help of Fast Digest Buffer, DTT, ATP and T4 DNA Ligase.

sgRNA cloning into (p)LentiCRISPR v2 (Puro) plasmid

Cloning of specific sgRNAs into the *(p)LentiCRISPR v2 (Puro)* backbone was achieved as described in "sgRNA cloning into *pSpCas9(BB)-2A-Puro (PX459) V2.0*", with the only exception that the restriction enzyme BsmBI was used instead of BpiI. Oligonucleotides no. 49 to 108 were used for these purpose (see chapter 4.1.10.2, starting on page 104).

4.2.4 Working with proteins

4.2.4.1 Dual-Luciferase Reporter (DLR) assay

Cells were seeded, transfected and treated as described in section 4.2.2.6 (page 115). On the day of harvesting, cells were washed once with 1x PBS. PBS was removed and 100 µL 1x Passive Lysis Buffer was added to the cells. Plates were shaken for 15 minutes at an orbital shaker for cell lysis. Then, plates were transferred to a -80 °C freezer for at least overnight.

On the day of measurement, plates were thawn and 20 µL cell lysate was pipetted into one well of a white-walled 96-well plate (Greiner Bio-One). Every sample was measured

at least in triplicates. Luciferase activity was then determined according to the manual using the multimode microplate reader TriStar LB 941 (Berthold Technologies GmbH & Co KG, Bad Wildbad, Germany) and the software MikroWin2010. First, Reagent A is added to start the *Firefly* reaction, emitting light signal, which is then quantified. This reaction is then stopped by the addition of Reagent B+C, which at the same time starts the *Renilla* luciferase reaction. *Renilla* luciferase catalyzed then the chemical reaction from coelenterazine into coelenteramide, thereby generating another stabilized luminescent signal, which is then quantified.

For analysis, measured luminescent signals were exported to MS Office Excel. There, the ratio of the *Firefly* luciferase signal and the *Renilla* luciferase signal of each well was calculated to normalize the *Firefly* luciferase signals. Then, the mean values of the technical replicates were determined and all samples were divided by the wildtype and/or normoxia sample to have a common reference.

4.2.4.2 Western blotting

Cell lysis

Cells were seeded and treated as described in section 4.2.2 (page 113).
For harvesting of cell lysate, cells were washed once with 1x PBS. Then, an appropriate amount of Laemmli buffer was added to cover the cells. A cell scaper (TPP Techno Plastic Products AG, Trasadingen, Switzerland) was used to collect the cell lysate in one corner of the cell dish or plate and the cell lysate was collected into a 1.5 mL reaction tube and stored on ice.
To shear genomic DNA, the lysate was sonicated for 60 seconds (Sonoplus, Bandelin electronic GmbH). Subsequently, the lysate was incubated at 95 °C for five minutes to denature the proteins. The protein lysate was then stored at -20 °C until further use.

Determination of protein concentration

For determining the protein concentration, the Lowry method was used [119]. A two-step reactions leads to color development, whose absorbance is then measured at 750 nm using the multimode microplate reader (Berthold Technologies). Here, the colorimetric DC Protein Assay Reagents Package was used according to the manufacturer's instructions. Pure Laemmli buffer was used as a blank measurement. The protein concentration was then determined using a calibration curve determined with increasing concentrations of BSA.

Sample preparation

To prepare the sample for SDS-PAGE run, a defined amount of sample (corresponding to 30 to 50 µg of total protein) was mixed with Laemmli buffer and 4x Sample Buffer in a way to yield enough solution to load 20 µL per gel well. Those samples were then heated at 95 °C for five minutes to denature the proteins.

SDS-PAGE

The denatured proteins were separated according to their size using sodium dodecyl sulfate-polyacrylamide gel electrophoresis (SDS-PAGE). Here, addition of SDS renders the proteins identically charged per unit mass, which enables the size-dependent separation. For standard discontinuous SDS-PAGE, the Mini-PROTEAN 3 system (Bio-Rad Laboratories, Hercules, California, USA) with 15-well combs was used. Per well, 20 µL of denatured protein sample was loaded onto 8 %/12 % double-percentage gels or 10 % single-percentage gels with 4 % stacking gel. Gel was run initially at 80 V and then at 120 V after the proteins reached the separating gel.

Blotting

Separated proteins were transferred to 0.45 µm PVDF transfer membranes (#88518, Thermo Fisher Scientific) at 125 mA per blot using the same Mini-PROTEAN 3 system (Bio-Rad) for two hours.

Detection of protein bands

The following steps were all carried out under shaking. After blotting, membranes were incubated for at least one hour in 5 % milk blocking buffer to prevent unspecific antibody binding. Then, blots were cut according to the proteins to be detected and incubated in primary antibody solutions (see Tab. 4.1.4.1) at 4 °C overnight. On the next day, blots were washed three times 15 minutes in washing buffer and were then incubated for at least one hour with the appropriate HRP-coupled secondary antibody (see Tab. 4.1.4.2) at room temperature. Then, blots were washed twice in washing buffer and once in 1x PBS for each 15 minutes.

To detect protein bands, chemiluminescent signal was produced by incubating the membranes with Pierce ECL Western Blotting Substrate, Western Lightning Plus ECL, or a 9:1 mixture of SuperSignal West Pico PLUS Chemiluminescent Substrate and Super Signal West Femto Maximum Sensitiviy Substrate (SOCS3 only) for up to 5 minutes. Then, ECL reagent was removed and the blots were transferred to a transparent plate and covered with foil. Detection of bands was achieved by using the ChemoStar Western blot imager (INTAS Science Imaging Instruments GmbH, Göttingen, Germany) with adding

exposure times up to 1 hour. Pictures were then saved as raw data.

Membrane stripping

In case the same membrane part needed to be incubated with another primary antibody, the blots were stripped of bound antibodies by adding stripping buffer two times for each 20 minutes with shaking at room temperature. Afterwards, membranes were washed three times for 10 minutes in PBS-T to remove the acidic buffer. Then, membranes were blocked with blocking buffer for at least one hour again and probed with the next primary antibody.

Analysis and post processing

Raw data of the ChemoStar Western blot imager were loaded into FIJI/ImageJ and contrast settings were adjusted, always applied to the whole blot. Extracts of the blots were then copied and assembled in Inkscape to the final figure.

Abstract

Cancer is a leading cause of death worldwide, with brain tumors and lung cancers demonstrating particularly high mortality rates. The role of the complex tumor microenvironment (TME) and the interactions of cancer cells with the tumor stroma are the focus of intense investigation to better understand cancer progression and to test potential therapeutic options. In many solid tumors, regions with reduced oxygen availability (hypoxia) are present in the TME, along with active hypoxia inducible factor (HIF) signaling, the main cellular oxygen-sensing pathway. While the core HIF pathway is well characterized, its regulation remains to be fully elucidated. Uncovering the regulation of HIF signaling is key to understand how brain and lung tumors develop, adapt to low or fluctuating oxygen tensions and hijack the HIF pathway for progression, e. g., to induce invasion and metastasis.

To discover novel HIF pathway regulators, *in vitro* fluorescent reporters (FRs) were developed to monitor the activation status of this signaling pathway in cells. Selected FRs were further examined in glioblastoma and/or lung adenocarcinoma cell lines to generate fluorescent reporter systems (FRSs). The best-performing FRSs were used to optimize the experimental conditions for a CRISPR knock-out (KO) screen targeting the whole coding genome. This screening in a glioblastoma FRS identified several known and previously unknown candidate regulators of the HIF signaling pathway in normoxia. Selected top hits were independently validated in both glioblastoma and lung adenocarcinoma FRSs. Moreover, initial functional analyses on a top hit, suppressor of cytokine signaling 3 (SOCS3), were performed in several cancer cell lines, including additional glioblastoma as well as renal cell carcinoma cell lines, in order to uncover the role of SOCS3 in HIF regulation.

The development and application of the FRSs have moved us closer to decoding the regulation of the HIF signaling pathway in multiple cancers. Going forward, we will follow up on these findings to gain mechanistic insights into how SOCS3 regulates the HIF pathway. In addition, the versatile FRSs will help us to identify additional regulators under varying tumor microenvironmental conditions, such as hypoxia.
By uncovering the regulation of the HIF signaling pathway in more detail, these studies may contribute to the development of innovative therapeutic strategies, paving the way to more effectively combat cancer.

Zusammenfassung

Krebs ist eine der häufigsten Todesursachen weltweit; insbesondere Hirntumore und Lungenkrebs weisen eine hohe Mortalität auf. Die Rolle der komplexen Tumor-Mikroumgebung (TME, engl. *tumor microenvironment*) und der Interaktion von Krebszellen mit dem Tumorstroma sind Gegenstand intensiver Forschung, um die Krebsentwicklung besser zu verstehen und potentielle Therapieansätze zu prüfen. In vielen soliden Tumoren liegen im TME Regionen mit einer reduzierten Sauerstoffversorgung (Hypoxie) vor, in denen der Hypoxia Inducible Factor (HIF)-Signalweg aktiviert ist, welcher für die Reaktion der Zellen auf veränderte Sauerstoffkonzentrationen verantwortlich ist. Während die Hauptkomponenten des HIF-Signalwegs bereits bekannt sind, sind seine Regulierungsmechanismen bisher nicht vollständig aufgeklärt. Die Aufdeckung der Regulation des HIF-Signalweges ist der Schlüssel, um zu verstehen wie Gehirn- und Lungentumoren entstehen, sich an niedrige oder schwankende Sauerstofflevel anpassen und den HIF-Signalweg für die weitere Entwicklung, beispielweise die Induktion der Invasion und Metastasierung, ausnutzen.

Um neue regulatorische Proteine des HIF-Signalweges zu identifizieren, haben wir *in vitro* Fluoreszenzreporter (FR) entwickelt, die den Aktivierungsstatus des HIF-Signalwegs in Zellen anzeigen. Ausgewählte FR wurden in Glioblastom- (bösartiger Hirntumor) und/oder Lungenadenokarzinomzelllinien getestet, um Fluoreszenzreportersysteme (FRS) zu etablieren. Die performantesten FRS wurden verwendet, um die experimentellen Bedingungen für ein CRISPR-knockout(KO)-Screening zu optimieren, welches auf das gesamte kodierende Genom abzielte. Dieses Screening unter Verwendung eines Glioblastom-FRS identifizierte zahlreiche bereits bekannte aber auch bisher unbeschriebene Regulatoren des HIF-Signalweges unter Normoxie. Ausgewählte Top-Regulatoren wurden unabhängig sowohl in Glioblastom- als auch in Lungenadeno-karzinom-FRS validiert. Darüber hinaus wurden erste funktionelle Untersuchungen eines Top-Kandidaten, Suppressor of cytokine signaling 3 (SOCS3), in verschiedenen Zelllinien durchgeführt, darunter weitere Glioblastom- sowie Nierenzellkarzinomzelllinien, um die Rolle von SOCS3 in der Regulation von HIF aufzudecken.

Die Entwicklung und Anwendung der FRS hat uns näher an die Entschlüsselung der Regulation des HIF-Signalweges in mehreren Krebsentitäten herangeführt. Um zu verstehen, wie SOCS3 den HIF-Signalweg reguliert, werden wir die hier vorgestellten Ergebnisse weiter verfolgen und vertiefen. Weiterhin werden uns die vielfältigen

FRS helfen, zusätzliche Regulatoren des HIF-Signalweges auch unter anderen Tumor-Mikroumgebungsbedingungen, beispielsweise der Hypoxie, zu identifizieren.
Indem wir die Regulation des HIF-Signalweges besser verstehen, könnten diese Untersuchungen zur Entwicklung neuer therapeutischer Strategien beitragen und damit den Weg zu einem effektiveren Kampf gegen Krebs ebnen.

Abbreviations

2-OG	2-oxoglutarate
aa	amino acid
ACO1	aconitase 1
ADRB2	beta-2 adrenergic receptor
AHR	aryl hydrocarbon receptor
AIP	aryl hydrocarbon receptor-interacting protein
α-KG	α-ketoglutarate
AMPK	5’ AMP-activated protein kinase
APOBEC3	apolipoprotein B mRNA editing enzyme catalytic polypeptide 3
ARNT	aryl hydrocarbon receptor nuclear translocator
ATF4	activating transcription factor 4
ATM	ataxia telangiectasia mutated
BSA	bovine serum albumin
bHLH	basic helix-loop-helix domain
bp	base pair
BOLA3	BolA family member 3
Cas	CRISPR-associated protein
ChIP-seq	chromatin immune precipitation sequencing
CNS	central nervous system
CUL2	Cullin-2
CTAD	C-terminal transactivation domain
CBP	CREB binding protein
CBFB	core-binding factor subunit beta
CDCA7L	cell division cycle associated 7 like
CDK	cyclin-dependent kinase
c-Myc	cellular myelocytomatose oncogene
ccRCC	clear-cell renal cell carcinoma
CRISPR	clustered regularly interspaced short palindromic repeats
CSC	cancer stem cell
CODD	C-terminal ODD

ccRCC	clear-cell renal carcinoma
c-SRC	cellular sarcoma
CNTF	ciliary neurotrophic factor
CMV	cytomegalovirus
DLR	dual luciferase reporter
DMOG	dimethyloxaloylglycine
DNA	deoxyribonucleic acid
DNMT3A	DNA methyltransferase 3A
DNMT3L	DNA methyltransferase 3 like
DSB	double strand break
DNAJC19	DnaJ heat shock protein family (Hsp40) member C19
ECM	extracellular matrix
EGFR	epidermal growth factor receptor
EGLN	EGL nine homolog
EMT	epithelial-to-mesenchymal transition
EPAS1	endothelial PAS domain-containing protein 1
EPO	erythropoietin
EPOR	erythropoietin receptor
ET	endogenous tagging
ERK	extracellular-signal regulated kinase
ELO	elongin
FACS	fluorescence activated cell sorting
FAK1	focal adhesion kinase 1
FASTKD2	FAST kinase domains 2
FbFP	flavin mononucleotide (FMN)–based fluorescent proteins
FBS	fetal bovine serum
FC	flow cytometry
Fe^{2+}	ferrous iron
FH	fumarate hydratase
FI	fluorescence intensity
FIH	factor inhibiting HIF
FITC	fluorescein isothiocyanate
FR	fluorescent reporter
FRS	fluorescent reporter system
gDNA	genomic DNA
GFP	green fluorescent protein

gRNA	guide RNA
GSK3β	glycogen synthase kinase-3β
G-CSFR	granulocyte colony stimulating factor receptor
GHR	growth hormone receptor
GAS	gamma activated site
HA	homology arm
HIF	hypoxia inducible factor
HR	homologous recombination
HRE	hypoxia responsive element
HOTAIR	homeobox transcript antisense RNA
HDR	homology-directed repair
HSP90	heat shock protein 90
IDH	isocitrate dehydrogenase
IQR	interquartile range
IL	interleukin
IF	interferon
IR	insulin receptor
IRS	insulin receptor substrate
IDO	indolamin-2,3-dioxygenase
JAK	janus kinase
KO	knock-out
KI	knock-in
KIR	kinase inhibitory region
KRAB	krüppel associated box
KRAS	kirsten rat sarcoma virus
LFC	log-fold change
LIAS	lipoic acid synthetase
lncRNA	long non-coding RNA
LIPT2	lipoyl(octanoyl) transferase 2
LEP-R	leptin receptor
LIF	leukemia inhibitory factor
Luc2	*Firefly* luciferase 2
MANEAL	mannosidase endo-alpha like
MAX	myc-associated factor X
MDM2	mouse double minute 2 homolog
miRNA	micro RNA

MOI	multiplicity of infection
mRNA	messenger RNA
MRP	mitochondrial ribosomal protein
mTOR	mammalian target of rapamycin
mTORC1	mTOR complex 1
NC	negative control
NDUFA	NADH dehydrogenase ubiquinone 1 alpha subcomplex subunit
NHEJ	non-homologous end joining
NTC	non-targeting control
NGS	next generation sequencing
NTAD	N-terminal transactivation domain
NF-κB	nuclear factor “kappa-light-chain-enhancer” of activated B-cells
NSCLC	non-small cell lung cancer
NODD	N-terminal ODD
ODD	oxygen-dependent degradation domain
OE	overexpression
OGDH	oxoglutarate dehydrogenase
ORM2	orosomucoid 2
OXPHOS	oxidative phosphorylation
O_2	oxygen
OSM	oncostatin M
PAM	protospacer adjacent motif
PC	positive control
PDK1	pyruvate dehydrogenase kinase 1
PPP3CA	protein phosphatase 3 catalytic subunit alpha
PHD	prolyl hydroxylase domain
POI	protein of interest
PAS	Per-ARNT-Sim
PAC	PAS-associated C-terminal
PI3K	phosphoinositide 3-kinase
PKA	protein kinase A
PLK3	Polo-like kinase 3
PuroR	puromycin N-acetyltransferase
POR	pLenti6-ODD-Fluc-Rluc
RBX1	ring-box 1
ROS	reactive oxygen species

RACK1	receptor of activated protein C kinase 1
RPUSD3	RNA pseudouridine synthase D3
RBX2	RING box protein 2
SCC	single cell clone
SCLC	small cell lung cancer
SDH	succinate dehydrogenase
SETD7	SET domain containing 7
SH2	Src-homology 2
SIAH	seven-in-absentia homolog
SOCS3	suppressor of cytokine signaling 3
sgRNA	single-guide RNA
siRNA	small interfering RNA
STAT	signal transducers and activators of transcription
STAT3	signal transducers and activators of transcription 3
STK11	serine/threonine kinase 11
SWI/SNF	SWItch/sucrose non-fermentable
SMARCB1	SWI/SNF related, matrix associated, actin dependent regulator of chromatin, subfamily B, member 1
Siglec	sialic acid binding Ig-like lectin
SIEL	sis-inducible element (SIE)-like
SDS-PAGE	sodium dodecyl sulfate-polyacrylamide gel electrophoresis
SMG1	SMG1 nonsense mediated mRNA decay associated PI3K related kinase
TET	ten-eleven translocation
TC	tissue culture
TCEB	transcription elongation factor B polypeptide
TCA	tricarboxylic acid cycle
TME	tumor microenvironment
TIM14	mitochondrial import inner membrane translocase 14
TYK2	tyrosine kinase 2
TGF	transforming growth factor
T2A	Thosea asigna virus 2A
VEGF	vascular endothelial growth factor
VHL	von-Hippel-Lindau
wt	wildtype
WSB1	WD repeat and SOCS box-containing protein 1

Index of figures and tables

List of figures

List of tables

References

[1] T. Acker et al. “Genetic evidence for a tumor suppressor role of HIF-2alpha.” In: *Cancer Cell* 8.2 (2005), pp. 131–41.

[2] A. Albanese et al. “The Role of Hypoxia-Inducible Factor Post-Translational Modifications in Regulating Its Localisation, Stability, and Activity.” In: *Int J Mol Sci* 22.1 (2020).

[3] R. J. Appelhoff et al. “Differential function of the prolyl hydroxylases PHD1, PHD2, and PHD3 in the regulation of hypoxia-inducible factor.” In: *J Biol Chem* 279.37 (2004), pp. 38458–65.

[4] J. D. Arroyo et al. “A Genome-wide CRISPR Death Screen Identifies Genes Essential for Oxidative Phosphorylation.” In: *Cell Metab* 24.6 (2016), pp. 875–885.

[5] A. Augstein et al. “Cell-specific and hypoxia-dependent regulation of human HIF-3alpha: inhibition of the expression of HIF target genes in vascular cells.” In: *Cell Mol Life Sci* 68.15 (2011), pp. 2627–42.

[6] M. Baba et al. “Tumor suppressor protein VHL is induced at high cell density and mediates contact inhibition of cell growth.” In: *Oncogene* 20.22 (2001), pp. 2727–36.

[7] J. J. Babon and N. A. Nicola. “The biology and mechanism of action of suppressor of cytokine signaling 3.” In: *Growth Factors* 30.4 (2012), pp. 207–19.

[8] X. Bao et al. “The crosstalk between HIFs and mitochondrial dysfunctions in cancer development.” In: *Cell Death Dis* 12.2 (2021), p. 215.

[9] R. Barrangou et al. “CRISPR provides acquired resistance against viruses in prokaryotes.” In: *Science* 315.5819 (2007), pp. 1709–12.

[10] L. Barthel et al. “Glioma: molecular signature and crossroads with tumor microenvironment.” In: *Cancer Metastasis Rev* (2021).

[11] I. Berger et al. “Mitochondrial complex I deficiency caused by a deleterious NDUFA11 mutation.” In: *Ann Neurol* 63.3 (2008), pp. 405–8.

[12] E. Berra et al. “HIF prolyl-hydroxylase 2 is the key oxygen sensor setting low steady-state levels of HIF-1alpha in normoxia.” In: *EMBO J* 22.16 (2003), pp. 4082–90.

[13] T. Bishop and P. J. Ratcliffe. “Signaling hypoxia by hypoxia-inducible factor protein hydroxylases: a historical overview and future perspectives.” In: *Hypoxia (Auckl)* 2 (2014), pp. 197–213.

[14] T. Burckstummer et al. “A reversible gene trap collection empowers haploid genetics in human cells.” In: *Nat Methods* 10.10 (2013), pp. 965–71.

[15] S. P. Burr et al. “Mitochondrial Protein Lipoylation and the 2-Oxoglutarate Dehydrogenase Complex Controls HIF1alpha Stability in Aerobic Conditions.” In: *Cell Metab* 24.5 (2016), pp. 740–752.

[16] W. Cai and H. Yang. “The structure and regulation of Cullin 2 based E3 ubiquitin ligases and their biological functions.” In: *Cell Div* 11 (2016), p. 7.

[17] N. S. Chandel et al. “Reactive oxygen species generated at mitochondrial complex III stabilize hypoxia-inducible factor-1alpha during hypoxia: a mechanism of O2 sensing.” In: *J Biol Chem* 275.33 (2000), pp. 25130–8.

[18] B. Chen et al. “Dynamic imaging of genomic loci in living human cells by an optimized CRISPR/Cas system.” In: *Cell* 155.7 (2013), pp. 1479–91.

[19] R. Q. Chen et al. “Kinome siRNA screen identifies SMG-1 as a negative regulator of hypoxia-inducible factor-1alpha in hypoxia.” In: *J Biol Chem* 284.25 (2009), pp. 16752–16758.

[20] R. Chowdhury et al. “Structural basis for oxygen degradation domain selectivity of the HIF prolyl hydroxylases.” In: *Nature Communications* 7.1 (2016).

[21] K. Chylinski, A. Le Rhun, and E. Charpentier. “The tracrRNA and Cas9 families of type II CRISPR-Cas immunity systems.” In: *RNA Biol* 10.5 (2013), pp. 726–37.

[22] F. Ciccarone et al. “Aconitase 2 inhibits the proliferation of MCF-7 cells promoting mitochondrial oxidative metabolism and ROS/FoxO1-mediated autophagic response.” In: *Br J Cancer* 122.2 (2020), pp. 182–193.

[23] P. E. Clark. “The role of VHL in clear-cell renal cell carcinoma and its relation to targeted therapy.” In: *Kidney Int* 76.9 (2009), pp. 939–45.

[24] M. E. Cockman et al. “Lack of activity of recombinant HIF prolyl hydroxylases (PHDs) on reported non-HIF substrates.” In: *Elife* 8 (2019).

[25] D. Collias and C. L. Beisel. “CRISPR technologies and the search for the PAM-free nuclease.” In: *Nat Commun* 12.1 (2021), p. 555.

[26] G. D’Angelo et al. “Hypoxia up-regulates prolyl hydroxylase activity: a feedback mechanism that limits HIF-1 responses during reoxygenation.” In: *J Biol Chem* 278.40 (2003), pp. 38183–7.

[27] L. D’Ignazio, D. Bandarra, and S. Rocha. “NF-kappaB and HIF crosstalk in immune responses.” In: *FEBS J* 283.3 (2016), pp. 413–24.

[28] L. Dai et al. “Emerging roles of suppressor of cytokine signaling 3 in human cancers.” In: *Biomed Pharmacother* 144 (2021), p. 112262.

[29] L. Dai et al. “SOCS3 Acts as an Onco-immunological Biomarker With Value in Assessing the Tumor Microenvironment, Pathological Staging, Histological Subtypes, Therapeutic Effect, and Prognoses of Several Types of Cancer.” In: *Front Oncol* 12 (2022), p. 881801.

[30] C. V. Dang et al. “The interplay between MYC and HIF in cancer.” In: *Nat Rev Cancer* 8.1 (2008), pp. 51–6.

[31] C. J. De Saedeleer et al. “Lactate activates HIF-1 in oxidative but not in Warburg-phenotype human tumor cells.” In: *PLoS One* 7.10 (2012), e46571.

[32] A. Dekanty et al. “Drosophila genome-wide RNAi screen identifies multiple regulators of HIF-dependent transcription in hypoxia.” In: *PLoS Genet* 6.6 (2010), e1000994.

[33] F. Diao and B. H. White. “A novel approach for directing transgene expression in Drosophila: T2A-Gal4 in-frame fusion.” In: *Genetics* 190.3 (2012), pp. 1139–44.

[34] M. R. Doe et al. “Myc posttranscriptionally induces HIF1 protein and target gene expression in normal and cancer cells.” In: *Cancer Res* 72.4 (2012), pp. 949–57.

[35] K. Doege et al. “Inhibition of mitochondrial respiration elevates oxygen concentration but leaves regulation of hypoxia-inducible factor (HIF) intact.” In: *Blood* 106.7 (2005), pp. 2311–7.

[36] J. G. Doench. “Am I ready for CRISPR? A user’s guide to genetic screens.” In: *Nat Rev Genet* 19.2 (2018), pp. 67–80.

[37] J. G. Doench et al. “Optimized sgRNA design to maximize activity and minimize off-target effects of CRISPR-Cas9.” In: *Nat Biotechnol* 34.2 (2016), pp. 184–191.

[38] H. Dopeso et al. “PHD3 Controls Lung Cancer Metastasis and Resistance to EGFR Inhibitors through TGFalpha.” In: *Cancer Res* 78.7 (2018), pp. 1805–1819.

[39] R. J. Dotson et al. “Influence of Cholesterol on the Oxygen Permeability of Membranes: Insight from Atomistic Simulations.” In: *Biophys J* 112.11 (2017), pp. 2336–2347.

[40] T. Drepper et al. “Reporter proteins for in vivo fluorescence without oxygen.” In: *Nat Biotechnol* 25.4 (2007), pp. 443–5.

[41] S. L. Dunwoodie. “The role of hypoxia in development of the Mammalian embryo.” In: *Dev Cell* 17.6 (2009), pp. 755–73.

[42] R. Erapaneedi et al. “A novel family of fluorescent hypoxia sensors reveal strong heterogeneity in tumor hypoxia at the cellular level.” In: *EMBO J* 35.1 (2016), pp. 102–13.

[43] V. Ernani and T. E. Stinchcombe. “Management of Brain Metastases in Non-Small-Cell Lung Cancer.” In: *J Oncol Pract* 15.11 (2019), pp. 563–570.

[44] A. G. Evdokimov et al. “Structural basis for the fast maturation of Arthropoda green fluorescent protein.” In: *EMBO Rep* 7.10 (2006), pp. 1006–12.

[45] M. A. Farooq et al. “Mitochondrial DNA instability in cells lacking aconitase correlates with iron citrate toxicity.” In: *Oxid Med Cell Longev* 2013 (2013), p. 493536.

[46] A. Filatova et al. “Acidosis Acts through HSP90 in a PHD/VHL-Independent Manner to Promote HIF Function and Stem Cell Maintenance in Glioma.” In: *Cancer Res* 76.19 (2016), pp. 5845–5856.

[47] A. Finch et al. “Advances in Research of Adult Gliomas.” In: *Int J Mol Sci* 22.2 (2021).

[48] J. D. Firth et al. “Oxygen-regulated control elements in the phosphoglycerate kinase 1 and lactate dehydrogenase A genes: similarities with the erythropoietin 3’ enhancer.” In: *Proc Natl Acad Sci U S A* 91.14 (1994), pp. 6496–500.

[49] G. H. Fong and K. Takeda. “Role and regulation of prolyl hydroxylase domain proteins.” In: *Cell Death and Differentiation* 15.4 (2008), pp. 635–641.

[50] G. Gabriely et al. “Role of AHR and HIF-1alpha in Glioblastoma Metabolism.” In: *Trends Endocrinol Metab* 28.6 (2017), pp. 428–436.

[51] B. K. Garvalov et al. “PHD3 regulates EGFR internalization and signalling in tumours.” In: *Nat Commun* 5 (2014), p. 5577.

[52] S. Geisler and J. Coller. “RNA in unexpected places: long non-coding RNA functions in diverse cellular contexts.” In: *Nat Rev Mol Cell Biol* 14.11 (2013), pp. 699–712.

[53] Robert Koch-Institut (Hrsg) und die Gesellschaft der epidemiologischen Krebsregister in Deutschland e.V. (Hrsg). “Krebs in Deutschland für 2017/2018.” In: *Zentrum für Krebsregisterdaten* 13. Ausgabe (2018), pp. 1–172.

[54] D. Ghezzi et al. “FASTKD2 nonsense mutation in an infantile mitochondrial encephalomyopathy associated with cytochrome c oxidase deficiency.” In: *Am J Hum Genet* 83.3 (2008), pp. 415–23.

[55] L. A. Gilbert et al. “CRISPR-mediated modular RNA-guided regulation of transcription in eukaryotes.” In: *Cell* 154.2 (2013), pp. 442–51.

[56] D. M. Gilkes, G. L. Semenza, and D. Wirtz. “Hypoxia and the extracellular matrix: drivers of tumour metastasis.” In: *Nat Rev Cancer* 14.6 (2014), pp. 430–9.

[57] L. A. Gross et al. “The structure of the chromophore within DsRed, a red fluorescent protein from coral.” In: *Proc Natl Acad Sci U S A* 97.22 (2000), pp. 11990–5.

[58] D. Hanahan. “Hallmarks of Cancer: New Dimensions.” In: *Cancer Discov* 12.1 (2022), pp. 31–46.

[59] S. Hara et al. “Expression and characterization of hypoxia-inducible factor (HIF)-3alpha in human kidney: suppression of HIF-mediated gene expression by HIF-3alpha.” In: *Biochem Biophys Res Commun* 287.4 (2001), pp. 808–13.

[60] T. Hart et al. “Evaluation and Design of Genome-Wide CRISPR/SpCas9 Knockout Screens.” In: *G3 (Bethesda)* 7.8 (2017), pp. 2719–2727.

[61] R. Heim, D. C. Prasher, and R. Y. Tsien. “Wavelength mutations and posttranslational autoxidation of green fluorescent protein.” In: *Proc Natl Acad Sci U S A* 91.26 (1994), pp. 12501–4.

[62] P. Heir et al. “Oxygen-dependent Regulation of Erythropoietin Receptor Turnover and Signaling.” In: *J Biol Chem* 291.14 (2016), pp. 7357–72.

[63] A. T. Henze et al. “Loss of PHD3 allows tumours to overcome hypoxic growth inhibition and sustain proliferation through EGFR.” In: *Nat Commun* 5 (2014), p. 5582.

[64] A. T. Henze et al. “Prolyl hydroxylases 2 and 3 act in gliomas as protective negative feedback regulators of hypoxia-inducible factors.” In: *Cancer Res* 70.1 (2010), pp. 357–66.

[65] G. T. Hess et al. “Directed evolution using dCas9-targeted somatic hypermutation in mammalian cells.” In: *Nat Methods* 13.12 (2016), pp. 1036–1042.

[66] I. B. Hilton et al. “Epigenome editing by a CRISPR-Cas9-based acetyltransferase activates genes from promoters and enhancers.” In: *Nat Biotechnol* 33.5 (2015), pp. 510–7.

[67] M. Hirsila et al. “Characterization of the human prolyl 4-hydroxylases that modify the hypoxia-inducible factor.” In: *J Biol Chem* 278.33 (2003), pp. 30772–80.

[68] C. W. Hsu et al. “Identification of approved and investigational drugs that inhibit hypoxia-inducible factor-1 signaling.” In: *Oncotarget* 7.7 (2016), pp. 8172–83.

[69] R. Y. Huang et al. “An EMT spectrum defines an anoikis-resistant and spheroidogenic intermediate mesenchymal state that is sensitive to e-cadherin restoration by a src-kinase inhibitor, saracatinib (AZD0530).” In: *Cell Death Dis* 4 (2013), e915.

[70] J. D. Hunter. “Matplotlib: A 2D Graphics Environment.” In: *Computing in Science and Engineering* 9.3 (2007), pp. 90–95.

[71] L. Iommarini et al. “Non-Canonical Mechanisms Regulating Hypoxia-Inducible Factor 1 Alpha in Cancer.” In: *Front Oncol* 7 (2017), p. 286.

[72] M. Ivan and Jr. Kaelin W. G. “The EGLN-HIF O2-Sensing System: Multiple Inputs and Feedbacks.” In: *Mol Cell* 66.6 (2017), pp. 772–779.

[73] M. Ivan et al. “HIFalpha targeted for VHL-mediated destruction by proline hydroxylation: implications for O2 sensing.” In: *Science* 292.5516 (2001), pp. 464–8.

[74] Ferlay J et al. *Global Cancer Observatory: Cancer Today.* 2020.

[75] P. Jaakkola et al. “Targeting of HIF-alpha to the von Hippel-Lindau ubiquitylation complex by O2-regulated prolyl hydroxylation.” In: *Science* 292.5516 (2001), pp. 468–72.

[76] I. H. Jain et al. “Genetic Screen for Cell Fitness in High or Low Oxygen Highlights Mitochondrial and Lipid Metabolism.” In: *Cell* 181.3 (2020), 716–727 e11.

[77] I. H. Jain et al. “Hypoxia as a therapy for mitochondrial disease.” In: *Science* 352.6281 (2016), pp. 54–61.

[78] R. Jansen et al. “Identification of genes that are associated with DNA repeats in prokaryotes.” In: *Mol Microbiol* 43.6 (2002), pp. 1565–75.

[79] Q. K. Ji et al. “CDCA7L promotes glioma proliferation by targeting CCND1 and predicts an unfavorable prognosis.” In: *Mol Med Rep* 20.2 (2019), pp. 1149–1156.

[80] X. Jin and P. Mu. “Targeting Breast Cancer Metastasis.” In: *Breast Cancer (Auckl)* 9.Suppl 1 (2015), pp. 23–34.

[81] M. Jinek et al. “RNA-programmed genome editing in human cells.” In: *Elife* 2 (2013), e00471.

[82] D. E. Johnson, R. A. O’Keefe, and J. R. Grandis. “Targeting the IL-6/JAK/STAT3 signalling axis in cancer.” In: *Nat Rev Clin Oncol* 15.4 (2018), pp. 234–248.

[83] R. S. Johnson. “Profile of William Kaelin, Peter Ratcliffe, and Greg Semenza, 2016 Albert Lasker Basic Medical Research Awardees.” In: *Proceedings of the National Academy of Sciences* 113.49 (2016), pp. 13938–13940.

[84] S. Joshi, A. R. Singh, and D. L. Durden. “MDM2 regulates hypoxic hypoxia-inducible factor 1alpha stability in an E3 ligase, proteasome, and PTEN-phosphatidylinositol 3-kinase-AKT-dependent manner.” In: *J Biol Chem* 289.33 (2014), pp. 22785–22797.

[85] Jr. Kaelin W. G. and P. J. Ratcliffe. “Oxygen sensing by metazoans: the central role of the HIF hydroxylase pathway.” In: *Mol Cell* 30.4 (2008), pp. 393–402.

[86] Jr. Kaelin W. G., P. J. Ratcliffe, and G. L. Semenza. “Pathways for Oxygen Regulation and Homeostasis: The 2016 Albert Lasker Basic Medical Research Award.” In: *JAMA* 316.12 (2016), pp. 1252–3.

[87] A. Karagiota et al. “Protein phosphatase PPP3CA (calcineurin A) down-regulates hypoxia-inducible factor transcriptional activity.” In: *Arch Biochem Biophys* 664 (2019), pp. 174–182.

[88] B. Keith, R. S. Johnson, and M. C. Simon. “HIF1alpha and HIF2alpha: sibling rivalry in hypoxic tumour growth and progression.” In: *Nat Rev Cancer* 12.1 (2011), pp. 9–22.

[89] K. B. Kennel et al. “The PHD1 oxygen sensor in health and disease.” In: *J Physiol* 596.17 (2018), pp. 3899–3913.

[90] N. S. Kenneth et al. “SWI/SNF regulates the cellular response to hypoxia.” In: *J Biol Chem* 284.7 (2009), pp. 4123–31.

[91] N. J. Kershaw et al. “SOCS3 binds specific receptor-JAK complexes to control cytokine signaling by direct kinase inhibition.” In: *Nat Struct Mol Biol* 20.4 (2013), pp. 469–76.

[92] M. Kilic-Eren, T. Boylu, and V. Tabor. “Targeting PI3K/Akt represses Hypoxia inducible factor-1alpha activation and sensitizes Rhabdomyosarcoma and Ewing’s sarcoma cells for apoptosis.” In: *Cancer Cell Int* 13 (2013), p. 36.

[93] J. J. Kim et al. “WSB1 promotes tumor metastasis by inducing pVHL degradation.” In: *Genes Dev* 29.21 (2015), pp. 2244–57.

[94] H. J. Knowles et al. “Effect of ascorbate on the activity of hypoxia-inducible factor in cancer cells.” In: *Cancer Res* 63.8 (2003), pp. 1764–8.

[95] J. Koditz et al. “Oxygen-dependent ATF-4 stability is mediated by the PHD3 oxygen sensor.” In: *Blood* 110.10 (2007), pp. 3610–7.

[96] M. Koshy et al. “Improved survival time trends for glioblastoma using the SEER 17 population-based registries.” In: *J Neurooncol* 107.1 (2012), pp. 207–12.

[97] M. Krieg et al. “Up-regulation of hypoxia-inducible factors HIF-1alpha and HIF-2alpha under normoxic conditions in renal carcinoma cells by von Hippel-Lindau tumor suppressor gene loss of function.” In: *Oncogene* 19.48 (2000), pp. 5435–43.

[98] A. Kumagai et al. “A bilirubin-inducible fluorescent protein from eel muscle.” In: *Cell* 153.7 (2013), pp. 1602–11.

[99] B. Laderian et al. “Emerging Therapeutic Implications of STK11 Mutation: Case Series.” In: *Oncologist* 25.9 (2020), pp. 733–737.

[100] M. J. Lamberti et al. “Transcriptional activation of HIF-1 by a ROS-ERK axis underlies the resistance to photodynamic therapy.” In: *PLoS One* 12.5 (2017), e0177801.

[101] D. Lando et al. “FIH-1 is an asparaginyl hydroxylase enzyme that regulates the transcriptional activity of hypoxia-inducible factor.” In: *Genes Dev* 16.12 (2002), pp. 1466–71.

[102] J. J. Landry et al. “The genomic and transcriptomic landscape of a HeLa cell line.” In: *G3 (Bethesda)* 3.8 (2013), pp. 1213–24.

[103] B. Langmead and S. L. Salzberg. “Fast gapped-read alignment with Bowtie 2.” In: *Nat Methods* 9.4 (2012), pp. 357–9.

[104] E. Laughner et al. “HER2 (neu) signaling increases the rate of hypoxia-inducible factor 1alpha (HIF-1alpha) synthesis: novel mechanism for HIF-1-mediated vascular endothelial growth factor expression.” In: *Mol Cell Biol* 21.12 (2001), pp. 3995–4004.

[105] E. Lebigot et al. “Impact of mutations within the [Fe-S] cluster or the lipoic acid biosynthesis pathways on mitochondrial protein expression profiles in fibroblasts from patients.” In: *Mol Genet Metab* 122.3 (2017), pp. 85–94.

[106] J. W. Lee et al. “Hypoxia signaling in human diseases and therapeutic targets.” In: *Exp Mol Med* 51.6 (2019), pp. 1–13.

[107] M. Lee et al. “Expression of human inducible nitric oxide synthase in response to cytokines is regulated by hypoxia-inducible factor-1.” In: *Free Radic Biol Med* 130 (2019), pp. 278–287.

[108] S. Lee et al. “Neuronal apoptosis linked to EglN3 prolyl hydroxylase and familial pheochromocytoma genes: developmental culling and cancer.” In: *Cancer Cell* 8.2 (2005), pp. 155–67.

[109] S. Lee et al. “Nuclear/cytoplasmic localization of the von Hippel-Lindau tumor suppressor gene product is determined by cell density.” In: *Proc Natl Acad Sci U S A* 93.5 (1996), pp. 1770–5.

[110] S. Li et al. “EglN3 hydroxylase stabilizes BIM-EL linking VHL type 2C mutations to pheochromocytoma pathogenesis and chemotherapy resistance.” In: *Proc Natl Acad Sci U S A* 116.34 (2019), pp. 16997–17006.

[111] W. Li et al. “MAGeCK enables robust identification of essential genes from genome-scale CRISPR/Cas9 knockout screens.” In: *Genome Biol* 15.12 (2014), p. 554.

[112] X. S. Li et al. “Mammalian SWI/SNF–a subunit BAF250/ARID1 is an E3 ubiquitin ligase that targets histone H2B.” In: *Mol Cell Biol* 30.7 (2010), pp. 1673–88.

[113] X. Lin et al. “A chemical genomics screen highlights the essential role of mitochondria in HIF-1 regulation.” In: *Proc Natl Acad Sci U S A* 105.1 (2008), pp. 174–9.

[114] Z. Lin et al. “Establishment of age group classification for risk stratification in glioma patients.” In: *BMC Neurol* 20.1 (2020), p. 310.

[115] C. Lindemann et al. “SOCS3 promoter methylation is mutually exclusive to EGFR amplification in gliomas and promotes glioma cell invasion through STAT3 and FAK activation.” In: *Acta Neuropathologica* 122.2 (2011), pp. 241–251.

[116] X. Liu et al. “Repression of hypoxia-inducible factor alpha signaling by Set7-mediated methylation.” In: *Nucleic Acids Res* 43.10 (2015), pp. 5081–98.

[117] Y. Liu et al. “Hypoxia regulates vascular endothelial growth factor gene expression in endothelial cells. Identification of a 5’ enhancer.” In: *Circ Res* 77.3 (1995), pp. 638–43.

[118] D. N. Louis et al. “The 2021 WHO Classification of Tumors of the Central Nervous System: a summary.” In: *Neuro Oncol* 23.8 (2021), pp. 1231–1251.

[119] O. H. Lowry et al. “Protein measurement with the Folin phenol reagent.” In: *J Biol Chem* 193.1 (1951), pp. 265–75.

[120] G. MacLeod et al. “Genome-Wide CRISPR-Cas9 Screens Expose Genetic Vulnerabilities and Mechanisms of Temozolomide Sensitivity in Glioblastoma Stem Cells.” In: *Cell Reports* 27.3 (2019), 971–986.e9.

[121] L. Magraner-Pardo et al. “Systematic Analysis of FASTK Gene Family Alterations in Cancer.” In: *Int J Mol Sci* 22.21 (2021).

[122] B. Mair et al. “Essential Gene Profiles for Human Pluripotent Stem Cells Identify Uncharacterized Genes and Substrate Dependencies.” In: *Cell Rep* 27.2 (2019), 599–615 e12.

[123] K. S. Makarova et al. “A putative RNA-interference-based immune system in prokaryotes: computational analysis of the predicted enzymatic machinery, functional analogies with eukaryotic RNAi, and hypothetical mechanisms of action.” In: *Biol Direct* 1 (2006), p. 7.

[124] C. Marinaccio et al. “LKB1/STK11 Is a Tumor Suppressor in the Progression of Myeloproliferative Neoplasms.” In: *Cancer Discov* 11.6 (2021), pp. 1398–1410.

[125] M. Martin. “Cutadapt removes adapter sequences from high-throughput sequencing reads.” In: *2011* 17.1 (2011), p. 3.

[126] M. Martini et al. “Prognostic relevance of SOCS3 hypermethylation in patients with glioblastoma multiforme.” In: *International journal of cancer Journal international du cancer* 123.12 (2008), pp. 2955–2960.

[127] I. D. Mascanfroni et al. “Metabolic control of type 1 regulatory T cell differentiation by AHR and HIF1-alpha.” In: *Nat Med* 21.6 (2015), pp. 638–46.

[128] N. Mashtalir et al. “Modular Organization and Assembly of SWI/SNF Family Chromatin Remodeling Complexes.” In: *Cell* 175.5 (2018), 1272–1288.e20.

[129] P. H. Maxwell et al. “The tumour suppressor protein VHL targets hypoxia-inducible factors for oxygen-dependent proteolysis.” In: *Nature* 399.6733 (1999), pp. 271–5.

[130] M. A. Maynard et al. “Multiple splice variants of the human HIF-3 alpha locus are targets of the von Hippel-Lindau E3 ubiquitin ligase complex.” In: *J Biol Chem* 278.13 (2003), pp. 11032–40.

[131] G. Melillo et al. “A hypoxia-responsive element mediates a novel pathway of activation of the inducible nitric oxide synthase promoter.” In: *J Exp Med* 182.6 (1995), pp. 1683–93.

[132] E. Metzen. “Enzyme substrate recognition in oxygen sensing: how the HIF trap snaps.” In: *Biochem J* 408.2 (2007), e5–6.

[133] A. L. Miles et al. “The vacuolar-ATPase complex and assembly factors, TMEM199 and CCDC115, control HIF1alpha prolyl hydroxylation by regulating cellular iron levels.” In: *Elife* 6 (2017).

[134] P. Mittal and C. W. M. Roberts. “The SWI/SNF complex in cancer - biology, biomarkers and therapy.” In: *Nat Rev Clin Oncol* 17.7 (2020), pp. 435–448.

[135] S. Mohan and R. D. Burk. “von Hippel-Lindau protein complex is regulated by cell density.” In: *Oncogene* 22.34 (2003), pp. 5270–80.

[136] L. Mohrmann and C. P. Verrijzer. “Composition and functional specificity of SWI2/SNF2 class chromatin remodeling complexes.” In: *Biochim Biophys Acta* 1681.2-3 (2005), pp. 59–73.

[137] D. Mokranjac et al. “Tim14, a novel key component of the import motor of the TIM23 protein translocase of mitochondria.” In: *EMBO J* 22.19 (2003), pp. 4945–56.

[138] S. Morita et al. “Targeted DNA demethylation in vivo using dCas9-peptide repeat and scFv-TET1 catalytic domain fusions.” In: *Nat Biotechnol* 34.10 (2016), pp. 1060–1065.

[139] S. Movafagh, S. Crook, and K. Vo. “Regulation of hypoxia-inducible factor-1a by reactive oxygen species: new developments in an old debate.” In: *J Cell Biochem* 116.5 (2015), pp. 696–703.

[140] K. Nakashima et al. “Synergistic signaling in fetal brain by STAT3-Smad1 complex bridged by p300.” In: *Science* 284.5413 (1999), pp. 479–82.

[141] K. Nakayama, J. Qi, and Z. Ronai. “The ubiquitin ligase Siah2 and the hypoxia response.” In: *Mol Cancer Res* 7.4 (2009), pp. 443–51.

[142] C. A. Opitz et al. “An endogenous tumour-promoting ligand of the human aryl hydrocarbon receptor.” In: *Nature* 478.7368 (2011), pp. 197–203.

[143] B. M. Ortmann et al. “The HIF complex recruits the histone methyltransferase SET1B to activate specific hypoxia-inducible genes.” In: *Nat Genet* (2021).

[144] Q. T. Ostrom et al. “CBTRUS Statistical Report: Primary Brain and Other Central Nervous System Tumors Diagnosed in the United States in 2014-2018.” In: *Neuro Oncol* 23.12 Suppl 2 (2021), pp. iii1–iii105.

[145] H. F. Ozbakir et al. “Beyond the Green Fluorescent Protein: Biomolecular Reporters for Anaerobic and Deep-Tissue Imaging.” In: *Bioconjug Chem* 31.2 (2020), pp. 293–302.

[146] Y. Pan et al. “Multiple factors affecting cellular redox status and energy metabolism modulate hypoxia-inducible factor prolyl hydroxylase activity in vivo and in vitro.” In: *Mol Cell Biol* 27.3 (2007), pp. 912–25.

[147] L. Peretz et al. “Combined shRNA over CRISPR/cas9 as a methodology to detect off-target effects and a potential compensatory mechanism.” In: *Scientific Reports* 8.1 (2018).

[148] V. Petrova et al. “The hypoxic tumour microenvironment.” In: *Oncogenesis* 7.1 (2018), p. 10.

[149] R. V. Pisal et al. “Detection of Mycoplasma Contamination Directly from Culture Supernatant Using Polymerase Chain Reaction.” In: *Folia Biol (Praha)* 62.5 (2016), pp. 203–206.

[150] A. M. Porcelli et al. “The genetic and metabolic signature of oncocytic transformation implicates HIF1alpha destabilization.” In: *Hum Mol Genet* 19.6 (2010), pp. 1019–32.

[151] *Press release: The Nobel Prize in Chemistry 2020*. 2020.

[152] *Press release: The Nobel Prize in Physiology or Medicine 2019*. 2019.

[153] C. W. Pugh and P. J. Ratcliffe. "New horizons in hypoxia signaling pathways." In: *Exp Cell Res* 356.2 (2017), pp. 116–121.

[154] F. A. Ran et al. "Genome engineering using the CRISPR-Cas9 system." In: *Nat Protoc* 8.11 (2013), pp. 2281–2308.

[155] E. B. Rankin, J. M. Nam, and A. J. Giaccia. "Hypoxia: Signaling the Metastatic Cascade." In: *Trends Cancer* 2.6 (2016), pp. 295–304.

[156] B. G. Reid and G. C. Flynn. "Chromophore formation in green fluorescent protein." In: *Biochemistry* 36.22 (1997), pp. 6786–91.

[157] M. Riihimaeki et al. "Metastatic sites and survival in lung cancer." In: *Lung Cancer* 86.1 (2014), pp. 78–84.

[158] J. Rodriguez et al. "PHD3 Regulates p53 Protein Stability by Hydroxylating Proline 359." In: *Cell Rep* 24.5 (2018), pp. 1316–1329.

[159] A. J. Rubin et al. "Coupled Single-Cell CRISPR Screening and Epigenomic Profiling Reveals Causal Gene Regulatory Networks." In: *Cell* 176.1-2 (2019), 361–376 e17.

[160] M. Safran et al. "Mouse model for noninvasive imaging of HIF prolyl hydroxylase activity: Assessment of an oral agent that stimulates erythropoietin production." In: *Proceedings of the National Academy of Sciences* 103.1 (2005), pp. 105–110.

[161] A. Saint-Martin, M. C. Castañeda-Patlán, and M. Robles-Flores. "The Role of Hypoxia-Inducible Factors in Cancer Resistance." In: *J Cell Signal* 2.154 (2017).

[162] N. E. Sanjana, O. Shalem, and F. Zhang. "Improved vectors and genome-wide libraries for CRISPR screening." In: *Nat Methods* 11.8 (2014), pp. 783–784.

[163] S. Schick et al. "Systematic characterization of BAF mutations provides insights into intracomplex synthetic lethalities in human cancers." In: *Nature genetics* 51.9 (2019), pp. 1399–1410.

[164] J. Schindelin et al. "Fiji: an open-source platform for biological-image analysis." In: *Nat Methods* 9.7 (2012), pp. 676–82.

[165] K. Schmid et al. "SangeR: The high-throughput Sanger sequencing analysis pipeline." In: *Bioinformatics Advances* (Jan. 2022). vbac009.

[166] J. Schodel et al. "High-resolution genome-wide mapping of HIF-binding sites by ChIP-seq." In: *Blood* 117.23 (2011), e207–17.

[167] C. J. Schofield and Z. Zhang. "Structural and mechanistic studies on 2-oxoglutarate-dependent oxygenases and related enzymes." In: *Curr Opin Struct Biol* 9.6 (1999), pp. 722–31.

[168] A. Schoolmeesters, D. D. Brown, and Y. Fedorov. "Kinome-wide functional genomics screen reveals a novel mechanism of TNFalpha-induced nuclear accumulation of the HIF-1alpha transcription factor in cancer cells." In: *PLoS One* 7.2 (2012), e31270.

[169] S. Seidel et al. "A hypoxic niche regulates glioblastoma stem cells through hypoxia inducible factor 2 alpha." In: *Brain* 133.Pt 4 (2010), pp. 983–95.

[170] M. A. Selak et al. "Succinate links TCA cycle dysfunction to oncogenesis by inhibiting HIF-alpha prolyl hydroxylase." In: *Cancer Cell* 7.1 (2005), pp. 77–85.

[171] G. L. Semenza. “A compendium of proteins that interact with HIF-1alpha.” In: *Exp Cell Res* 356.2 (2017), pp. 128–135.

[172] G. L. Semenza. “Heritable disorders of oxygen sensing.” In: *Am J Med Genet A* 185.8 (2021), pp. 2576–2581.

[173] G. L. Semenza. “Oxygen sensing, hypoxia-inducible factors, and disease pathophysiology.” In: *Annu Rev Pathol* 9 (2014), pp. 47–71.

[174] G. L. Semenza. “Targeting HIF-1 for cancer therapy.” In: *Nat Rev Cancer* 3.10 (2003), pp. 721–32.

[175] G. L. Semenza et al. “Hypoxia-inducible nuclear factors bind to an enhancer element located 3’ to the human erythropoietin gene.” In: *Proc Natl Acad Sci U S A* 88.13 (1991), pp. 5680–4.

[176] G. L. Semenza et al. “Transcriptional regulation of genes encoding glycolytic enzymes by hypoxia-inducible factor 1.” In: *J Biol Chem* 269.38 (1994), pp. 23757–63.

[177] M. Serocki et al. “miRNAs regulate the HIF switch during hypoxia: a novel therapeutic target.” In: *Angiogenesis* 21.2 (2018), pp. 183–202.

[178] O. Shalem et al. “Genome-scale CRISPR-Cas9 knockout screening in human cells.” In: *Science* 343.6166 (2014), pp. 84–87.

[179] B. A. Sherf et al. “Dual-Luciferase(R) reporter assay: An advanced co-reporter technology integrating firefly and Renilla luciferase assays.” In: *Promega Notes* 57 (1996), pp. 2–9.

[180] T. Shibata, A. J. Giaccia, and J. M. Brown. “Development of a hypoxia-responsive vector for tumor-specific gene therapy.” In: *Gene Ther* 7.6 (2000), pp. 493–8.

[181] M. C. Simon. “Siah Proteins, HIF Prolyl Hydroxylases, and the Physiological Response to Hypoxia.” In: *Cell* 117.7 (2004), pp. 851–853.

[182] F. Skoulidis et al. “Co-occurring genomic alterations define major subsets of KRAS-mutant lung adenocarcinoma with distinct biology, immune profiles, and therapeutic vulnerabilities.” In: *Cancer Discov* 5.8 (2015), pp. 860–77.

[183] K. A. Smith, G. B. Waypa, and P. T. Schumacker. “Redox signaling during hypoxia in mammalian cells.” In: *Redox Biol* 13 (2017), pp. 228–234.

[184] S. W. Son et al. “The Hypoxia-Long Noncoding RNA Interaction in Solid Cancers.” In: *Int J Mol Sci* 22.14 (2021).

[185] T. Song et al. “MiR-138 suppresses expression of hypoxia-inducible factor 1alpha (HIF-1alpha) in clear cell renal cell carcinoma 786-O cells.” In: *Asian Pac J Cancer Prev* 12.5 (2011), pp. 1307–11.

[186] V. Srinivas et al. “Oxygen sensing and HIF-1 activation does not require an active mitochondrial respiratory chain electron-transfer pathway.” In: *J Biol Chem* 276.25 (2001), pp. 21995–8.

[187] P. Stepper et al. “Efficient targeted DNA methylation with chimeric dCas9-Dnmt3a-Dnmt3L methyltransferase.” In: *Nucleic Acids Res* 45.4 (2017), pp. 1703–1713.

[188] T. A. Takeda et al. “Continuous de novo biosynthesis of haem and its rapid turnover to bilirubin are necessary for cytoprotection against cell damage.” In: *Sci Rep* 5 (2015), p. 10488.

[189] C. C. Tan et al. “Feedback modulation of renal and hepatic erythropoietin mRNA in response to graded anemia and hypoxia.” In: *Am J Physiol* 263.3 Pt 2 (1992), F474–81.

[190] A. A. Thai et al. “Lung cancer.” In: *Lancet* 398.10299 (2021), pp. 535–554.

[191] P. D. Tiburcio, H. Choi, and L. E. Huang. “Complex role of HIF in cancer: the known, the unknown, and the unexpected.” In: *Hypoxia (Auckl)* 2 (2014), pp. 59–70.

[192] A. Toschi et al. “Differential dependence of hypoxia-inducible factors 1 alpha and 2 alpha on mTORC1 and mTORC2.” In: *J Biol Chem* 283.50 (2008), pp. 34495–9.

[193] R. Triepels et al. “The nuclear-encoded human NADH:ubiquinone oxidoreductase NDUFA8 subunit: cDNA cloning, chromosomal localization, tissue distribution, and mutation detection in complex-I-deficient patients.” In: *Hum Genet* 103.5 (1998), pp. 557–63.

[194] R. Y. Tsien. “The green fluorescent protein.” In: *Annu Rev Biochem* 67 (1998), pp. 509–44.

[195] C. C. Uphoff and H. G. Drexler. “Comparative PCR analysis for detection of mycoplasma infections in continuous cell lines.” In: *In Vitro Cell Dev Biol Anim* 38.2 (2002), pp. 79–85.

[196] D. Villar et al. “Identification of a region on hypoxia-inducible-factor prolyl 4-hydroxylases that determines their specificity for the oxygen degradation domains.” In: *Biochemical Journal* 408.2 (2007), pp. 231–240.

[197] A. Vito, N. El-Sayes, and K. Mossman. “Hypoxia-Driven Immune Escape in the Tumor Microenvironment.” In: *Cells* 9.4 (2020).

[198] G. S. Waldo et al. “Rapid protein-folding assay using green fluorescent protein.” In: *Nat Biotechnol* 17.7 (1999), pp. 691–5.

[199] J. Walter et al. “Flavin mononucleotide-based fluorescent proteins function in mammalian cells without oxygen requirement.” In: *PLoS One* 7.9 (2012), e43921.

[200] J. Wan et al. “SOCS3 blocks HIF-1alpha expression to inhibit proliferation and angiogenesis of human small cell lung cancer by downregulating activation of Akt, but not STAT3.” In: *Mol Med Rep* 12.1 (2015), pp. 83–92.

[201] G. L. Wang et al. “Hypoxia-inducible factor 1 is a basic-helix-loop-helix-PAS heterodimer regulated by cellular O2 tension.” In: *Proc Natl Acad Sci U S A* 92.12 (1995), pp. 5510–4.

[202] M. Waskom and the seaborn development team. *Seaborn*. Version v0.11.0. Sept. 2020.

[203] M. Wegner et al. “Circular synthesized CRISPR/Cas gRNAs for functional interrogations in the coding and noncoding genome.” In: *Elife* 8 (2019).

[204] R. H. Wenger et al. “Frequently asked questions in hypoxia research.” In: *Hypoxia (Auckl)* 3 (2015), pp. 35–43.

[205] C. A. White and N. A. Nicola. “SOCS3: An essential physiological inhibitor of signaling by interleukin-6 and G-CSF family cytokines.” In: *JAKSTAT* 2.4 (2013), e25045.

[206] M. S. Wiesener et al. “Induction of endothelial PAS domain protein-1 by hypoxia: characterization and comparison with hypoxia-inducible factor-1alpha.” In: *Blood* 92.7 (1998), pp. 2260–8.

[207] S. E. Wilkins et al. “Targeting Protein-Protein Interactions in the HIF System.” In: *ChemMedChem* 11.8 (2016), pp. 773–86.

[208] L. Xie et al. “Oxygen-regulated beta(2)-adrenergic receptor hydroxylation by EGLN3 and ubiquitylation by pVHL.” In: *Sci Signal* 2.78 (2009), ra33.

[209] Q. Xu et al. “Targeting Stat3 blocks both HIF-1 and VEGF expression induced by multiple oncogenic growth signaling pathways.” In: *Oncogene* 24.36 (2005), pp. 5552–60.

[210] C. Xue and E. C. Greene. “DNA Repair Pathway Choices in CRISPR-Cas9-Mediated Genome Editing.” In: *Trends Genet* 37.7 (2021), pp. 639–656.

[211] K. Yokogami, S. Yamashita, and H. Takeshima. “Hypoxia-induced decreases in SOCS3 increase STAT3 activation and upregulate VEGF gene expression.” In: *Brain Tumor Pathol* 30.3 (2013), pp. 135–143.

[212] M. N. Zaini et al. “Endogenous HIF2A reporter systems for high-throughput functional screening.” In: *Sci Rep* 8.1 (2018), p. 12063.

[213] Q. Zhang and H. Yang. “The Roles of VHL-Dependent Ubiquitination in Signaling and Cancer.” In: *Front Oncol* 2 (2012), p. 35.

[214] H. Zhou et al. “Reciprocal regulation of SOCS 1 and SOCS3 enhances resistance to ionizing radiation in glioblastoma multiforme.” In: *Clinical Cancer Research* 13.8 (2007), pp. 2344–2353.

Appendix

Plasmid map of pLenti6 5xHRE CMVp HIF2α-ODD(aa354-581)=UnaG-V5 reporter plasmid

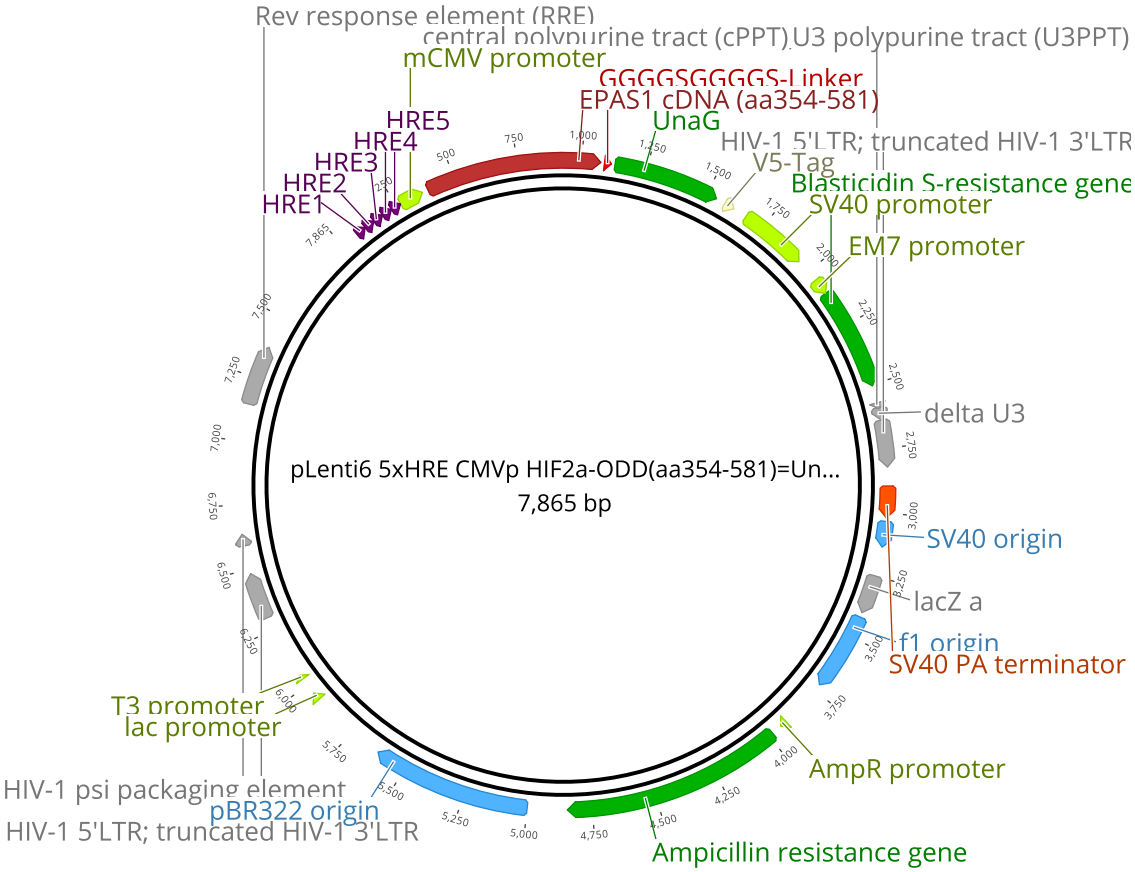

Figure 4.1: Plasmid map of pLenti6 5xHRE CMVp HIF2α-ODD(aa354-581)=UnaG-V5 reporter plasmid.
HRE = hypoxia responsive element; mCMV promoter = minimal cytomegalovirus promoter; EPAS1 cDNA = coding sequence for HIF2α protein.

Descriptive statistic tables of boxplots inside violin plots

The following pages contain tables showing the respective descriptive statistic measures of the boxplots inside the violin plots (flow cytometry analyses).

		UnaG Fluorescence Intensity [AU]: Descriptive statistic measures					
SCC	**Treatment**	**Min.**	**1st Qu.**	**Median**	**Mean**	**3rd Qu.**	**Max.**
A1	Normoxia	156.9	791.8	966.4	1,020.8	1,182.5	46,935.2
	Hypoxia	230.9	7,676.8	11,820.8	13,601.7	17,824.3	95,867.0
	DMOG	318.2	7,277.2	10,133.6	11,892.4	14,637.2	91,114.7
B11	Normoxia	204.2	842.1	1,041.9	1,100.1	1,287.6	27,954.2
	Hypoxia	424.8	7,223.9	10,626.4	12,088.2	15,553.3	136,299.0
	DMOG	581.6	6,883.5	9,991.5	11,464.7	14,620.1	62,938.5
C2	Normoxia	156.9	661.6	805.1	851.2	991.6	5,410.9
	Hypoxia	436.6	3,597.9	5,714.3	7,039.5	9,112.4	62,932.6
	DMOG	352.2	3,457.3	4,826.3	5,860.1	7,155.8	46,002.8
E7	Normoxia	103.6	592.0	744.4	783.6	932.4	18,545.9
	Hypoxia	179.1	4,941.7	8,484.8	10,249.5	13,952.4	81,746.3
	DMOG	229.4	4,271.3	6,778.4	8,507.6	11,311.6	58,738.2
F9	Normoxia	77.0	549.1	686.7	721.9	851.0	3,176.1
	Hypoxia	236.8	2,718.8	4,428.2	5,146.7	6,867.2	37,003.0
	DMOG	303.4	1,835.2	2,853.4	3,593.1	4,665.0	25,655.8
Pool	Normoxia	108.0	574.2	754.8	839.6	1,007.9	52,275.1
	Hypoxia	111.0	3,678.9	6,656.3	8,896.1	11,578.0	129,038.0
	DMOG	84.4	3,038.8	5,329.5	7,333.8	9,356.6	98,723.4
wt	Normoxia	25.2	313.8	405.5	445.9	528.4	5,884.5
	DMOG	57.7	353.7	457.3	488.0	584.6	1,744.9

Table 4.4: Descriptive statistic measures corresponding to Fig. 2.8.
SCC = single cell clone; AU = arbitrary units; Min. = minimum; Qu. = quartile; Max. = maximum; DMOG = dimethyloxaloylglycine.

SCC	Treatment	UnaG Fluorescence Intensity [AU]: Descriptive Statistic measures					
		Min.	1st Qu.	Median	Mean	3rd Qu.	Max.
P3A5	Normoxia	68.1	504.7	633.4	792.1	793.3	81,815.9
	Hypoxia	245.7	22,248.8	29,089.4	30,338.3	36,966.7	129,299.0
	DMOG	338.9	23,234.9	29,648.8	30,797.2	37,073.6	110,093.0
P3A6	Normoxia	48.8	408.5	510.6	553.0	640.8	41,126.2
	Hypoxia	84.4	12,332.8	19,049.1	19,279.8	25,784.6	84,638.2
	DMOG	171.7	12,982.6	17,062.9	18,150.3	22,163.0	91,131.0
P3B4	Normoxia	59.2	411.4	515.0	538.4	639.4	2,223.0
	Hypoxia	269.4	11,988.0	17,146.6	17,601.9	22,619.9	77,671.9
	DMOG	248.6	14,717.1	18,855.2	19,674.0	23,757.0	77,777.0
P3B8	Normoxia	25.2	353.7	447.0	470.2	558.0	10,031.4
	Hypoxia	149.5	8,042.3	11,495.2	11,948.2	15,250.3	51,589.8
	DMOG	164.3	8,496.7	11,144.4	11,741.9	14,277.6	52,796.0
P4B3	Normoxia	7.4	296.0	375.9	394.1	467.7	17,108.8
	Hypoxia	77.0	4,232.1	9,645.2	9,917.2	14,361.9	76,926.0
	DMOG	62.2	4,650.2	7,903.2	8,485.8	11,508.5	66,019.8
P4D1	Normoxia	29.6	288.6	368.5	396.4	467.7	27,351.9
	Hypoxia	47.4	1,003.4	7,584.3	8,790.7	13,726.6	69,133.8
	DMOG	62.2	5,242.2	8,991.0	10,263.9	13,866.1	77,714.8
P5A3	Normoxia	34.0	418.8	537.2	568.0	682.3	5,298.4
	Hypoxia	193.9	5,363.5	9,910.1	10,309.9	14,396.0	62,346.5
	DMOG	145.0	8,064.5	9,938.2	10,429.4	12,276.6	33,143.1
P5H5	Normoxia	41.4	371.5	467.7	496.7	586.1	26,375.1
	Hypoxia	180.6	7,590.2	12,717.6	13,267.9	18,014.6	72,037.5
	DMOG	72.5	754.8	12,113.8	12,024.9	19,059.4	81,164.7
P6A7	Normoxia	28.1	421.8	531.3	622.4	667.5	44,158.8
	Hypoxia	182.0	14,114.4	20,486.9	21,198.3	27,414.4	88,205.0
	DMOG	312.3	11,076.3	14,721.6	15,839.6	19,339.2	70,541.2
P6C2	Normoxia	99.2	489.9	626.0	1,229.0	811.0	66,457.9
	Hypoxia	108.0	18,555.9	25,968.9	26,734.2	34,006.0	130,495.0
	DMOG	164.3	12,719.1	16,487.2	17,659.3	21,352.0	80,396.6
P6G12	Normoxia	53.3	378.9	476.6	505.6	599.4	22,139.3
	Hypoxia	16.3	7,978.7	13,750.0	14,457.3	19,823.1	84,391.1
	DMOG	65.1	12,981.1	17,543.9	18,556.7	22,989.6	95,720.5
wt	Normoxia	11.8	266.4	347.8	372.5	448.4	2,575.2
	Hypoxia	1.5	278.2	373.0	409.4	492.8	3,574.2
	DMOG	1.5	267.9	355.2	386.3	467.7	2,908.2

Table 4.5: Descriptive statistic measures corresponding to Fig. 2.9.
SCC = single cell clone; AU = arbitrary units; Min. = minimum; Qu. = quartile; Max. = maximum; DMOG = dimethyloxaloylglycine.

Cell line	Seeded cells	Treatment	UnaG Fluorescence Intensity [AU]: Descriptive statistic measures					
			Min.	1st Qu.	Median	Mean	3rd Qu.	Max.
G141 SCC#A1	75,000	Normoxia	262.0	827.3	994.6	1,046.2	1,213.6	32,409.0
		Hypoxia	501.7	3,270.8	5,933.3	8,087.8	10,952.0	100,334.0
		DMOG	362.6	4,660.5	6,230.8	7,073.3	8,583.6	44,978.7
	150,000	Normoxia	293.0	1,036.0	1,240.2	1,307.8	1,509.6	42,455.3
		Hypoxia	327.1	8,991.0	14,160.6	16,334.2	21,579.2	116,747.0
		DMOG	436.6	7,086.2	9,506.0	10,862.9	13,195.7	148,740.0
	200,000	Normoxia	216.1	1,058.2	1,281.7	1,347.2	1,561.4	42,582.6
		Hypoxia	737.0	11,581.0	17,928.7	20,040.9	26,268.5	141,189.0
		DMOG	442.5	8,456.7	11,618.0	13,371.8	16,401.4	114,166.0
A549 SCC#P3A5	75,000	Normoxia	16.3	259.0	331.5	461.9	421.8	43,661.5
		Hypoxia	16.3	14,379.7	20,153.2	20,801.3	26,626.7	85,800.0
		DMOG	211.6	16,577.5	20,851.7	21,633.0	25,872.3	69,009.4
	150,000	Normoxia	57.7	309.3	392.2	636.7	506.2	90,121.6
		Hypoxia	88.8	19,367.3	26,280.4	27,425.1	34,452.2	101,019.0
		DMOG	216.1	22,444.2	28,461.9	29,607.5	35,539.2	93,503.4
	200,000	Normoxia	5.9	319.7	411.4	688.5	537.2	90,670.7
		Hypoxia	79.9	20,277.5	27,748.5	29,007.0	36,375.1	105,965.0
		DMOG	174.6	24,386.0	31,424.8	32,645.2	39,484.9	130,277.0

Table 4.6: Descriptive statistic measures corresponding to Fig. 2.11.
SCC = single cell clone; AU = arbitrary units; Min. = minimum; Qu. = quartile; Max. = maximum; DMOG = dimethyloxaloylglycine.

Cell line	FBS-Conc.	Treatment	UnaG Fluorescence Intensity [AU]: Descriptive statistic measures					
			Min.	1st Qu.	Median	Mean	3rd Qu.	Max.
G141 SCC#A1	1 %	Normoxia	165.76	1038.96	1260.96	1347.81	1552.52	85360.5
		Hypoxia(in)	134.68	11356	17723.75	19800.21	26031.7	170653
		Hypoxia(out)	412.92	7469.56	12442.4	14455.89	19425	116648
		DMOG	251.6	11057.1	15298.8	17437.9	21525.1	99316.9
	5 %	Normoxia	409.96	1141.08	1367.52	1457.36	1669.44	66389.8
		Hypoxia(in)	266.4	11122.2	17227.2	19310.4	25322	131898
		Hypoxia(out)	467.68	7784.8	12676.2	14550.42	19420.6	149224
		DMOG	648.24	10556.8	14462.6	16500.63	20261.2	99278.4
	10 %	Normoxia	173.16	1095.2	1326.08	1411.95	1636.88	61837.4
		Hypoxia(in)	282.68	11129.6	17379.6	19485.62	25676.5	136110
		Hypoxia(out)	4.44	7126.2	12145.65	14186.77	19248.9	148583
		DMOG	389.24	10725.6	14834	17023.06	21004.2	123272
A549 SCC#P3A5	1 %	Normoxia	50.32	309.32	390.72	830.64	498.76	110984
		Hypoxia(in)	136.16	24731.17	34213.2	36277.31	45920	128824
		Hypoxia(out)	105.08	25407.55	34082.15	35721.14	44395.22	181481
		DMOG	57.72	29459.4	37482.5	39263.27	47224.55	139631
	5 %	Normoxia	8.88	318.2	398.12	819.53	506.16	124847
		Hypoxia(in)	74	25662.8	34999	37034.9	46445.4	146101
		Hypoxia(out)	133.2	25537.4	34225	35741.3	44342.3	174625
		DMOG	168.72	31978.75	40460.95	42267.13	50734.4	162298
	10 %	Normoxia	11.84	318.2	401.08	843.67	509.12	108515
		Hypoxia(in)	146.52	24782.6	34034.1	35756.43	45052.7	153941
		Hypoxia(out)	179.08	24795.9	33254.1	34800.22	43130.9	179816
		DMOG	142.08	31198.4	39423.5	41134.97	49217.4	150020

Table 4.7: Descriptive statistic measures corresponding to Fig. 2.12.
AU = arbitrary units; Min. = minimum; Qu. = quartile; Max. = maximum; FBS-Conc. = concentration of fetal bovine serum in FACS buffer; DMOG = dimethyloxaloylglycine; in = cells harvested inside the hypoxia chamber; put = cells harvested outside of the hypoxia chamber.

Cell line	Treatment	Incub. time	UnaG Fluorescence Intensity [AU]: Descriptive statistic measures					
			Min.	1st Qu.	Median	Mean	3rd Qu.	Max.
G141 SCC#A1	Normoxia	0 h	179.1	954.6	1,151.4	1,214.2	1,403.0	27,433.3
	Hypoxia	0 h	299.0	9,905.6	15,976.6	18,061.5	24,150.6	171,403.0
		0.5 h	337.4	9,260.4	14,434.4	16,263.4	21,455.6	114,838.0
		1 h	303.4	8,218.4	12,994.4	14,788.7	19,630.7	134,400.0
		2 h	362.6	7,540.6	12,081.2	13,947.1	18,579.9	106,819.0
		3 h	370.0	7,014.1	10,968.3	12,651.8	16,621.9	106,532.0
	DMOG	0 h	330.0	4,601.3	6,295.9	7,341.5	8,970.3	112,890.0
A549 SCC#P3A5	Normoxia	0 h	140.6	615.7	788.8	1,805.4	1,028.6	176,890.0
	Hypoxia	0 h	423.3	50,496.9	68,370.1	72,007.8	89,727.6	262,143.0
		0.5 h	313.8	53,152.0	70,709.2	74,436.0	91,654.2	262,143.0
		1 h	361.1	46,019.1	60,276.0	62,822.5	76,822.4	262,143.0
		2 h	356.7	45,594.4	59,802.4	62,208.7	76,277.7	262,143.0
		3 h	488.4	47,397.0	61,326.8	63,934.5	77,837.6	236,535.0

Table 4.8: Descriptive statistic measures corresponding to Fig. 2.13.
AU = arbitrary units; Min. = minimum; Qu. = quartile; Max. = maximum; Incub. time = incubation time on ice before measurement in hours; DMOG = dimethyloxaloylglycine.

Cell line	sgRNA	Treatment	UnaG Fluorescence Intensity [AU]: Descriptive statistic measures					
			Min.	1st Qu.	Median	Mean	3rd Qu.	Max.
G141 SCC#A1	No KO	Normoxia	362.6	1,224.0	1,462.2	1,532.8	1,764.2	21,650.9
		Hypoxia	544.6	14,544.0	23,674.1	27,349.5	36,876.8	200,340.0
	NC#1	Normoxia	325.6	1,263.9	1,515.5	1,592.0	1,839.6	17,967.2
		Hypoxia	449.9	12,130.5	19,282.9	22,342.9	29,863.4	139,058.0
	NC#2	Normoxia	315.2	1,309.8	1,582.1	1,661.7	1,932.9	105,925.0
		Hypoxia	390.7	9,213.0	14,999.8	17,677.0	23,779.2	233,309.0
	NC#3	Normoxia	310.8	1,352.7	1,623.6	1,705.2	1,968.4	63,785.0
		Hypoxia	512.1	9,023.6	14,697.9	17,315.0	23,172.4	130,795.0
	PHD2#3	Normoxia	421.8	1,691.6	2,536.7	6,381.5	7,639.4	118,501.0
		Hypoxia	692.6	8,091.2	12,649.6	15,147.0	19,612.3	128,054.0
	PHD3#8	Normoxia	281.2	1,315.7	1,591.0	1,719.0	1,950.6	88,813.3
		Hypoxia	478.0	13,602.7	21,688.7	24,431.0	32,580.7	162,106.0
	VHL#2	Normoxia	669.0	20,671.2	27,906.9	30,391.9	37,958.7	162,022.0
		Hypoxia	741.5	22,544.8	30,538.3	33,407.6	41,983.2	135,802.0
	VHL#3	Normoxia	389.2	5,499.7	19,620.4	21,241.1	31,124.4	148,281.0
		Hypoxia	880.6	18430.4	26677.8	29823.2	38766	182602
A549 SCC#P3A5	No KO	Normoxia	77.0	452.9	571.3	739.2	726.7	105,136.0
		Hypoxia	273.8	40,538.7	53,605.6	56,435.8	69,101.2	208,621.0
	NC#1	Normoxia	8.9	411.4	518.0	576.6	651.2	74,896.9
		Hypoxia	7.4	35,151.1	47,426.6	49,924.6	62,076.0	218,035.0
	NC#2	Normoxia	41.4	404.0	510.6	565.6	640.8	71,879.2
		Hypoxia	50.3	34,352.3	46,591.9	48,809.5	60,869.8	219,659.0
	NC#3	Normoxia	41.4	396.6	504.7	556.2	633.4	69,207.8
		Hypoxia	47.4	32,320.6	44,530.2	46,430.7	58,571.0	159,877.0
	PHD2#3	Normoxia	65.1	429.2	563.9	1,952.7	769.6	97,922.7
		Hypoxia	130.2	29,786.5	41,332.0	42,903.8	54,410.0	167,274.0
	PHD3#8	Normoxia	57.7	414.4	525.4	604.6	663.0	95,251.3
		Hypoxia	44.4	40,523.9	53,832.0	55,933.9	69,097.9	189,339.0

Table 4.9: Descriptive statistic measures corresponding to Fig. 2.14 and Fig. 2.15.
sgRNA = single guide RNA; AU = arbitrary units; Min. = minimum; Qu. = quartile; Max. = maximum.

Screening hit list (p <0.005, ΔLFC >1)

The following pages contain the screening hits with p <0.005 and ΔLFC >1.

Rank	Gene ID	*p*	ΔLFC	Rank	Gene ID	*p*	ΔLFC
1	STK11	0.00000233	9.68	**51**	MRPS31	0.00247370	6.34
2	EGLN1	0.00000026	8.89	**52**	FKBP1A	0.00332580	6.27
3	TCEB2	0.00000026	8.86	**53**	MRPL41	0.00063998	6.17
4	TCEB1	0.00000026	8.82	**54**	TNC	0.00468290	6.17
5	VHL	0.00000026	8.59	**55**	MAMDC4	0.00360550	6.00
6	SMARCB1	0.00000855	7.33	**56**	C9orf135	0.00159880	5.95
7	CUL2	0.00000181	7.06	**57**	LOC286238	0.00215820	5.87
8	NDUFA11	0.00003548	6.83	**58**	SSNA1	0.00381380	5.75
9	MANEAL	0.00004999	5.88	**59**	STIL	0.00390180	5.58
10	MRPS21	0.00002409	5.80	**60**	FBXO8	0.00284250	5.56
11	MRPS2	0.00000285	5.63	**61**	DNAJB1	0.00183710	5.56
12	SOCS3	0.00000026	5.60	**62**	MTIF2	0.00244550	5.52
13	ORM2	0.00003963	5.11	**63**	INSL4	0.00218100	5.39
14	AIP	0.00000285	4.93	**64**	P2RX4	0.00252030	5.36
Excl.	ATP13A1	0.00000803	4.56	**65**	NFIB	0.00175160	5.35
15	ARID1A	0.00004170	4.45	**66**	C10orf2	0.00200490	5.26
16	AHR	0.00000026	4.36	**67**	OBP2B	0.00497300	5.21
17	LIPT2	0.00000803	3.71	**68**	MRPS18A	0.00105180	5.14
18	RPUSD3	0.00000389	2.94	**69**	CSK	0.00157600	5.14
19	ACO1	0.00005569	12.18	**70**	TAS2R39	0.00132630	5.12
20	BOLA3	0.00007589	9.12	**71**	HOXA11	0.00228830	5.12
21	DNAJC19	0.00015410	8.03	**72**	FAM166B	0.00105490	5.07
22	FASTKD2	0.00026444	7.68	**73**	CBWD1	0.00356510	5.06
23	CDCA7L	0.00041310	7.21	**74**	PPP1R13B	0.00059647	5.04
24	NDUFA8	0.00046956	6.75	**75**	RGCC	0.00136260	4.99
25	CBFB	0.00006242	6.66	**76**	NME6	0.00251360	4.90
26	TMEM141	0.00035146	6.26	**77**	YTHDC1	0.00118340	4.83
27	CHCHD1	0.00009661	6.14	**78**	POR	0.00385050	4.79
28	ADIG	0.00022714	4.77	**79**	KHSRP	0.00201060	4.70
29	RMND1	0.00041362	4.14	**80**	DAP3	0.00079383	4.68
30	KIAA0368	0.00011629	3.92	**81**	TRUB2	0.00479480	4.68
31	TIMM8A	0.00029707	3.83	**82**	PGM5	0.00426650	4.66
32	PPOX	0.00016136	3.71	**83**	UAP1	0.00359570	4.64
33	MRPS11	0.00012769	3.66	**84**	HMBS	0.00253070	4.60
34	MRPL17	0.00010956	3.64	**85**	N4BP3	0.00279020	4.60
35	GNAQ	0.00040689	3.47	**86**	NDUFB4	0.00442400	4.59
36	PARL	0.00025149	3.22	**87**	INPPL1	0.00294820	4.58
37	KMT2B	0.00025978	2.22	**88**	NDUFV1	0.00322430	4.57
38	NDUFAF4	0.00253690	9.25	**89**	NOA1	0.00146260	4.56
39	PSG1	0.00063118	8.98	**90**	BACH1	0.00109790	4.49
40	PRMT8	0.00480000	8.70	**91**	NDUFB9	0.00375780	4.48
41	GATC	0.00414680	8.12	**92**	ETV3L	0.00157450	4.48
42	EXD3	0.00200650	8.10	**93**	KLF4	0.00112640	4.48
43	OR10A4	0.00211370	7.49	**94**	FCN1	0.00190390	4.48
44	CYB5RL	0.00280880	6.94	**95**	FTSJ2	0.00144600	4.46
45	CCDC57	0.00197900	6.90	**96**	ARFGEF2	0.00178990	4.45
46	CCIN	0.00076897	6.84	**97**	MTERF4	0.00444990	4.45
47	STYK1	0.00121960	6.74	**98**	ADORA3	0.00481400	4.42
48	YME1L1	0.00059492	6.52	**99**	NTMT1	0.00099896	4.38
49	NDUFB11	0.00072468	6.51	**100**	XCL2	0.00470680	4.36
50	IQSEC1	0.00414420	6.40	**101**	CCL21	0.00311810	4.35

Rank	Gene ID	*p*	ΔLFC	Rank	Gene ID	*p*	ΔLFC
102	SIRPA	0.00240070	4.34	**153**	OR10J1	0.00306680	2.87
103	NDUFS2	0.00110000	4.32	**154**	ALAD	0.00127350	2.87
104	UROD	0.00100150	4.29	**155**	TBC1D13	0.00477050	2.82
105	CR1L	0.00359050	4.21	**156**	MNDA	0.00424370	2.81
106	NGFR	0.00266170	4.09	**157**	MSMP	0.00317610	2.72
107	WDR63	0.00191740	3.99	**158**	GLRX5	0.00412560	2.69
108	SNAPIN	0.00104560	3.97	**159**	ERV3-1	0.00320670	2.68
109	NDUFB6	0.00374640	3.96	**160**	DNASE2	0.00400590	2.66
110	EGLN3	0.00408570	3.94	**161**	FRRS1L	0.00105800	2.66
111	IFNA17	0.00467470	3.91	**162**	SNX3	0.00259540	2.64
112	RWDD3	0.00432860	3.87	**163**	KTN1	0.00175680	2.59
113	KLHL29	0.00351540	3.87	**164**	FDX1	0.00058145	2.56
114	C19orf38	0.00357240	3.84	**165**	FECH	0.00127040	2.56
115	TRIM72	0.00199510	3.83	**166**	APC2	0.00100720	2.48
116	SERTAD1	0.00057783	3.80	**167**	RPS14	0.00332220	2.45
117	IL11RA	0.00055866	3.78	**168**	LYSMD2	0.00457260	2.44
118	GPRIN1	0.00369930	3.72	**169**	LACTBL1	0.00351690	2.38
119	RAB3D	0.00256490	3.72	**170**	CRB2	0.00324340	2.36
120	LIAS	0.00172780	3.70	**171**	HIST1H2BM	0.00498080	2.35
121	PRKACG	0.00402820	3.70	**172**	FCRL6	0.00136160	2.21
122	C9orf40	0.00373090	3.69	**173**	RAB27B	0.00233120	2.06
123	AGL	0.00379610	3.63	**174**	ERN1	0.00239500	2.03
124	MRC2	0.00392100	3.60	**175**	FGD3	0.00236130	2.01
125	MRPS14	0.00115590	3.59	**176**	RAD51D	0.00259080	1.64
126	SPINK4	0.00087697	3.58	**177**	NCOR2	0.01678800	10.16
127	CYSRT1	0.00286480	3.56	**178**	TMC4	0.01771400	10.02
128	TUFM	0.00239240	3.55	**179**	IL18BP	0.03783700	9.97
129	FAM53A	0.00401270	3.55	**180**	MYL12B	0.03050000	9.41
130	INHBC	0.00235250	3.54	**181**	GOLGA1	0.01791500	9.07
131	CYB5B	0.00053224	3.48	**182**	SAP18	0.00676060	8.82
132	SLC30A1	0.00098549	3.46	**183**	TREML2	0.03955900	8.61
133	ZBTB34	0.00254830	3.41	**184**	CNTLN	0.01356900	8.51
134	CIC	0.00211010	3.40	**185**	UGT1A10	0.02612900	8.43
135	GUK1	0.00349470	3.39	**186**	PCNP	0.00746560	8.28
136	GDF15	0.00300210	3.37	**187**	MARS2	0.02598900	8.26
137	MBD3L4	0.00343040	3.35	**188**	ZNF23	0.02125600	8.01
138	ADAM28	0.00361540	3.34	**189**	CCDC34	0.03509800	7.87
139	ANO9	0.00320250	3.30	**190**	MRFAP1	0.02133400	7.86
140	C19orf66	0.00088448	3.29	**191**	OR13C9	0.01106300	7.80
141	LOC100130880	0.00300410	3.13	**192**	IFNA10	0.04011000	7.78
142	ZNF484	0.00262390	3.06	**193**	MARCH1	0.03364900	7.77
143	NDUFS7	0.00291970	3.03	**194**	ZSCAN4	0.03242700	7.65
144	MTRF1L	0.00270260	3.01	**195**	SNX27	0.00810690	7.64
145	LHX6	0.00301400	2.98	**196**	C9orf171	0.02562800	7.63
146	DIRAS1	0.00335480	2.97	**197**	TRPC5OS	0.00554130	7.57
147	PRUNE	0.00269380	2.97	**198**	MRPL20	0.01561000	7.57
148	MRPL57	0.00377180	2.97	**199**	LDLRAD3	0.03924200	7.53
149	TMEM165	0.00149470	2.95	**200**	CCDC183	0.01094000	7.49
150	MTG1	0.00465550	2.94	**201**	PPAT	0.04442500	7.28
151	RBM15	0.00068350	2.93	**202**	TGIF1	0.00764490	7.16
152	LIN37	0.00375210	2.91	**203**	SENP3	0.02279900	7.02

Rank	Gene ID	*p*	ΔLFC	Rank	Gene ID	*p*	ΔLFC
204	CRYGS	0.03660200	7.00	**255**	P2RX1	0.03179000	5.82
205	MIA3	0.04121600	6.96	**256**	IFNA1	0.00608880	5.80
206	C9orf142	0.01432700	6.86	**257**	TRPM1	0.04440800	5.80
207	MSGN1	0.02295700	6.84	**258**	NDUFAF7	0.02047000	5.78
208	OVOL2	0.03418500	6.82	**259**	MX1	0.04284300	5.76
209	SCAI	0.02656100	6.81	**260**	SIK3	0.01653100	5.75
210	GPAM	0.03805000	6.78	**261**	OR1I1	0.04524300	5.75
211	UBA2	0.02815200	6.69	**262**	B4GALT3	0.03366500	5.66
212	HDGFRP2	0.04712400	6.68	**263**	DNAH11	0.01309100	5.65
213	HADH	0.02291600	6.61	**264**	AP5Z1	0.02804600	5.61
214	PCP4L1	0.02253900	6.59	**265**	FBXW5	0.00814470	5.58
215	RNF138	0.04891200	6.59	**266**	MRPL21	0.02389300	5.55
216	ZNF714	0.03194600	6.58	**267**	WEE1	0.03104300	5.55
217	TCEB3CL2	0.00697720	6.56	**268**	CAPRIN1	0.01500400	5.53
218	SUCLG1	0.00598360	6.53	**269**	MRPL37	0.01444700	5.51
219	MRPL46	0.03111400	6.52	**270**	AMIGO3	0.04017300	5.51
220	SERTAD3	0.03138400	6.52	**271**	SCAF1	0.00509220	5.50
221	ZNF625	0.04227100	6.48	**272**	LPAR1	0.03696500	5.48
222	DMC1	0.03882300	6.48	**273**	DMRT1	0.04652300	5.48
223	C11orf80	0.03912300	6.46	**274**	ZNF563	0.01718700	5.47
224	CTAG1B	0.02393200	6.41	**275**	ZIC2	0.01416200	5.47
225	CCNY	0.04130100	6.40	**276**	KIAA1804	0.02535900	5.44
226	SEMA4D	0.01099800	6.35	**277**	TMEM81	0.03549000	5.43
227	ABHD4	0.04771100	6.33	**278**	LIPT1	0.01262000	5.43
228	DDX28	0.04094200	6.32	**279**	PEX16	0.02219900	5.43
229	FOXD4L3	0.02016400	6.31	**280**	CEACAM4	0.01256500	5.42
230	CGREF1	0.04306500	6.30	**281**	ASB8	0.03613200	5.42
231	ASB18	0.02092700	6.29	**282**	STRBP	0.03409300	5.42
232	SUPT4H1	0.01247100	6.26	**283**	C9orf106	0.01334700	5.41
233	ZNF462	0.01286100	6.23	**284**	EVX1	0.04074700	5.39
234	MANBA	0.03128200	6.23	**285**	NUTM2G	0.00604890	5.38
235	CCDC18	0.01509800	6.23	**286**	PGLYRP4	0.01822400	5.33
236	LOC113230	0.02034400	6.22	**287**	VPS39	0.01123300	5.32
237	PAPOLA	0.04623600	6.21	**288**	NDUFA1	0.00988990	5.31
238	ZBTB40	0.01844600	6.18	**289**	RGMA	0.04015300	5.30
239	GOLGA2	0.02219400	6.10	**290**	HBA1	0.04396700	5.28
240	ANKLE1	0.02372100	6.07	**291**	TMEM261	0.00528230	5.28
241	C21orf140	0.03476500	6.00	**292**	FANCG	0.01440500	5.26
242	GGCT	0.03211800	5.99	**293**	NAP1L2	0.01010600	5.26
243	HIST2H2BF	0.00786030	5.98	**294**	ZNF543	0.04484300	5.25
244	ZNF687	0.01766500	5.97	**295**	KRT222	0.02028100	5.25
245	HIST1H2BL	0.04688700	5.96	**296**	RHOB	0.02225300	5.25
246	NAA50	0.03457200	5.94	**297**	KHDRBS2	0.01762500	5.15
247	VPS26B	0.04812500	5.92	**298**	NFU1	0.04606500	5.15
248	SLC25A26	0.00839850	5.86	**299**	C15orf27	0.01063700	5.15
249	ZNF564	0.01274100	5.85	**300**	GGN	0.00547760	5.14
250	FBL	0.01856300	5.85	**301**	OR1L1	0.04160900	5.14
251	MEGF6	0.01750400	5.84	**302**	MRRF	0.02935800	5.13
252	OSTC	0.04180100	5.83	**303**	MRPS7	0.00820120	5.13
253	SMAD7	0.04300300	5.82	**304**	OR10H3	0.00880360	5.11
254	KCNJ3	0.01837200	5.82	**305**	CLPP	0.02862700	5.10

Rank	Gene ID	*p*	ΔLFC	Rank	Gene ID	*p*	ΔLFC
306	HIST2H4A	0.01581400	5.10	**357**	SLC4A4	0.04748200	4.62
307	TMEM121	0.04407800	5.08	**358**	HPGDS	0.01560400	4.61
308	ST6GALNAC6	0.01230100	5.07	**359**	DIRC1	0.04828300	4.60
309	KCNV2	0.00691190	5.06	**360**	REM1	0.04494200	4.58
310	LMO7	0.03415100	5.06	**361**	CTBS	0.04039500	4.54
311	GAL3ST2	0.02314400	5.06	**362**	RGS7	0.01103600	4.54
312	ZNF587	0.02450900	5.03	**363**	DEDD	0.01024600	4.53
313	SNX30	0.00587120	5.02	**364**	HES1	0.04338100	4.52
314	LTBR	0.04939900	5.01	**365**	BLOC1S5	0.03639700	4.51
315	CYP19A1	0.03883100	4.91	**366**	BNIPL	0.01565500	4.50
316	PARD6G	0.01126300	4.90	**367**	AURKAIP1	0.02462800	4.50
317	OR4A5	0.01774100	4.88	**368**	NT5DC1	0.04422100	4.48
318	ZNF883	0.01303500	4.88	**369**	SLC35C1	0.01086300	4.47
319	CEL	0.00720870	4.88	**370**	CYP4F22	0.02104800	4.47
320	FCHO2	0.00831930	4.88	**371**	ADGRL3	0.01718000	4.45
321	KRTAP5-1	0.02531800	4.88	**372**	C9orf47	0.03064100	4.44
322	OR52L1	0.04675200	4.88	**373**	LILRB2	0.04569100	4.44
323	SDC3	0.04299100	4.86	**374**	PPDPF	0.01132000	4.44
324	TXNDC12	0.02437200	4.86	**375**	LSMEM1	0.04053900	4.43
325	TMEM222	0.02973300	4.85	**376**	MRPL4	0.00856220	4.42
326	L2HGDH	0.02485200	4.85	**377**	DHRS9	0.02516000	4.42
327	BICD2	0.04953300	4.85	**378**	SNRNP70	0.01318000	4.41
328	HTR3D	0.04229800	4.84	**379**	TSPYL1	0.03208800	4.40
329	ISCA1	0.02471200	4.83	**380**	ENTPD5	0.02054200	4.40
330	SMLR1	0.01960300	4.83	**381**	ATP9B	0.01067700	4.38
331	ZFAND5	0.03509100	4.82	**382**	C9orf24	0.01707700	4.38
332	NDUFC2	0.01140700	4.82	**383**	COLEC11	0.04170600	4.35
333	PPP1R14A	0.03396000	4.81	**384**	SOSTDC1	0.04662000	4.35
334	BRI3	0.00843380	4.80	**385**	CDK20	0.04349700	4.35
335	AMACR	0.04670700	4.79	**386**	ENPP6	0.04704800	4.35
336	PTPRD	0.02157700	4.77	**387**	PPM1L	0.03154200	4.34
337	ABL2	0.01021900	4.77	**388**	MRPS23	0.00925270	4.34
338	SLC25A19	0.03056700	4.77	**389**	AP3D1	0.01356600	4.34
339	RAI2	0.00897460	4.76	**390**	EIF4G2	0.01479100	4.33
340	TRIO	0.04990200	4.76	**391**	FSD1L	0.01018000	4.33
341	IL1A	0.04636700	4.74	**392**	BAP1	0.02805800	4.33
342	ASMTL	0.04101800	4.73	**393**	FAM129B	0.01254500	4.33
343	MRPS35	0.00866320	4.70	**394**	STX6	0.04015800	4.31
344	MRPS18B	0.04462900	4.70	**395**	CAPG	0.00662340	4.31
345	RPS6KA2	0.01412800	4.67	**396**	C8B	0.02868100	4.31
346	FAM208B	0.02291100	4.67	**397**	UNG	0.00677050	4.30
347	HEMK1	0.03305900	4.67	**398**	ZNF506	0.02666200	4.29
348	LPAR4	0.01036700	4.66	**399**	TARS2	0.02689900	4.29
349	DCP1B	0.02964300	4.65	**400**	TMOD1	0.03656000	4.28
350	LTK	0.02863700	4.64	**401**	TMC2	0.02587800	4.28
351	TEFM	0.00761530	4.64	**402**	TBC1D3F	0.01382800	4.28
352	MIPEP	0.02880900	4.63	**403**	NDUFA2	0.00639650	4.28
353	QRSL1	0.00739880	4.62	**404**	NUBPL	0.00608980	4.27
354	GATB	0.01110300	4.62	**405**	SLC39A6	0.01930100	4.27
355	TIAL1	0.00903210	4.62	**406**	MECR	0.02859400	4.26
356	P3H4	0.02886700	4.62	**407**	SIAH2	0.03136800	4.26

Rank	Gene ID	*p*	ΔLFC	Rank	Gene ID	*p*	ΔLFC
408	MTG2	0.01673200	4.26	**459**	LYNX1	0.03909600	3.96
409	GOLT1A	0.02735800	4.26	**460**	FKBP7	0.02320400	3.95
410	ABCA7	0.04209000	4.25	**461**	PAGE1	0.01003200	3.95
411	DEFB116	0.04703500	4.25	**462**	ITM2C	0.00525740	3.94
412	CSN2	0.03552000	4.25	**463**	PSIP1	0.00881140	3.93
413	DAAM2	0.01859800	4.24	**464**	DDRGK1	0.00977950	3.93
414	OR5AR1	0.02075200	4.23	**465**	AP1M2	0.04375400	3.92
415	ZNF648	0.04263400	4.22	**466**	C11orf70	0.03965200	3.90
416	SPDL1	0.03881000	4.22	**467**	CIRBP	0.04608500	3.90
417	CLSTN1	0.02921800	4.21	**468**	APOH	0.02246300	3.90
418	LZTS3	0.01921500	4.20	**469**	ERBB2	0.04415900	3.89
419	ATF3	0.03032700	4.19	**470**	AKR1C3	0.03887800	3.89
420	TPD52L3	0.00978500	4.19	**471**	C2orf42	0.04276200	3.87
421	ATP1A4	0.04630900	4.18	**472**	NDC80	0.04287500	3.87
422	MZF1	0.02454700	4.18	**473**	NEURL4	0.03967300	3.84
423	BCO1	0.02134200	4.18	**474**	SLC9A7	0.03942000	3.83
424	MTIF3	0.01482000	4.17	**475**	TRPM6	0.00877150	3.83
425	CSRP1	0.04918500	4.17	**476**	FGF7	0.00652030	3.83
426	MRPS33	0.01256500	4.15	**477**	ADAMTS13	0.01404300	3.83
427	RTBDN	0.01730100	4.15	**478**	RAB3IP	0.03280900	3.82
428	RNF187	0.04554600	4.15	**479**	HBZ	0.03102100	3.82
429	RBPJ	0.00905850	4.13	**480**	GREM2	0.03341200	3.81
430	OR2T2	0.01162500	4.13	**481**	PRKAG2	0.00791890	3.81
431	UPF3B	0.02912200	4.12	**482**	GC	0.03807000	3.81
432	RHPN2	0.03749300	4.11	**483**	PROK1	0.02147500	3.81
433	GDF5	0.00525840	4.11	**484**	ZSCAN18	0.02194200	3.81
434	PARS2	0.00988160	4.11	**485**	CSRNP3	0.02134800	3.81
435	GRSF1	0.00825610	4.10	**486**	ACTL7A	0.01256500	3.80
436	CTSV	0.02862800	4.10	**487**	MAGIX	0.03564100	3.79
437	DACT2	0.01858600	4.09	**488**	LCE6A	0.03314200	3.79
438	SLC37A1	0.01912900	4.09	**489**	MRPL10	0.00549850	3.79
439	RABGAP1	0.00956200	4.05	**490**	ISL2	0.02620100	3.78
440	OR1E2	0.04000800	4.04	**491**	RSPH3	0.02379500	3.78
441	ENKUR	0.03673300	4.04	**492**	LSP1	0.04638300	3.77
442	RRP1B	0.04172200	4.04	**493**	REXO2	0.00880050	3.76
443	TP53INP2	0.04273200	4.03	**494**	C1orf233	0.04719400	3.76
444	NDUFAF3	0.04787600	4.02	**495**	NPRL3	0.04797300	3.76
445	UCK1	0.01504000	4.02	**496**	GMIP	0.04377000	3.75
446	TOR4A	0.02429500	4.00	**497**	TOR1B	0.03033700	3.74
447	GALNT2	0.04671700	4.00	**498**	GJA4	0.01833700	3.74
448	RNF141	0.02505100	4.00	**499**	DNALI1	0.03425400	3.74
449	RAB12	0.01065900	4.00	**500**	TPTE	0.02854800	3.73
450	KDM4C	0.04297100	4.00	**501**	KLF11	0.01465000	3.73
451	FMO2	0.01918700	3.99	**502**	IFIT2	0.01819300	3.73
452	S100A7L2	0.01969600	3.99	**503**	IFNK	0.02364200	3.72
453	STUB1	0.00624210	3.99	**504**	ALPPL2	0.02304500	3.71
454	RPL36AL	0.02054300	3.98	**505**	TMEM251	0.03321200	3.69
455	ZRSR2	0.03098500	3.98	**506**	SV2B	0.04113100	3.69
456	ANKRD18A	0.04881200	3.98	**507**	TIMM17A	0.02367700	3.68
457	GBA	0.02984200	3.97	**508**	TMEM191C	0.02205500	3.67
458	MALSU1	0.00658300	3.97	**509**	OSCP1	0.00893730	3.67

Rank	Gene ID	*p*	ΔLFC	Rank	Gene ID	*p*	ΔLFC
510	DARS2	0.01255000	3.67	**561**	CDKN2A	0.00895540	3.41
511	TMEM221	0.01955500	3.66	**562**	LARS2	0.04195700	3.41
512	ZNF507	0.02253200	3.66	**563**	CST9	0.01488000	3.40
513	UROS	0.00664930	3.66	**564**	PITHD1	0.01775300	3.40
514	TMEM56	0.03136000	3.66	**565**	EFCAB9	0.00979090	3.39
515	FAM73B	0.01294500	3.65	**566**	CLIC1	0.01999100	3.39
516	KCNT1	0.03188200	3.65	**567**	UCKL1	0.02082800	3.39
517	RBCK1	0.01672300	3.65	**568**	TRIM58	0.01702200	3.39
518	OR5B12	0.02103500	3.64	**569**	QSOX2	0.04410800	3.38
519	GFM1	0.04529300	3.64	**570**	SLC35F3	0.00599810	3.38
520	OTOGL	0.04601000	3.63	**571**	SARS2	0.04750000	3.38
521	HAVCR1	0.01189800	3.62	**572**	HSF2BP	0.02065800	3.37
522	DRAXIN	0.03036500	3.62	**573**	PERP	0.02520000	3.36
523	CLCA1	0.01495400	3.62	**574**	OR2G6	0.03437400	3.36
524	NPDC1	0.03216600	3.62	**575**	HSD17B4	0.01778000	3.36
525	ZNF804B	0.01492900	3.61	**576**	MIB1	0.04753700	3.36
526	SEC23B	0.02371800	3.61	**577**	GPR157	0.03455200	3.35
527	CYGB	0.00740300	3.60	**578**	LCE1E	0.03141600	3.35
528	SLC2A10	0.04604900	3.59	**579**	CA7	0.01777200	3.34
529	SYCN	0.00630270	3.58	**580**	OSTF1	0.00858240	3.34
530	SMIM17	0.01409400	3.57	**581**	PTGES2	0.03018500	3.34
531	CCDC30	0.03221100	3.56	**582**	FARP2	0.00838770	3.34
532	PDCD2L	0.02615600	3.56	**583**	ZNF316	0.01738100	3.32
533	INSRR	0.03191900	3.56	**584**	MPO	0.01101500	3.32
534	AGRN	0.02145200	3.56	**585**	MPND	0.02983300	3.31
535	CCDC60	0.01609400	3.53	**586**	MLLT11	0.00564640	3.31
536	DISP1	0.01258400	3.53	**587**	CPOX	0.01385800	3.30
537	ATP4B	0.02027400	3.53	**588**	WTAP	0.01977300	3.29
538	OXA1L	0.02758000	3.52	**589**	OSTM1	0.04264400	3.29
539	PGAM2	0.03773200	3.52	**590**	TMEM134	0.00560600	3.28
540	COQ7	0.00563810	3.49	**591**	MR1	0.01194000	3.28
541	LCN9	0.02713900	3.49	**592**	RAC2	0.02616000	3.28
542	GAN	0.01578600	3.49	**593**	MYLPF	0.03997600	3.27
543	OR52W1	0.02251100	3.47	**594**	RUNX1	0.04013400	3.27
544	MAN2C1	0.03350800	3.46	**595**	EMILIN3	0.01135800	3.27
545	CES4A	0.02349300	3.46	**596**	BARX2	0.03580700	3.27
546	TBC1D9	0.01351100	3.46	**597**	CFHR3	0.01396300	3.26
547	C17orf75	0.03194100	3.45	**598**	TMOD4	0.02007400	3.26
548	FAM47E-STBD1	0.03180600	3.45	**599**	LRP4	0.04645300	3.26
549	MRPS9	0.01067700	3.45	**600**	MUC12	0.02099300	3.25
550	AIDA	0.02264600	3.45	**601**	PDE6H	0.03237900	3.25
551	PLEKHG2	0.02392800	3.45	**602**	MINPP1	0.01556000	3.25
552	RASAL3	0.03617900	3.44	**603**	MIDN	0.04023800	3.25
553	C18orf65	0.02216700	3.44	**604**	SFT2D2	0.02798200	3.25
554	LZTS1	0.01022300	3.44	**605**	HOXD10	0.02572500	3.23
555	JAG1	0.01847800	3.43	**606**	CASKIN1	0.02395500	3.23
556	BDKRB2	0.04462400	3.43	**607**	PAMR1	0.00902270	3.23
557	SRCAP	0.03763300	3.42	**608**	CORO7	0.04866000	3.22
558	GRID2IP	0.01047400	3.42	**609**	RFX7	0.02579300	3.21
559	MRPL54	0.00816540	3.42	**610**	VN1R2	0.03870800	3.21
560	ZNF570	0.03426300	3.41	**611**	CERCAM	0.03951700	3.21

Rank	Gene ID	*p*	ΔLFC	Rank	Gene ID	*p*	ΔLFC
612	NAB2	0.02078500	3.21	**663**	GTPBP3	0.01361800	2.99
613	CD8A	0.04847100	3.21	**664**	LKAAEAR1	0.00609450	2.99
614	MKL1	0.02588300	3.20	**665**	MRPL55	0.01183100	2.98
615	TFF1	0.04318800	3.18	**666**	GTF3C1	0.03646100	2.98
616	PSG6	0.03232100	3.18	**667**	CCER2	0.04086200	2.98
617	CBR1	0.02157900	3.18	**668**	B3GNT6	0.01775500	2.98
618	PNKD	0.04751700	3.17	**669**	DMBX1	0.02062600	2.98
619	OR4A47	0.00871500	3.17	**670**	GAREM	0.02084100	2.97
620	FOXD2	0.03742100	3.16	**671**	ZNF726	0.03036900	2.97
621	PEBP4	0.01544100	3.16	**672**	TAS2R5	0.00807270	2.95
622	GCSH	0.04992000	3.15	**673**	FBXO7	0.03484200	2.95
623	FAM120A	0.00549100	3.15	**674**	PPP1R37	0.01652600	2.95
624	ADTRP	0.02982300	3.14	**675**	MAN2A1	0.04654800	2.94
625	DSG2	0.01458400	3.14	**676**	AGBL4	0.00775930	2.94
626	HARBI1	0.01644400	3.13	**677**	CDKN1C	0.03947400	2.94
627	CCL4	0.04311300	3.13	**678**	OR7C2	0.03608500	2.94
628	TICAM2	0.02773200	3.13	**679**	BRD4	0.03920600	2.93
629	C22orf29	0.01701300	3.13	**680**	CYP4F8	0.02169600	2.93
630	CD34	0.03660700	3.13	**681**	CLN8	0.04311000	2.93
631	C5orf45	0.04637000	3.13	**682**	CHSY1	0.04224100	2.93
632	SRL	0.04508400	3.12	**683**	CSF3	0.04374700	2.93
633	LRP11	0.01350300	3.11	**684**	KIRREL	0.04996600	2.92
634	EEF1A2	0.03973900	3.10	**685**	NLRP8	0.02849000	2.91
635	OR4D10	0.01133000	3.10	**686**	HK2	0.03121200	2.91
636	ZNF510	0.00698490	3.10	**687**	NDUFB10	0.04019100	2.91
637	CALCB	0.03853000	3.10	**688**	UQCR11	0.01083400	2.91
638	NANOS1	0.03314200	3.08	**689**	HSPA8	0.04000200	2.91
639	CNTFR	0.00776190	3.08	**690**	ALPL	0.04403500	2.91
640	HRNR	0.01902500	3.08	**691**	HNF4G	0.04767400	2.91
641	TSPY2	0.01856900	3.06	**692**	ARRDC5	0.01487500	2.90
642	NOTCH1	0.01885700	3.06	**693**	PTGER1	0.03471900	2.90
643	ZDBF2	0.03644800	3.05	**694**	KDM6B	0.03840000	2.90
644	DPP9	0.01238500	3.05	**695**	NDUFA5	0.01720100	2.90
645	FCRLA	0.04328800	3.05	**696**	ZSCAN1	0.01768100	2.89
646	PNPLA4	0.02857700	3.05	**697**	PEAR1	0.00808980	2.89
647	GPR61	0.04649500	3.05	**698**	MRPL32	0.03626800	2.89
648	ST8SIA3	0.04206100	3.05	**699**	PPAPDC2	0.03618700	2.88
649	OR52B6	0.04723500	3.05	**700**	TRIM68	0.02899900	2.88
650	ZNF106	0.02424000	3.04	**701**	C9orf66	0.03752100	2.88
651	KRTAP12-3	0.03449100	3.04	**702**	AP1M1	0.02843800	2.88
652	RSPH10B	0.01645400	3.04	**703**	PDE12	0.01417600	2.88
653	EGF	0.01033300	3.03	**704**	FBXO25	0.03775300	2.88
654	ADRM1	0.04247900	3.02	**705**	PEF1	0.00973290	2.87
655	OR52E8	0.00634930	3.02	**706**	FCGR2A	0.01490900	2.87
656	GPR35	0.04737600	3.02	**707**	PHLPP1	0.04887900	2.87
657	FAM213A	0.03076100	3.01	**708**	LOC339862	0.02271100	2.87
658	GSK3A	0.02536400	3.01	**709**	RCE1	0.02836900	2.86
659	HARS2	0.01061800	3.00	**710**	MRPL13	0.01583000	2.86
660	SMAD3	0.01323700	3.00	**711**	ABHD17B	0.04632200	2.86
661	NXNL2	0.00727030	3.00	**712**	GSG2	0.01943400	2.86
662	LOC100505478	0.03926600	3.00	**713**	TMEM107	0.04942900	2.86

Rank	Gene ID	*p*	ΔLFC	Rank	Gene ID	*p*	ΔLFC
714	LPIN1	0.01034500	2.86	**765**	CR1	0.01581400	2.69
715	OPN3	0.03021800	2.85	**766**	CCNF	0.00976710	2.69
716	ADAMTSL2	0.04945700	2.85	**767**	PUS1	0.00625770	2.69
717	LGALS7B	0.04140600	2.84	**768**	PMFBP1	0.04923900	2.68
718	CDX2	0.02208900	2.84	**769**	NMRK1	0.04357400	2.68
719	KLHDC2	0.03199600	2.84	**770**	CYP4A11	0.04572300	2.68
720	NFASC	0.01044400	2.84	**771**	GDI2	0.03575900	2.67
721	LHCGR	0.03813900	2.83	**772**	CASP14	0.01455100	2.67
722	ARAP1	0.04737300	2.83	**773**	STXBP2	0.04438200	2.67
723	ST14	0.00674460	2.83	**774**	C7orf71	0.01159600	2.67
724	LCE1A	0.03866800	2.83	**775**	TAS2R20	0.04147100	2.67
725	TMC6	0.00693420	2.82	**776**	LHX4	0.02010200	2.66
726	FCRL1	0.02106000	2.82	**777**	OR13C3	0.00691090	2.66
727	DPP3	0.01658000	2.82	**778**	PPARGC1B	0.02251500	2.66
728	RRH	0.04079400	2.81	**779**	LYG1	0.00920820	2.65
729	C1orf94	0.01830200	2.80	**780**	USP26	0.03736600	2.65
730	COX17	0.03072400	2.79	**781**	RBL1	0.02164000	2.65
731	ADNP	0.03294200	2.79	**782**	TOMM7	0.02539200	2.64
732	MTO1	0.00536930	2.79	**783**	HS2ST1	0.03245700	2.63
733	CD48	0.02842300	2.78	**784**	SOX2	0.04878400	2.63
734	ATP2B1	0.04914300	2.78	**785**	SAP130	0.04009400	2.62
735	FOXK2	0.03667400	2.78	**786**	ABCB5	0.03148000	2.62
736	ZXDB	0.01831400	2.78	**787**	SUPV3L1	0.04297100	2.61
737	SH3RF1	0.03381400	2.78	**788**	DNM1	0.00756200	2.61
738	AQP1	0.01123600	2.77	**789**	DNAH7	0.04640200	2.61
739	TBCA	0.02836600	2.76	**790**	PMCH	0.04096400	2.61
740	MRPL9	0.00811290	2.76	**791**	SPAG8	0.02849100	2.61
741	RPS6KA4	0.04791000	2.76	**792**	CGA	0.03137200	2.61
742	NR5A1	0.00883050	2.76	**793**	NRTN	0.00778780	2.61
743	SBK2	0.01232300	2.76	**794**	KRBA1	0.03209600	2.60
744	FARSB	0.03502000	2.76	**795**	TTC9	0.02629600	2.60
745	FAM118A	0.00952930	2.75	**796**	CKS2	0.00850370	2.60
746	RFX5	0.02949700	2.75	**797**	ZNF444	0.02722200	2.60
747	NBEAL2	0.03541500	2.75	**798**	OR51M1	0.02785100	2.60
748	SOX7	0.02502800	2.75	**799**	QSER1	0.04309600	2.59
749	TRIM17	0.04088300	2.75	**800**	CALR	0.00957490	2.59
750	KLHL36	0.02232100	2.75	**801**	MRPL33	0.04755900	2.59
751	ISL1	0.01467700	2.74	**802**	TNFSF8	0.03323600	2.59
752	BLZF1	0.01668300	2.74	**803**	WDR83OS	0.00917550	2.57
753	DDIT4	0.04076400	2.74	**804**	ZNF91	0.00738330	2.57
754	CXCL6	0.00548220	2.73	**805**	TCTE1	0.02188900	2.56
755	CORO2A	0.01014800	2.73	**806**	RIC1	0.04313900	2.56
756	ANGPTL5	0.03279700	2.72	**807**	ECHDC3	0.01439800	2.56
757	AK8	0.04461500	2.72	**808**	LHFP	0.01845000	2.56
758	TAB3	0.04597000	2.72	**809**	KIAA0040	0.03367400	2.56
759	AGFG2	0.04207000	2.72	**810**	LOC388282	0.02859200	2.55
760	RASGRP4	0.04494500	2.71	**811**	TCTE3	0.04987800	2.55
761	MYOT	0.02438700	2.71	**812**	HRH2	0.03707000	2.55
762	IFNA2	0.01462600	2.70	**813**	NTSR2	0.04807800	2.54
763	SERPINA9	0.03080600	2.70	**814**	ACP5	0.03881200	2.54
764	ZNF568	0.01891400	2.70	**815**	RAB4A	0.02811100	2.54

Rank	Gene ID	*p*	ΔLFC	Rank	Gene ID	*p*	ΔLFC
816	BCAN	0.04664700	2.54	**867**	C10orf71	0.02419800	2.36
817	FAM170B	0.02111400	2.53	**868**	ERVMER34-1	0.03543900	2.36
818	DCT	0.01590400	2.53	**869**	OSBPL10	0.03399700	2.36
819	PHYH	0.04793800	2.52	**870**	KCTD15	0.00697610	2.36
820	FBXO28	0.03591300	2.52	**871**	SERPINA10	0.00571580	2.35
821	USP2	0.00683060	2.52	**872**	DEGS1	0.01315800	2.35
822	MRPS17	0.01357300	2.52	**873**	AK1	0.00963710	2.35
823	RPS20	0.00544650	2.52	**874**	TMEM168	0.02752300	2.35
824	UBR7	0.02073500	2.52	**875**	FAM3B	0.03941700	2.35
825	SHC3	0.00834570	2.51	**876**	PRRC2B	0.03103200	2.35
826	PKN3	0.00683990	2.51	**877**	DNAJA1	0.02134600	2.35
827	PNMA2	0.03615700	2.51	**878**	KCP	0.03086300	2.34
828	SNX22	0.02683000	2.51	**879**	PGRMC2	0.04360800	2.34
829	MAN1C1	0.04291600	2.51	**880**	DMKN	0.04069300	2.34
830	PCDHGB3	0.04418600	2.50	**881**	CENPU	0.03550200	2.33
831	KLC3	0.03055400	2.50	**882**	RIC3	0.04499600	2.33
832	MDH2	0.00581270	2.49	**883**	LAMB3	0.04950600	2.33
833	EPGN	0.04706200	2.49	**884**	ZNF579	0.00813800	2.32
834	TMEM74B	0.02923100	2.49	**885**	CYP7B1	0.04750800	2.32
835	NUDT8	0.03458800	2.47	**886**	SLC25A44	0.02695700	2.32
836	ACTG2	0.04065100	2.47	**887**	SPP1	0.02819500	2.32
837	PRDM8	0.02999200	2.47	**888**	TIRAP	0.04730400	2.30
838	PLIN5	0.04382900	2.47	**889**	CCSAP	0.02809700	2.30
839	RCC2	0.04130900	2.47	**890**	EFHC2	0.02183700	2.29
840	IBA57	0.03302200	2.47	**891**	IER5L	0.04256400	2.29
841	SLC25A46	0.04175900	2.47	**892**	GPSM1	0.04675100	2.28
842	TFB1M	0.03456000	2.47	**893**	ZER1	0.00993540	2.28
843	NDUFS8	0.02834600	2.46	**894**	BTBD19	0.03464600	2.28
844	ZNF547	0.01878400	2.46	**895**	APBB3	0.02651300	2.28
845	CALD1	0.03368200	2.45	**896**	MAP3K11	0.03081200	2.27
846	FCRL3	0.03901700	2.45	**897**	GSTA4	0.02335400	2.27
847	SCN1A	0.04623900	2.45	**898**	TMEM120B	0.03922200	2.26
848	SPATA31D4	0.00934540	2.45	**899**	MMP3	0.00637320	2.25
849	KIAA2013	0.02100700	2.44	**900**	JUND	0.04811100	2.25
850	TOPORS	0.00774480	2.44	**901**	KRCC1	0.03951400	2.25
851	C10orf91	0.01999600	2.43	**902**	HNF1A	0.02428200	2.25
852	JAG2	0.00569300	2.43	**903**	ZNF75D	0.04289400	2.25
853	PTRH1	0.02649300	2.42	**904**	DEFB106B	0.04253700	2.24
854	ERGIC3	0.01381400	2.42	**905**	ZNF467	0.02744000	2.24
855	MTFMT	0.04815200	2.41	**906**	37865	0.02339900	2.24
856	RBAK	0.04971700	2.40	**907**	CCDC159	0.00840580	2.23
857	ZDHHC12	0.02417800	2.40	**908**	MARK1	0.02267700	2.22
858	KCNJ18	0.04120400	2.40	**909**	LEMD2	0.03599000	2.22
859	LCOR	0.03242500	2.39	**910**	SMIM15	0.01861400	2.22
860	HEXA	0.01992200	2.39	**911**	TPM1	0.02634400	2.22
861	CPLX3	0.00780540	2.38	**912**	HSD11B1	0.01368600	2.22
862	HENMT1	0.04007900	2.38	**913**	POU4F3	0.01586100	2.22
863	ZCCHC5	0.04767800	2.38	**914**	MYCBP2	0.02899700	2.21
864	MAGEC1	0.02044600	2.37	**915**	YBEY	0.04975000	2.21
865	FAM159A	0.00622090	2.37	**916**	MOB3A	0.04888100	2.20
866	WNT16	0.01561500	2.37	**917**	HMG20B	0.02293000	2.19

Rank	Gene ID	*p*	ΔLFC	Rank	Gene ID	*p*	ΔLFC
918	SIRPB1	0.02508900	2.19	**969**	LRFN1	0.00764170	1.99
919	C20orf62	0.00502480	2.18	**970**	CHRNA10	0.02150400	1.99
920	IGFBP4	0.03947600	2.18	**971**	VSNL1	0.03925500	1.98
921	FURIN	0.00566920	2.18	**972**	CLDND1	0.04647600	1.97
922	SRGAP1	0.04527800	2.18	**973**	MCC	0.02254600	1.97
923	MRPS34	0.00546150	2.17	**974**	RAPSN	0.03431200	1.96
924	DOK1	0.04704900	2.17	**975**	FAT2	0.03203600	1.96
925	ZNF429	0.02977100	2.17	**976**	PPM1J	0.04276700	1.95
926	C1orf186	0.03306700	2.17	**977**	GREB1L	0.01043900	1.94
927	C9orf131	0.03641800	2.16	**978**	EHD1	0.00966500	1.94
928	CHST12	0.04488100	2.16	**979**	TLX3	0.02263700	1.94
929	TSPEAR	0.02296600	2.15	**980**	DHX30	0.04079100	1.92
930	KLK5	0.03316500	2.15	**981**	MUM1L1	0.04304000	1.92
931	TCOF1	0.01776000	2.15	**982**	ZFP37	0.01225100	1.90
932	SLC39A1	0.01229900	2.15	**983**	MAGI3	0.03352800	1.89
933	CXCL9	0.04849100	2.15	**984**	GRK5	0.04405500	1.89
934	GNB2	0.02174600	2.14	**985**	ATF6	0.02861000	1.88
935	MARCH5	0.00720710	2.14	**986**	RASSF5	0.04588100	1.87
936	ZNF610	0.03235700	2.14	**987**	TLL1	0.04509100	1.87
937	DNAJB5	0.00985410	2.14	**988**	MYDGF	0.02528200	1.86
938	ZNF197	0.01020500	2.14	**989**	KDM4E	0.04333200	1.86
939	CAPZA1	0.03083800	2.14	**990**	PROP1	0.01621800	1.86
940	LOC100506422	0.01838500	2.13	**991**	TFAM	0.04218300	1.85
941	SYNPO2	0.01940100	2.12	**992**	MTMR11	0.03049800	1.85
942	SNPH	0.03479700	2.11	**993**	DISC1	0.04065900	1.85
943	SLC43A1	0.04087400	2.11	**994**	LARGE	0.01582500	1.84
944	FAF1	0.02122800	2.11	**995**	TWF2	0.03323600	1.84
945	UQCC1	0.04916000	2.11	**996**	CCDC89	0.02386300	1.84
946	IQGAP3	0.01797200	2.10	**997**	KCNQ2	0.03478100	1.84
947	PHYHIPL	0.03797100	2.10	**998**	CCRN4L	0.03110400	1.84
948	ELAC1	0.04655800	2.10	**999**	PPAP2B	0.03401900	1.83
949	CDH20	0.02333400	2.10	**1000**	SPACA5	0.04477500	1.83
950	RAD23A	0.02612900	2.10	**1001**	BTG2	0.03111000	1.81
951	GRIFIN	0.04315600	2.08	**1002**	GTPBP6	0.02006400	1.81
952	AUH	0.03236900	2.08	**1003**	MXRA5	0.01475000	1.80
953	FBN3	0.04394800	2.07	**1004**	GATA1	0.00940970	1.80
954	PVRL4	0.01127200	2.07	**1005**	PABPC5	0.04630100	1.80
955	GRAMD1A	0.00855450	2.07	**1006**	COX10	0.04588900	1.79
956	MCAT	0.01366400	2.06	**1007**	DCAF5	0.01685000	1.79
957	KRTAP10-3	0.02423600	2.05	**1008**	DKK3	0.04785700	1.79
958	MRPS28	0.02072000	2.04	**1009**	G0S2	0.00722730	1.79
959	AGT	0.03902900	2.04	**1010**	C1orf210	0.03053600	1.79
960	REEP6	0.02338300	2.03	**1011**	ETFA	0.03035900	1.76
961	LRSAM1	0.00941070	2.03	**1012**	RFWD2	0.02916000	1.75
962	CEBPD	0.02228600	2.03	**1013**	SYDE1	0.02324000	1.73
963	ASB15	0.01104600	2.02	**1014**	BHLHA15	0.03769300	1.73
964	BRPF1	0.02028900	2.02	**1015**	CRMP1	0.03598300	1.73
965	TIFA	0.01561600	2.01	**1016**	TXNDC15	0.03538500	1.73
966	TBX22	0.04583600	2.01	**1017**	GABRR1	0.03771800	1.73
967	TEX14	0.02420100	2.00	**1018**	CHI3L1	0.03781100	1.72
968	KLC2	0.03791800	2.00	**1019**	C9orf3	0.04865600	1.71

Rank	Gene ID	*p*	ΔLFC	Rank	Gene ID	*p*	ΔLFC
1020	MAU2	0.04287300	1.71	**1064**	DNAH14	0.02599400	1.45
1021	LBH	0.00858450	1.71	**1065**	PCSK6	0.03598200	1.45
1022	IER3IP1	0.02596000	1.70	**1066**	MEF2BNB-MEF2B	0.04144000	1.45
1023	MEF2D	0.01927200	1.70	**1067**	JAM3	0.04623800	1.45
1024	NDRG4	0.02896700	1.70	**1068**	RFK	0.03923300	1.40
1025	NOL4L	0.02509000	1.68	**1069**	FABP9	0.03787200	1.39
1026	SLC35B4	0.02302300	1.68	**1070**	KRTAP10-6	0.04754100	1.39
1027	PITPNM1	0.04800000	1.68	**1071**	GNA15	0.02842700	1.39
1028	DMRTC2	0.04886100	1.66	**1072**	BTAF1	0.03855100	1.39
1029	DRGX	0.01754000	1.66	**1073**	COQ3	0.04097300	1.38
1030	C11orf52	0.04711500	1.66	**1074**	BARX1	0.02576400	1.37
1031	WASL	0.03137900	1.66	**1075**	ARSA	0.03751600	1.37
1032	ZNF699	0.00693830	1.66	**1076**	FAM210B	0.02255700	1.33
1033	PEX11A	0.04761800	1.65	**1077**	WDTC1	0.02733200	1.33
1034	SDHAF1	0.02250800	1.63	**1078**	DPP9-AS1	0.04285400	1.31
1035	MRPL34	0.03450300	1.63	**1079**	BLCAP	0.04034300	1.31
1036	HDAC5	0.04284700	1.63	**1080**	LRRC63	0.02951600	1.30
1037	NCR3LG1	0.00759770	1.62	**1081**	TBRG4	0.03596100	1.29
1038	ZNF544	0.01686200	1.61	**1082**	STRA6	0.02165800	1.29
1039	CEP170B	0.03382300	1.61	**1083**	COQ6	0.00577070	1.28
1040	HRCT1	0.04380600	1.60	**1084**	OR13C4	0.04246400	1.28
1041	MVB12A	0.04387800	1.60	**1085**	RILPL1	0.04913200	1.28
1042	RRBP1	0.03897000	1.60	**1086**	SMCHD1	0.04429500	1.26
1043	CDK14	0.03286600	1.58	**1087**	LMO2	0.04032600	1.23
1044	C8orf59	0.03274100	1.57	**1088**	JSRP1	0.03333700	1.23
1045	KCTD2	0.01405300	1.56	**1089**	TUBB6	0.01610300	1.23
1046	IGFBPL1	0.04005100	1.56	**1090**	PPAPDC3	0.01753000	1.21
1047	USF2	0.01374500	1.54	**1091**	CRCP	0.01786300	1.20
1048	C9orf170	0.04133200	1.53	**1092**	GDAP1L1	0.02121000	1.17
1049	OR5V1	0.04411500	1.53	**1093**	C7orf62	0.04775600	1.16
1050	HNRNPH3	0.03677100	1.53	**1094**	C22orf34	0.03705300	1.15
1051	GPRC5C	0.00542580	1.52	**1095**	ECHDC1	0.01612900	1.15
1052	SLC41A1	0.04351500	1.50	**1096**	SMPDL3A	0.02338700	1.15
1053	KCNQ4	0.04033500	1.50	**1097**	DLL4	0.04038500	1.14
1054	C6orf62	0.03983400	1.49	**1098**	GADD45GIP1	0.00895590	1.13
1055	MPEG1	0.04545100	1.49	**1099**	ZNF546	0.03186600	1.12
1056	FAM91A1	0.00832140	1.48	**1100**	MIER1	0.00817110	1.11
1057	ZNF7	0.03464000	1.48	**1101**	UBASH3A	0.04245400	1.10
1058	PRDM4	0.04803400	1.48	**1102**	HELZ2	0.03459700	1.09
1059	CLUAP1	0.01526200	1.47	**1103**	AMOTL2	0.01294500	1.09
1060	ABTB2	0.01925900	1.47	**1104**	MAN2B1	0.04896600	1.07
1061	SPTA1	0.03564700	1.47	**1105**	ZMYND11	0.00552680	1.05
1062	DAND5	0.01244400	1.46	**1106**	H1FX	0.01992900	1.03
1063	PRM2	0.03390600	1.46				

Table 4.10: Screening hits rank no. 1 to 1106.
p = p-value of the comparison between UnaG-positive and unsorted CO cells; LFC = log fold change of a gene found in UnaG-positive or UnaG-negative cells compared to unsorted CO cells; ΔLFC = difference of the log fold changes of UnaG-positive minus UnaG-negative cells.

Ehrenwörtliche Erklärung

Hiermit erkläre ich, dass ich die vorliegende Arbeit selbstständig und ohne unzulässige Hilfe oder Benutzung anderer als der angegebenen Hilfsmitel angefertigt habe. Alle Textstellen, die wörtlich oder sinngemäß aus veröffentlichten oder nichtveröffentlichten Schriften entnommen sind, und alle Angaben, die auf mündlichen Auskünften beruhen, sind als solche kenntlich gemacht. Bei den von mir durchgeführten und in der Dissertation erwähnten Untersuchungen habe ich die Grundsätze guter wissenschaftlicher Praxis, wie sie in der „Satzung der Justus-Liebig-Universität Gießen zur Sicherung guter wissenschaftlicher Praxis“ niedergelegt sind, eingehalten sowie ethische, datenschutzrechtliche und tierschutzrechtliche Grundsätze befolgt. Ich versichere, dass Dritte von mir weder unmittelbar noch mitelbar geldwerte Leistungen für Arbeiten erhalten haben, die im Zusammenhang mit dem Inhalt der vorgelegten Dissertation stehen, und dass die vorgelegte Arbeit weder im Inland noch im Ausland in gleicher oder ähnlicher Form einer anderen Prüfungsbehörde zum Zweck einer Promotion oder eines anderen Prüfungsverfahrens vorgelegt wurde. Alles aus anderen Quellen und von anderen Personen übernommene Material, das in der Arbeit verwendet wurde oder auf welches direkt Bezug genommen wird, wurde als solches kenntlich gemacht. Insbesondere wurden alle Personen genannt, die direkt und indirekt an der Entstehung der vorliegenden Arbeit beteiligt waren. Mit der Überprüfung meiner Arbeit durch eine Plagiatserkennungssoftware bzw. ein internetbasiertes Softwareprogramm erkläre ich mich einverstanden.

Giessen,
Ort, Datum Unterschrift (Nadja Ritschel)

Acknowledgements

This endeavor would not have been possible without my supervisor Prof. Dr. Till Acker, who provided me the opportunity to work on this fascinating topic and guided me through good and turbulent times in the laboratory. I would also like to thank Prof. Dr. Reinhard Dammann for his interest in my studies and for accepting the second supervision of this work. Furthermore, I'm extremely grateful for the support provided by our former and current lab leaders. First, Dr. Boyan Garvalov lightened the start in the project and provided excellent supervision. Later, PD Dr. Attila Németh took over and supported me with scientific and personal advice whenever needed. I am deeply indebted to Prof. Dr. Laura Steenpass, who became a scientific and personal role model since we met during my master's studies.

Additionally, many thanks go to my cooperation partners from the Institute of Biochemistry II, Goethe University Frankfurt and the Department of Medicine V, Internal Medicine, Infectious Diseases and Infection Control, Justus Liebig University Giessen for technical help and long discussions.

I am also grateful for my former and present colleagues from the Institute of Neuropathology, namely Carmen, Daniel, Huike, Julia, Salisa, Sandra, Meng-Miao, Sabine, Weam, Isabel, Elisabeth, Yasmine, Sascha, Omelyan, Nuray, Aya, Kai, Jannik, and Nazli. Thank you for your friendship, motivation and all the lessons you taught me. Thanks should also go to all colleagues from the diagnostics department for technical and organizational support.

I would like to express my deepest gratitude to my closest friends Kathey and Selina for being always there for me and listening to all my troubles but also celebrating my achievements. Thanks go also to my good friends Kati and Caro for discussing about science and sharing the struggles of doing research since our master's studies. Furthermore, I would like to thank all the other great friends, accompanying me through all these years.

I could not have undertaken this journey without my family. My deepest gratitude for their unconditional love, support and believe in me go to my mother Iris, my father Hans-Günter, my siblings Alex and Nici and my sister in law Becky. Moreover, I would like to extend my deepest thanks to my husband Kai. No words can describe how much impact he had in where I am now as a scientist and, moreover, as a person. Kai, this whole journey would not have been possible without you - thank you!